APPLICATION OF ATR-FTIR SPECTROSCOPY FOR THE DIRECT DETECTION OF STIMULANTS IN BIOFLUIDS

Sayali Sangamnerkar MSc

A thesis submitted in fulfilment of the requirements for the degree of Doctor of Philosophy

Supervisors:

Dr Alison Nordon

Dr Matthew J Baker

Department of Pure and Applied Chemistry

University of Strathclyde

August 2023

This thesis is the result of the author's original research. It has been composed by the author and has not been previously submitted for the examination which has led to the award of a degree.

Signed: 

Date: 31st August 2023

“Life is not easy for any of us. But what of that? We must have perseverance and above all, confidence in ourselves.”

Marie Curie

Acknowledgements

I am grateful to so many people who helped me reach this moment, without whom I would not have made it through or enjoyed my experience as much as I have – even when sometimes it got difficult!

Firstly, I would like to express my deepest gratitude to my supervisor, Matt, for giving me this opportunity to learn from you, for your innovative take on my original idea, and for your constant guidance personally and professionally. Without your support and patience in the beginning as well as throughout my PhD journey and those consistent "How are you doing with everything?" at the beginning of every meeting to check in on me, I would not be here. I hope our paths cross again in the future!

I am also very thankful to Alison, who took over from Matt, for taking me on as a student, for all her support especially in the statistics part of my thesis – which no one ever teaches you, and for always having a kind and encouraging word for me – especially in the late stages when things got very difficult for me.

Sam, my brilliant and amazing post-doc and even more awesome friend – girl, I would not be here without your help and guidance in writing and coding, and an unbelievable amount of patience and support throughout this process! You have pushed me, motivated me, kept me going and reminded me of my self-worth when I didn't remember it myself! I love you and I am very grateful to have you in my life!

I would like to thank all my friends in the research group for welcoming me and sharing all the night outs and laughs and wonderful memories in Scotland! In particular, I must mention James and Justin, I am grateful for all the time that you spent helping me understand coding – which might as well be rocket science to me, and answered all my questions at odd hours! Ashton and Chris – Thank you for keeping me company in the lab during those long hours of data collection!

Alex and Kelly - My bananas! I am so grateful for all your love, tea (coffee in my case ☺) breaks, Italian and Scottish sweets, laughs and memes! I could not have asked for more supportive PhD colleagues and even better friends (although friend doesn't seem enough of

a word to describe you two) in a city where I didn’t know a single soul! I will forever cherish the memories I had with you two and I can’t wait for future adventures together!

Finally, to my family, my mom and my brother, Sumedh, I would not be the person I am without your constant support and love. Sumedh, I want to thank you for your your laughs, and memes and all the jokes (even the ones that I don’t find funny or were ill-timed) reminded me of the funnier side of life when things were dark in the moments. Mom, you taught me to break the stereotypes and aim for the sky through your actions and your life. I am so very grateful for all your support through school, university and all my other adventures. I love you both very much and this thesis is for you!

Abstract

Drug detection has become a necessity with dynamic drug markets, the increasing and diverse number of compounds consumed by the world population, the rise of novel psychoactive substances (NPSs) and poly-drug use and lies at the heart of all drug-related issues, policies and legislation. The current screening tests provide inconsistent results across various classes of drugs, especially NPSs, and in different biofluids with high false-positive rates, necessitating secondary testing using expensive confirmatory techniques at already overloaded laboratories. To this effect, the potential of attenuated total reflectance – Fourier transform infrared (ATR-FTIR) spectroscopy in combination with chemometric analyses is evaluated in this thesis as a direct, rapid, adaptable and inexpensive screening method for the detection of methamphetamine (MA) in serum and urine. The method developed here required no prior sample preparation and is demonstrated to distinguish MA from drug-free samples in forensically and clinically relevant concentrations with sensitivities and specificities of ~91% in serum and ~95.5% in urine. Furthermore, discrimination of MA from its metabolites in serum and urine is also demonstrated as they are more likely to be found alongside MA in real-world samples. Limits of detection and quantification of ATR-FTIR spectroscopy for MA are also established at 0.1 mg/mL and 0.3 mg/mL in serum and 0.29 mg/mL and 0.9 mg/mL in urine respectively to establish the applicability of this method in various settings. The suitability of this method as an alternative screening test is demonstrated by successfully discriminating MA from the common prescription drugs known to give false positives on immunoassays in a clinical setting. Finally, the suitability of this method in forensic toxicological screening is illustrated by distinguishing MA from its NPS analogues, synthetic cathinones. Through this work, the great potential of ATR-FTIR spectroscopy is demonstrated for the direct detection of drugs in biological samples to keep up with the ever-evolving drug markets.

Publications and Presentations

A. G. Theakstone, C. Rinaldi, H. J. Butler, J. M. Cameron, L. R. Confield, S. H. Rutherford, A. Sala, **S. Sangamnerkar**, M. J. Baker, Fourier-transform infrared spectroscopy of biofluids: A practical approach. Translational Biophotonics. 3, e202000025 (2021).
DOI: https://www.doi.org/10.1002/tbio.202000025

Analytical Biosciences Group, Royal Society of Chemistry, May 2022. *Presentation.*

List of Abbrieviations

2C	2-(4-bromo-2,5-dimethoxyphenyl)ethanamine
2C-H	2,5-dimethoxyphenethylamine
2D	two dimensions
3D	three dimensions
4-CMC	4-chloromethcathinone
4-MEC	4-methylethcathinone
4-MeO-α-PVP	4'-Methoxy-α-pyrrolidinopentiophenone
AM	Amphetamine
API	Active pharmaceutical ingredient
ATR-FTIR	Attenuated total reflectance- Fourier transform infrared
ATS	Amphetamine-type substances
AU	Artificial urine
AUC	Area under the receiver operator characteristic curve
βK-2C-B	2-Amino-1-(4-bromo-2,5-dimethoxyphenyl)ethan1-one
BlankAU	Blank Artificial urine
BlankS	Blank serum
BU	Bupropion
CAL	Calibration
CNS	Central nervous system
CV	Cross-validation
DART	Direct analysis in real time
DESI	Desorption electrospray ionisation
DLLME	Dispersive liquid-liquid microextraction
DUID	Driving under the influence of drugs
EMA	European medicines agency
EMCDDA	European Monitoring Centre for Drugs and Drug Addiction
EU	European union
EWA	Early warning advisory
FDA	Food and Drug administration
FID	Flame ionisation detector
GC-MS	Gas chromatography mass spectrometry

Ge	Germanium
HIV	Human immunodeficiency virus
IA	Immunoassay
IR	Infrared
IRE	Internal reflection element
LB	Labetalol
LC-MS/MS	Liquid chromatography tandem mass spectrometry
LDA	Linear discriminant analysis
LiTaO3	Lithium Tantalate
LLE	Liquid-liquid extraction
LOD	Limit of detection
LOQ	Limit of quantification
LSD	Lysergic acid
LV	Latent variable
MA	Methamphetamine
MAL	Methallylescaline
MDA	3,4-Methylenedioxyamphetamine
MDMA	3,4-Methylenedioxymethamphetamine
MET	Metformin
MRM	Multiple reaction monitoring
MSM	Dimethyl sulfone
NBOMe	N-methoxybenzyl
NIPALS	Non-linear iterative partial least squares
NIST	National Institute of Standards and Technology
NOR	Norephedrine
NPS	Novel psychoactive substances
OF	Ofloxacin
p-OHAM	p-hydroxyamphetamine
p-OHMA	p-hydroxymethamphetamine
Para	Paracetamol
PCA	Principal components analysis
PLS-DA	Partial least squares discriminant analysis
PLS-R	Partial least squares regression analysis

PR	Promethazine
PSA	Psychoactive Substances Act
QCL	Quantum cascade lasers
RB	Rubberband
RF	Random forest
RMSEC	Root mean square error of calibration
RMSECV	Root mean square error of cross-validation
RMSEP	Root mean square error of prediction
ROC	Receiver operating characteristic curve
SAMHSA	Substance Abuse and Mental Health Services Administration
SERS	Surface enhanced Raman spectroscopy
SG	Savitzky-Golay
SMOTE	Synthetic minority over-sampling technology
SNR	Signal-to-noise ratio
SPAM	Powder amphetamine in serum
SPBU	Powder bupropion in serum
SPE	Solid-phase extraction
SPLB	Powder labetalol in serum
SPMA	Powder methamphetamine in serum
SPMAMSM	Powder methamphetamine and dimethylsulfone in serum
SPMAPara	Powder methamphetamine and paracetamol in serum
SPMASug	Powder methamphetamine and sugar in serum
SPMET	Powder metformin in serum
SPMSM	Powder dimethylsulfone in serum
SPNOR	Powder norephedrine in serum
SPOF	Powder ofloxacin in serum
SPPara	Powder paracetamol in serum
SPpOHAM	Powder p-hydroxyamphetamine in serum
SPpOHMA	Powder p-hydroxyamethamphetamine in serum
SPPR	Powder promethazine in serum
SPSug	Powder sugar in serum
SPTR	Powder trazodone in serum
Sug	Sugar

SWGDRUG	Scientific Working Group for Analysis of Seized Drugs
TCE	Tetrachloroethylene
TIR	Total internal reflection
TN	True negative
TP	True positive
TR	Trazodone
UK	United Kingdom
UNODC	United Nations Office of Drugs and Crime
UPAM	Powder amphetamine in urine
UPBU	Powder bupropion in urine
UPLB	Powder labetalol in urine
UPMA	Powder methamphetamine in urine
UPMAMSM	Powder methamphetamine and dimethylsulfone in urine
UPMAPara	Powder methamphetamine and paracetamol in urine
UPMASug	Powder methamphetamine and sugar in serum
UPMET	Powder metformin in urine
UPMSM	Powder dimethylsulfone in urine
UPNOR	Powder norephedrine in urine
UPOF	Powder ofloxacin in urine
UPPara	Powder paracetamol in urine
UPpOHAM	Powder p-hydroxyamphetamine in urine
UPpOHMA	Powder p-hydroxyamphetamine in urine
UPPR	Powder promethazine in urine
UPSug	Powder sugar in urine
UPTR	Powder trazodone in urine
US	United States
UV	Ultraviolet
WHO	World Health Organisation

Table of Contents

CHAPTER ONE

INTRODUCTION

1.1 Introduction

Drug markets and patterns of drug use are becoming ever more dynamic, diverse, and complex with approximately 275 million drug users worldwide.[1] The consumption of drugs is typically characterised by the use and abuse of illicit drugs as well as the non-medical use of pharmaceutical drugs. Globalization, new technology and the growth of online markets have led to an explosion of counterfeit drugs; not only for controlled psychoactive substances and lifestyle drugs but also for life-saving medicines such as antibiotics, antimalarials and cardiovascular, as well as cancer medicines.[2-4] New psychoactive substances (NPS), also known as 'designer drugs', are being produced at an alarming rate to circumvent the global prohibitive legislation.[3, 5] In the case of clinically approved pharmaceuticals, the adulteration stems from uncontrolled/illicit manufacturing practices as well as deliberate fraudulent production.[6, 7] The greater availability and selection of substances leading to poly-drug use adds another layer of complexity whereby more than one drug is consumed simultaneously or consecutively by individuals.[8] In turn, when drugs are then encountered, whether, in seizures by authorities, or consumers, it has become increasingly difficult to know their composition. In order to tackle this complex issue, there is a need for further technological advances in collection methods as well as sophisticated detection methods.

1.2 Background

Pharmaceutical products are highly regulated through various regulatory frameworks put in place by the likes of the European Medicines Agencies (EMA) or the Food and Drug Administration (FDA) bodies for individual countries. Further guiding principles are also provided by the World Health Organisation (WHO) for medicinal products. However, there are many instances where all these systems of checks and balances fail and the products that reach the consumer are not authentic. The WHO (1999, p. 8) defines counterfeit medicines as:

> One which is deliberately and fraudulently mislabelled with respect to identity and/or source. Counterfeiting can apply to both branded and generic products and counterfeit products may include products with the correct ingredients or with the wrong ingredients, without active ingredients, with insufficient active ingredient or with fake packaging.

This is a blanket term used to describe tampering of any kind with the original product. The term 'substandard medicines', usually preferred by the European Union, , refers to a drug that upon laboratory inspections fails to meet the specifications it claims to comply with.[7, 9, 10] Falsified medicines is another term used to describe such products whereby the products are deliberately and fraudulently designed to mimic the real medicines but in reality contain wrong dosages or no active pharmaceutical ingredient (API), or the wrong API.[10, 11] The terms substandard and falsified are still preferred over the more inclusive term, 'counterfeit' so as to not confuse intellectual property issues with clinical, pharmacological and toxicological concerns.[12, 13]

Counterfeit drugs, in the entirety of their definition, pose a serious threat to public health.[13-15] The UK is not a prime location for the manufacture of counterfeits, though it makes an attractive target for the sale and transit of such medicines. In 2021, over 3 million medicines were seized by the UK border authorities as part of a global operation, valued at over £9 million.[16] These seizures included drugs such as antidepressants, anabolic steroids, analgesics/painkillers, anti-cancer medication, antimalarials, hypnotic and sedative medication, erectile dysfunction pills and various medical devices.[16] Following examination of 710,000 packages, these medicines were seized amongst legitimate products, and over 3,100 online adverts were closed down. However, many medicines still make it into the legitimate supply chain. In such situations, they only come to light if the dispensing chemists can identify counterfeits visually or, in worse cases, the consumer following an adverse reaction. The UK supply chain is a complex system and allows for approximately 900 million medications to be prescribed annually in the UK. Though there are many safeguards in place to avoid counterfeit and falsified drugs from reaching the consumer, it is difficult to estimate the scale of this problem due to the lack of a systematic monitoring process.[17, 18]

The inexorable growth of online pharmacies particularly popular in high-income countries such as the United States where between 19 and 26 million people buy medicines online, makes even the most regulated supply chains vulnerable.[19] As part of Interpol's Operation Pangea in 2015 to tackle illegal online sales of medicines, more than 6 million doses of lifestyle drugs such as slimming pills and erectile dysfunction medications as well as life-saving drugs for cancer, depression and epilepsy were seized in the UK.[20, 21] The internet provides counterfeiters access to various markets for parallel trading or those without strict regulatory oversight. Furthermore, current legislation and regulations do not provide a

strong enough deterrent, either through enforcement or penalties, for counterfeiters.[7] In such situations, the drug users become the first to detect counterfeiting from an online sale. In the case of antimicrobials, it can cause drug resistance in people due to wrong doses in falsified drugs.[22-24] While not many fatalities are officially attributed to counterfeits in the UK, such cases have been identified in other countries like the United States.[6, 7, 25] Notwithstanding the direct harm to public health, counterfeit medicines are expensive to investigate, costly to the overall healthcare system, and can be detrimental to the reputation of drug companies.[26] Therefore, it becomes necessary to be able to identify counterfeit medicines not only in their original form but also in biological fluids once they have been consumed.

Of the 275 million users of drugs, almost 13% of these suffer from drug use disorders due to the misuse of prescription drugs, traditional illicit drugs, and novel substances or any combination thereof.[1] Traditional drugs of abuse such as cocaine and methamphetamine have a long history of abuse and misuse across the world. These drugs, though initially introduced for innocuous reasons such as improving efficiency by staying awake and working long hours, have high addiction potential. Their dependence, associated long-term health risks and crime place a huge burden on the healthcare systems.

While these traditional illicit drugs are strictly monitored globally, illicitly produced new compounds are difficult to predict and monitor. As of 2021, over 1150 individual NPSs were reported by 133 countries to the Early Warning Advisory (EWA) of the United Nations Office of Drugs and Crime (UNODC).[27] These are categorised into six groups based on their effect, most of which mimic traditional drugs (Figure 1-1).[27] Due to the clandestine manufacture and consumption of these compounds, little is known about their pharmacology, potency, toxicity and long-term health effects.[28]

The Council of the European Union has provided a more formal definition for NPSs that includes any ‘new narcotic or psychotropic drug, in pure form or in preparation, that is not controlled by the United Nations drug conventions, but which may pose a public health threat comparable to that posed by substance listed in these conventions’.[29] However, this

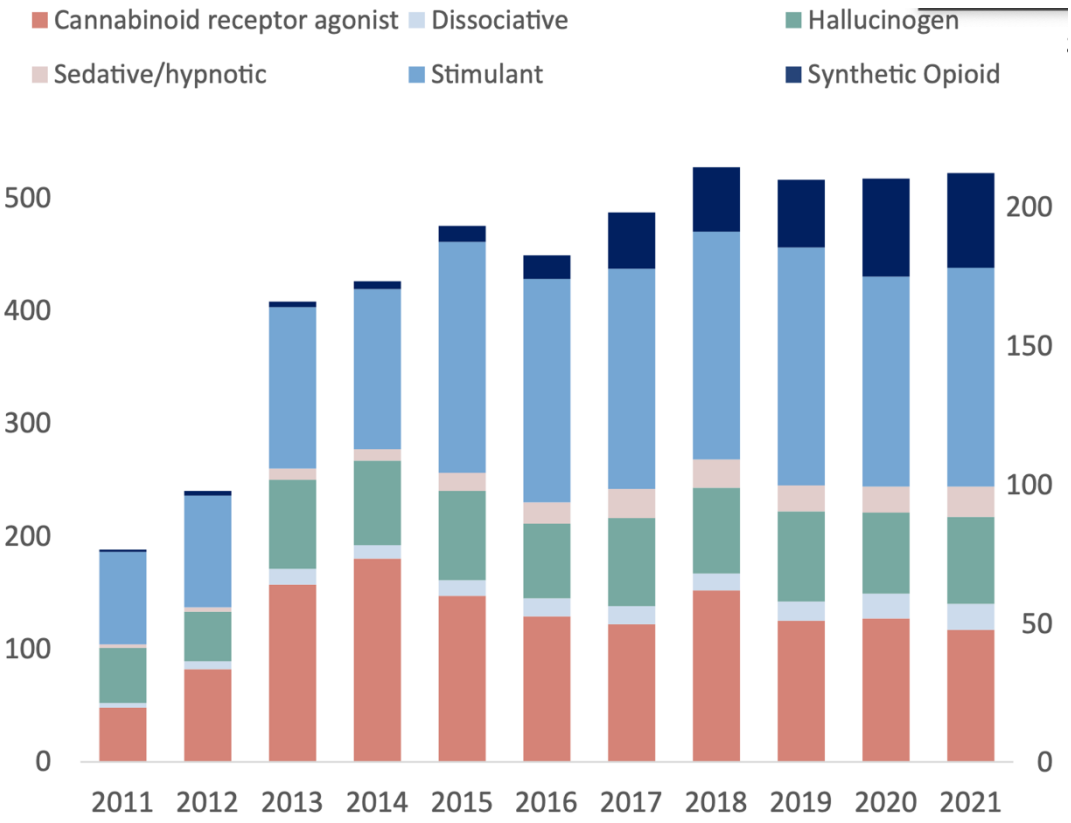

Figure 1-1: Emergence of NPS by effect group reported to the UNODC EWA 2009-2021. Figure reproduced from UNODC NPS report.[27] Stimulants are shown in blue which is one of the two biggest contributors to drugs seized worldwide.

is a legal, not medical or pharmacological definition. The initial development of these substances stems from failed pharmaceutical drug campaigns with expired patents that provide clandestine chemists with a large array of structures and synthetic routes to exploit.[30] Newer compounds however are purposely created either by making small chemical alterations to traditional drugs or with an aim to achieve the same physiological effects or the same 'high' as the traditional drugs. These are marketed as 'legal highs' or 'research chemicals' or 'substances not for human consumption', often under the guise of 'bath salts' or 'plant food' to circumvent drug and food legislation appearing not so dangerous to the consumers.[31, 32] All these terms further add to the confusion in legal, and clinical situations when multiple substances are used in blends and sold under the names of traditional drugs.[30, 33, 34]

In the UK, there were over 3284 drug-related deaths reported in 2021, out of which at least 439 were linked to the use of at least one NPS.[29] Of those monitored by EWA, there are as many as 730 NPSs that are not routinely screened for in laboratories.[35, 36] Traditional

psychoactive substances with a long history of use have clinical, pharmacological and toxicological data for reference.[37] In the case of NPSs, such information is only found anecdotally from clinical cases, poison centres and self-reported use, and is difficult to keep up to date for emerging compounds.[38, 39] Targeted NPS analysis is only carried out if the surrounding environment indicates the use of NPSs.[36, 40] Commercially available reference libraries do not always have the necessary data for constantly emerging new compounds. Moreover, the reference samples are difficult to obtain and maintain due to the immense variety and constant turnover in the drug markets. Similarly, appropriately validating methods for testing such compounds is a time-consuming process that takes longer than their lifespan in these markets. This highlights the possibility that the NPS statistics are underestimating the issue in cases of adverse reactions and fatalities. The differences in the capabilities of forensic and clinical laboratories, standard operating procedures for post-mortem toxicology investigations for suspected drug-related deaths, as well as inconsistent recording and quality of reporting systems over time and across countries further complicate quantifying the impact of NPSs.[8, 29]

Consequently, when considering patterns of drug use in the real world, the delineation between 'good' and 'bad' drugs and even 'licit' and 'illicit' drugs becomes increasingly blurred. The use of non-controlled medications in a non-prescribed way is one such example of 'grey' areas where there may be no legal precedent, but the potential for harm still exists. The use of NPSs to achieve the same effect as traditional drugs is another instance where the legislation falls short while the harm to human life continues.

On a global scale, the production, supply and use of substances which are recognised as "drugs" or "controlled substances" are regulated by various international treaties; including Single Convention on Narcotic Drugs 1961, the Convention on Psychotropic Substances 1971, and the United Nations Convention Against Illicit Traffic in Narcotic Drugs and Psychotropic Substances 1988. Additionally, the UNODC has a global reporting system where new and emerging trends in controlled substances and their prevalence across the world are identified and reported. Most of this international legislation tends to be prohibitive and punitive in nature.[41] Overall, these three conventions regulate the manufacture, use and distribution of psychotropic substances across the world, for individual as well as scientific research purposes.

In recent years, national bodies subscribing to these treaties have become more liberal in their attitude towards drug use and are seriously discussing more tolerant and pragmatic strategies for the use of controlled substances.[41] Instead of introducing a blanket ban like in Ireland or Poland, on all substances with psychoactive properties, some countries like New Zealand have chosen to interpret the international documents to make up legislations that focus on the psychoactive properties of the substances.[28,41] While these regulations are trying to remain relevant, the advances in modern chemistry, technology and communications, and scientific innovation have found more loopholes in the current legislation.[42] In particular, national legislations that control the misuse of potentially hazardous chemicals on an individual drug compound basis haven't been effective in dealing with NPSs that mimic traditional drugs.

In the UK, international conventions are translated into two main acts that control drug use; medicines are controlled by the Medicines Act while traditional recreational drugs are controlled under the Misuse of Drugs Act (MDA) 1971 and the Psychoactive Substances Act (PSA) 2016.[43, 44] The MDA 1971 restricts and prohibits the production, supply, intention to supply, possession with intent to supply, import and export, and the unlawful use of any premises for the production or supply of controlled drugs without a licence.[43] The Psychoactive Substances Act (PSA) 2016 was created to introduce a blanket ban on the production, distribution, sale and supply of psychoactive substances in the UK intended for human consumption. The primary driving force behind the PSA was the constant struggle to control misuse of the novel analogues of existing controlled substances under the MDA.[45] More importantly, the PSA defined the term 'psychoactive substance' as any substance that is either stimulating or depressing to the central nervous system (CNS) of the consumer, whereby the person's mental and emotional state is altered.[46] However, NPSs are rarely tested prior to their distribution and use, which means that their 'psychoactivity' is either unknown or not scientifically proven creating difficulties for the effective execution of such legislation.

Drug detection lies at the heart of all drug-related issues, policies and legislation. This is highlighted in the current drug policies and strategies for the future where the need for an evidence-based approach is stipulated.[8] The ever-changing 'market' of drug compounds and their popularity in recent years has demanded the application of screening tools and detection capabilities to a variety of situations.[37] While drug-induced fatalities get the most

attention in the press, they consist of only a small portion of the entire drug detection field. Routine drug detection is carried out in numerous situations including quality monitoring and assurance in pharmacovigilance studies, workplace testing,[46-48] anti-doping drug test in sporting events,[49-52] drug monitoring in the clinical setting,[37, 53-55] drug testing for driving-under-influence situations,[56-58] as well as routine forensic testing of seized materials and post-mortem samples.[59-61] These differing situations hold unique and potentially massive implications for developing efficient, inexpensive, accurate and high-throughput detection methods that can be adapted to the evolving drug market.

1.3 Methamphetamine

Amphetamine-type stimulants (ATS) which include methamphetamine (MA) are one of the six drug categories highlighted by the UNODC with a persistent prevalence of abuse and misuse globally.[1] MA was selected as the drug of choice in this study as it is the second most-consumed drug in the world with a plethora of legal, economic, pharmacological, analytical, clinical and forensic research available.[62]

Figure 1-2: Images were taken from US DEA seizures for Desoxyn and the EMCDDA report for Captagon.[63] The Desoxyn tablets on the top left are real while those in the top right are counterfeit. The Captagon tablets (bottom left) are real, which are visually different from the counterfeit versions (bottom right).

While MA can be extracted naturally from the *Ephedra* tree bark and synthesized legitimately as pharmaceutical preparations, most of the MA currently found on the drug market is illicitly manufactured either in small clandestine labs or in large-scale productions with global trafficking networks.[62] There are various pharmaceutical preparations of ATSs such as 'Captagon', 'Adderall' and 'Desoxyn', which are prescribed for attention deficit hyperactivity disorder (ADHD) and narcolepsy, respectively (Figure 1-2).[63-65] Illicit MA is produced in many forms including tablets, powders and crystals which are known by various street names including 'crank', 'crystal meth', and 'ice'.[62] The tablet form, especially those that resemble pharmaceutical preparations such as Adderall is especially dangerous in that they target non-traditional drug users and have been linked to many drug-related deaths.[62, 66] Furthermore, mixing MA with other drugs such as fentanyls has become an increasingly common practice which has caused a sharp rise in MA-related deaths.[62, 67-69]

The core of ATSs is best characterised by its simplest molecule, amphetamine, which contains all the structural elements responsible for their psychostimulant activity, this drug category also includes other structurally and functionally similar compounds such as methylenedioxy derivatives. Furthermore, synthetic cathinones such as mephedrone, 4-methylethcathinone (4-MEC) and 4-chloromethcathinone (4-CMC) are stimulants that are structurally similar to MA and form the second-largest group of NPS monitored by the UNODC.[36, 38] Any subtle differences in the structures of these compounds creates drastic changes in their pharmacodynamic activity as well as the interactions with the several target proteins altering their abuse potential and toxicity.[70] For instance, the addition of the *N*-methyl group on the side chain seen in MA increases the lipid solubility of the drug, causing rapid diffusion into the central nervous system.[71, 72] Following its uptake, methamphetamine is readily distributed to various parts of the body including the lungs, liver, brain and kidneys.[73] Therefore, the toxicity associated with methamphetamine ingestion occurs not only from the high initial dose or its chronic use but also from the accumulation in various parts of the body.[74-76] This means that the detection and identification of methamphetamine are not only important in the immediate case of drug use but also in long-term policies for chronic users.

Methamphetamine is also a drug substance that crosses socio-economic boundaries and has a long history of abuse, there is longitudinal data to show that chronic use of MA causes neurological damage that takes a long time to revert even after discontinuing the drug use.[77, 78] A lack of Naloxone-type treatment for MA and other stimulants means that it is a difficult

road to recovery requiring behavioural therapy with consistent commitment from patients.[79-81] Furthermore, the use of MA is associated with a culture of needle sharing and risky sexual behaviour where contraction of diseases such as HIV and Hepatitis B and C is likely.[82-84] This puts a further burden on the healthcare system not only in terms of treating misuse of MA but also its long-term consequences. Therefore, the need for drug detection methods for various biological fluids and more specifically, the adaptability of those methods to newer analogues of traditional drugs such as MA is persistent. The use of MA as an example target drug in this thesis is two-fold because it allows for the detection of MA and its distinction from compounds that mimic its effects on consumers. With this in mind, the following sections will briefly discuss the advantages and shortcomings of various biological fluids and detection methods used to identify drugs of abuse.

1.4 Biological Fluids

The term biofluid is used generally for any biological fluid obtained from the body, including those that are excreted such as urine or sweat; those that are secreted such as breast milk or bile; those that develop as a result of pathology such as cyst fluids; and those that can be obtained by a needle such as blood or cerebrospinal fluid. These fluids are extremely valuable in that they contain several biomolecules which have been in direct contact with internal organs throughout the human body.[85-87] These biomolecules include carbohydrates, lipids, nucleic acids and proteins that fundamentally share a structure and function relationship influenced by the environment they are produced or found in.[85-87] Consequently, these can be treated as biomarkers that can be used to not only identify and diagnose pathologies but also monitor the progression of diseases and treatments over time.[85, 88, 89]

Whole blood, serum and urine samples remain the preferred biological matrices in antemortem and post-mortem detection of drugs and other foreign substances as most administered drugs are excreted in these biofluids.[90] Furthermore, saliva, sweat and hair are also used for the detection of drugs as they can provide information on the timing of ingestion, metabolism, and chronic drug use.[91-102] While these alternative matrices are much easier to collect, the interpretation of concentrations based on their use can be problematic.

The reasons for choosing one matrix over another are situation-dependent - on their availability and ease of collection, the window of exposure represented, as well as the sensitivity and specificity of the parent drugs and their metabolites. The complex nature of

biofluids and their subsequent interactions with these compounds for example variations due to blood pH levels, diffusion rates and influence of interferents both inherent in the matrix and additives (food and body sprays) result in permutations and deviations from the normal matrix.[37, 103, 104] Furthermore, comparative literature across biological matrices for the same compounds is lacking as the limits of detection (LOD) and limits of quantification (LOQ) are significantly different in various biological fluids. Traditionally, urine samples are commonly submitted in clinical toxicology, while forensic toxicological investigations usually focus on serum samples as only blood samples are submitted for laboratory analysis.[105] In the case of NPS, interpretation of concentrations from any biofluid can be problematic as controlled preclinical studies in humans and reliable concentration data are often missing or yet to be established.[106, 107] Human serum and urine were the matrices employed in this study, as such they are discussed in more detail below.

Blood samples are difficult to collect and contain many complex proteins within them that complicate toxicological analyses.[131] Furthermore, the stability of various drugs and their metabolites in the blood can be extremely variable and is affected by the time lapse between sample collection and actual analysis, and storage/transportation of samples, requiring speedy analysis for detection.[108] Drugs that metabolise extensively can have a short detection window in blood as they are rapidly excreted in the urine. Moreover, the use of anticoagulants/preservatives in storing blood samples can interact with the analytes of interest, causing further problems during analysis. However, the main reason for using blood samples is that amount of drug detected in blood samples can be easily and properly correlated with the amount of drug consumed, thus making it a valuable matrix for drug detection.[90, 109] While some of the complex components are removed when analysing only the serum component of whole blood, most analytical techniques will require a complete sample clean-up step to only extract the exogenous compounds for analysis.

Urine is the preferred biological matrix of choice when analysing drugs of abuse because it is a compositionally simple matrix with a convenient and non-invasive collection.[91, 110, 111] Moreover, consumed drugs along with their metabolites are present in urine at much higher concentrations than in blood and are detectable for longer periods.[111-113] However, it is also a matrix that can be easily tampered with before and after collection.[109, 114] Furthermore, by the time some drugs such as synthetic cannabinoids, are excreted in the urine, the structures of their metabolites are so different from the parent drug that it is difficult to correlate

them.[113] The use of real human urine in research environments is problematic because urine composition is dependent on gender, age, race, food intake, exercise and the presence of medications.[115-117] In addition, urine composition significantly changes throughout the day even for the same individual and presents challenges for collection and storage.[116] The use of real urine samples also comes with the risk of exposure to pathogens during collection and handling.

The biological fluids mentioned above can also be collected in post-mortem situations along with liver, lung, kidney, spleen, muscle, brain, heart and bile tissue samples for the detection of foreign substances.[101, 118] In toxicology samples, the issue of characterising the composition and concentrations of a drug and its metabolites are complicated by the effects of decomposition, post-mortem redistribution and lack of appropriate reference standards in those matrices. It is commonly known that considering the time after death, factors such as body positioning can redistribute fluids in the body.[119] This redistribution of blood into and out of organs can convolute the amounts of any foreign substances present. Redistribution is demonstrated in heart muscle and lung tissue areas for methamphetamine, and it is fairly constant in peripheral blood resulting in it being the best sample for analysis.[120] Similarly, this can apply to amphetamine as it is just as readily absorbed and distributed across the body antemortem.[121] However, specific studies for many NPSs are lacking and can have implications for the interpretation of results.

1.5 Drug Detection Methods

Typically, drug detection is carried out as a two-step process, whether it is on suspicious samples or confiscated cargo, or to detect drug consumption in a person. Initial screening is carried out using presumptive tests to establish the presence of drugs and potentially identify the class of drugs. In the case of seized samples, these are mainly colour spot tests carried out in the field. For detecting drug consumption, for example at a roadside, or at a workplace, a screening test is generally carried out using biological fluids, preferably non-invasive biofluids such as oral fluid, urine and sweat. These tests are aimed at maximising the diagnostic throughput in order to identify all the presumptive positives in the sample. Following this, a confirmatory analysis is carried out on a sample, powder or blood/urine sample, at a centralised laboratory to accurately confirm the presence of drugs, and identify the chemical compound and its concentration.[56, 122] These are focused on maximising the specificity, i.e. correctly identifying drugs present in all the positive presumptives.

The identification process will typically consist of a sequence of techniques that are most efficient and cost-effective to provide reliable and accurate results. The Scientific Working Group for the Analysis of Seized Drugs (SWGDRUG) along with UNODC has provided guidelines for building an analytical scheme utilising various combinations of methods that can be used to obtain results that are legally sound.[123-126] The methods are grouped into three categories, A, B and C, and arranged in a hierarchy of increasing selectivity (Figure 1-3).[126] However, it is prudent to note that this list is not all-inclusive, nor is there only one correct analytical technique/scheme. While the choice of methods is ultimately a balance between the information required, cost-effectiveness, analysis time, and the situation where drug analysis is needed, it is possible to compile a list of desired features that might be used to evaluate novel methods for their application to drug detection. These include portability and

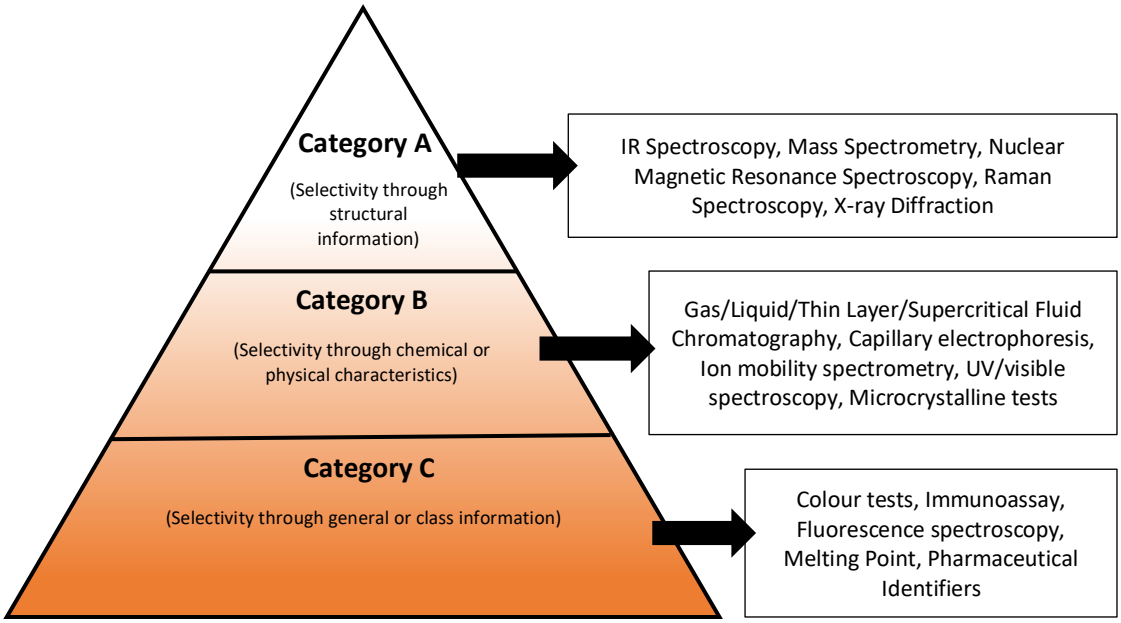

Figure 1-3: Schematic showing the categories of various analytical techniques employed in the analysis of seized drug samples. The image is adapted from SWGDRUG documentation.

short response time to allow rapid analysis to allow in-field analysis, high specificity in order to avoid social, legal and economic ramifications, multidrug detection ability in complex matrices, high accuracy and reproducibility of results to withstand rigorous method validation, user-friendly, low-cost and environmentally friendly operation, ease of data interpretation and finally the ability to transmit data securely to authorities.[90] With this in mind, the following section will briefly discuss the techniques and methods used in presumptive, on-site screening and those employed in the lab for confirmatory drug testing.

1.5.1 Presumptive Tests

1.5.1.1 Colour Tests

According to the International Collaborative Exercise carried out by the UNODC involving 310 laboratories from 86 countries in 2020-2021, colourimetric (spot) tests are one of the most commonly employed screening tests for analysis of seized materials.[127] In these tests, chemical reagents are added to a small sample of seized materials where a colour change in specific reagents is indicative of a specific drug class present in the sample.[37, 128-130] Colour tests are usually employed in a predetermined sequence to ascertain the type of drug class while using a minimum number of tests. These tests are rapid, portable, low cost and require no sample preparation which accounts for their prevalence in the field as well as in the laboratory.[37, 130] While these are classed as having the least discriminating power, they are widely employed in the field for ruling out samples containing no drugs due to their operational simplicity and lack of training as a low-cost way of analysing a large number of samples.

The most commonly used reagents of ATS detection are Marquis reagent (a mixture of formaldehyde and concentrated sulfuric acid), Mandelin reagent (a mixture of ammonium vanadate in sulfuric acid) and Simon's reagent (a mixture of sodium nitroprusside, sodium carbonate and acetaldehyde). Marques and Mandelin reagents are broad-spectrum reagents that react with multiple classes of drugs including anti-depressants and opiates, while Simon's reagent is used to detect secondary amines such as MA and MDMA. Samples containing MA produce dark yellowish green and deep reddish orange-dark reddish brown colours when analysed with Marques and Mandelin reagents respectively.[130, 131] Simon's reagent on the other hand is a functional group selective reagent for secondary amines producing a blue-coloured product.[130]

O'Neal and colleagues carried out a detailed validation of twelve such colour tests to report a sensitivity of 10-100 μg for amphetamines for the three aforementioned reagents. However, this study highlighted that these tests are not always specific to a particular drug or drug class as false positives were recorded for innocuous compounds such as aspirin, salt, sugar and mace.[131] Murray *et al*. showed that a combination of multiple reagents was insufficient to correctly identify pure MDMA tablets from those adulterated with MA, where the combined sensitivity, specificity, positive predictive value and negative predictive value were 58%, 50%, 28% and 77%, respectively.[132] While this study was comprehensive enough

in terms of including novice and expert analysts for performing and interpreting the tests, it still relied on the analyst's perception of colour.

As of July 2022, 204 unique synthetic cathinones have been reported to the UNODC EWA by 86 countries across the world.[133] This group of structurally similar compounds is usually consumed to achieve the same physiological effect as MA and does not have an appropriate specific colour test. Recent guidance published by UNODC has suggested the use of Zimmerman's reagent that produced immediate colour change for 13 out of 16 cathinone compounds that were tested.[134] However, an earlier study of 11 cathinones by Toole and colleagues showed that Marques reagent was able to identify methylenedioxy substituents while methcathinone-type compounds were better identified by Liebermann's reagent.[135] Another more extensive study by Philp *et al.*[136] utilised a Cu(II)-neocuproine reagent to test for 120 substances including cathinones and other substances regularly used as cutting agents. While an extensive range of compounds was included in this study, the majority of compounds produced the same resultant colour including some commonly used cutting agents such as paracetamol.[136] Furthermore, this test required heating samples at 80 ^{o}C for 10 mins, reducing its applicability in the field.

One of the main issues highlighted in these studies is the precise characterisation of colour as it is subjective to the operator's perception. In the case of NPS commonly cut with other chemicals, this issue is exacerbated as these could also react with the reagents producing a different overall colour for the combination of reactions by the drug mixture.[129] The use of a digital camera or a smartphone followed by analysis using an image processing software such as Adobe Photoshop, an image processing toolbox in Matlab or applications such as ColorAssist is a common solution proposed in the literature for more accurate and reliable characterisation of colour.[128, 137-141] Another solution was the use of a UV-Vis spectrometer to record the absorbance spectra for the coloured products during the detection of amphetamines.[136, 142]

In spite of the above advances in objective quantification of colour, the inherent issue of the lack of specificity of the colour tests still remains. In a recent street control incident run by the police in North-East Italy, approximately 3 kg of white powder and blue heart-shaped tablets were identified as ATS by both Marques and Mandelin reagents.[143] However, upon confirmatory analysis by GC-MS, it was determined that they contained anabolic steroids

with no amphetamine-type substances present.[143] As the mechanisms of many colour tests are not fully understood, their applicability to the ever-increasing number of new compounds needs to be tested for every individual drug. This is an enormous and cumbersome task which increases exponentially when drug mixtures are taken into account.

In addition, the colour tests not only analyse extremely potent substances but also contain hazardous chemicals which pose safety risks for those conducting these tests in the field. While some of these safety concerns are mitigated with the use of commercially available drug testing kits, the lack of knowledge/training and adequate quality assurance can have potentially disastrous consequences.[132, 144, 145] For some reagents such as Scott's reagent, the sensitivity of the test is dependent on ambient temperature, making them unsuitable in hotter climates.[146] In addition, the long-term stability and storage of these kits also need to be considered as most reagents mentioned above need fresh preparation and refrigeration before analysis.[146]

1.5.1.2 Immunoassays

While colour spot tests are the first screening test for seized powder samples, immunoassays are the primary on-site screening methods used for biological specimens.[127, 147] Immunoassays (IAs) are widely employed in clinical and toxicological screening as they are quick, cheap and relatively accurate in ruling out negative samples.[148] IAs rely on the bonding of antigens (molecules of interest) and specially patterned antibodies. Numerous commercial IA kits exist that allow for the detection of a single class of drugs or a panel of drug classes that can be either predetermined or a customised set.[149-153] However, one of the recurring issues with IAs is the cross-reactivity observed between structurally similar compounds. Because AM and MA are very simple molecules, developing very specific antibodies for these molecules is difficult. In addition, other structurally similar compounds such as ephedrine – one of its precursors as well as 3,3-methylenedioxymethamphetamine – an illicit street stimulant, show some cross-reactivities across commercial immunoassay kits.

Dasgupta *et al.* and Hsu *et al.* demonstrated this by evaluating the efficacy of amphetamine IA kits. Both EMIT® d.a.u and EMIT® II monoclonal AM/MA assay gave positive results for 18 samples, which were determined to contain no AM or MA by further GC-MS analysis in the Dasgupta study.[151] In addition, the authors found that the GC-MS analysis of samples showed the presence of ephedrine, pseudoephedrine, phentermine and phenylpropanolamine

highlighting their cross-reactivity for these compounds.[151] Hsu and colleagues expanded such analysis to include 8 IA kits. The authors indicated that the cross-reactivities across these four compounds are lower when their concentrations are higher, Synchron CX® and TDx®-Amp kits which are specifically designed for AM/MA showed ≧50% cross-reactivity to MDMA and MDA, and EMIT-Amp showed higher cross-reactivity to MDA but was not effective in the detection of MDMA at lower than 500 ng/mL concentration.[152]

The compounds mentioned in the above studies, MDMA and MDA, have been on the drug market for a long time, therefore it is possible to predict and evaluate the ability of commercial immunoassays for their detection. However, novel stimulants have a diverse range of structures making it challenging to not only create new specific immunoassays but also to predict the suitability of current kits for their detection.[154] To this effect, a study by Petrie and colleagues evaluated the suitability of three commercial amphetamine screening kits for the detection of 42 amphetamine-type substances which included numerous NPS drug classes.[155] The authors focused on the amine functionality of these kits by including NPS classes such as 2,5-dimethoxyphenethylamines (2C), piperazines, β-keto amphetamines, 2,5-dimethoxyamphetamines and 4-substituted amphetamines to show that only 14 out of 42 compounds showed cross-reactivity for all three kits. Another extensive study by Regester *et al.* evaluated the performance of five commercial IA screening kits for the detection of 92 designer drugs of classes including 2,5-dimethoxyamphetamines, 2C series, tryptamines, α-pyrrolidinopropiophenones, β-keto amphetamines, piperazines, substituted amphetamines and phencyclidine analogues.[148] Of the 94 compounds included in this study, 80 of them tested positive on at least one of the kits, while none of the NPS tested in this study showed positive results for all the kits.[148] While this study was extensive in its list of included compounds, the Petrie *et al.* study provided valuable 2D and 3D structural similarity data used to predict the cross-reactivities of 261 additional compounds.[155] Of these 261 compounds which included amphetamine-like substances as well as metabolites, only 4 were predicted to cross-react with all three immunoassay kits included in this study. Interestingly, mephedrone, a very popular illicit drug on the current drug market, showed no cross-reactivity to any of the kits in the Petrie *et al.* study and only reacted to one of the amphetamine screening kits in the Regester *et al.* study. Furthermore, neither study considered the effects of adulterants, cutting agents and other diluents commonly found with designer drugs. Therefore, while immunoassays have certain advantages, they can not be relied upon for the detection of all amphetamine-type compounds found worldwide.

Instead of relying on the immunoassay results alone, Tupper *et al.* employed the use of Fourier transform infrared (FTIR) spectroscopy to investigate the adulteration of fentanyl in Canada. In light of the massive opioid crisis in North America, this combined approach was applied as a means of harm reduction whereby samples of illicit substances are checked and individualised feedback is provided to the users.[156] During this six-month pilot study, the authors found that 907 of 1714 tested samples were expected to be "heroin" by the clients while only 160 samples actually contained any diacetylmorphine or 6-monoacetylmorphine.[156] Interestingly, 822 of the supposed "heroin" samples tested positive for the fentanyl immunoassay kit, and the FTIR results did not show the presence of diacetylmorphine or 6-monoacetylmorphine. Furthermore, FTIR results were able to identify adulterants such as caffeine, mannitol, xylitol or sorbitol which were not detected by the fentanyl immunoassays.[156] The authors also reported that of the 256 samples that were sold as amphetamines or methamphetamine, 15 samples tested positive for fentanyl. Other unexpected compounds found instead of the drug compounds included pumice stone, feldspar dust, plaster, oxazepam (a benzodiazepine sedative), and N-ethylbyphedrone (a synthetic cathinone).[156] At the end of the study, the authors concluded that the combined use of immunoassay and FTIR spectroscopy was reported to be valuable by the clients and showed much greater utilisation at the clinic. Though only powder samples were tested in this study and more expensive laboratory-based confirmatory techniques were not available due to resource constraints, this study illustrated the efficacy of FTIR spectroscopy as a cheap, reliable, portable and non-destructive screening technique in a point-of-care setting.

1.5.2 Techniques Coupled to Mass Spectrometry

Hyphenated separation methods such as gas chromatography-mass spectrometry (GC-MS) and liquid chromatography-(tandem) mass spectrometry (LC-MS/MS) are the gold standard for final confirmatory drug testing in forensic and clinical toxicology.[125-127] The analytes firstly are separated chromatographically based on their retention times following which the compounds are identified based on their characteristic fragmentation patterns. In forensic drug analyses of powders and biofluids, these techniques can be used to screen for unknown compounds in an untargeted manner or they can be used in a targeted approach to identify commonly encountered drugs of abuse with high sensitivity.[105, 157-170] For many years, GC-MS has been the standard for drug screening and it still remains one of the most commonly used methods for screening urine samples.[105] However, some highly polar, non-volatile and thermally unstable substances are better suited to be analysed by LC-MS/MS methods.

Therefore, the screening strategies for drug analyses consist of a combination of these two techniques. For biofluid analysis, sample preparation steps such as dilution, extraction using solid-phase or liquid-liquid extraction (SPE and LLE) methods, derivatisation (in the case of GC-MS) and reconstitution into an appropriate solvent are of paramount importance for the recovery of analytes and increasing the sensitivity of the method.[171-173] The subsequent MS data analysis is carried out by trained experts for compound identification either by using molecular formula-based on multiple reaction monitoring (MRM) transitions and their ratios and/or by matching the product ion spectra with reference spectra from an information-rich library. However, spectra matching using reference libraries remains the preferred method for unambiguous identification and is in association with the recent guidelines published by the EU.[172, 174]

Alsenedi and Morrison carried out long-term stability studies in urine samples and demonstrated the use of GC-MS combined with the SPE method for the detection of 29 stimulants including MA, AM and synthetic cathinones.[160] A similar study by Mercieca and colleagues demonstrated the use of GC-MS for the detection of 25 stimulants in blood and urine.[159] With the full-scan mode acquisition, and a total analysis time of ~22 mins, Mercieca *et al.* demonstrated a relatively high-throughput method for the separation and identification of compounds as well as its application to real-case samples to detect stimulants in whole blood. Furthermore, the use of DLLME in comparison to SPE was found to be more environmentally friendly and cost-effective due to the use of low volumes of solvents. However, both studies focused on a single class of drugs which limits their application to broad-spectrum screening of unknown samples in the era of poly-drug use.

Odoardi and colleagues expanded the application of the DLLME extraction procedure combined with ultra high-performance LC-MS/MS to identify 70 NPS from several classes in whole blood with sample preparation times of 15 mins, analytical run times of ~14 mins and detection limits within 0.2 - 2 ng/mL ranges with acceptable recoveries and negligible matrix.[170] Mollerup *et al.* proposed a combined targeted and untargeted screening approach using high-resolution MS instrumentation to authentic driving-under-the-influence-of-drugs (DUID) whole blood samples with simple acetonitrile-based protein precipitation as a sample preparation step.[167] Both these studies incorporated necessary aspects of drug detection such as the inclusion of metabolites and low detection limits, their approaches were complex

requiring expert analysis and interpretation making their application outwith a fully equipped laboratory with expensive instrumentation and trained personnel difficult.

The ambient ionisation techniques such as DESI (desorption electrospray ionisation) and DART (direct analysis in real-time) combined with miniature MS instruments allow the analysis of samples with minimal sample preparation, no chromatographic separation and often total analysis times of under 1 min in non-laboratory settings e.g. police stations, doctors' surgeries and prisons.[175-179] McCullough and colleagues demonstrated portable MS for the analysis of solid samples from 50 UK drug seizures, 49 of which were correctly identified using the NIST MS database.[175] Similarly, Gomez-Rios *et al.* and Schepens *et al.* illustrated the applicability of ambient ionisation combined with portable MS to the analysis of drugs of abuse in liquid matrices such as orange juice, lemon tea and oral fluid.[176, 179] Damon and colleagues expanded this further to include more complex biofluids such as whole blood, serum and urine for the analysis of drugs of abuse by using specially prepared hydrophobic paper with handheld MS instrumentation.[180] While all these studies were able to reach accepted limits of detection, and perform quick analysis with minimal sample preparation, numerous problems were identified that included missed identification due to an incomplete reference library for the McCullough *et al.* study,[175] an increase in noise levels and a lack of specificity due to the use of a single quadrupole in the Gomez-Rios *et al.*[176] and Schepens *et al.*[179] studies as well as the extensive time required for preparation of paper substrates along with the dependence of detection limits on the drug-protein binding capacities in the Damon *et al.*[180] study. Furthermore, the elimination of chromatography shifts the separation burden onto the MS which could be problematic for structurally similar drug compounds.[181, 182] Therefore, it is prudent to note that while ambient ionisation MS methods have a bright future in drug screening in the field by decentralising drug analysis, currently they can only be classed as "category B" methods according to SWGDRUG guidelines.[175]

Though the traditional GC-MS and LC-MS/MS methods are highly sensitive and specific, they require extensive sample pre-treatment, availability of reference standards, expensive instrumentation, constant maintenance and expert operators for analysis and interpretation limiting their use in the field. Though the propensity of complex biofluids to matrix effects can be reduced with specific sample pretreatment procedures and matrix-matched method validation, this is a time-consuming process that could fail to catch new compounds and

might exceed the lifespan of some NPS.[37, 172, 183] Consequently, when NPSs are encountered in routine testing, they may be lost in the extraction process or go unnoticed during instrumental analysis due to a lack of information surrounding the NPS structure, knowledge of their metabolites and time required to produce reference standards for the parent drug and the metabolites. While some of these issues such as the removal of chromatography are solved by ambient ionisation portable MS instrumentation, those methods come with their own set of problems highlighted previously. All MS methods rely on extensive reference libraries which are necessary for untargeted drug screenings, the major drawback of transferability of MS libraries across instruments and laboratories still remains to be resolved.[172] Therefore, the search for direct, rapid, cost-effective, and portable drug detection methods remains ongoing for the analysis of traditional drugs and NPSs in biological fluids both in the field as well as in a forensic laboratory setting.

1.5.3 Alternative Detection Methods

1.5.3.1 Electrochemical Methods

Other than the primary methods of detection reviewed in the previous sections, electrochemical sensors are a promising tool employed for the detection of illicit substances in the field of drug analysis and forensic toxicology. The electrochemical techniques are mainly divided into voltammetry where the desired potential is applied to measure the current output from the oxidation-reduction of an electroactive compound and potentiometry where a difference in voltage between the working electrode and reference electrode is measured. The main advantages of these techniques include their simplicity in setup and sample preparation, short analysis times, good performance in a variety of matrices and very good analytical capabilities in terms of LODs and concentration ranges.[90, 184] With the advent of screen-printed electrodes, these sensors have not only dramatically reduced in cost, but are also readily customised with the inclusion of nanoparticles, antibodies and receptors allowing them to increase selectivity toward target analytes.

Balbino *et al.*[185] and Frietas *et al*.[186] reported the use of modified platinum screen-printed electrodes and unmodified boron-doped diamond electrodes for the analysis of drugs and any adulterants present with detection limits of 0.028 µM and 0.89 µM respectively. While the detection limits of 0.028 µM were lower than conventional systems, Frietas *et al.*[186] were able to detect a range of adulterants and provide results comparable with GC with a flame ionisation detector (FID). Unlike these studies that are analyte-specific, Van Echelpoel and

colleagues developed an electrochemical sensor for MDMA in seized tablets and evaluated its selectivity against 72 compounds including common drugs of abuse, licit pharmaceuticals, NPS and adulterants.[187] Unlike the colour tests and spectroscopic techniques such as near-infrared and Raman that are affected by the colour of tablets and the presence of other substances, the electrochemical sensor was able to identify all 39 MDMA tablets correctly.[187] While all of these studies showed excellent selectivity to the target analytes, portability and a means of rapid and reliable analysis, none of the studies are suitable for general drug screening and did not evaluate the efficacy of this method in the analysis of biological fluids.

More recently, these methods were expanded to allow for the detection of drugs of abuse such as MA[188] and MDMA[189, 190] as well as NPS[191] such as synthetic cathinones in biological fluids such as human urine and serum. Garrido *et al.* used glassy carbon electrodes for the detection of MDMA and achieved detection limits of 2.4 μM in human serum.[190] Švorc and colleagues conducted voltammetric measurements with boron-doped diamond electrodes to detect MA in human urine with a detection limit of 0.05 μM.[188] Another study by Razavipanah *et al.*[191] reported a spiked study for the detection of mephedrone in plasma and urine samples with detection limits of 3 nM and no interferences from the complex biological matrices highlighting the ability of this sensor in future forensic applications.[191] While all these studies showed excellent promise in targeted analyses, the authors did not evaluate their performance for other similar compounds, illicit drugs or adulterants. As street drugs frequently tend to be mixed with other compounds, the application of these methods to samples of unknown composition is limited. Furthermore, voltammetric analysis of biological matrices is rife with biofouling processes whereby components in biofluids such as proteins adhere to the sensors eventually leading to foreign responses.[90]

1.5.3.2 Spectroscopic Techniques

Spectroscopic techniques mainly FTIR and Raman are other types of detection methods employed in the forensic analysis of drugs. Raman spectroscopy is based on the inelastic (Raman) scattering of photons which results in the photons having lower (Stokes) or higher (anti-Stokes) energies than the excitation source. This difference in energy between the excitation source and the scattered photons provides the vibrational fingerprint for the sample. IR spectroscopy on the other hand is based on the measurement of the amount of IR radiation absorbed or emitted by a sample as a function of wavelength (for a detailed

explanation see Chapter 2). Both methods, therefore, are highly structurally selective and are included in category A of the SWGDRUG scheme (Figure 1-3).

Both techniques are non-destructive, fast and allow for analysis of most sample types.[3, 192, 193] One distinct advantage of spectroscopic techniques over the chromatographic techniques described earlier is that analysis can be done directly, without the need for any sample pretreatment or extraction. Notwithstanding initial purchase costs, this allows for minimising costs and reagent used per sample for a high throughput analysis and makes these techniques green and sustainable in the long term. Furthermore, the miniaturisation of the spectrometers in the form of handheld devices has increased their portability allowing for on-site analysis in the field. This, paired with chemometrics and a searchable library of reference spectra, these instruments provide a powerful analytical methodology.

In 2016, Moreira *et al.*[194] demonstrated the use of Raman spectroscopy combined with chemometrics in the direct analysis of ecstasy tablets seized by the police in Brazil. Each tablet was scanned as is to identify the presence of caffeine, clobezorex, dextromethorphan and β-keto MDMA analogue along with some excipients such as titanium dioxide and starch and the absence of MDMA using FT-Raman spectral band assignments.[194] Calvo-Calvo-Castro *et al*.[195] demonstrated that a combination of Raman spectroscopy with chemometric models has the potential to be applied to 'unknown' NPS that continue to pop up on the drug markets and are likely to be absent from spectral libraries. The authors used hierarchical clustering to categorise 478 NPS compounds into 21 categories based on their common structural core, which were then further divided into 79 subcategories. The PCA model was able to classify MA from the test set with N-ethylamphetamine due to their structural similarities reflected in their similar Raman profiles and also align βk-2C-B with category 2 representing the phenethylamine backbone and more specifically with 4-MeO-α-PVP within category 2 as they both contain carbonyl functionality characteristic of the cathinone drug class.[195] While the authors presented excellent results from the classification analysis of these pure compounds, the effects of adulterants, precursors and cutting agents commonly present in NPS samples were not investigated. Furthermore, the study was conducted in solid/powder form which meant that the predictive capabilities of this model on other sample types such as tablets with heterogeneous compositions and drugs in biofluids were not evaluated. On the whole, however, this study showed tremendous promise in addressing

the large structural diversity in NPS that commonly plagues most analytical techniques but it also presented a valuable approach for future

The use of surface-enhanced Raman spectroscopy (SERS) has greatly enhanced the sensitivity of Raman spectroscopy.[196-198] Nuntawong *et al.*[197] demonstrated that specially prepared SERS chips with self-assembled, vertically aligned silver nanorods can be employed for the detection of a series of mixtures of MA and its primary metabolite AM in urine samples with a detection limit of 50 µg/mL which was then lowered to 5 pg/mL by pre-treating the urine samples with nitric acid.[197] A similar study by Yang *et al.*[198] used gold nanoparticles dotted magnetic nanocomposite modified with inositol hexakisphosphate as SERS substrate for the detection of benzoylecgonine (a metabolite of cocaine) and cotinine (a metabolite of nicotine) in saliva with LODs of 29 ppb and 8.8 ppb respectively, as well as nicotine (plus its metabolites) in eccrine sweat in latent fingerprints with LODs of 17.6 ng/mL.[198] Muhamodali *et al.*[199] expanded the application of the SERS protocol combined with chemometrics for the discrimination of four classes of NPS including methcathinones, aminoindanes, diphenidines and synthetic cannabinoids. Although the PCA model created for solid and aqueous samples showed good discrimination between the four classes, some overlap was seen across methcathinone and aminoindane classes due to their structural similarities.[199] The LODs reported here (between 2 mM and 51 mM) were much higher than those achieved in the previously mentioned Nuntawong *et al.*[197] study and those achieved using mass spectrometric methods, Muhamadali *et al.*[199] were able to obtain them without any sample pretreatment demonstrating its potential applicability as a portable on-site method.

However, all these studies required tedious preparation processes for the modification of SERS substrates, required expert interpretation for manual identifications, only focused on a single drug compound at a time and did not investigate the presence of interfering compounds as is common in polydrug use. The higher detection limits meant that the application of this method for the detection of more potent compounds such as fentanyls might be limited until further sensitivity improvements can be made. The application of these protocols to NPS or as yet unknown compounds remains problematic because the pharmacokinetic data required in interpreting urinary and oral fluid concentrations based on the dosage is still lacking or anecdotal at best.

FTIR spectroscopy has been applied to direct analysis of counterfeit medicines, drugs of abuse and NPSs in powder form as well as in the analysis of biofluids for disease diagnosis and drug detection making it a powerful analytical tool when combined with chemometrics.[3, 200-202] Custers and colleagues reported an application of attenuated total reflection (ATR)-FTIR spectroscopy combined with chemometrics for the analysis of 209 samples that included genuine Viagra® and Cialis®, generic products of Viagra® and counterfeit samples containing sildenafil, tadalafil or both or placebo samples.[3] Similarly the studies conducted within the same research group by Pereira *et al.*[203, 204] demonstrated that the combination of ATR-FTIR spectroscopy with PLS-DA can be used to analyse illicit MDMA tablets as well as a complex matrix represented here by the blotter paper samples containing NPS from the NBOMe series. These models were able to correctly classify all but one MDMA sample as well discriminate between the various hallucinogens categorised as the NBOMe series, 2C-H series and methallylescaline (MAL) and blank paper with the exception of those samples containing lysergic acid (LSD) which were misclassified as blank paper. Though these studies reported promising results, samples containing more than one illicit drug were not included in the analysis. Low sensitivity common to IR instruments was evident in these studies and spectral identification was performed by library matching limiting its use to unknown samples where an extensive dataset is not available. However, an approach previously described by Calvo-Castro *et al.*[195] applied here with FTIR spectral data might provide a way to overcome this problem.

All major biomolecular groups such as carbohydrates, lipids, nucleic acids and proteins, display fundamental vibrational absorptions in the mid-IR region. Upon detection, the differences in their concentrations observed in the IR spectrum can provide valuable information for disease diagnosis and clinical analysis. The deficiency of phospholipids has been used as a depression marker,[205, 206] changes in specific proteins like immunoglobulin G and human serum albumin can indicate inflammation and infection,[207] and variations in the nucleic acids have recently been linked to the early detection of cancer.[85, 208] In addition, biofluids such as blood, urine, saliva and sweat are also analysed to detect foreign substances including drugs and their metabolites.[169, 209-212] In cases of chronic and long-term drug use, it is also likely that drugs accumulate in the tissue and can potentially be observed in IR spectra.

ATR-FTIR spectroscopic studies for the analysis of drugs have mainly focused on oral fluid as the biological matrix of choice for the direct detection of cocaine and MDMA.[213-217] Mostly

carried out within the same research group, the first study by Hans *et al.*[213] explored the IR spectra of cocaine in water and oral fluid as well as common interferents such as diluents, masking agents, common medications and soft drinks with an aim of building an easy-to-use test device (Figure 1-4). Using the spectral region of 1800-1710 cm^{-1}, real saliva samples spiked with cocaine were analysed to achieve a LOD of 0.02 mg/mL which remained unaffected in the presence of interferents such as mouthwash, alcohol and caffeine/energy drinks.[213] Although the authors acknowledged the issues arising from inconsistent drying of saliva samples on the ATR crystal and insufficient sensitivity in their methodology, this study presented a promising first step towards drug detection in biofluids using ATR-FTIR spectroscopy.

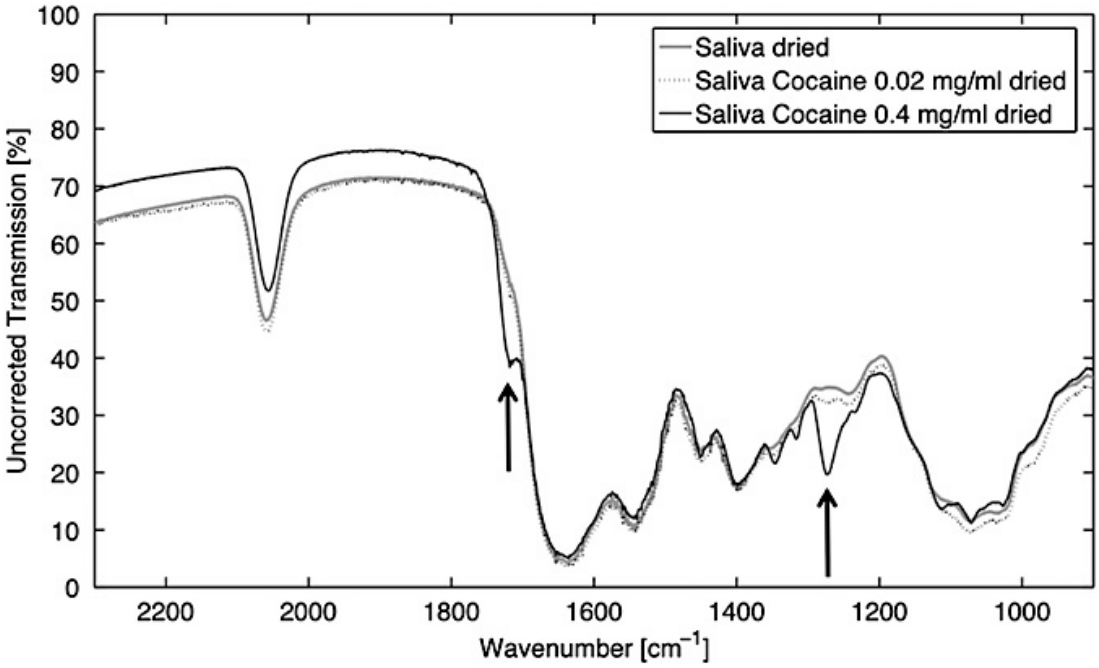

Figure 1-4: Uncorrected transmission spectra of pure dried saliva from a fasting person and saliva spiked with cocaine. The graphs show the transmission spectrum of dried saliva (grey), of dried saliva with cocaine (0.02 mg/mL; black dotted) and of dried saliva spiked with cocaine (0.4 mg/ml; black solid). The characteristic change in transmission of the cocaine is now clearly visible (indicated by the arrows). The resolution of the FTIR spectrometer was 1 cm^{-1}. Reproduced from ref. 217 with permission from Hans, Müller and Sigrist, © 2012 John Wiley & Sons, Inc.

Subsequent works from this research group have focused on improving the sensitivity of the method, firstly by developing a simple-one-step extraction protocol for isolating cocaine from the oral fluid into an IR-transparent solvent, tetrachloroethylene (TCE)[214] and secondly by using quantum cascade lasers at ~1750 cm^{-1} (where least absorption interference was

observed for cocaine) following the extraction process.[216] This process consisted of mixing TCE solvent with the saliva sample without the need for bulky or expensive instrumentation. The use of a QCL unit combined with either ATR crystal or transmission cell was employed to analyse these TCE-extracted, cocaine-spiked saliva samples which achieved detection limits of 3 µg/mL and ~10 µg/mL respectively.[215] Acknowledging the semi-quantitative nature of ATR crystal use due to variable sample drying, the later study by Hans *et al.*[216] applied this protocol to saliva samples spiked with street cocaine to achieve detection limits of ~1 µg/mL (Figure 1-5). Further reduction in detection limit to ~100 ng/mL was achieved by preconcentrating cocaine during the extraction process. However, the adulterants in street cocaine visible in TCE-dissolved samples were not visible in the spiked saliva samples that were analysed using the same process.[216]

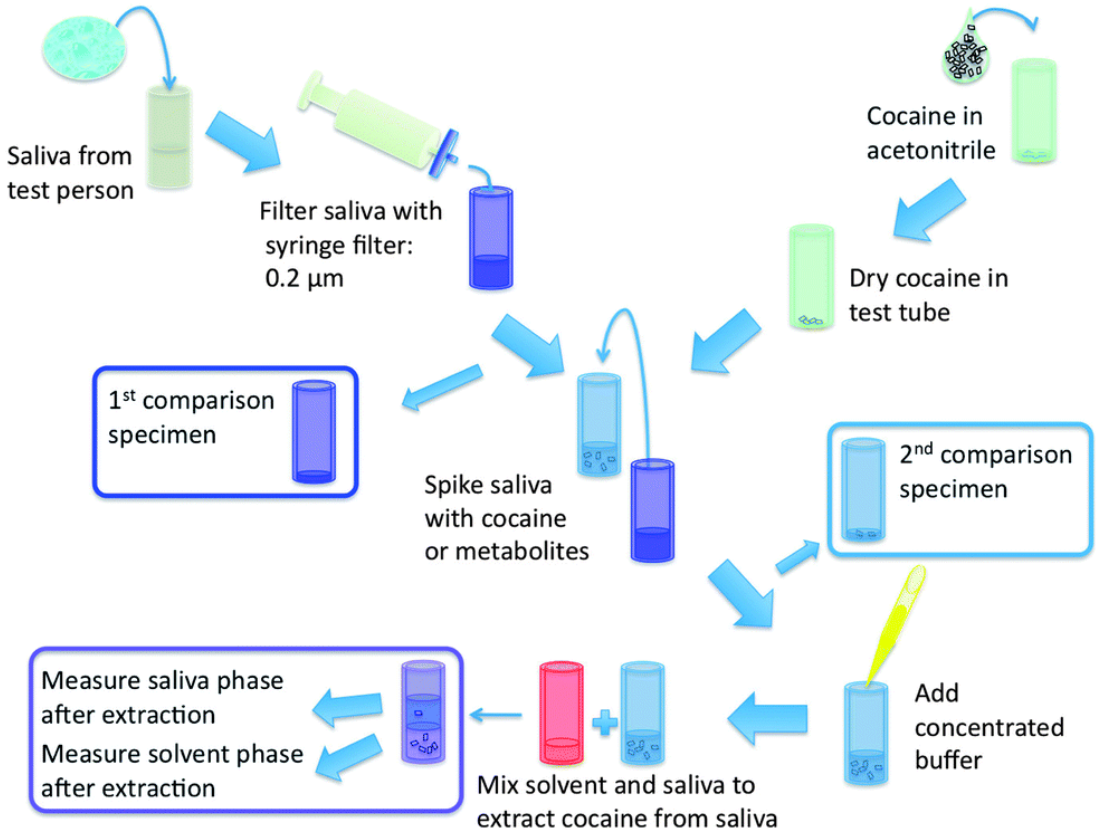

Figure 1-5: Preparation and extraction of a saliva sample: after the acquisition the saliva is filtered. One part of the saliva is kept for the first comparison measurements. The other part is mixed with cocaine dried beforehand in a test tube. This sample is again split into the second comparison specimen and the sample that will be extracted. The mixing of the solvent and saliva is done manually after the stabilization of the pH. The separation of the two liquids is a self-organised process. Reproduced from ref. 220 with permission from Hans, Müller, Petrosyan and Sigrist, © 2014 John Wiley & Sons, Inc.

Hans *et al.* emphasised that the best results were achieved when saliva samples were extracted immediately after collection and preparation as their previous studies noted spectral changes in the saliva samples from varying storage conditions.[213, 214] While these successive studies demonstrated the power of ATR-FTIR spectroscopy for drug detection in biofluids, its application to other drugs remains to be evaluated. While some spectral processing was performed, none of the studies employed chemometrics when its usefulness in spectroscopic studies is well-known. Moreover, the suitability of the extraction solvent, TCE, needs to be investigated for a range of compounds and in a variety of biofluids. TCE is environmentally dangerous and is classed as a carcinogen and a CNS depressant that enters the body through respiratory and dermal exposure, therefore the risk associated with the widespread application of the proposed methodology in the field with unprotected personnel has to be carefully considered. Furthermore, in the case of NPS, pharmacokinetics and toxicology data are not available for interpretation of initial doses based on oral fluid concentrations which limits the application of this method. In spite of these limitations, this protocol shows promise in developing a rapid field testing device based on ATR-FTIR spectroscopy.

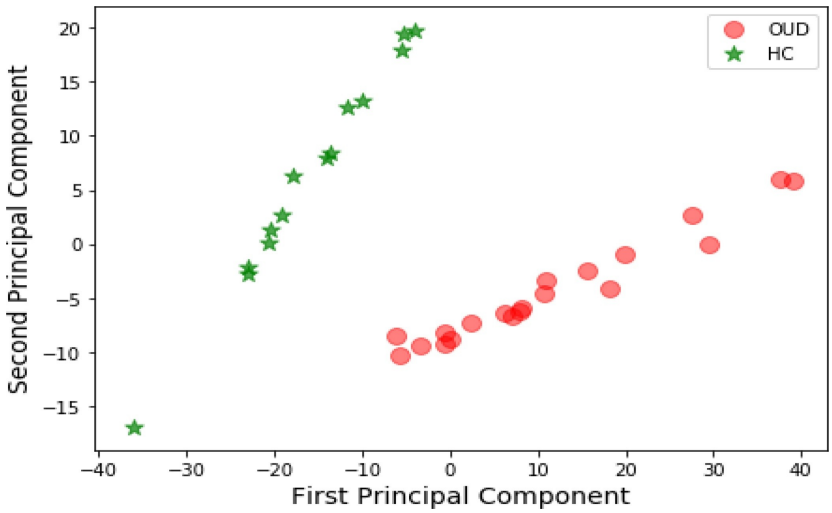

Figure 1-6: PCA results of the second derivation of ATR-IR spectra of OUD and HC serum discriminated by PCA in the region 1800 cm^{-1} to 900 cm^{-1}. Reproduced from ref. 222 with permission from Guleken, Ünübol, Bilici, Saribal, Toraman, Gündüz and Kuruca © 2020 Elsevier.

More recently in 2020, Guleken *et al.*[218] employed ATR-FTIR spectroscopy combined with chemometrics to investigate biochemical changes in the IR spectra of serum of patients with opioid addiction on an average daily dose of 2.95 g of opioids for 7.31 years prior to inclusion

in the study. With the use of PCA and LDA, this study was able to distinguish healthy serum samples from those of the opioid users with 92.85% sensitivity and 100% specificity, because chronic long-term use of opioids alters the amounts and ratios of plasma proteins thus altering their serum profiles (Figure 1-6).[218] While this study did not look at the detection of drugs in serum and only evaluated changes in relation to opioids, it was valuable in that long-term changes in chronic users have the potential to be presented in serum spectra in combination with the drug spectral signatures such as those presented in the spiked studies by Hans and colleagues.[213, 216]

Table 1-1 provides a summary of important characteristics necessary for the techniques covered in this chapter. On the whole, hyphenated chromatographic techniques remain the gold standard in terms of extremely low detection limits, these are also dependent on the availability of expert analysts, reference standards and extensive libraries for their implementation. Spectroscopic techniques offer many advantages for their application in routine drug detection. While Raman spectroscopy, mainly SERS, has demonstrated much greater sensitivity, it usually suffers from fluorescence interferences which can mask identifying spectral signatures.[196] As shown by the SWGDRUG guidelines, FTIR spectroscopy is highly structurally selective in that it allows for the characterisation of compounds without such interferences. This is of great importance, especially when identifying closely related compounds such as NPS within the same class. Minimal to no sample preparation required in their operation means that no parts of the sample are lost during the extensive extractions necessary for mass spectrometric methods, making them suitable for in-field analysis. Numerous commercially available spectroscopic handheld instruments operate similarly to benchtop instruments, allowing for convenient translation of developed methodologies from the lab into the field. While the application of IR spectroscopy to biofluids is problematic due to interferences from water initially and then from the overwhelming spectral signatures from biomolecules, some solutions have been presented in the literature. The drying of liquid biological samples is able to minimise water contributions, and the development of one-step extraction procedures has the potential to increase the sensitivity of ATR-FTIR spectroscopy.[214, 216] Furthermore, the use of chemometrics such as for classification purposes or more extensively such as that presented by Calvo-Castro *et al.* with the aim of including unknown substances reveals the real power of FTIR spectroscopy.[195]

Table 1-1: Summary of techniques and characteristics required in a drug detection method. ('X' = No, '✓' = Yes, '★' to '★★★★★' indicates a relative scale from low/minimal to high/extensive respectively.)

Technique	Minimal Sample preparation	Non-destructive	Ease of operation/ Analysis	High Structural Discrimination	Cost	Portability	Point of Care
Colour Tests	★★★★★	★★★★★	★★★★★	★	★★	★★★★★	X
Immuno-assays	★★★	★★★★★	★★★	★★★★	★★★	★★★	✓
Electro-chemical Methods	★	★★★★★	★★★	★★★	★★★	★★★	X
MS-based Methods	★	★★★★★	★	★★★★★	★★★★★	★	X
FTIR Spectroscopy	★★★★★	★	★★★★★	★★★★★	★	★★★★★	✓

1.6 Aims and Objectives

Drug detection methods remain one of the primary means of getting evidence-based information on the discovery of new drug compounds, drug manufacturing, consumption and trafficking in the licit and illicit drug markets. With over 275 million drug users and 1150 new substances reported in 2022, a direct, rapid and inexpensive drug detection method can represent a solution to overburdened laboratories and provide timely intelligence in clinical situations and forensic investigations.[1, 27]

The PhD research outlined in this thesis aims to test the hypothesis that it is possible to distinguish adulterated/counterfeit drugs from their pure or legitimate forms in biological samples. To achieve this goal, this study aims to explore the application of ATR-FTIR spectroscopy for direct detection, identification and quantification of drug compounds in biological fluids, namely urine and human pooled serum as a novel, easy and inexpensive alternative to the current methods of drug detection. To achieve this, this thesis will:

- Conduct a proof-of-concept study to detect and quantify the concentration of methamphetamine, and its four metabolites, in urine and pooled serum without any sample pre-treatment (**Chapter 3**).
- Investigate the ability of ATR-FTIR spectroscopy to discriminate between pure and illicitly adulterated methamphetamine in pooled serum and urine (**Chapter 4**).
- Explore the application of ATR-FTIR spectroscopy as an alternative to immunoassays for the detection of methamphetamine (**Chapter 5**).
- Investigate the ability of ATR-FTIR spectroscopy to discriminate between methamphetamine and synthetic cathinones as novel analogues of the traditional stimulant in pooled serum and urine (**Chapter 6**).

1.7 References

1. United Nations Office of Drugs and Crime, *World Drug Report Booklet 2*, United Nations Office of Drugs and Crime, Vienna, Austria, 2021.

2. U. Holzgrabe, in *Encyclopedia of Spectroscopy and Spectrometry*, eds. J. C. Lindon, G. E. Tranter and D. Koppenaal, Academic Press, Amsterdam, 3rd edn., 2017, pp. 393-395.

3. D. Custers, T. Cauwenbergh, J. L. Bothy, P. Courselle, J. O. De Beer, S. Apers and E. Deconinck, *Journal of Pharmaceutical and Biomedical Analysis*, 2015, **112**, 181-189.

4. G. Jackson, S. Patel and K. S., *International Journal of Clinical Practice*, 2011, **66**, 241-250.

5. European Monitoring Centre for Drugs and Drug Addiction, *European Drug Report - Trends and Developments* European Monitoring Centre for Drugs and Drug Addiction,, Luxemburg, 2017.

6. H. M. Sammons and I. Choonara, *British Medical Journal: Paediatrics* 2017, **1**, bmjpo-2017-000007.

7. A. Johnston and D. Holt, *British Journal of Clinical Pharmacology*, 2013, **78**, 218-243.

8. European Monitoring Centre for Drugs and Drug Addiction, *European Drug Report: Trends and Developments*, European Monitoring Centre for Drugs and Drug Addiction,, Luxemburg, 2021.

9. D. McManus and B. D. Naughton, *BMJ Global Health*, 2020, **5**, e002393.

10. C. Hauk, N. Hagen and L. Heide, *American Journal of Tropical Medicine and Hygiene*, 2021, **104**, 1936-1945.

11. I. M. E. Bakker-'t Hart, D. Ohana and B. J. Venhuis, *Journal of Pharmaceutical and Biomedical Analysis*, 2021, **197**, 113948.

12. K. Degardin, Y. Roggo and P. Margot, *Journal of Pharmaceutical and Biomedical Analysis*, 2014, **87**, 167-175.

13. J. G. Schier, C. S. Rubin, D. Miller, D. Barr and M. A. McGeehin, *Journal of Public Health Policy*, 2009, **30**, 127-143.

14. D. B. Blossom, A. J. Kallen, P. R. Patel, A. Elward, L. Robinson, G. Gao, R. Langer, K. M. Perkins, J. L. Jaeger, K. M. Kurkjian, M. Jones, S. F. Schillie, N. Shehab, D. Ketterer, G. Venkataraman, T. K. Kishimoto, Z. Shriver, A. W. McMahon, K. F. Austen, S. Kozlowski, A. Srinivasan, G. Turabelidze, C. V. Gould, M. J. Arduino and R. Sasisekharan, *New England Journal of Medicine*, 2008, **359**, 2674-2684.

15. V. Keoluangkhot, M. D. Green, L. Nyadong, F. M. Fernández, M. Mayxay and P. N. Newton, *American Journal of Tropical Medicine and Hygiene*, 2008, **78**, 552-555.

16. INTERPOL, *Thousands of Fake Online Pharmacies Shut Down in Interpol Operation*, 2021.

17. S. Chaplin, *Prescriber*, 2007, **18**, 16-21.

18. B. J. Venhuis, A. E. Oostlander, D. D. Giorgio, R. Mosimann and I. du Plessis, *The Lancet Oncology*, 2018, **19**, e209-e217.

19. World Health Organisation, *Global Surveillance and Monitoring System for Substandard and Falsified Medical Products*, World Health Organisation Geneva, 2017.

20. Medicines and Healthcare products Regulatory Agency, Over 3 Million Medicines and Devices Seized in Uk as Part of Global Crackdown, https://www.gov.uk/government/news/over-3-million-medicines-and-devices-seized-in-uk-as-part-of-global-crackdown, (accessed 6 December, 2021).

21. S. Houlton, *Prescriber*, 2018, **29**, 33-35.

22. G. M. L. Nayyar, J. G. Breman, P. N. Newton and J. Herrington, *The Lancet Infectious Diseases*, 2012, **12**, 488-496.

23. D. Reddy and J. Banerji, *The Lancet Infectious Diseases*, 2012, **12**, 829.

24. L. Parasa, L. Kumar, S. Para, V. Atluri, K. Santhisree, P. Kumar and C. Setty, *Reviews in Infection*, 2010, **1**, 117-123.

25. R. M. Smith, M. K. Schaefer, M. A. Kainer, M. Wise, J. Finks, J. Duwve, E. Fontaine, A. Chu, B. Carothers, A. Reilly, J. Fiedler, A. D. Wiese, C. Feaster, L. Gibson, S. Griese, A. Purfield, A. A. Cleveland, K. Benedict, J. R. Harris, M. E. Brandt, D. Blau, J. Jernigan, J. T. Weber and B. J. Park, *New England Journal of Medicine*, 2012, **369**, 1598-1609.

26. L. O. Gostin and G. J. Buckley, *Countering the Problem of Falsified and Substandard Drugs*, The National Academies Press, Washington, DC, 2013.

27. Early Warning Advisory and United Nations Office of Drugs and Crime, *Current Nps Threats Volume V*, United Nations Office of Drugs and Crime, Vienna, Austria, 2022.

28. I. Al-Banaa, L. Hawkins, S. L. Hill, D. J. Lupton, G. Jackson, E. A. Sandilands, S. M. Bradberry, J. P. Thompson, S. Rushton and S. H. L. Thomas, *International Journal of Drug Policy*, 2020, **77**, 102672.

29. European Monitoring Centre for Drugs and Drug Addiction, *Drug-Related Deaths and Mortality in Europe: Update from the Emcdda Expert Network*, European Monitoring Centre for Drugs and Drug Addiction,, Luxemburg, 2021.

30. S. Beharry and S. Gibbons, *Forensic Science International*, 2016, **267**, 25-34.

31. T. C. Ayres and J. W. Bond, *BMJ Open*, 2012, **2**, e000977.

32. R. A. S. Couto, L. M. Gonçalves, F. Carvalho, J. A. Rodrigues, C. M. P. Rodrigues and M. B. Quinaz, *Critical Reviews in Analytical Chemistry*, 2018, **48**, 372-390.

33. L. R. Cumba, A. V. Kolliopoulos, J. P. Smith, P. D. Thompson, P. R. Evans, O. B. Sutcliffe, D. R. do Carmo and C. E. Banks, *Analyst*, 2015, **140**, 5536-5545.

34. D. Angelov, J. O'Brien and P. Kavanagh, *Drug Testing and Analysis*, 2013, **5**, 145-149.

35. J. B. Morrow, J. D. Ropero-Miller, M. L. Catlin, A. D. Winokur, A. B. Cadwallader, J. L. Staymates, S. R. Williams, J. G. McGrath, B. K. Logan, M. M. McCormick, K. B. Nolte, T. P. Gilson, M. J. Menendez and B. A. Goldberger, *Journal of Analytical Toxicology*, 2019, **43**, 1-9.

36. M. Kraemer, A. Boehmer, B. Madea and A. Maas, *Forensic Science International*, 2019, **298**, 186-267.

37. S. Graziano, L. Anzillotti, G. Mannocchi, S. Pichini and F. P. Busardo, *Journal of Pharmaceutical and Biomedical Analysis*, 2019, **163**, 170-179.

38. K. Layne, P. I. Dargan and D. M. Wood, in *Novel Psychoactive Substances*, eds. P. Dargan and D. Wood, Academic Press, Boston, 2nd edn., 2022, ch. 13, pp. 333-380.

39. J. R. H. Archer, in *Novel Psychoactive Substances*, eds. P. Dargan and D. Wood, Academic Press, Boston, 2nd Edition edn., 2022, pp. 131-156.

40. D. Gerostamoulos, S. Elliott, H. C. Walls, F. T. Peters, M. Lynch and O. H. Drummer, *Journal of Analytical Toxicology*, 2016, **40**, 318-320.

41. D. Bewley-Taylor and M. Jelsma, *Legislative Reform of Drug Policies*, 2012, **18**, 1-24.

42. P. Reuter and B. Pardo, *International Journal of Drug Policy*, 2017, **40**, 117-122.

43. Home Office - United Kingdom, Misuse of Drugs Act 1971, https://www.legislation.gov.uk/uksi/2016/1109/made, (accessed 11 November, 2022).

44. Home Office - United Kingdom, Psychoactive Substances Act 2016, https://www.legislation.gov.uk/ukpga/2016/2/contents/enacted, (accessed 11 November, 2022).

45. R. G. Hill, *British Journal of Clinical Pharmacology*, 2019, **86**, 499-504.

46. E. J. Cone, *Forensic Science International*, 2001, **121**, 7-15.

47. E. Gerace, S. P. Bakanova, D. Di Corcia, A. Salomone and M. Vincenti, *Forensic Science International*, 2021, **318**, 110561.

48. D. E. Smith, L. Marzilli and L. D. Davidson, in *Textbook of Addiction Treatment: International Perspectives*, eds. N. el-Guebaly, G. Carrà, M. Galanter and A. M. Baldacchino, Springer International Publishing, Cham, 2021, pp. 733-756.

49. W. H. Kwok, T. L. S. Choi, K. Y. Kwok, G. H. M. Chan, J. K. Y. Wong and T. S. M. Wan, *Journal of Chromatography A*, 2016, **1451**, 41-49.

50. L. Gheddar, A.-L. Pélissier, J. Desfeux, F. Niort, J.-S. Raul and P. Kintz, *Journal of Analytical Toxicology*, 2021, bkab091.

51. F. Klont, S. Jahn, C. Grivet, S. König, R. Bonner and G. Hopfgartner, *Talanta*, 2020, **211**, 1-9.

52. L. D. Bowers and X. Bigard, *Medicine and Sport Science*, 2017, **62**, 77-90.

53. H. Y. Tey and H. H. See, *Journal of Chromatography A*, 2021, **1635**, 1-29

54. A. N. Cohen, G. Collins, F. C. Nucifora, R. Strobel, D. B. Wait and A. S. Young, *Psychiatric Services*, 2017, **69**, 345-348.

55. J. Esteve-Romero, J. Albiol-Chiva and J. Peris-Vicente, *Analytica Chimica Acta*, 2016, **926**, 1-16.

56. M. A. Alhefeiti, J. Barker and I. Shah, *Molecules*, 2021, **26**, 3291-3317.

57. J. Maurer, E. Vergalito, A.-F. Prior, N. Donzé, A. Thomas and M. Augsburger, *Forensic Science International*, 2021, **329**, 111081.

58. M. Dagar, S. Yadav, V. V. R. Sai, J. Satija and H. Bhatia, *Talanta*, 2022, **238**, 123048.

59. L. E. Jones, A. Stewart, K. L. Peters, M. McNaul, S. J. Speers, N. C. Fletcher and S. E. J. Bell, *Analyst*, 2016, **141**, 902-909.

60. R. Risoluti, S. Materazzi, A. Gregori and L. Ripani, *Talanta*, 2016, **153**, 407-413.

61. A. M. Leffler, P. B. Smith, A. de Armas and F. L. Dorman, *Forensic Science International*, 2014, **234**, 50-56.

62. United Nations Office of Drugs and Crime, *World Drug Report Booklet 4* United Nations Office of Drugs and Crime, Vienna, Austria, 2021.

63. European Monitoring Centre for Drugs and Drug Addiction, *Captagon: Understanding Today's Illicit Market*, European Monitoring Centre for Drugs and Drug Addiction, Luxemberg, 2018.

64. D. J. Heal, S. L. Smith, J. Gosden and D. J. Nutt, *Journal of Psychopharmacology*, 2013, **27**, 479-496.

65. D. J. Heal, S. C. Cheetham and S. L. Smith, *Neuropharmacology*, 2009, **57**, 608-618.

66. Drug Enforcement Administration, *2020 National Drug Threat Assessment*, US Department of Justice - Drug Enforcement Administration, United States, 2021.

67. H. M. Hazani, I. Naina Mohamed, M. Muzaimi, W. Mohamed, M. F. Yahaya, S. L. Teoh, R. M. Pakri Mohamed, M. F. Mohamad Isa, S. M. Abdulrahman, R. Ramadah, M. R. Kamaluddin and J. Kumar, *Frontiers in Pharmacology*, 2022, **13**.

68. M. Kariisa, L. Scholl, N. Wilson, P. Seth and B. Hoots, *Morbidity and Mortality Weekly Report*, 2019, **68**, 388-395.

69. J. E. Zibbell, S. D. Clarke, A. H. Kral, N. J. Richardson, D. Cauchon and A. Aldridge, *Drug and Alcohol Dependence*, 2022, **232**, 1-8.

70. M. Reyes-Parada, P. Iturriaga-Vasquez and B. K. Cassels, *Frontiers in Pharmacology*, 2020, **10**.

71. R. De La Torre, S. Yubero-Lahoz, R. Pardo-Lozano and M. Farre, *Frontiers in Genetics*, 2012, **3**, 1-8.

72. J. S. Fowler, C. Kroll, R. Ferrieri, D. Alexoff, J. Logan, S. L. Dewey, W. Schiffer, D. Schlyer, P. Carter, P. King, C. Shea, Y. Xu, L. Muench, H. Benveniste, P. Vaska and N. D. Volkow, *Journal of Nuclear Medicine*, 2007, **48**, 1724-1732.

73. D. J. Wagner, J. E. Sager, H. Duan, N. Isoherranen and J. Wang, *Drug Metabolism and Disposition*, 2017, **45**, 770.

74. G. J. Rivière, W. B. Gentry and S. M. Owens, *Journal of Pharmacology and Experimental Therapeutics*, 2000, **292**, 1042-1047.

75. S. Yu, L. Zhu, Q. Shen, X. Bai and X. Di, *Behavioural Neurology*, 2015, **2015**, 1-11.

76. R. de la Torre, M. Farre, M. Navarro, R. Pacifici, P. Zuccaro and S. Pichini, *Clinical Pharmacokinetics*, 2004, **43**, 157-185.

77. T. Akindipe, D. Wilson and D. J. Stein, *Metabolic Brain Disease*, 2014, **29**, 351-357.

78. D. E. Rusyniak, *Psychiatric Clinics of North America*, 2013, **36**, 261-275.

79. J. Ballester, G. Valentine and M. Sofuoglu, *Expert Review of Clinical Pharmacology*, 2017, **10**, 305-314.

80. K. C. Morley, J. L. Cornish, A. Faingold, K. Wood and P. S. Haber, *Expert Opinion on Investigational Drugs*, 2017, **26**, 563-578.

81. A. Moszczynska, *Current Neuropharmacology*, 2021, **19**, 2077-2091.

82. National Institute on Drug Abuse, Methamphetamine Research Report 2019, (accessed 12 December, 2022).

83. R. J. Ellis, M. E. Childers, M. Cherner, D. Lazzaretto, S. Letendre and I. Grant, *Journal of Infectious Diseases*, 2003, **188**, 1820-1826.

84. N. Fairbairn, T. Kerr, M. J. Milloy, R. Zhang, J. Montaner and E. Wood, *Addictive Behaviours*, 2011, **36**, 762-763.

85. A. Rohman, A. Windarsih, E. Lukitaningsih, M. Rafi, K. Betania and N. A. Fadzillah, *Biomedical Spectroscopy and Imaging*, 2019, **8**, 55-71.

86. J. N. Adkins, S. M. Varnum, K. J. Auberry, R. J. Moore, N. H. Angell, R. D. Smith, D. L. Springer and J. G. Pounds, *Analysis By Multidimensional Separation Coupled With Mass Spectrometry*, 2002, **1**, 947-955.

87. T. D. Veenstra, T. P. Conrads, B. L. Hood, A. M. Avellino, R. G. Ellenbogen and R. S. Morrison, *Molecular & Cellular Proteomics*, 2005, **4**, 409-418.

88. X. Xu and T. D. Veenstra, *PROTEOMICS – Clinical Applications*, 2008, **2**, 1403-1412.

89. A. Zhang, H. Sun, P. Wang, Y. Han and X. Wang, *Journal of Proteomics*, 2012, **75**, 1079-1088.

90. A.-M. Dragan, M. Parrilla, B. Feier, R. Oprean, C. Cristea and K. De Wael, *Trends in Analytical Chemistry*, 2021, **145**, 116447.

91. V. Blandino, J. Wetzel, J. Kim, P. Haxhi, R. Curtis and M. Concheiro, *Current Pharmaceutical Biotechnology*, 2017, **18**, 796-805.

92. B. De Martinis, *Current Pharmaceutical Analysis*, 2008, **4**, 274-278.

93. C. Gambelunghe, N. Fucci, K. Aroni, M. Bacci, A. Marcelli and R. Rossi, *Therapeutic Drug Monitoring*, 2016, **38**, 634-639.

94. A. J. Barnes, M. L. Smith, S. L. Kacinko, E. W. Schwilke, E. J. Cone, E. T. Moolchan and M. A. Huestis, *Clinical Chemistry*, 2008, **54**, 172-180.

95. M. J. Burgueno, A. Alonso and S. Sanchez, *Forensic Science International*, 2016, **265**, 47-53.

96. B. Flinders, E. Cuypers, T. Porta, E. Varesio, G. Hopfgartner and R. M. A. Heeren, *Methods Molecular Biology*, 2017, **1618**, 137-147.

97. J. Barbosa, J. Faria, F. Carvalho, M. Pedro, O. Queiros, R. Moreira and R. J. Dinis-Oliveira, *Bioanalysis*, 2013, **5**, 895-914.

98. R. Dams, R. E. Choo, W. E. Lambert, H. Jones and M. A. Huestis, *Drug Alcohol Dependance*, 2007, **87**, 258-267.

99. D. Borg, E. Kolb, C. Lantigua and R. Stripp, *Journal of Analytical Toxicology*, 2018, **42**, 25-32.

100. K. N. Ellefsen, M. Concheiro, S. Pirard, D. A. Gorelick and M. A. Huestis, *Forensic Science International*, 2016, **260**, 95-101.

101. M. Barroso, E. Gallardo and J. A. Queiroz, *Bioanalysis*, 2009, **1**, 977-1000.

102. H. Gjerde, K. Langel, D. Favretto and A. G. Verstraete, *Forensic Science International*, 2015, **256**, 42-45.

103. P. Adamowicz, *Clinical Toxicology*, 2021, **59**, 648-654.

104. C. J. Briscoe and D. S. Hage, *Bioanalysis*, 2009, **1**, 205-220.

105. M. Grapp, C. Kaufmann, F. Streit and L. Binder, *Forensic Science International*, 2018, **287**, 63-73.

106. L. H. J. Richter, V. Flockerzi, H. H. Maurer and M. R. Meyer, *Journal of Pharmaceutical and Biomedical Analysis*, 2017, **143**, 32-42.

107. L. Mercolini and M. Protti, *Journal of Pharmaceutical and Biomedical Analysis*, 2016, **130**, 202-219.

108. M. A. Huestis and M. L. Smith, *Trends Molecular Medicine*, 2018, **24**, 156-172.

109. A. T. M. d. Silva, C. D. P. B. Bessa, W. d. S. Borges and K. B. Borges, *Trends in Analytical Chemistry*, 2018, **108**, 323-346.

110. M. Vandevenne, H. Vandenbussche and A. Verstraete, *Acta Clinica Belgica*, 2016, **55**, 323-333.

111. K. R. Allen, *Annals of Clinical Biochemistry*, 2011, **48**, 531-541.

112. A. G. Verstraete, *Therapeutic Drug Monitoring*, 2004, **26**, 200-205.

113. P. Adamowicz and A. Malczyk, *Forensic Science International*, 2019, **295**, 36-45.

114. M. A. Huestis and E. J. Cone, *Annals of the New York Academy of Sciences*, 2007, **1098**, 104-121.

115. B. Barr Dana, C. Wilder Lynn, P. Caudill Samuel, J. Gonzalez Amanda, L. Needham Lance and L. Pirkle James, *Environmental Health Perspectives*, 2005, **113**, 192-200.

116. E. N. Taylor and G. C. Curhan, *Journal of the American Society of Nephrology*, 2007, **18**, 654.

117. N. Sarigul, F. Korkmaz and İ. Kurultak, *Scientific Reports*, 2019, **9**, 20159.

118. S. R. Saenz, R. J. Lewis, M. K. Angier and J. R. Wagner, *Journal of Analytical Toxicology*, 2017, **41**, 508-516.

119. D. J. Pounder and G. R. Jones, *Forensic Science International*, 1990, **45**, 253-263.

120. F. Musshoff, *Drug Metabolism Reviews*, 2000, **32**, 15-44.

121. F. Moriya and Y. Hashimoto, *Journal of Analytical Toxicology*, 2000, **24**, 153-154.

122. E. Kim, S. Choe, J. Lee, M. Jang, H. Choi and H. Chung, *Forensic Science International*, 2016, **265**, 186-192.

123. United Nations International Drug Control Programme, *Rapid on-Site Screening of Drugs of Abuse Part I: Biological Specimens* Vienna, Austria, 2001.

124. United Nations Office of Drugs and Crime, *Rapid Testing Methods of Drugs of Abuse*, United Nations Office of Drugs and Crime, Vienna, Austria, 1994.

125. United Nations Publication, *Recommended Methods for the Identification and Analysis of Amphetamine, Methamphetamine and Their Ring-Substituted Analogues in Seized Materials*, United Nations Office on Drugs and Crime, 2006.

126. Scientific Working Group for the Analysis of Seized Drugs (SWGDRUG), *Swgdrug Recommendations Version 8.0*, United States Department of Justice, Washington DC, 2019.

127. United Nations Office of Drugs and Crime, *International Collaborative Exercises - Drug Analysis Report*, United Nations Office of Drugs and Crime, Vienna, Austria, 2021.

128. A. Choodum and N. Nic Daeid, *Talanta*, 2011, **86**, 284-292.

129. E. Cuypers, A.-J. Bonneure and J. Tytgat, *Drug Testing and Analysis*, 2016, **8**, 136-140.

130. M. Philp and S. Fu, *Drug Testing and Analysis*, 2018, **10**, 95-108.

131. C. O'Neal, D. J. Couch and A. A. Fatah, *Forensic Science International*, 2000, **109**, 189-201.

132. R. A. Murray, P. L. Doering, L. A. Boothby, M. L. Merves, R. R. McCusker, C. W. Chronister and B. A. Goldberger, *Pharmacotherapy: The Journal of Human Pharmacology and Drug Therapy*, 2003, **23**, 1238-1244.

133. Early Warning Advisory and United Nations Office of Drugs and Crime, *Large Seizures of Synthetic Cathinones in Europe Reflect Their Growing Importance on the Illicit Stimulants Market*, United Nations Office of Drugs and Crime, Vienna, Austria, 2022.

134. United Nations Office of Drugs and Crime, *Recommended Methods for the Identification and Analysis of Synthetic Cathinones in Seized Materials*, United Nations Office of Drugs and Crime, Vienna, Austria, 2020.

135. K. E. Toole, R. Shimmon, N. Krayem and S. Taflaga, *Microgram* 2012, **9**, 27-32.

136. M. Philp, R. Shimmon, M. Tahtouh and S. Fu, *Forensic Chemistry*, 2016, **1**, 39-50.

137. A. Choodum and N. N. Daeid, *Drug Testing and Analysis*, 2011, **3**, 277-282.

138. A. Choodum, P. Kanatharana, W. Wongniramaikul and N. N. Daeid, *Talanta*, 2013, **115**, 143-149.

139. G. O. da Silva, W. R. de Araujo and T. R. L. C. Paixão, *Talanta*, 2018, **176**, 674-678.

140. K. M. Elkins, A. C. Weghorst, A. A. Quinn and S. Acharya, *Drug Testing and Analysis*, 2017, **9**, 306-310.

141. A. Carrio, C. Sampedro, J. L. Sanchez-Lopez, M. Pimienta and P. Campoy, *Sensors*, 2015, **15**, 29569-29593.

142. G. J. Mohr, M. Wenzel, F. Lehmann and P. Czerney, *Analytical and Bioanalytical Chemistry*, 2002, **374**, 399-402.

143. D. Favretto, F. Castagna, S. Maietti, R. Boscolo-Berto and S. D. Ferrara, *Journal of Pharmaceutical and Biomedical Analysis*, 2013, **83**, 260-264.

144. J. C. Matthews and W. S. Wassif, *British Journal of Biomedical Science*, 2010, **67**, 218-220.

145. L. P. de Oliveira, D. P. Rocha, W. R. de Araujo, R. A. A. Muñoz, T. R. L. C. Paixão and M. O. Salles, *Analytical Methods*, 2018, **10**, 5135-5163.

146. National Institute of Standards Technology - Office of Law Enforcement Standards, *Color Test Reagents/Kits for Preliminary Identification of Drugs of Abuse*, National Institute of Justice - US Department of Justice, , Gaithersburg, 2000.

147. United Nations International Drug Control Programme, *Rapid on-Site Screening of Drugs of Abuse Part I: Biological Specimens*, United Nations Office of Drugs and Crime, Vienna, Austria, 2001.

148. L. E. Regester, J. D. Chmiel, J. M. Holler, S. P. Vorce, B. Levine and T. Z. Bosy, *Journal of Analytical Toxicology*, 2015, **39**, 144-151.

149. D. A. Armbruster, E. C. Hubster, M. S. Kaufman and M. K. Ramon, *Clinical Chemistry*, 1995, **41**, 92-98.

150. Y. H. Caplan, B. Levine and B. Goldberger, *Clinical Chemistry*, 1987, **33**, 1200-1202.

151. A. Dasgupta, S. Saldana, G. Kinnaman, M. Smith and K. Johansen, *Clinical Chemistry*, 1993, **39**, 104-108.

152. J. Hsu, C. Liu, C. P. Hsu, W.-I. Tsay, J.-H. Li, D.-L. Lin and R. H. Liu, *Journal of Analytical Toxicology*, 2003, **27**, 471-478.

153. A. G. Verstraete and F. V. Heyden, *Journal of Analytical Toxicology*, 2005, **29**, 359-364.

154. A. Saitman, H. D. Park and R. L. Fitzgerald, *Journal of Analytical Toxicology*, 2014, **38**, 387-396.

155. M. Petrie, K. L. Lynch, S. Ekins, J. S. Chang, R. J. Goetz, A. H. B. Wu and M. D. Krasowski, *Clinical Toxicology*, 2013, **51**, 83-91.

156. K. W. Tupper, K. McCrae, I. Garber, M. Lysyshyn and E. Wood, *Drug and Alcohol Dependence*, 2018, **190**, 242-245.

157. T. J. Gelmi, M. Verrijken and W. Weinmann, *Regulatory Toxicology and Pharmacology*, 2020, **116**, 104747.

158. H. S. Bombana, M. F. dos Santos, D. R. Muñoz and V. Leyton, *Journal of Chromatography B*, 2020, **1139**, 121973.

159. G. Mercieca, S. Odoardi, M. Cassar and S. Strano Rossi, *Journal of Pharmaceutical and Biomedical Analysis*, 2018, **149**, 494-501.

160. K. A. Alsenedi and C. Morrison, *Journal of Chromatography B*, 2018, **1076**, 91-102.

161. S. Lehmann, T. Kieliba, J. Beike, M. Thevis and K. Mercer-Chalmers-Bender, *Journal of Chromatography B*, 2017, **1064**, 124-138.

162. F. Vaiano, F. P. Busardò, D. Palumbo, C. Kyriakou, A. Fioravanti, V. Catalani, F. Mari and E. Bertol, *Journal of Pharmaceutical and Biomedical Analysis*, 2016, **129**, 441-449.

163. P. M. O'Byrne, P. V. Kavanagh, S. M. McNamara and S. M. Stokes, *Journal of Analytical Toxicology*, 2013, **37**, 64-73.

164. C. Bell, C. George, A. T. Kicman and A. Traynor, *Drug Testing and Analysis*, 2011, **3**, 496-504.

165. M. Concheiro, S. Anizan, K. Ellefsen and M. A. Huestis, *Analytical and Bioanalytical Chemistry*, 2013, **405**, 9437-9448.

166. A. I. Al-Asmari, *Forensic Science International*, 2020, **309**, 110193.

167. C. B. Mollerup, P. W. Dalsgaard, M. Mardal and K. Linnet, *Drug Testing and Analysis*, 2017, **9**, 1052-1061.

168. J. C. Eichhorst, M. L. Etter, P. L. Hall and D. C. Lehotay, *Methods in Molecular Biology*, 2012, **902**, 29-41.

169. M. K. Wozniak, M. Wiergowski, J. Aszyk, P. Kubica, J. Namiesnik and M. Biziuk, *Journal of Pharmaceutical and Biomedical Analysis*, 2018, **148**, 58-64.

170. S. Odoardi, M. Fisichella, F. S. Romolo and S. Strano-Rossi, *Journal of Chromatography B*, 2015, **1000**, 57-68.

171. F. T. Peters, *Clinical Biochemistry*, 2011, **44**, 54-65.

172. D. Remane, D. K. Wissenbach and F. T. Peters, *Clinical Biochemistry*, 2016, **49**, 1051-1071.

173. Z. Niu, W. Zhang, C. Yu, J. Zhang and Y. Wen, *Trends in Analytical Chemistry*, 2018, **102**, 123-146.

174. 2002/657/Ec: Commission Decision of 12 August 2002 Implementing Council Directive 96/23/Ec Concerning the Performance of Analytical Methods and the Interpretation of Results (Notified under Document Number C (2002) 3044), https://eur-lex.europa.eu/legal-content/EN/TXT/?uri=CELEX:32002D0657, (accessed 11 November, 2022).

175. B. J. McCullough, K. Patel, R. Francis, P. Cain, D. Douce, K. Whyatt, S. Bajic, N. Lumley and C. Hopley, *Journal of the American Society for Mass Spectrometry*, 2020, **31**, 386-393.

176. G. A. Gómez-Ríos, T. Vasiljevic, E. Gionfriddo, M. Yu and J. Pawliszyn, *Analyst*, 2017, **142**, 2928-2935.

177. T. H. Chen, H. Y. Hsu and S. P. Wu, *Forensic Science International*, 2016, **267**, 1-6.

178. Z. E. Lawton, A. Traub, W. L. Fatigante, J. Mancias, A. E. O'Leary, S. E. Hall, J. R. Wieland, H. Oberacher, M. C. Gizzi and C. C. Mulligan, *Journal of the American Society for Mass Spectrometry*, 2017, **28**, 1048-1059.

179. E. Schepens, S. Inman, B. J. McCullough and C. Hopley, *Forensic Chemistry*, 2017, **4**, 75-81.

180. D. E. Damon, K. M. Davis, C. R. Moreira, P. Capone, R. Cruttenden and A. K. Badu-Tawiah, *Analytical Chemistry*, 2016, **88**, 1878-1884.

181. N. E. Manicke, B. J. Bills and C. Zhang, *Bioanalysis*, 2016, **8**, 589-606.

182. T. R. Croley, K. D. White, J. H. Callahan and S. M. Musser, *Journal of the American Society for Mass Spectrometry*, 2012, **23**, 1569-1578.

183. F. T. Peters and D. Remane, *Analytical and Bioanalytical Chemistry*, 2012, **403**, 2155-2172.

184. L. Shaw and L. Dennany, *Current Opinion in Electrochemistry*, 2017, **3**, 23-28.

185. M. A. Balbino, É. N. Oiye, M. F. M. Ribeiro, J. W. C. Júnior, I. C. Eleotério, A. J. Ipólito and M. F. de Oliveira, *Journal of Solid State Electrochemistry*, 2016, **20**, 2435-2443.

186. J. M. Freitas, D. L. O. Ramos, R. M. F. Sousa, T. R. L. C. Paixão, M. H. P. Santana, R. A. A. Muñoz and E. M. Richter, *Sensors and Actuators B: Chemical*, 2017, **243**, 557-565.

187. R. Van Echelpoel, R. F. Kranenburg, A. C. van Asten and K. De Wael, *Forensic Chemistry*, 2022, **27**, 100383.

188. Ľ. Švorc, M. Vojs, P. Michniak, M. Marton, M. Rievaj and D. Bustin, *Journal of Electroanalytical Chemistry*, 2014, **717-718**, 34-40.

189. R. A. S. Couto, S. S. Costa, B. Mounssef, J. G. Pacheco, E. Fernandes, F. Carvalho, C. M. P. Rodrigues, C. Delerue-Matos, A. A. C. Braga, L. Moreira Gonçalves and M. B. Quinaz, *Sensors and Actuators B: Chemical*, 2019, **290**, 378-386.

190. E. M. Garrido, J. M. Garrido, N. Milhazes, F. Borges and A. M. Oliveira-Brett, *Bioelectrochemistry*, 2010, **79**, 77-83.

191. I. Razavipanah, E. Alipour, B. Deiminiat and G. H. Rounaghi, *Biosensors and Bioelectronics*, 2018, **119**, 163-169.

192. J. Ollesch, S. L. Drees, H. M. Heise, T. Behrens, T. Brüning and K. Gerwert, *Analyst*, 2013, **138**, 4092-4102.

193. A. A. Bunaciu, Ş. Fleschin, V. D. Hoang and H. Y. Aboul-Enein, *Critical Reviews in Analytical Chemistry*, 2017, **47**, 67-75.

194. R. V. Moreira, J. L. da Costa, M. R. Menezes and D. L. A. de Faria, *Vibrational Spectroscopy*, 2016, **87**, 104-110.

195. J. Calvo-Castro, A. Guirguis, E. G. Samaras, M. Zloh, S. B. Kirton and Jacqueline L. Stair, *RSC Advances*, 2018, **8**, 31924-31933.

196. R. Dong, S. Weng, L. Yang and J. Liu, *Analytical Chemistry*, 2015, **87**, 2937-2944.

197. N. Nuntawong, P. Eiamchai, W. Somrang, S. Denchitcharoen, S. Limwichean, M. Horprathum, V. Patthanasettakul, S. Chaiya, A. Leelapojanaporn, S. Saiseng, P. Pongsethasant and P. Chindaudom, *Sensors and Actuators B: Chemical*, 2017, **239**, 139-146.

198. T. Yang, X. Guo, H. Wang, S. Fu, Y. wen and H. Yang, *Biosensors and Bioelectronics*, 2015, **68**, 350-357.

199. H. Muhamadali, A. Watt, Y. Xu, M. Chisanga, A. Subaihi, C. Jones, D. I. Ellis, O. B. Sutcliffe and R. Goodacre, *Frontiers in Chemistry*, 2019, **7**.

200. R. M. Correia, E. Domingos, F. Tosato, N. A. dos Santos, J. d. A. Leite, M. da Silva, M. C. A. Marcelo, R. S. Ortiz, P. R. Filgueiras and W. Romão, *Analytical Methods*, 2018, **10**, 593-603.

201. L. S. A. Pereira, F. L. C. Lisboa, J. Coelho Neto, F. N. Valladão and M. M. Sena, *Forensic Science International*, 2018, **288**, 227-235.

202. C. Negoita, M. Praisler and A. Ion, *AIP Conference Proceedings*, 2019, **2075**, 170026.

203. L. S. A. Pereira, F. L. C. Lisboa, J. Coelho Neto, F. N. Valladao and M. M. Sena, *Forensic Science International*, 2018, **288**, 227-235.

204. L. S. A. Pereira, F. L. C. Lisboa, J. C. Neto, F. N. Valladão and M. M. Sena, *Microchemical Journal*, 2017, **133**, 96-103.

205. T. Baghai, G. Varallo-Bedarida, C. Born, S. Häfner, C. Schüle, D. Eser, R. Rupprecht, B. Bondy and C. Schacky, *The Journal of Clinical Psychiatry*, 2010, **72**, 1242-1247.

206. H. Tiemeier, H. R. van Tuijl, A. Hofman, A. J. Kiliaan and M. M. Breteler, *The American Journal of Clinical Nutrition*, 2003, **78**, 40-46.

207. M. J. Baker, C. S. Hughes and K. A. Hollywood, *Biophotonics: Vibrational Spectroscopic Diagnostics*, Morgan & Claypool Publishers, San Rafael, California, 2016.

208. K. Spalding, F. Bonnier, C. Bruno, H. Blasco, R. Board, I. Benz-de Bretagne, H. J. Byrne, H. J. Butler, I. Chourpa, P. Radhakrishnan and M. J. Baker, *Vibrational Spectroscopy*, 2018, **99**, 50-58.

209. A. Ameline, C. Richeval, J. M. Gaulier, J. S. Raul and P. Kintz, *Drug Testing and Analysis*, 2019, **11**, 223-229.

210. F. Wu, T. L. Scroggin, T. D. Metz and G. A. McMillin, *Journal of Analytical Toxicology*, 2018, **42**, 42-48.

211. M. T. Truver and M. J. Swortwood, *Journal of Analytical Toxicology*, 2018, **42**, 554-561.

212. T. G. Rosano, P. Y. Ohouo and M. Wood, *Journal of Analytical Toxicology*, 2017, **41**, 536-546.

213. K. M. Hans, S. Müller and M. W. Sigrist, *Drug Testing and Analysis*, 2012, **4**, 420-429.

214. K. M.-C. Hans, M. Gianella and M. Sigrist, *Proceedings of Society of Photo-Optical Instrumentation Engineers*, 2012, **8229**.

215. K. M.-C. Hans, M. Müller, M. Gianella, P. Wägli and M. Sigrist, *Proceedings of Society of Photo-Optical Instrumentation Engineers*, 2013, **8591**.

216. K. M. C. Hans, M. Müller, T. Petrosyan and M. W. Sigrist, *Analytical Methods*, 2014, **6**, 666-673.

217. P. Wägli, Y.-C. Chang, A. Homsy, L. Hvozdara, H. P. Herzig and N. F. de Rooij, *Analytical Chemistry*, 2013, **85**, 7558-7565.

218. Z. Guleken, B. Ünübol, R. Bilici, D. Sarıbal, S. Toraman, O. Gündüz and S. Erdem Kuruca, *Journal of Pharmaceutical and Biomedical Analysis*, 2020, **190**, 113553.

CHAPTER TWO

THEORY AND METHODS

2.1 Vibrational Spectroscopy

Spectroscopy is the study of the interaction of light with matter in the form of absorption, emission and scattering.[1] Light, more appropriately labelled as electromagnetic radiation, consists of radio waves, microwaves, infrared, visible and ultra-violet radiation, X-rays, gamma rays and cosmic rays; each with increasing frequency. Electromagnetic radiation can be thought of as consisting of small packets of energy, or photons that behave both like particles and waves.[2] Their wave-like behaviour shows two distinct in-phase components, the electric and magnetic fields, which oscillate perpendicular to each other and travel concurrently at the speed of light (Figure 2-1).[3]

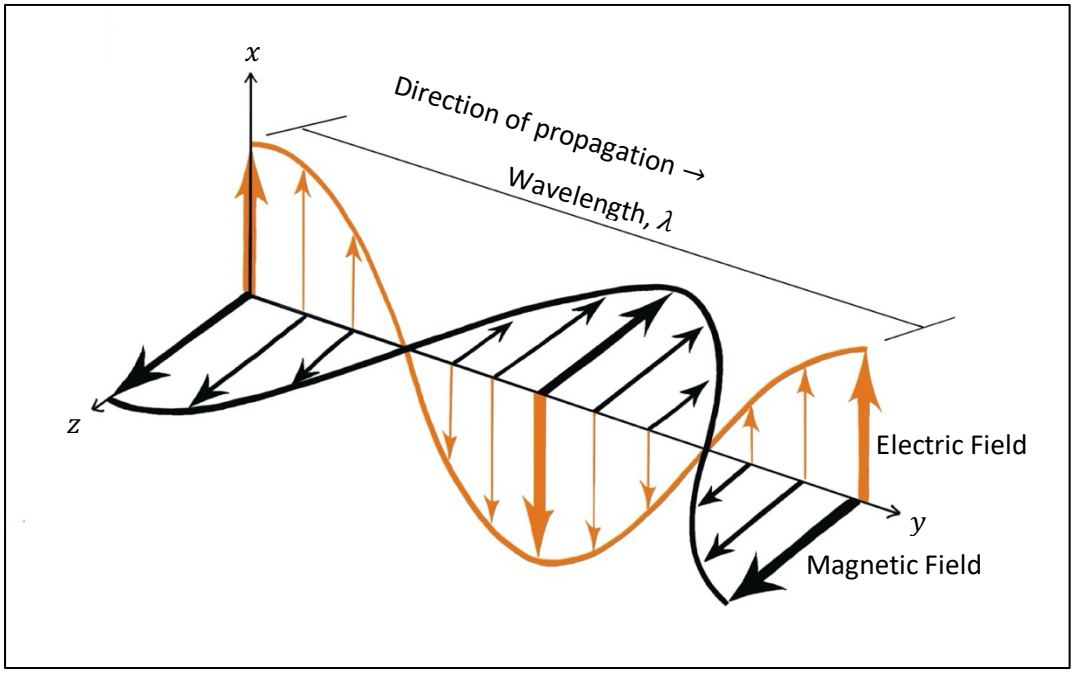

Figure 2-1: Perpendicular relationship between electric and magnetic fields of an electromagnetic wave, showing wavelength, λ.

The wavelength is defined as the distance between two consecutive peaks or two consecutive troughs, while the frequency is the number of waves that travel past a given point in a unit of time.[4] The frequency (ν) and wavelength (λ) of a wave are inversely proportional to each other and can be used to calculate the energy (E) of the photon using an expansion of Planck's Law as shown in the following equations:

$$\nu = \frac{c}{\lambda} \tag{2.1}$$

$$E = h\nu = \frac{hc}{\lambda} \quad (2.2)$$

where c is the velocity of light and h is Planck's constant.

From Equation (2.2), the energy of a wave is inversely proportional to the wavelength (1/ λ) and this quantity is known as the wavenumber, $\bar{\nu}$. Wavenumbers can also be thought of as the number of cycles per unit distance and are measured in cm^{-1}.[5]

Vibrational spectroscopy is a term used to describe the optical techniques of infrared (IR) and Raman spectroscopy and relates to the absorption, emission or scattering of electromagnetic radiation.[6] IR spectroscopy can be further divided into three types that include near-IR (12,500-4000 cm^{-1}), mid-IR (4000-400 cm^{-1}) and far-IR (400-30 cm^{-1}) as defined by the ISO20473:2007 (E) standards.[7]

The principles of IR spectroscopy rely on the characteristic behaviour of the bonds between atoms within molecules.[5] Most compounds, including the drug and biological molecules of interest in this thesis, show strong absorption bands in the mid-IR region which are linked to the rotational and vibrational movements of atoms within those molecules.[8, 9] The pattern of absorption created using mid-IR spectroscopy is characteristic of bonding arrangements of atoms known as functional groups and can be used to create a spectral fingerprint of the compounds in question.[8] Therefore, mid-IR spectroscopy is useful in analytical investigations where the determination of chemical structures and identification of unknowns in a sample is required.[8, 10] Other advantages of this method include its rapid, and non-destructive analysis as well as using only a small sample volume, which makes it a popular technique employed across a variety of fields.[11-16] Each experimental chapter in this thesis utilises mid-IR spectroscopy and therefore this chapter will focus on describing its theoretical basis, instrumentation and methods used for data analysis.

2.1.1 Molecular Transitions

The Born-Oppenheimer approximation is useful in understanding molecular transitions and the total energy of a molecule. It assumes that electronic and nuclear motion are separate and due to the large disparity in the mass of an electron in comparison with the size of the nucleus, nuclear motion is minimal relative to the electrons.[1] Therefore, the total energy of

molecules can be described as the sum of its electronic (ΔE_e), vibrational (E_v), rotational (E_r),, and translational (E_t), energies with respect to electronic motion within the molecules (equation 2.3):[17]

$$\Delta E = \Delta E_e + \Delta E_v + \Delta E_r + \Delta E_t \quad (2.3)$$

At the molecular level, the quantised nature of electromagnetic radiation is more relevant. Photons of specific energy can be absorbed or emitted by a molecule which results in the transfer of energy. The electronic transitions occur when an electron is moved from its ground electronic state to its excited electronic state, while vibrational transitions occur between different vibrational levels of the same electronic state (Figure 2-2).[17] For each electronic transition there are many vibrational energy levels and for each vibrational level, there exist many rotational levels for each molecule (Figure 2-2).[17] Electronic transitions require higher energy radiation than vibrational transitions, which require higher energy incoming photons than that for rotational movements within a molecule.[17]

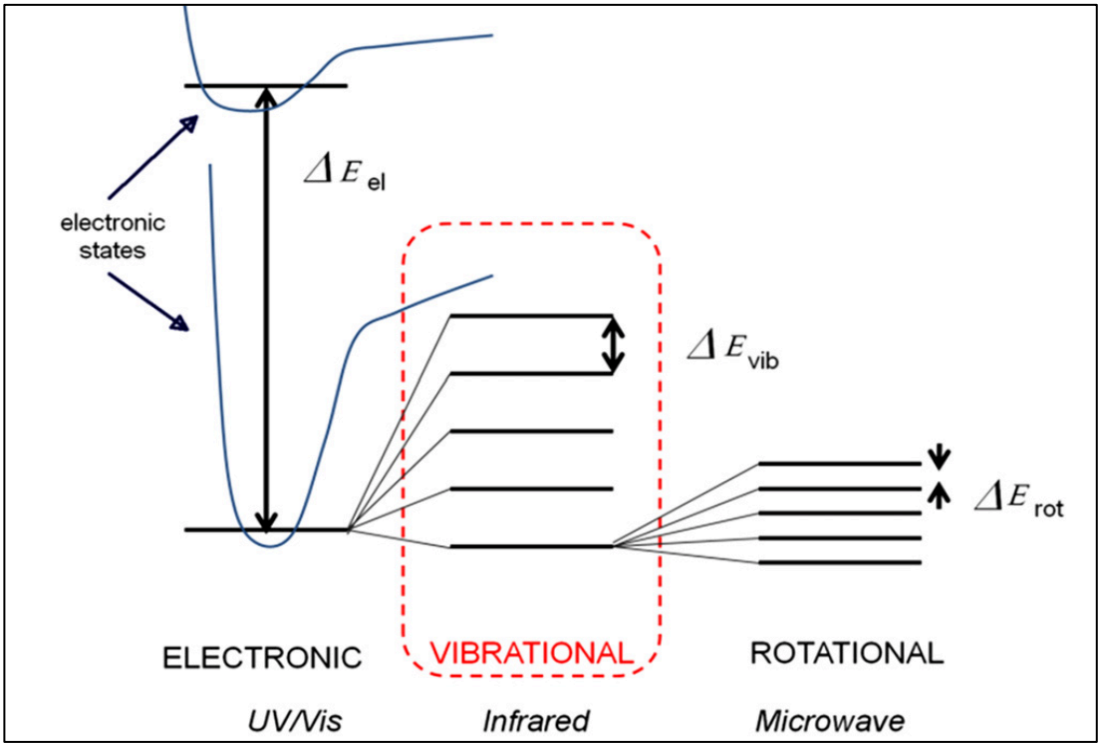

Figure 2-2: Energy transitions with varying energy of the incident radiation (reproduced from Baker *et al.* 2016).

For an electronic transition, the higher energy of ultraviolet, visible or x-ray radiation is needed, while infrared radiation is able to excite vibrational transitions. In a molecule with stable bonds, there is a balance of attractive and repulsive forces between the positive nucleus and negative electrons allowing the molecule to settle at an equilibrium inter-nuclear distance and reach an energetic minimum (Figure 2-3).

For a simple diatomic molecule, the motion of atoms along the bond length resembles the harmonic oscillator - the motion of two weights attached to either side of a spring and therefore can be modelled using Hooke's Law (Equation 2.4):[18]

$$F = -kx \tag{2.4}$$

where F is the force, k is the force constant and x is the displacement from equilibrium. In molecular terms, the two masses are atoms, and the spring is the bond length between the atoms. Any displacement from the equilibrium of the molecule can be viewed as vibrations

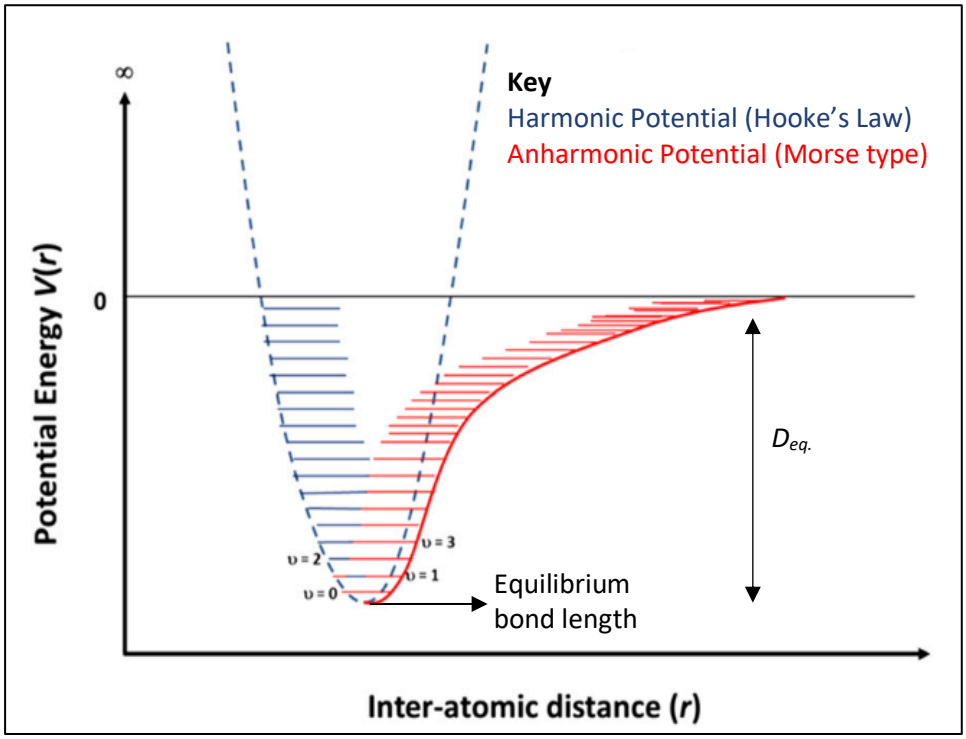

Figure 2-3: Morse potential energy diagram for harmonic (blue) and anharmonic (red) oscillation (adapted from Baker *et al.* 2016).

and the frequency with which they vibrate are vibrational modes for that molecule. The energy associated with these vibrations is quantised, taking only specific values illustrated by

the discrete vibrational levels.[2] For each vibrational mode, *j*, the energy of the molecule, E_{vib}, is described by Equation 2.5:

$$E_{vib} = h\nu_j \left(\upsilon_j + \frac{1}{2}\right) \tag{2.5}$$

where υ_j is the quantum number for the *j*th mode, and the ν_j is the fundamental frequency for that vibrational mode. However, this molecular description is oversimplified as bonds between atoms can be broken, which is not reflected in the harmonic potential model. Additionally, the anharmonicity of chemical bonds is better represented by the Morse potential rather than the simple harmonic description (Figure 2-3). The allowed potential energies of the anharmonic model are described by the Morse-type potential (Equation 2.6)

$$E_{vib} = h\nu_j \left(\upsilon_j + \frac{1}{2}\right) - h\nu_j x_j \left(\upsilon_j + \frac{1}{2}\right)^2 \tag{2.6}$$

where x_j is the anharmonicity constant.

The vibrational frequency of these atoms depends on a variety of factors including the atomic mass, bond strength, bond length and the surrounding molecular environment, thus are characteristic of the molecule. The fundamental vibrational frequency of a diatomic molecule is given by following equation 2.7:[2]

$$\nu = \left(\frac{1}{2\pi}\right)\sqrt{\frac{k}{\mu}} \tag{2.7}$$

where the quantity $\mu = \frac{m_1 m_2}{(m_1+m_2)}$ represents the reduced mass of two atoms in the diatomic molecule and m_1 and m_2 are the masses of atoms 1 and 2, respectively.[2]

For anharmonic behaviour, the relationship between force and displacement is nonlinear leading to non-equidistant energy levels that are dependent on the amplitude of the displacement.[2, 17] The energy levels get increasingly closer together as the vibrational quantum number, υ, increases, forming a continuum of energy levels as shown by the red section of the graph in Figure 2-3. When the potential energy wavefunction reaches zero, known as the dissociation energy, D_{eq}, the bond is broken, and the atoms are no longer bound (Figure 2-3).

Selection rules are used to govern the transitions from the ground state to the excited state. Initially, for infrared absorption to occur the vibrational excitation must induce a change in the transitional dipole moment, μ, these vibrations are known to be IR active.[3] For vibrational transitions, the selection rules are stated in terms of the change in the vibrational quantum number, υ, which must be an integer value. The fundamental transition is defined as the transition of the molecule from the ground vibrational state to the first excited vibrational state ($\upsilon_0 \rightarrow \upsilon_1$).[17] For anharmonic vibrations, the $\Delta\upsilon = \pm 1$ selection rule is no longer valid and υ can be any number. This gives rise to overtone and combination vibrational modes which result from the transition of the ground state to higher energy levels. Overtones occur when a vibrational mode is excited from $\upsilon_0 \rightarrow \upsilon_2$, which is known as the first overtone, or $\upsilon_0 \rightarrow \upsilon_3$, the second overtone, etc. While the overtone bands tend to be multiples of fundamental frequencies in the harmonic oscillator, the anharmonic oscillator calculations indicate that overtones are usually less than the multiples of the fundamental frequency.[3, 19] As the energy levels are much closer together in the anharmonic model (red lines in Figure 2-3), there is a higher chance of them being occupied. This is reflected in the form of weaker intensity bands in the IR spectra. While most overtone bands appear in the near-IR region, for some functional groups such as those involving aromatic rings, some appear in the mid-IR region providing additional information about their molecular structure.[20] When two fundamental bands appear at the same frequency, combination bands are often shown in the IR spectrum.

2.1.2 Vibrational Modes

The number of vibrational modes for a given molecule is dependent on its structure and the change in dipole moment due to the motion of atoms.[19] For centrosymmetric molecules, there is no change in the transition dipole moment, and hence they are IR inactive. In heteronuclear molecules such as HCl and CO, the dipoles are permanent making them IR active with strong absorption bands, while the diatomic homonuclear molecules such as N_2 and O_2 have no dipole moments and are thus IR inactive.[21] The position of each atom in a molecule can be expressed across three axes, x, y, and z, which allows for three degrees of freedom for molecular motion. For a non-linear molecule with N atoms, there are 3N – 6 vibrational modes, while there are 3N – 5 modes of vibrations in a linear molecule due to the loss of one of the rotational degrees of freedom.[3]

In the mid-IR region, there are usually two types of vibrations observed, vibrations along the bond length, also known as the stretching vibrations (*v*) and vibrations involving changes in

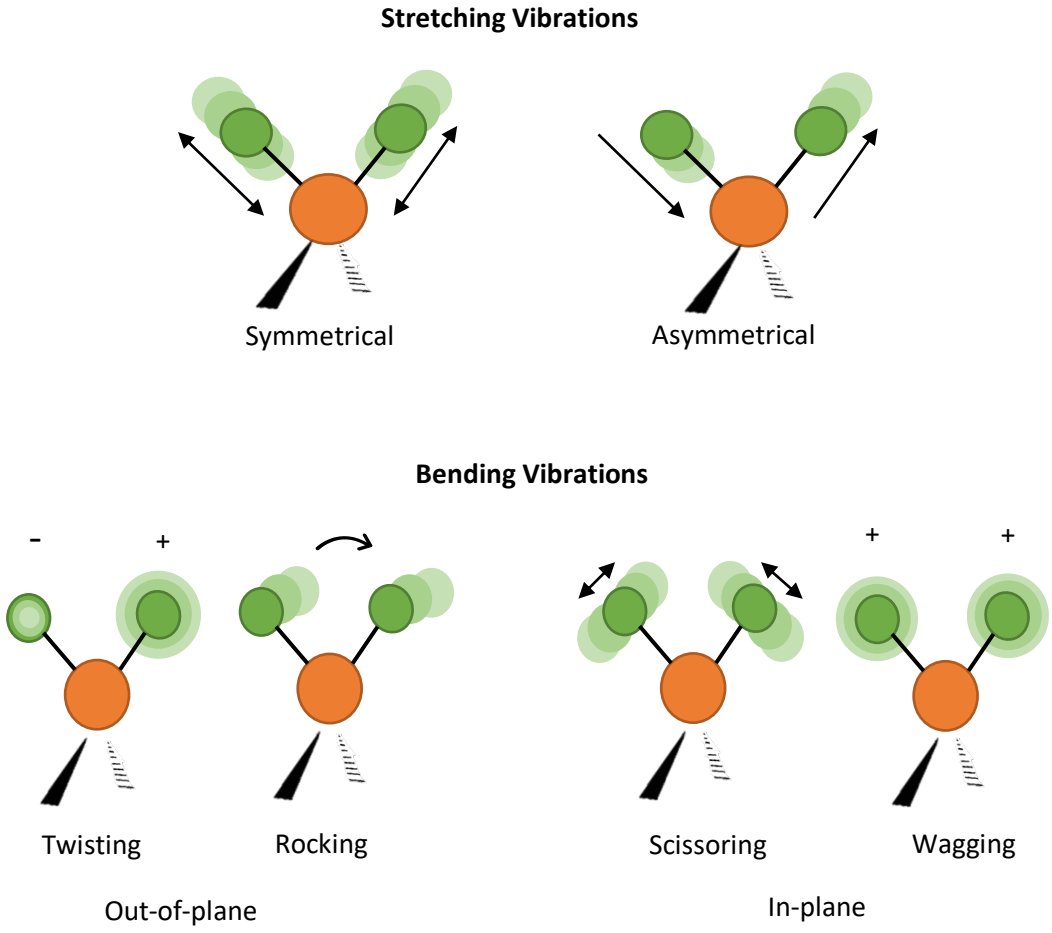

Figure 2-4: Molecular vibrations observed for non-linear molecules in mid-IR spectroscopy.

bond angles also known as bending vibrations (δ – in-plane; π – out of plane).[22] A summary of these vibrations is shown in Figure 2-4. The stretching vibrations can be symmetric or asymmetric and alter the bond length, while the bending vibrations due to changing bond angles can be described as twisting, rocking, scissoring, and wagging.

During these light-induced bond vibrations, the incident light shone upon a sample can be transmitted, reflected, absorbed, or scattered when it encounters the sample. The fundamental principle of IR spectroscopy is governed by Beer-Lambert's Law, which relates the absorbance of the intensity of the incident radiation before, I_0 and after, I, is passed through the sample.[2] The absorbance of IR light, A, is directly proportional to the

concentration of a given sample, c, the molar absorptivity, ε, in L mol^{-1} cm^{-1} and the pathlength, *l,* in cm.

$$A = \varepsilon cl = log_{10}(\frac{I_0}{I}) \quad (2.8)$$

Therefore, IR spectroscopy can be used to quantify the concentrations of substances present in the sample. Various functional groups show characteristic vibrational bands across the mid-IR range of 4000 – 400 cm^{-1} and are thus used to identify compounds. This makes IR spectroscopy a valuable technique for the identification of a variety of molecules including chemicals and biomolecules such as lipids, proteins, and carbohydrates in biofluids.

2.2 Fourier Transform Infrared Spectroscopy

Fourier transform infrared (FTIR) spectrometers were developed to achieve faster spectral collection and better spectral sensitivities in comparison to their older counterparts.[23] Faster acquisition times achieved through the use of an interferometer in an FTIR spectrometer allows for multiple scans to be collected and co-added which leads to improved spectral quality. Furthermore, with the use of sensitive detectors, a higher signal-to-noise ratio is achieved using FTIR instrumentation. In this thesis, an FTIR spectrometer with an ATR sampling accessory was used for all analyses. The principles of these are described in more detail in this section.

2.2.1 Instrumentation

Fourier transform infrared spectrometers consist of a light source, an interferometer and a detector that is used to collect the spectrum. The light source generates IR radiation, which interacts with the sample after collimation via an interferometer and is later collected at the detector. This signal is amplified and converted into a digital signal which is then transferred to a computer. A Fourier transform is applied to the signal which converts a time-dependent interferogram into a frequency spectrum. Typically, it is presented as wavenumbers plotted against the transmission (%T) or absorbance (-log$_{10}$ of the transmittance spectrum).

2.2.1.1 Light Sources

The most common light source used in a traditional benchtop FTIR instrument in the mid-IR region is a silicon carbide rod, also known as Globar, and is resistively heated by passing an electric current through it to produce IR radiation.[19] This behaves as a blackbody source

where the radiance is dependent on its heating, creating IR radiation in the wavenumber range of 7000 – 600 cm^{-1}.[24]

2.2.1.2 Michelson Interferometer

A Michelson interferometer is an integral part of all FTIR instruments available today. It consists of a beam splitter and two mirrors (one stationary and one moving) at a perpendicular angle to each other (Figure 2-5). The IR light is split into two paths by the beam-splitter, one is transmitted to the moving mirror while the other is transmitted to the fixed mirror before being recombined at the same beam-splitter and then sent to the detector.[23] The moving mirror oscillates at a precise velocity, and so the distance travelled by this beam is different to that of the stationary beam, creating a path difference between the two beams. Therefore, when they are recombined, the frequencies will interact either constructively or destructively creating an interference pattern, also known as an interferogram, which is the measurement of IR light intensity as a function of time. To correctly calculate the exact difference between the path lengths, a He:Ne laser experiencing the same optical path difference is used as a reference.[23]

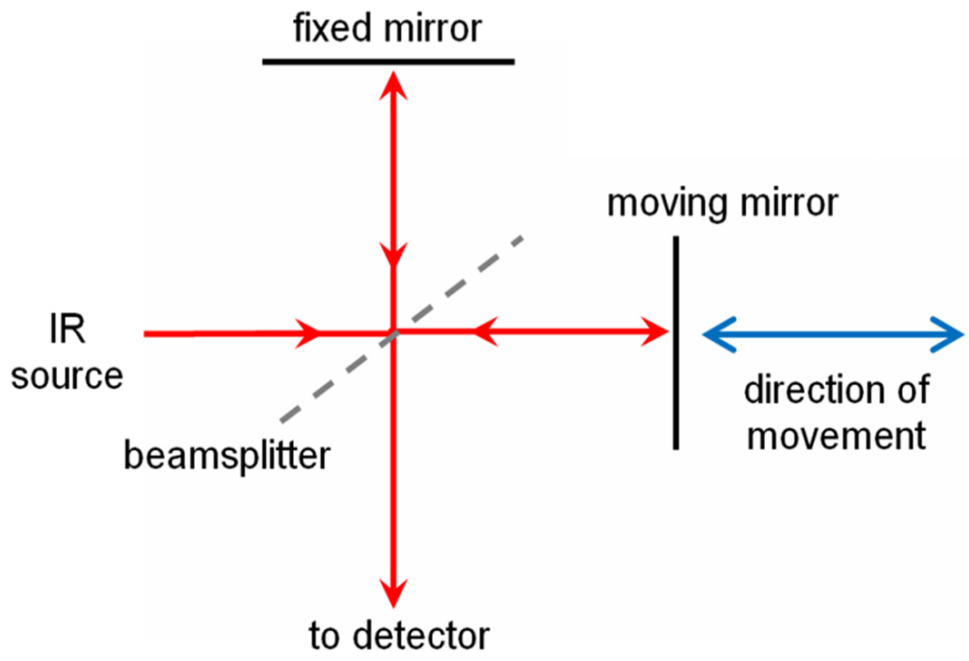

Figure 2-5: Schematic of a Michelson interferometer used to measure an FTIR interferogram. Figure adapted from Baker *et al*. 2016.

2.2.1.3 Detectors

There are commonly two types of FTIR detectors, thermal and quantum. Pyroelectric detectors are one type of thermal detector that consists of a ferroelectric material such as deuterated triglycine sulfate (DTGS) and lithium tantalate ($LiTaO_3$). The thermal detectors treat the IR beam as heat and detect the changes in temperature of the absorbing material. This change is measured by one of the physical properties of that material, such as resistivity, magnetisation, and pressure. Such materials exhibit a large spontaneous electrical polarisation at temperatures below their Curie point which is the temperature at which certain materials lose their permanent magnetic properties, to be replaced by induced magnetism.[19] The degree of polarisation is dependent on the temperature. By placing this material between two electrodes, a temperature-dependent capacitor is created. This capacitance changes with the heat applied through the incident IR radiation. This change in the capacitance is measured as the detector response in voltage.

While both DGTS and LiTaO3 detectors are high performance, a FTIR instrument with a $LiTaO_3$ detector was used in this thesis. The DGTS detector has a high signal-to-noise ratio but require temperature monitoring as it has a Curie point close to room temperature making its response very sensitive to temperature changes. LiTaO3 other the other hand, do not require cooling due to its higher Curie temperature allowing for simpler instrumentation and higher working temperatures.[25, 26]

Therefore, it must be used in conjunction with a thermostat for best performance. The $LiTaO_3$ detector on the other hand does not require temperature control eliminating the need for a thermostat and simplifying the electronics in the instrumentation. Additionally, low manufacturing costs of the IRE material also contribute to the overall cost saving. While the DTGS detector tends to be more sensitive, a comparable signal-to-noise performance is achieved with a $LiTaO_3$ detector by measuring sixteen scans of the sample with only a few extra seconds.

2.2.2 Background Spectrum

It is standard protocol to collect a background spectrum before sample analysis. An example of this is shown in Figure 2.6 where bands associated with atmospheric gases such as water vapour and carbon dioxide are highlighted. These two gases are commonly present in the ambient environment in high enough concentrations that they can result in unwanted bands.

In single-beam instruments, these can interfere with the spectral signatures of the sample by adding unwanted bands or obscuring important sample peaks. Therefore, collecting background spectrum removes all the environmental influences and allows for collecting a more accurate information about the sample.

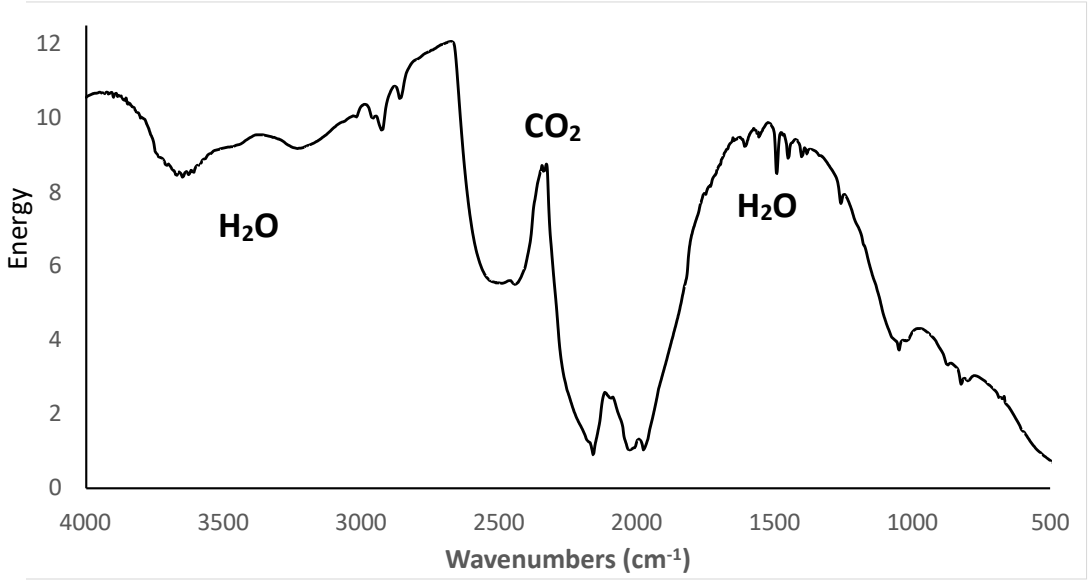

Figure 2-6: A background spectrum collected before sample analysis that shows atmospheric gases such as water vapour and carbon dioxide.

2.3 Sampling Modes

The main sampling modes employed in FTIR spectroscopy are transmission, reflectance (diffuse and specular) and attenuated total reflectance (ATR).[27] In transmission mode, light from the interferometer passes through the sample and the transmitted energy is measured at the detector to generate a spectrum. This mode can analyse many types of samples, but it can require extensive sample preparation, for example, making of KBr discs which can be time-consuming and may not be possible in the case of polymers. Diffuse reflectance measures the light that is scattered off the sample and is therefore useful in analysing rough samples such as powders. Specular reflectance, on the other hand, measures the light that is reflected off the surface of a sample and is useful in analysing flat, shiny samples or surface coatings. While these modes are useful in their own right, the ATR mode was used in this study. The principles and reasons for choosing this mode are described below.

2.3.1 Attenuated Total Reflectance (ATR) Mode

ATR utilises the principle of total internal reflection (TIR) without the IR beam directly passing through the sample. When a beam of IR radiation passes through a medium with a higher refractive index into a medium with a lower refractive index, total internal reflection (TIR) occurs at the interface provided that the angle of incidence is greater than the critical angle (Figure 2-7). This internal reflection creates an evanescent wave that extends beyond the crystal, also known as the internal reflection element (IRE) and into the sample on top of the IRE surface. The penetration depth of this wave into the sample is typically 0.5 – 5 µm and thus direct contact between the sample and the IRE is necessary. In the regions where the energy of the wave is absorbed by the sample, the evanescent wave is said to be attenuated and the resultant beam is sent to the detector. Attenuation of the evanescent wave happens at frequencies characteristic to the molecules being studied and creates the IR spectrum that is representative of the sample.

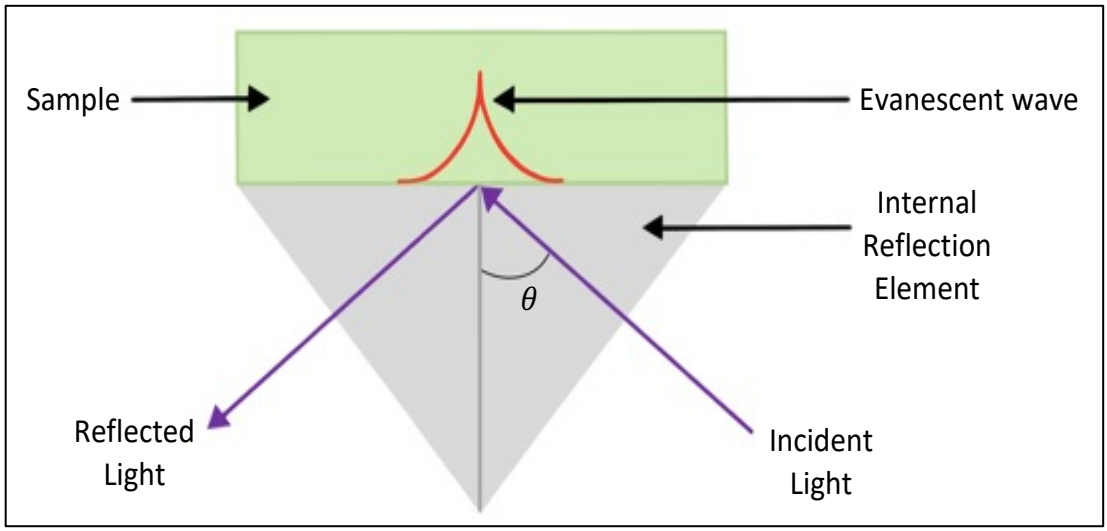

Figure 2-7 Schematic representation of the ATR sampling mode through a traditional diamond crystal (here labelled as internal reflection element), where θ represents the angle of incidence.

Two important factors in choosing the IRE material are a high refractive index and the depth of penetration of the evanescent wave. Commonly used IREs are diamond, germanium (Ge) and zinc selenide (ZnSe). These are chosen so that they have a much higher refractive index in relation to the samples being analysed. Diamond is the gold standard because it is a chemically inert and robust material. However, it is also the most expensive. ZnSe is a suitable alternative IRE material as it is inexpensive and has a high refractive index and depth of

penetration similar to diamond. Though ZnSe is a softer material than diamond, it is suitable for most routine analyses in 5 to 9 pH range including liquid samples such as the biofluids analysed in this thesis. The depth of penetration is dependent on other factors such as angle of incidence and sample properties such as thickness and composition. The angle of incidence was fixed in the instrument employed in this thesis. While it was not possible to exactly control the sample thickness, all processes relating to the deposition of the sample on the crystal were kept constant to maintain consistency across all analyses.

ATR mode is commonly used in routine analyses of surface studies, films and solutions because of non-destructive sampling with minimal to no sample preparation.[28-30] It is versatile, easy to use, and has low running costs with rapid data acquisition. One of the main advantages of the ATR mode is that in the case of air-dried liquid samples, which tend to create dry films of variable thickness, the signal is not impacted due to the smaller pathlength into the sample as defined by the penetration depth of the evanescent wave (0.5 – 5 μm). Moreover, consistent results obtained with small sample volumes (0.5 – 3 μL) and minimal expertise make this mode even more attractive in routine operations.[23, 31, 32] Finally, ATR-FTIR spectrometers are commonly found in most labs which reduces the costs associated with purchasing new instrumentation and makes use of already established equipment in an innovative approach.

There are some limitations to this sampling mode when measuring liquid samples such as biofluids. These include long drying times for liquid samples, the effects of the intense water vibrations in the mid-IR region, surface variations introduced by air drying such as the coffee-ring effect, cracking of dry films and the Vroman effect for serum samples.[32-36] Reducing the sample volume (0.5 – 3 μL) has been effective in reducing the drying times.[32] The spectral interferences from water absorption, and the Vroman effect, where low molecular weight proteins attach to the surface first, followed by the adsorption of larger protein molecules sometime after the drop is deposited on the surface, can be mitigated by allowing the sample to fully dry.[36, 37] The impact of spectral artefacts and variations caused by the cracking can be minimised by employing a variety of pre-processing methods following data collection.

2.3.2 Spectral Signatures of Biological Materials

The characteristic spectra for different biological materials are shown in Figure 2-8. Spectroscopically, the most important region in the IR spectrum is the fingerprint region (1800 – 900 cm^{-1}) as it contains fundamental vibrations of most of the biomolecules such as proteins, lipids and carbohydrates. There are naturally occurring variations observed in the concentrations of these biomolecules due to variations in age, sex, ethnicity, genetics, differences in collection times and other environmental factors.[11, 38] In the presence of foreign substances such as drugs, the inherent variations in biofluids are further complicated in their spectra. Pooled human serum purchased from a commercial tissue bank was used in this thesis to help mitigate some of the naturally occurring individual variations and obtain an average serum sample that is thoroughly tested for the presence of any other interfering factors.

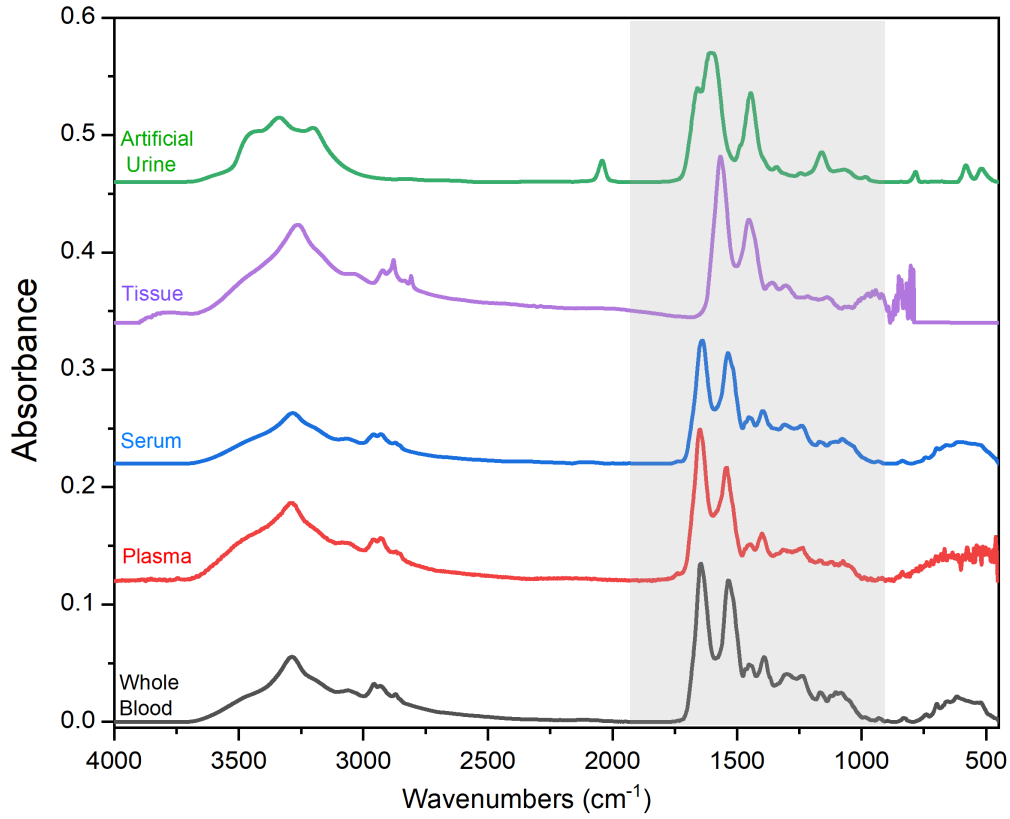

Figure 2-8 Stacked spectra of various biological samples including whole blood, plasma, serum, tissue, and artificial urine. The grey area highlights the fingerprint region (1800 – 900 cm^{-1}). All spectra were collected as part of this thesis.

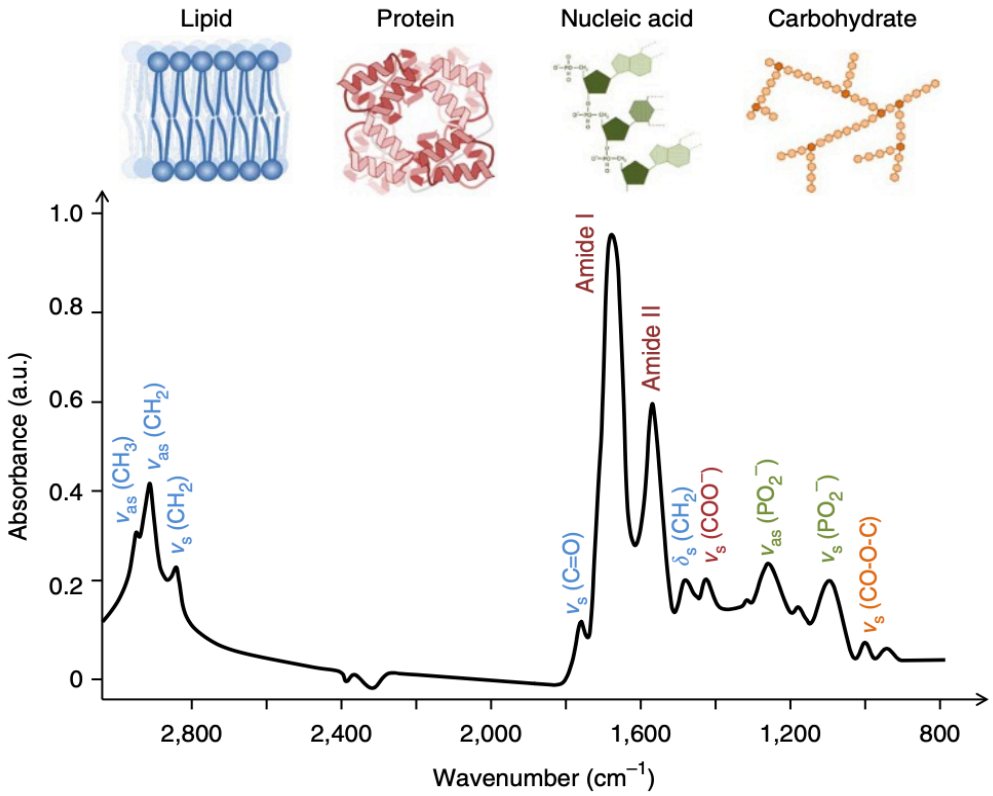

Figure 2-9: FTIR spectrum showing the four primary types of biomolecules found in a biological sample. The spectrum is labelled with peaks assigned to specific vibrations found in each of these biomolecules. (Reproduced from Baker *et al*. 2016).

For serum, some of the most important bands in the fingerprint region are the characteristic amide I and amide II bands representative of the amide (peptide) bonds that link amino acids in proteins and polypeptides (Figure 2-9). The stretching vibrations of the C=O bond lead to the amide I absorption band near 1650 cm^{-1}, with smaller contributions from CN stretching, and deformation of CCN and NH in-plane bending vibrations.[39] While the out-of-phase combination of the NH in-phase bend and the CN stretching vibration with minor contributions from CO in-plane bending and the CC and NC stretching vibrations gives rise to the amide II band at ~ 1550 cm^{-1}.[39, 40] Though the changes in location and amplitude of the amide I band and amide II are reflective of the secondary structures of a protein.[40] These are useful when looking at the presence of drug molecules in serum as a considerable portion of drug molecules are found to be protein-bound. Though it might be difficult to isolate these differences caused only by the protein-bound drug molecules without some prior sample preparation, they are still useful when identifying spectral signatures of the total amount of drugs present within the biofluids.

Similarly, IR characterisation of urine is useful in identifying variations in its components which can not only serve as potential biomarkers for disease diagnosis, but it can also allow for the identification of any foreign substances present in it. In this thesis, artificial urine, Surine™, was used for all urine analyses and the air-dried ATR-FTIR spectrum for a blank sample is shown in Figure 2-10. Artificial urine is used in this study to mitigate the effects of individual variation, to remove the need for the lengthy process of ethical approval and to address safety concerns as recent research into creating artificial alternatives to urine has shown great promise.[41] Spectroscopically, this artificial urine formulation is similar to real urine from healthy volunteers and other commercially available artificial urines as seen in the literature, though the exact peak positions vary slightly depending on the concentration of components.[41-44] Water (95%) is the predominant component of urine with the rest comprising urea (~9.3 mg/mL), creatinine (~1.5 mg/mL), uric acid (~0.03-0.6 mg/mL), ions such as sodium (~1.17 mg/mL), potassium (~0.75 mg/mL), chloride (~1.87 mg/mL), sulphate (~0.04-3.5 mg/mL), ammonia (~0.6-1.2 mg/mL) and other ions and molecules in trace amounts.[45, 46] While numerous other components have recently been identified as present

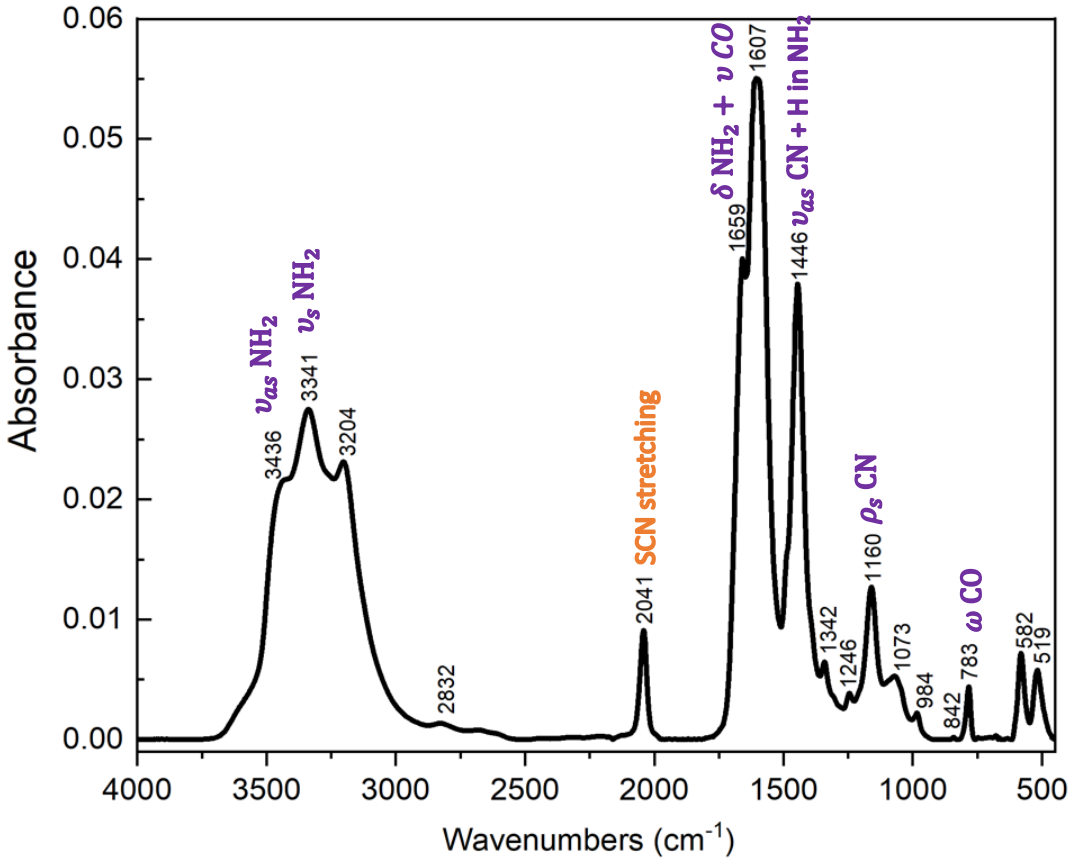

Figure 2-10: Air dried FTIR spectrum of artificial urine (Surine™) with tentative vibrational mode assignments.

in urine,[47] the main peaks observed in the IR spectrum are due to the components listed above. The high wavenumber region of the spectrum is dominated by the symmetric and asymmetric NH stretches of urea with and with minor contributions from CO stretches and NH_2 deformation vibrations (Figure 2-10).[48] Peaks seen in the lower wavenumber region at 1659, 1607, 1446, 1160 and 783 cm^{-1} are also mainly from urea with minor contributions from creatinine as illustrated by the assignments in Figure 2-10.[41, 48] Furthermore, the 2041 cm^{-1} peak is characteristic of thiocyanate presence in the urine, while the peaks below 950 cm^{-1} are a collection originating from urea, uric acid, creatinine and sodium phosphate.[41]

In post-mortem toxicology, the composition of biofluids is altered due to decomposition and is likely to have different IR spectra.[49-51] However these studies are mostly based on whole blood with the aim of identifying the time since death. Detailed spectroscopic investigations of other biofluids as well as any foreign substances found in them are lacking in the literature. This is an important distinction to note when comparing the results from the studies such as those presented in this thesis with that of post-mortem samples for interpretation.

2.4 Spectral Pre-processing

A raw IR spectrum of a biological sample is subject to spectral artefacts that arise from environmental conditions as well as instrument and sample variations. This section describes these artefacts and the necessary spectral pre-processing steps taken to minimise their effects prior to data analysis. All pre-processing was done using the PRFFECT version 2 toolbox written in the R programming language.[52] To that effect, the main aim of pre-processing is to improve the robustness and accuracy of the data, to allow easy interpretation and remove irrelevant information.[35] It is also customary to cut the IR spectrum to specific wavenumber ranges of relevance to the problem at hand, such as the 'fingerprint region' (1800 – 1000 cm^{-1}) that is of interest when examining biomolecules for disease-specific information. However, in the case of drug samples, it is more likely that the drug spectral signatures are spread across the entirety of the mid-IR spectrum. Therefore, the entire recorded spectrum was typically used in this study. In some cases, where relevant spectral signatures were more focused in a narrower wavenumber region for example 450-2200 cm^{-1} region for urine samples, the spectra were cut to this spectral region.

2.4.1 Baseline Correction

As IR spectroscopy is a technique that involves the interaction of light with matter, it is prone to the effects of scattering as well as the absorbance of IR radiation. As samples were air-dried it is not possible to have a perfectly flat sample surface without the presence of surface features, such as cracks, creating another source for scattering artefacts.[53, 54] This can cause an offset or sloping baseline, which makes spectral comparisons difficult and even replicates of the same sample can appear different.

Rubberband baseline correction was employed in this thesis which is appropriate when the distortions to the baseline are complex and irregular.[55] In this procedure, smoothing splines are fitted to the spectrum through the supporting points selected by an algorithm.[52, 54] The supporting points are chosen to find the troughs or convex hulls under the spectrum. The spectrum is then pulled down at these points to produce a corrected version. Noise cut-off levels of 0.1 were set during the application of this method to raw data in this thesis. This is illustrated in Figure 2-11 where the average raw spectrum of blank serum is depicted in black

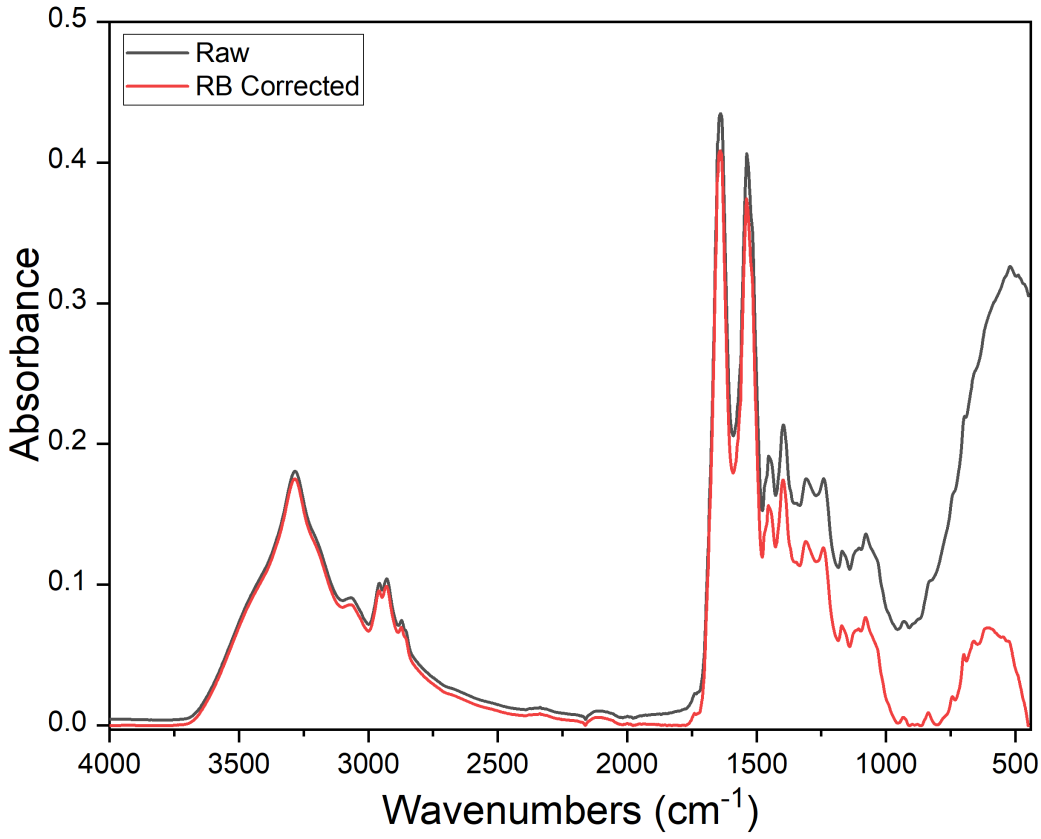

Figure 2-11: Average raw spectra for air-dried blank serum (in black) and baseline corrected using rubberband correction algorithm average spectra for blank serum (in red).

showing a variable baseline and the rubberband baseline-corrected spectrum is shown in red.

2.4.2 Normalisation

Some form of normalisation is often used in IR analysis to allow an effective comparison across different sets of samples so that they are all scaled within a similar range.[56] In the analysis of air-dried liquid samples it accounts for the differences in sample quantity and/or thickness due to air-drying. Throughout this thesis, the vector normalisation method was used. It contains two stages, initially by calculating the mean spectral absorbance which is subtracted from the spectrum, otherwise known as mean-centering, and secondly, each spectrum is divided by the square root of the sum of the squares of the mean-centered values.[54] In this way, the sum of all absorbance values squared is equal to one.[52, 54, 56] Figure 2-12 (blue trace) illustrates the reduction in spectral variability across the repeats achieved

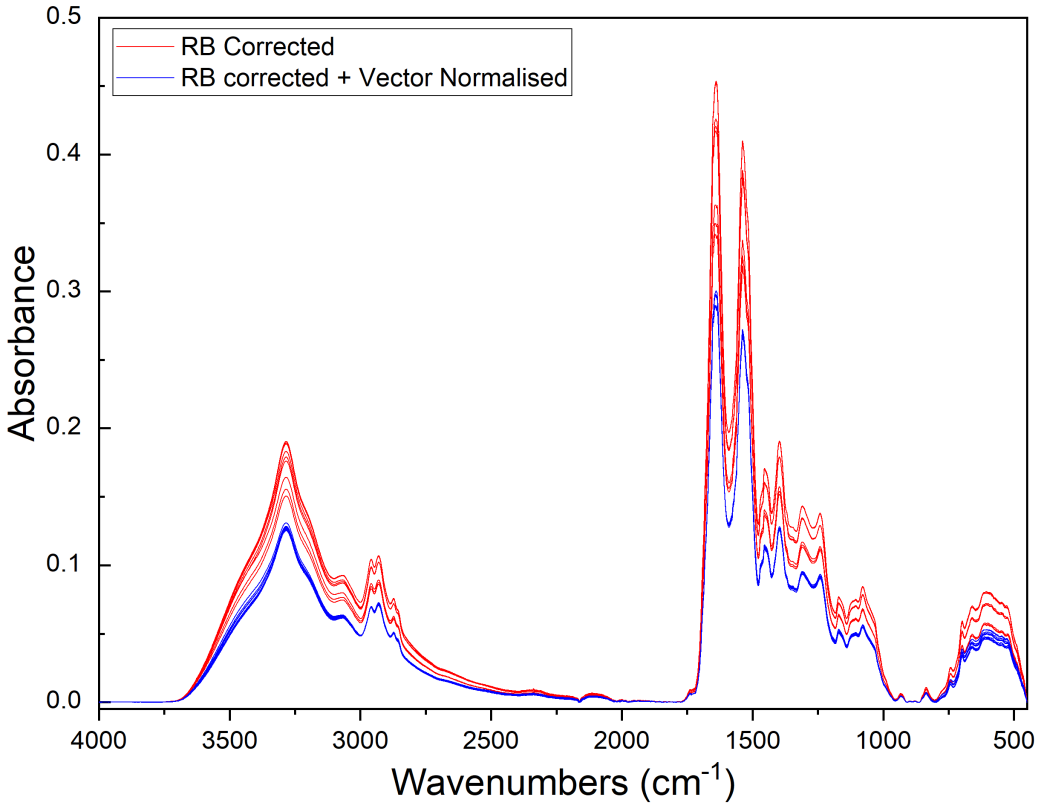

Figure 2-12: Baseline corrected spectra in red show variation across repeats, which is significantly reduced in the vector normalised spectra shown in blue.

through this process whereby normalised spectra for the same sample are virtually superimposed upon each other.

2.4.3 Smoothing

Smoothing algorithms are often applied to IR spectra to reduce inherent noise in the dataset. The most common method used for smoothing is known as the Savitzky-Golay (SG) filter, which minimises the high-frequency noise while maintaining peak morphology.[54] The SG filter fits a polynomial (order = 2) to a fixed number of data points within a moving window in order to smooth the signal.[57] This is illustrated by the spectra in black in Figure 2-13 where smoothing is applied along with other pre-processing methods previously mentioned. Therefore, the value of the pre-processing methods is demonstrated when the final result of all pre-processing methods is compared to that of the raw spectra.

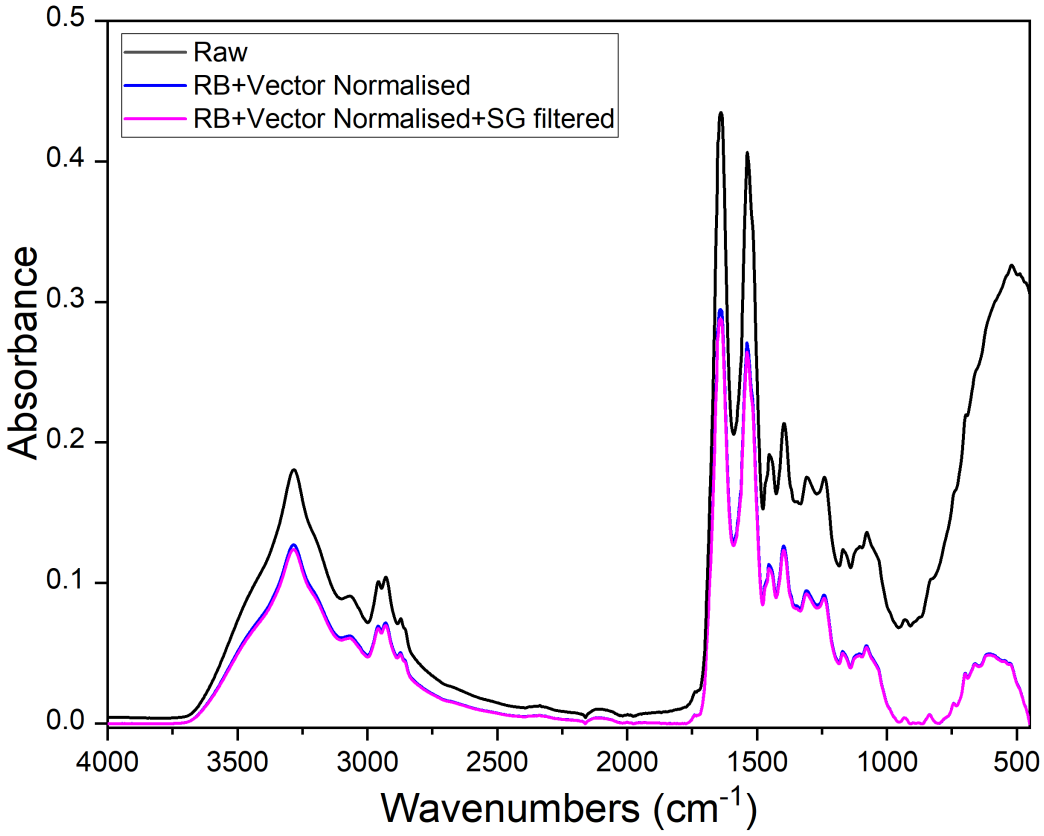

Figure 2-13: Final step of pre-processing where SG filter is applied for noise reduction (shown in magenta).

2.4.4 Spectral Derivatives

Spectral derivatisation is another way to remove baseline drifts and enhance spectral features.[56, 58] The derivatives are obtained by differentiating the absorbance intensity with

respect to wavelength and most commonly the first or second orders are used. The first-order derivative passes through zero at the same wavelength as the peak maximum in the raw spectrum and has a positive and negative band on either side in which the maximum and

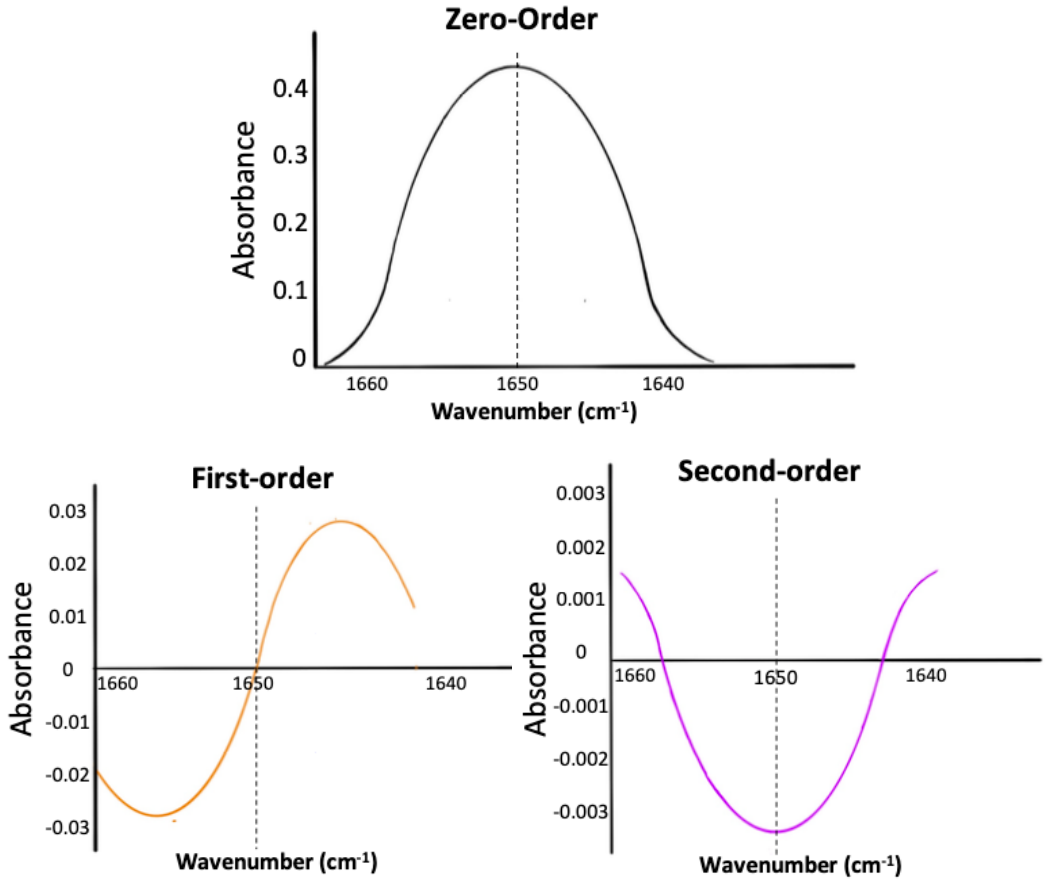

Figure 2-14: Representation of zero-order absorption band (top) and their corresponding first-order (bottom left) and second-order (bottom right) derivatives.

minimum fall at the inflection points in the absorbance band (Figure 2-14).[59] The second derivative displays a distinct negative peak at the same wavelength as the peak maximum on the original absorption spectra (Figure 2-14). Second-order derivatives are particularly useful in resolving overlapping broad peaks in the spectra and can lead to better classification models for predictive analysis.[36] However, noise is inadvertently introduced using this process and thus should only be used on spectra with high SNR. Second-order derivatives are utilised in later chapters in addition to the pre-processing options previously described for discrimination purposes.

2.5 Spectral Analysis

Spectroscopic investigations of biofluids lead to very large datasets whereby visual inspection or single peak analysis is neither helpful nor efficient. Hence it is essential to apply appropriate multivariate data analysis techniques for spectral interpretation. Previous work has shown that multivariate data analysis methods such as random forest (RF), partial least squares (PLS) - discriminant analysis and support vector machine have provided promising results in disease diagnostics in clinical setting.[60-64] This section describes two such methods – RF and PLS-DA that have been used in this thesis.

2.5.1 Random Forest

Data classification is a step-wise process which initially involves training a model on known data followed by testing the model on new, unseen, data. Random forest (RF) is a supervised machine learning method that builds a 'forest' or ensemble of decision trees which is used for classification or regression purposes. In a classification process, the observations or spectral features, here are represented in the branches of the tree, while the leaves represent the class labels (Figure 2-15). The classification predictions are made where each tree in the forest casts a vote for the class label of samples in the test data.[65] The final predictions are then reported as the majority vote of all the decision trees.

The decision trees are sensitive to the specific data they are trained on, in order to overcome this, data bagging is often utilised which allows RF to randomly sample the training dataset with replacement at each decision tree.[66] This means that the samples included in the original training dataset may occur zero, once or multiple times in any given tree. The features, which refer to wavenumbers in this instance, are selected from a random subset of a predetermined size from the full set of possible descriptors to allow for branching at each node.[52] This feature randomness creates distinct trees that are less correlated. In RF, the three main tuning parameters are the number of trees, *ntree*, the number of features/variables available at each decision tree for splitting, *mtry*, and the depth of trees which is referred to as *nodesize*.[67] The RF method was shown to be insensitive to training parameters *ntree*, *mtry* and *nodesize*.[66] While Palmer *et al*[66] suggested that values below 250 for *ntree* should not be used to prevent deterioration of data, higher values (greater than 500) did not show an improvement in classification but were only computationally cumbersome. While values lower than 40 for *mtry* mean that there are not enough

descriptors available at each split reducing the quality of the overall prediction, the values were obtained from the number of variables in the relevant dataset.[52, 66, 68] With this in mind, default values of 500 and 1 for *ntree* and *nodesize* respectively, were used. The parameter *mtry* was set at 59 which was derived by taking the square root of the number of variables (3550).

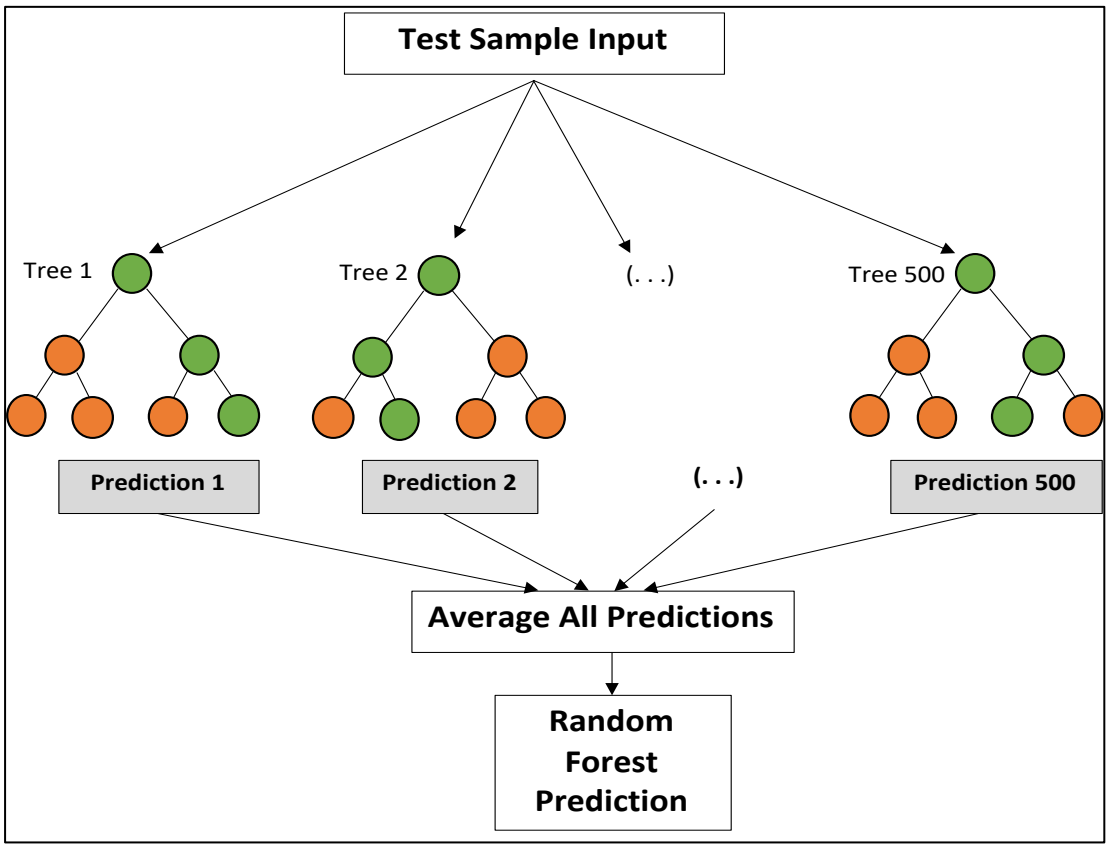

Figure 2-15: Generic structure of a random forest ensemble model.

In order to evaluate the accuracy and reliability of the classification algorithm (defined in the next section 2.5.2), the classification values are reported in terms of true positives (sensitivity), true negatives (specificity), false positives and false negatives. Another important result gathered from RF analysis is the RF importance plot that shows the Gini coefficient with respect to wavenumbers (Figure 2-16).[69] These rank the wavenumbers in the order of importance for that model and thus can be used to highlight spectral features of importance for discrimination (Figure 2-16).[47]

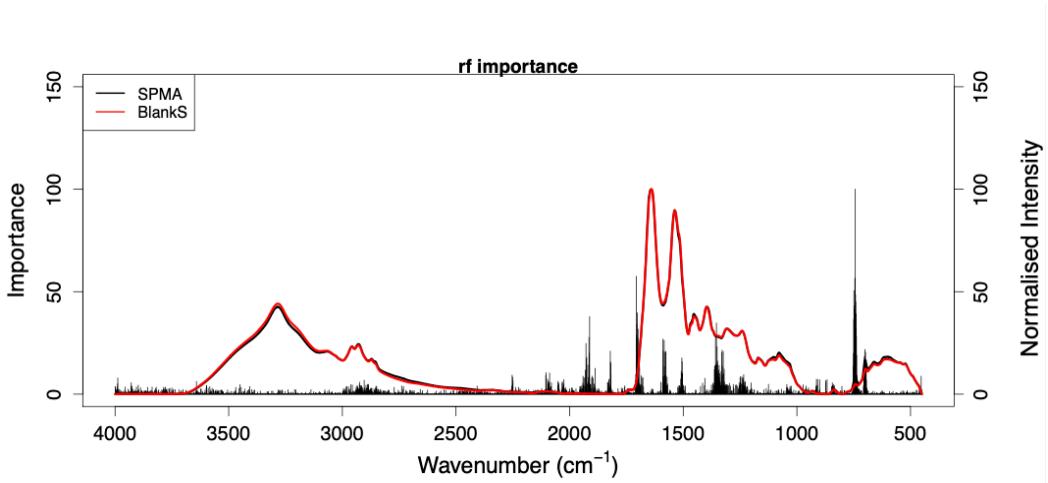

Figure 2-16: Average mean spectrum, superimposed on Gini Importance plot for RF analysis of serum samples with MA (labelled here as 'SPMA' shown in black) and blank serum samples (labelled here as 'BlankS' shown here in red).

2.5.2 Partial Least Squares analysis

The original non-linear iterative partial least squares (NIPALS) algorithm developed by Wold,[70] has been refined and extended to classification purposes in the field of chemometrics.[65] PLS – discriminant analysis is a variant of PLS regression (PLSR) where the Y variable is categorical instead of continuous as seen in the regression method.[71] PLS-DA is a supervised machine learning method that uses linear discriminators for classification purposes.[72] It extracts the necessary information from complex datasets with a large number of variables by reducing their dimensionality to understand the underlying patterns within the data.

The explanatory variables represented as a matrix, **X**, are the absorbance values for each of the wavenumbers being measured, while the response variables are represented as a **Y** matrix. For regression analysis, the response variables are continuous such as the concentration of analytes, while for classification analysis these are categorical such as the group membership of the sample spectra. The algorithm creates latent variables (LVs) that are linear combinations of the original variables in **X** as well as **Y** datasets in an iterative process in such a way that maximises covariance (correlation and variance) between **Y** and **X**. This separates the data allowing for discrimination between groups. This PLS model can then be used to test new unknown samples not used during model-building for the prediction of class membership.

The optimal number of components is chosen to minimise the cross-validation error which provides the most reliable model. The results of PLS-DA analysis are scores and loadings, whereby the loadings explain the variance by highlighting those wavenumbers in **X** with the greatest disparities in **Y** and the scores allow for visual discrimination between classes. The prediction accuracies and model reliability are determined through sensitivity, specificity, kappa and balanced accuracy parameters.

Sensitivities and specificities refer to the number of correct and incorrect predictions made by the model in the test set that is used for model evaluation (Equations 2.8 and 2.9). In a binary classification (blank serum samples versus those with drugs present), sensitivity denotes the ability of the model to accurately identify the samples with drugs present, while specificity refers to the ability of the model to correctly identify the blank samples. The values of true positives (TP) and true negatives (TN), as assigned by the model, were obtained when at least two or more spectra out of their 3 were correctly assigned to drug samples and to blank matrix samples respectively.

$$Sensitivity = \frac{True\ Positives}{True\ Positives + False\ Negatives} = \frac{True\ Positives}{Positives} \tag{2.8}$$

$$Specificity = \frac{True\ Negatives}{True\ Negatives + False\ Positives} = \frac{True\ Negatives}{Negatives} \tag{2.9}$$

In this situation the overall model performance was measured using the balanced accuracy which is defined as the average accuracy of each class, also known as the average of the sensitivity and specificity of the model (Equation 2.10):

$$Balanced\ accuracy = (\frac{TP}{P} + \frac{TN}{N})/2 \tag{2.10}$$

The reliability of the predictive model is determined by examining the Kappa value, κ, which quantifies the magnitude of agreement between the observed accuracy of prediction from the classification model with that of expected accuracy including that of a random chance.[73] The values of Kappa range from below zero to 1 and are reflective of the level of agreement between the classifiers. Values of $\kappa \leqq 0$, in general, indicate no agreement, 0.01-0.2 show

slight, 0.21-0.40 fair, 0.41-0.60 indicate moderate, 0.61-0.80 substantial and finally 0.81-1.00 show almost perfect agreement.[73, 74]

2.5.3 Sampling Methods

The models generated throughout this thesis are influenced by the samples used to build the model as well as the number of samples within each class. More specifically for drug samples in biological fluids, higher drug concentrations show greater spectral variation compared to lower concentration samples, which tend to be more subtle in their differences. The inclusion or exclusion of these samples from the dataset used to build the model can create a biased model.[65, 75] In addition, an uneven number of samples can bias the model to the class with the higher number of samples. In order to account for the class imbalance between the number of blank and drug samples, various resampling methods were employed in this thesis. Three sampling methods are used throughout this thesis, up-sampling, down-sampling and synthetic minority over-sampling (SMOTE) technique. The up-sampling method repeatedly samples the minority class with replacement to increase the number of samples for that class. Conversely, the down-sampling method reduces the majority class to the same size as the minority class by randomly selecting a subset of the majority class.[76] The SMOTE sampling on the other hand artificially generates 'new' data points to achieve a more balanced dataset.[75]

In simplest terms, up-sampling can be thought of as oversampling where samples from a minority class can be present in duplicates. The main advantage of this method is that no data points are deleted, and no information is lost. However, as this method is duplicating data, it can lead to overfitting. Down-sampling on the other hand is the opposite where samples from the majority class are discarded so that both classes are balanced. The main disadvantage of this method is that some data is lost in the process. However, this might not be a major issue if the large datasets and the class disparity are not too large. The SMOTE sampling can be effective in balancing out class inequalities, but it can also over-generalise the data especially if the existing minority class is not representative of the true distribution causing the synthetic samples not to reflect the actual diversity and nuances of the minority class. Ling and Li however have demonstrated that under-sampling of the minority class tends to lead to better results than up-sampling, and a combination of the two methods showed no significant improvement in the results.[77] With the dataset generated in this thesis,

all three methods were tried on all datasets where class imbalance was observed and those models that performed the best are reported.

2.6 References

1. A. Koleżyński, in *Molecular Spectroscopy—Experiment and Theory: From Molecules to Functional Materials*, eds. A. Koleżyński and M. Król, Springer International Publishing, Cham, 2019, pp. 1-48.

2. M. J. Hollas, *Basic Atomic and Molecular Spectroscopy*, Royal Society of Chemistry, Cambridge, 2002.

3. C. Banwell and E. McCash, *Fundamentals of Molecular Spectroscopy*, McGraw-Hill Publishing Company, London, 4th edn., 1994.

4. R. J. Ouellette and J. D. Rawn, in *Organic Chemistry*, eds. R. J. Ouellette and J. D. Rawn, Academic Press, London, 2nd edn., 2018, ch. 14, pp. 409-425.

5. B. C. Smith, *Fundamentals of Fourier Transform Infrared Spectroscopy* CRC Press, Boca Raton, 2nd edn., 2011.

6. P. J. Larkin, in *Infrared and Raman Spectroscopy*, ed. P. J. Larkin, Elsevier, Oxford, 2nd edn., 2018, ch. 1, pp. 1-5.

7. International Organization for Standardization, *Journal*, 2007.

8. L. Wang and B. Mizaikoff, *Analytical and Bioanalytical Chemistry*, 2008, **391**, 1641-1654.

9. D. Naumann, *Applied Spectroscopy Reviews*, 2001, **36**, 239-298.

10. L. M. Ng and R. Simmons, *Analytical Chemistry*, 1999, **71**, 343-350.

11. M. J. Baker, S. R. Hussain, L. Lovergne, V. Untereiner, C. Hughes, R. A. Lukaszewski, G. Thiefin and G. D. Sockalingum, *Chemistry Society Reviews*, 2016, **45**, 1803-1818.

12. H. H. Eysel, M. Jackson, A. Nikulin, R. L. Somorjai, G. T. D. Thomson and H. H. Mantsch, *Biospectroscopy*, 1997, **3**, 161-167.

13. A. A. Bunaciu, Ş. Fleschin, V. D. Hoang and H. Y. Aboul-Enein, *Critical Reviews in Analytical Chemistry*, 2017, **47**, 67-75.

14. D. Custers, T. Cauwenbergh, J. L. Bothy, P. Courselle, J. O. De Beer, S. Apers and E. Deconinck, *Journal of Pharmaceutical and Biomedical Analysis*, 2015, **112**, 181-189.

15. M.-M. Blum and H. John, *Drug Testing and Analysis*, 2012, **4**, 298-302.

16. A. Rohman, A. Windarsih, E. Lukitaningsih, M. Rafi, K. Betania and N. A. Fadzillah, *Biomedical Spectroscopy and Imaging*, 2019, **8**, 55-71.

17. M. J. Baker, C. S. Hughes and K. A. Hollywood, *Biophotonics: Vibrational Spectroscopic Diagnostics*, Morgan & Claypool Publishers, San Rafael, California, 2016.

18. G. M. Barrow, *Introduction to Molecular Spectroscopy*, McGraw-Hill Book Company, London, 1962.

19. Normal Modes in Polyatomic Molecules, https://chem.libretexts.org/@go/page/13672, (accessed 2021/10/13).

20. Vibrational Overtones, https://chem.libretexts.org/@go/page/2401, (accessed 2021/10/13).

21. P. J. Larkin, in *Infrared and Raman Spectroscopy (Second Edition)*, ed. P. J. Larkin, Elsevier, Oxford, 2nd edn., 2018, ch. 2, pp. 7-28.

22. C. Berthomieu and R. Hienerwadel, *Photosynthesis Research*, 2009, **101**, 157-170.

23. P. R. Griffiths and J. A. De Haseth, in *Fourier Transform Infrared Spectrometry*, ed. J. D. Winefordner, Wiley-Interscience, Hoboken, New Jersy, 2nd edn., 2007, ch. 15, pp. 321-348.

24. J. Stewart and J. Richmond, *Journal of Research of the National Bureau of Standards*, 1957, **59**, 405-409.

25. D. Skoog, D. West, J. Holler and S. Crouch, in *Fundamentals of Analytical Chemistry*, Thomson Brooks, Boston (MA, USA), 2007, ch. 25, pp. 683-721.

26. Z. Liang, S. Li, Z. Liu, Y. Jiang, W. Li, T. Wang and J. Wang, *Journal of Materials Science: Materials in Electronics*, 2015, **26**, 5400-5404.

27. B. Stuart, in *Kirk-Othmer Encyclopedia of Chemical Technology*, John Wiley & Sons, Inc United States of America, 2015, pp. 1-18.

28. C. Hughes, G. Clemens, B. Bird, T. Dawson, K. M. Ashton, M. D. Jenkinson, A. Brodbelt, M. Weida, E. Fotheringham, M. Barre, J. Rowlette and M. J. Baker, *Scientific Reports*, 2016, **6**, 20173.

29. E. Diessel, S. Willmann, P. Kamphaus, R. Kurte, U. Damm and H. M. Heise, *Applied Spectroscopy*, 2004, **58**, 442-450.

30. E. Goormaghtigh, V. Raussens and J.-M. Ruysschaert, *Biochimica et Biophysica Acta - Reviews on Biomembranes*, 1999, **1422**, 105-185.

31. M. J. Baker, J. Trevisan, P. Bassan, R. Bhargava, H. J. Butler, K. M. Dorling, P. R. Fielden, S. W. Fogarty, N. J. Fullwood, K. A. Heys, C. Hughes, P. Lasch, P. L. Martin-Hirsch, B. Obinaju, G. D. Sockalingum, J. Sulé-Suso, R. J. Strong, M. J. Walsh, B. R. Wood, P. Gardner and F. L. Martin, *Nature Protocols*, 2014, **9**, 1771-1791.

32. J. R. Hands, K. M. Dorling, P. Abel, K. M. Ashton, A. Bordbelt, C. Davis, T. Dawson, M. D. Jenkinson, R. W. Lea, C. Walker and M. J. Baker, *Journal of Biophotonics*, 2014, **7**, 189-199.

33. F. Bonnier, F. Petitjean, M. J. Baker and H. J. Byrne, *Journal of Biophotonics*, 2014, **7**, 167-179.

34. R. A. Shaw, S. Low-Ying, M. Leroux and H. H. Mantsch, *Clinical Chemistry*, 2000, **46**, 1493-1495.

35. K. Spalding, F. Bonnier, C. Bruno, H. Blasco, R. Board, I. Benz-de Bretagne, H. J. Byrne, H. J. Butler, I. Chourpa, P. Radhakrishnan and M. J. Baker, *Vibrational Spectroscopy*, 2018, **99**, 50-58.

36. J. M. Cameron, H. J. Butler, D. S. Palmer and M. J. Baker, *Journal of Biophotonics*, 2018, **11**, e201700299.

37. L. Vroman, in *Interfacial Phenomena in Biological Systems*, ed. M. Bender, CRC Press, New York, 1991, vol. 39.

38. M. J. Duffy, C. M. Sturgeon, G. Sölétormos, V. Barak, R. Molina, D. F. Hayes, E. P. Diamandis and P. M. M. Bossuyt, *Clinical Chemistry*, 2015, **61**, 809-820.

39. A. Barth and C. Zscherp, *Quarterly Reviews of Biophysics*, 2002, **35**, 369-430.

40. W. Gallagher, unpublished work.

41. N. Sarigul, F. Korkmaz and İ. Kurultak, *Nature - Scientific Reports*, 2019, **9**, 1-9.

42. S. Chutipongtanate and V. Thongboonkerd, *Analytical Biochemistry*, 2010, **402**, 110-112.

43. T. Brooks and C. W. Keevil, *Letters in Applied Microbiology*, 1997, **24**, 203-206.

44. M.-C. Yu, P. Rich, L. Foreman, J. Smith, M.-S. Yu, A. Tanna, V. Dibbur, R. Unwin and F. W. K. Tam, *Nature - Scientific Reports*, 2017, **7**, 4601.

45. D. F. Putnam, *Composition and Concentrative Properties of Human Urine*, National Aeronautics and Space Administration, California, 1971.

46. C. Rose, A. Parker, B. Jefferson and E. Cartmell, *Critical Reviews in Environmental Science and Technology*, 2015, **45**, 1827-1879.

47. S. Bouatra, F. Aziat, R. Mandal, A. C. Guo, M. R. Wilson, C. Knox, T. C. Bjorndahl, R. Krishnamurthy, F. Saleem, P. Liu, Z. T. Dame, J. Poelzer, J. Huynh, F. S. Yallou, N. Psychogios, E. Dong, R. Bogumil, C. Roehring and D. S. Wishart, *PLOS ONE*, 2013, **8**, e73076.

48. S. H. Overbury, A. I. Kolesnikov, G. M. Brown, Z. Zhang, G. S. Nair, R. L. Sacci, R. Lotfi, A. C. T. van Duin and M. Naguib, *Journal of the American Chemical Society*, 2018, **140**, 10305-10314.

49. H. Lin, Y. Zhang, Q. Wang, B. Li, P. Huang and Z. Wang, *Scientific Reports*, 2017, **7**, 13254.

50. Q. Wang, H. He, B. Li, H. Lin, Y. Zhang, J. Zhang and Z. Wang, *PLOS ONE*, 2017, **12**, e0182161.

51. J. Zhang, B. Li, Q. Wang, C. Li, Y. Zhang, H. Lin and Z. Wang, *Spectrochimica Acta Part A: Molecular and Biomolecular Spectroscopy*, 2017, **173**, 733-739.

52. B. R. Smith, M. J. Baker and D. S. Palmer, *Chemometrics and Intelligent Laboratory Systems*, 2018, **172**, 33-42.

53. P. Bassan, A. Kohler, H. Martens, J. Lee, H. J. Byrne, P. Dumas, E. Gazi, M. Brown, N. Clarke and P. Gardner, *Analyst*, 2010, **135**, 268-277.

54. H. J. Butler, B. R. Smith, R. Fritzsch, P. Radhakrishnan, D. S. Palmer and M. J. Baker, *Analyst*, 2018, **143**, 6121-6134.

55. A. G. Theakstone, C. Rinaldi, H. J. Butler, J. M. Cameron, L. R. Confield, S. H. Rutherford, A. Sala, S. Sangamnerkar and M. J. Baker, *Translational Biophotonics*, 2021, **3**, 1-20.

56. P. Lasch, *Chemometrics and Intelligent Laboratory Systems*, 2012, **117**, 100-114.

57. Å. Rinnan, F. v. d. Berg and S. B. Engelsen, *Trends in Analytical Chemistry*, 2009, **28**, 1201-1222.

58. J. Ollesch, S. L. Drees, H. M. Heise, T. Behrens, T. Brüning and K. Gerwert, *Analyst*, 2013, **138**, 4092-4102.

59. A. J. Owen, *Uses of Derivative Spectroscopy*, Agilent Technologies Ltd, Waldbrann, Germany, 1995.

60. J. Backhaus, R. Mueller, N. Formanski, N. Szlama, H.-G. Meerpohl, M. Eidt and P. Bugert, *Vibrational Spectroscopy*, 2010, **52**, 173-177.

61. J. M. Cameron, H. J. Butler, B. R. Smith, M. G. Hegarty, M. D. Jenkinson, K. Syed, P. M. Brennan, K. Ashton, T. Dawson and D. S. Palmer, *Analyst*, 2019, **144**, 6736-6750.

62. H. J. Butler, P. M. Brennan, J. M. Cameron, D. Finlayson, M. G. Hegarty, M. D. Jenkinson, D. S. Palmer, B. R. Smith and M. J. Baker, *Nature Communications*, 2019, **10**, 4501-4509.

63. J. R. Hands, G. Clemens, R. Stables, K. Ashton, A. Brodbelt, C. Davis, T. P. Dawson, M. D. Jenkinson, R. W. Lea, C. Walker and M. J. Baker, *Journal of Neuro-Oncology*, 2016, **127**, 463-472.

64. A. Staib, B. Dolenko, D. J. Fink, J. Früh, A. E. Nikulin, M. Otto, M. S. Pessin-Minsley, O. Quarder, R. Somorjai, U. Thienel, G. Werner and W. Petrich, *Clinica Chimica Acta*, 2001, **308**, 79-89.

65. M. Kuhn and K. Johnson, *Applied Predictive Modeling*, Springer, New York, 2013.

66. D. S. Palmer, N. M. O'Boyle, R. C. Glen and J. B. O. Mitchell, *Journal of Chemical Information and Modeling*, 2007, **47**, 150-158.

67. E. Scornet, *ESAIM: Proceedings and Surveys*, 2018, **60**, 144-162.

68. A. Liaw and M. Wiener, *R news*, 2002, **2**, 18-22.

69. B. R. Smith, K. M. Ashton, A. Brodbelt, T. Dawson, M. D. Jenkinson, N. T. Hunt, D. S. Palmer and M. J. Baker, *Analyst*, 2016, **141**, 3668-3678.

70. H. Wold, *Multivariate analysis*, 1966, 391-420.

71. D. Ruiz-Perez, H. Guan, P. Madhivanan, K. Mathee and G. Narasimhan, *BMC Bioinformatics*, 2020, **21**, 2.

72. R. G. Brereton and G. R. Lloyd, *Journal of Chemometrics*, 2014, **28**, 213-225.

73. M. L. McHugh, *Biochemia medica*, 2012, **22**, 276-282.

74. A. J. Viera and J. M. Garrett, *Fam Med*, 2005, **37**, 360-363.

75. N. V. Chawla, K. W. Bowyer, L. O. Hall and W. P. Kegelmeyer, *Journal of Artificial Intelligence Research*, 2002, **16**, 321-357.

76. M. Bourel, A. M. Segura, C. Crisci, G. López, L. Sampognaro, V. Vidal, C. Kruk, C. Piccini and G. Perera, *Water Research*, 2021, **202**, 117450.

77. C. X. Ling and C. Li, *Proceedings of International Conference on Knowledge Discovery from Data*, 1998, **98**, 73-79.

CHAPTER THREE

DETECTION AND IDENTIFICATION OF METHAMPHETAMINE AND ITS METABOLITES IN BIOFLUIDS USING ATR-FTIR SPECTROSCOPY

Abstract

Globalization, modern technology and easy access to the internet have led to an explosion of drug compounds available for public consumption. Methamphetamine (MA) is one such drug that has a long history of abuse and misuse worldwide and is consumed in licit and illicit forms. There are numerous state-of-the-art techniques developed for the screening of MA in biofluids, but these are plagued by tedious sample preparation, the need for solvents and expensive instrumentation. This is especially of consequence when consumption of illicit MA is suspected because all these methods are specifically developed for MA and will not always account for the presence of other impurities/substances in the sample.

FTIR spectroscopy has been employed in the analysis of powder samples from drug seizures as well as for the detection of biomarkers in biofluids. However, a combined approach to detecting drugs in biofluids has not been extensively explored. In this chapter, it is shown that ATR-FTIR spectroscopy can be applied in this context allowing for drug detection without prior sample extraction. Using methamphetamine (MA) as an example, this chapter outlines the proof-of-concept study to investigate the detection of MA and its metabolites in serum and urine using forensically and clinically relevant concentrations. The spectral signatures of MA were visible above the matrix background and were used in the multivariate classification of MA and 4 metabolites. Moreover, discrimination of MA samples from MA samples with one metabolite was demonstrated in this chapter to show the suitability of this method to analyse more complex, real-world samples.

3.1 Introduction

Recent years have seen an unprecedented increase in the use, misuse and abuse of traditional illicit drugs, prescription medications, as well as novel psychoactive substances (NPS) that mimic traditional drugs.[1] The drug market is evolving by not only creating new varieties with diverse chemistries to produce psychoactive effects but also new pre-precursors to mask the use of known precursors and identification of alternative routes of synthesis.[2, 3] This expansion of the range of synthetic drug products in an effort to widen or change the substances being offered to consumers, while retaining their psychoactive effects, is reflective of the drug and precursor control legislation globally. However, the manufacture, trafficking and use of traditional drugs remain at an all-time high.

Methamphetamine (MA) is one such traditional drug of abuse that is prevalent in all its forms amongst drug users with a long history of use, misuse and abuse.[4] It is internationally monitored and scheduled under national legislation in most countries along with its precursors.[2] According to the UNODC 2021 report, approximately 325 ton of MA was seized in 2019, and 24,000 clandestine labs were dismantled worldwide.[5] However, in comparison to the amount of internationally controlled precursor chemicals seized in that year, this only accounts for approximately 3 per cent of the total MA seized (10 tons).[5] This is reflective of the recent precursor control legislation and has created a wave of new non-controlled substances that are now used as precursors, also called pre-precursors, to produce common starting materials for MA.[3-5] This shows a dynamic shift in not only the traditional drugs themselves but also their starting materials which also need to be identified.

There are an estimated 27 million people who have or continue to use amphetamines in a variety of forms such as tablets, powders, and crystals administered via various routes including oral ingestion, smoking and intra-nasal/snorting, as well as intravenous injections.[6-12] While the purity and forms of MA vary across the world regions, it is a drug that permeates society across socio-economic boundaries with lasting effects in the community. The UNODC projections indicate that the number of drug users is more likely to increase in low-income countries over the next decade, with the production likely moving closer to the consumers.[13]

The most common screening methods are presumptive colourimetric tests that indicate the presence of specific classes of drugs by a change in colour.[14-18] While the commercial versions are developed for traditional drugs of abuse, these are often inadequate for NPS as the novel

precursors and pre-precursors can be structurally very similar and are not controlled under the current legislation.[3] Additionally, these methods cannot easily be applied to all types of forensic samples encountered such as blood, urine and saliva due to high detection limits, complexities in colour determination, and their lack of selectivity towards a drug class.[15]

Traditional methodologies such as GC-MS and LC-MS remain the gold standard for laboratory-based analytical techniques for the analysis of seized drugs and in forensic toxicology. While these methods have been employed in both targeted and untargeted approaches for screening and confirmatory analyses,[19-24] they require elaborate and time-consuming sample preparation steps using many solvents, particularly when analysing drugs of abuse in biofluids.[25-27] Furthermore, these instruments are expensive to purchase and maintain, require experienced staff to run and interpret data and are not suitable for field testing.[28] Therefore, it is increasingly important to develop a rapid, cost-effective and efficient detection method that can be deployed in the field in a decentralised manner (out of the lab) and that are also useful in the laboratory.

According to SWGDRUG guidelines for the analysis of unknown compounds, FTIR spectroscopy belongs to the group of techniques with the highest discrimination power.[29] In forensic science, FTIR spectroscopy has been employed in the analysis of seized powder drugs,[30-35] counterfeit medicines,[34, 36-38] explosives[39-41] and body fluids.[42-46] In the case of drugs of abuse, it is mostly used as a screening method to identify the drug compounds to guide more time-consuming and costly analyses such as GC-MS for confirmatory analyses. While it is also useful in screening for the adulterants and/or cutting agents present in seized drug samples, it is necessary to combine it with machine learning techniques for more convenient interpretation by a non-expert. It is also particularly adaptable and hence suitable for the constantly evolving drug markets.

When analysing body fluids in forensic science, on the other hand, it has mainly been applied to identify a specific type of fluid such as blood, semen and urine, as well as determine the time passed since their deposition at a crime scene.[46-49] More recently, Hans and colleagues have demonstrated the suitability of ATR-FTIR spectroscopy for the detection of cocaine in spoked saliva samples to obtain detection limits of 0.02 mg/mL.[50] This promising study was further developed to lower the detection limits to 3 µg/mL with one step extraction procedure and the use of a QCL unit with an ATR accessory.[51, 52] While these studies were the

first to analyse biofluids containing drugs with ATR-FTIR spectroscopy, its application to other drugs and biofluids remains to be evaluated. Moreover, these studies did not take advantage of the use of chemometrics in conjunction with FTIR spectroscopy which has been demonstrated in the literature.[28, 34, 53] Portable ATR-FTIR devices have already been demonstrated to be useful in a variety of applications.[54-56] Therefore, ATR-FTIR spectroscopy provides a unique opportunity to address the aforementioned analytical challenges by developing a combined approach with chemometrics for detecting drugs of abuse in biological fluids directly.

MA is a synthetic phenethylamine that consists of a chiral carbon which allows it to form two optical isomers also known as enantiomers (Figure 3-1). The *dextro*-stereoisomer (also called (+) or *d*- or *S-)* is a stronger CNS stimulant, while the *levo*-stereoisomer (also called (-)- or *l*- or *R-)* shows less stimulant activity in biological systems.[57] Psychostimulants such as methamphetamine affect the central nervous system usually by increasing the natural stimulating pathways in the brain which involves enhancing the effects of three main neurotransmitters; dopamine, norepinephrine and serotonin.[58, 59] The abuse liability of methamphetamine is attributed to potent psychostimulant effects which induce euphoria, increased alertness and endurance, improved cognitive and sensory performance, intensification of emotions including general improvement of mood, appetite suppression, as well as increased sexual arousal.[6, 12, 60-63] However, the strong abuse potential of the drug leads to tolerance building to the psychotropic effects mentioned above which can eventually lead to the consumption of toxic overdose.[61] The negative effects associated with the drug include tachycardia, arrhythmias, stroke, myocardial ischemia, hypertension, paranoia, seizures and psychosis.[10, 12, 62]

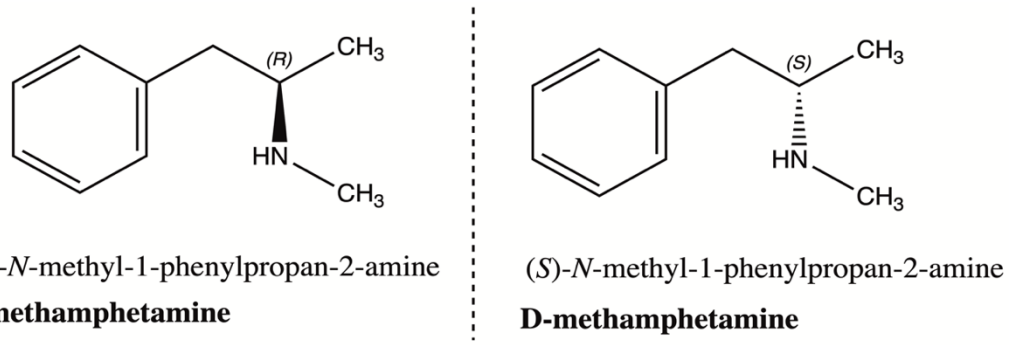

(*R*)-*N*-methyl-1-phenylpropan-2-amine
L-methamphetamine

(*S*)-*N*-methyl-1-phenylpropan-2-amine
D-methamphetamine

Figure 3-1: Structures of two optical isomers of methamphetamine – *levo* (on the left) and *dextro* (on the right).

The pharmacologically active dose for the *d*-isomer of methamphetamine is approximately 0.5 mg/kg, which for a 70 kg adult is ~35 mg.[64] The pharmaceutical preparation 'Desoxyn® Gradumet' is prescribed to make up an effective dose of 20 - 25 mg and 5 mg per day, for ADHD and obesity control, respectively.[65] The self-reported illicit doses of MA range from 50 - 500 mg totalling up to 4 g/day which lie outside the range of clinical experiments.[59, 66] The higher doses tolerated by chronic users are reflective of the accumulation of MA in the body. While fatal overdoes of methamphetamine are generally rare, illicitly acquired drugs can be combinations of various substances leading to fatal drug-drug interactions.[59]

Typically, the plasma half-life of MA is approximately 8-13 h with peak plasma concentrations occurring around 3-5 h after dosing,[67] which mirrors the duration of its stimulant effects making it one of the longer-lasting stimulants available on the drug market and thus leading to increased use and abuse.[11] The plasma-protein binding for MA is relatively low which implies that the majority of the drug is present in the biological fluid in free form.[68]

The hepatic metabolism of methamphetamine in humans is regulated by the polymorphic enzyme cytochrome P450, specifically, its CYP2D6 isozyme and results in the formation of two main metabolites, amphetamine and *p*-hydroxymethamphetamine and minor metabolites include *p*-hydroxyamphetamine and norephedrine (Figures 3-2).[69-71] The major active metabolite, amphetamine is formed through *N*-demethylation while *p*-hydroxymethamphetamine is formed *via* aromatic hydroxylation (Figure 3-2).[67, 72, 73] Amphetamine is further metabolised to 4-hydroxyamphetemine *via* hydroxylation at the 4-position on the benzene ring and to norephedrine, a psychoactive substance *via* oxidation (Figure 3-2).[57, 67, 70] Due to the high pK_a (~ 10) of methamphetamine, it is usually found in its ionised form.[74] Reabsorption of ionised drugs in the kidneys is highly pH dependent and as such approximately 43% of MA is excreted unchanged.[61, 69, 72, 75, 76] Consequently, resorption in alkaline conditions causes more degradation *via* the metabolic process which leads to changes in the metabolite concentrations found in biological fluids after initial ingestion.

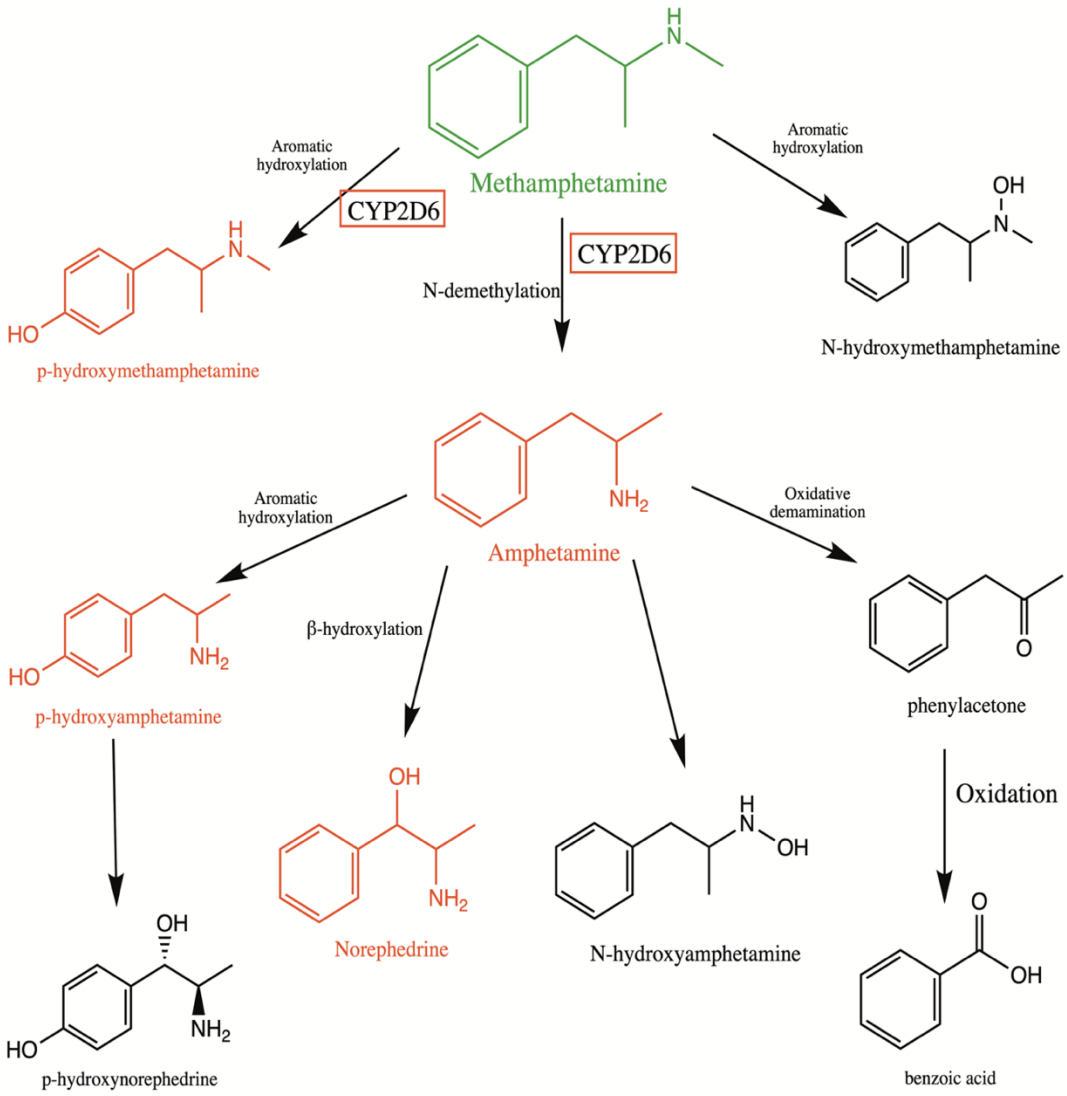

Figure 3-2: Simplified schematic of main metabolic pathways of methamphetamine in human. The parent drug, MA is shown in green and the metabolite structures of amphetamine, p-hydroxymethamphetamine, p-hydroxyamphetamine, norephedrine, are highlighted in red as they were chosen to be included in this study.

This chapter presents a proof-of-concept study of ATR-FTIR spectroscopy as a direct drug detection methodology, utilising MA as a model drug compound within two biological matrices, human pooled serum and urine. Considering the bioavailability of MA at 70% for oral ingestion and an excretion rate of 43% for the unchanged drug, the concentration ranges of MA found in serum and urine are likely to be in the ranges of 0.006 - 0.6 mg/mL and 0.035 - 4 mg/mL (for a 70 kg person with a total blood volume of 4.5 L and average urinary output of 0.5 mL/kg/hr over 12 hours) respectively. The lower end of these ranges is reflective of

therapeutic doses while the higher end is indicative of chronic users.[11, 61, 72, 77, 78] In addition, this is expanded to detect and quantify four metabolites of MA in two scenarios, as individual drugs and when combined with the parent drug in biofluids to reflect real-world samples.

3.2 Materials and Methods

3.2.1 Materials

(+)-Methamphetamine hydrochloride ($C_{10}H_{15}N$ • HCl, referred to as MA) and its four metabolites: (+)-Amphetamine hemisulfate ($C_9H_{13}N$ • 0.5 H_2SO_4, referred to as AM), para-hydroxymethamphetamine ($C_{10}H_{15}N$, referred to as p-OHMA), para-hydroxyamphetamine hydrobromide ($C_9H_{13}NO$ • HBr, referred to as p-OHAM) and DL-norephedrine hydrochloride ($C_9H_{13}NO$ • HCl, referred to as NOR) were purchased from Merck Chemicals Ltd. Human pooled serum (here referred to as serum) was purchased from TSC Life Sciences Ltd., which was stored at -80 °C in a freezer when not in use. For urinalysis, artificial urine, Surine™ Negative Urine Control was purchased from Merck Chemicals Ltd., which was stored at -4 °C in a refrigerator when not in use. All powder drugs were used as received. All solutions were prepared directly in the two matrices, pooled serum and artificial urine without any additional solvents or reagents.

3.2.2 Sample Preparation

For MA, AM, NOR and pOHAM, 10 mg/mL stock solutions were prepared in each biological matrix, however, due to the lower solubility of pOHMA, the maximum possible stock concentration of 3 mg/mL was prepared in each biofluid. These were then diluted using the blank matrices (serum or urine without any drug in them) to prepare a range of concentrations. The set of calibration standards consisted of samples in the concentration ranges of 0.1 - 0.9 and 1 - 10 mg/mL with an increment of 0.1 and 1, respectively, prepared for MA, AM, NOR and pOHAM in pooled serum and artificial urine. For pOHMA, the concentration ranges consisted of 0.1-0.9 and 1-3 mg/mL (in increments of 0.1 and 1, respectively). The higher concentrations in these ranges were greater then those typically found in therapeutic or chronic users. Without any previous research in this specific method of analysis, the higher concentrations were employed to ensure that drug spectral signatures were visible and then the concentration range was extended to include the relevant forensic and clinical range. The complete list of samples is provided in Table 3-1.

Table 3-1: Summary of all samples studied in this chapter.

Drug	Abbreviation	Sample concentrations (mg/mL)	No. of samples
Blank	Serum: BlankS	0 mg/mL	26
	Urine: BlankAU	0 mg/mL	17
MA	Serum: SPMA	10, 9, 8, 7, 6, 5, 4, 3, 2, 1, 0.9, 0.8, 0.7, 0.6, 0.5, 0.4, 0.3, 0.2, 0.1	26
	Urine: UPMA	10, 9, 8, 7, 6, 5, 4, 3, 2, 1, 0.9, 0.8, 0.7, 0.6, 0.5, 0.4, 0.3, 0.2, 0.1	19
AM	Serum: SPAM	10, 9, 8, 7, 6, 5, 4, 3, 2, 1, 0.9, 0.8, 0.7, 0.6, 0.5, 0.4, 0.3, 0.2, 0.1	25
	Urine: UPAM	10, 9, 8, 7, 6, 5, 4, 3, 2, 1, 0.9, 0.8, 0.7, 0.6, 0.5, 0.4, 0.3, 0.2, 0.1	20
NOR	Serum: SPNOR	10, 9, 8, 7, 6, 5, 4, 3, 2, 1, 0.9, 0.8, 0.7, 0.6, 0.5, 0.4, 0.3, 0.2, 0.1	26
	Urine: UPNOR	10, 9, 8, 7, 6, 5, 4, 3, 2, 1, 0.9, 0.8, 0.7, 0.6, 0.5, 0.4, 0.3, 0.2, 0.1	19
pOHMA	Serum: SPpOHMA	3, 2, 1, 0.9, 0.8, 0.7, 0.6, 0.5, 0.4, 0.3, 0.2, 0.1	12
	Urine: UPpOHMA	3, 2, 1, 0.9, 0.8, 0.7, 0.6, 0.5, 0.4, 0.3, 0.2, 0.1	12
pOHAM	Serum: SPpOHAM	10, 9, 8, 7, 6, 5, 4, 3, 2, 1, 0.9, 0.8, 0.7, 0.6, 0.5, 0.4, 0.3, 0.2, 0.1	19
	Urine: UPpOHAM	10, 9, 8, 7, 6, 5, 4, 3, 2, 1, 0.9, 0.8, 0.7, 0.6, 0.5, 0.4, 0.3, 0.2, 0.1	18

Table 3-2: Summary of samples with a single drug belonging to the independent test set are listed.

Sample ID	Drug present	Concentration (mg/mL)
9001	NOR	0.4
9002	MA	0.3
9003	AM	0.37
9004	MA	0.5
9005	MA	1
9006	MA	4
9007	MA	9
9008	AM	2
9009	AM	5
9010	AM	7
9011	NOR	1
9012	NOR	3
9013	NOR	9

Table 3-3: Summary of samples with a combination of parent drug with one metabolite. These were included in the independent test set.

Sample ID	Actual drug combination present
9014	0.6 mg/mL MA + 0.1 mg/mL AM
9015	0.8 mg/mL MA + 0.12 mg/mL NOR
9016	1 mg/mL MA + 0.17 mg/mL AM
9017	0.3 mg/mL MA + 0.1 mg/mL NOR

In order to test classification and regression models built on the data, blind samples were prepared independently by a colleague in the research group using the same stock solutions following the same method outlined above (Tables 3-2 and 3-3). A total of 16 blind samples were created which consisted of samples with a single drug (n = 13) and samples with drug-metabolite mixtures (n = 4). The concentrations and combinations were recorded and referred to after data analysis. The purpose of these blind samples was two-fold – these were created to evaluate the efficacy of statistical models by (a) creating an independent test set and (b) to simulate a real-world situation where drug mixtures are commonplace.

3.2.3 Spectral Collection

A PerkinElmer UATR Two FT-IR spectrometer with the PerkinElmer ATR diamond accessory was used for the collection of all spectra in this analysis. Spectra were acquired in the range of 4000-450 cm^{-1}, at a resolution of 4 cm^{-1} and averaged over 16 co-added scans. All powder spectra were scanned as pure drug powders without the need for milling to identify the pure spectral characteristics of the drug. This was carried out by depositing enough (~2 μg) drug powder onto the crystal surface so that the entire surface was covered. Following this, the sample was clamped down to ensure intimate contact between the sample and the crystal surface. The clamping force was maintained at approximately 70% in the Spectrum software provided by Perkin Elmer and the sample was scanned three times. This process was repeated three times per sample to acquire 9 spectra per sample.

For biofluid samples, 3 μL of serum and 0.5 μL of AU were deposited onto the diamond crystal surface. A lower volume for the AU samples was selected, however, owing to the effects of air drying. Usually, a coffee ring or a halo effect is seen in dried liquid samples,[79] but for urine this halo formed outside the crystal surface when 3 μL was deposited. Therefore, 0.5 μL of

urine samples were used to ensure that the entire dried sample was on the crystal surface. The samples were allowed to air dry on the surface. The drying times were between 10-15 mins for HPS samples and 4-6 mins for AU samples. While the drying times were dependent on the humidity and temperature of the day in the laboratory environment, the sample profiles were monitored during the drying process. When the profiles were no longer changing and resembled those published in the literature,[79-81] the dried samples were scanned three times. This process was repeated three times per sample which yielded a total of nine dried spectra per sample. Prior to the spectral collection for each spot of each sample, a background spectrum was taken.

3.2.4 Spectral Pre-processing

The PRFFECT toolbox within R statistical computing environment software was utilised to pre-process the spectral data.[82] There are a range of pre-processing steps that can be employed to reduce such spectral variation and the order in which they are performed remains an important but contested topic in the literature.[83] The optimum protocol followed here was developed through a trial-and-error basis to maximise the sensitivity and specificity of the classification without adding to the overall data analysis time. The specific pre-processing protocol followed here included Savitzky-Golay (SG) filter for smoothing, vector normalisation and rubberband baseline correction in that order, following which nine spectra per sample were averaged to a single spectrum per sample. The second derivative is applied for some analyses in addition to the pre-processing steps mentioned and is specified when discussing those results. In addition, urine spectra were cut to 2000 – 450 cm^{-1} region. The data was mean-centred and scaled during the model construction stage. The details of these pre-processing steps are described in section 2.4.

3.2.5 Spectral Analysis

For multivariate classification analysis, two machine learning methods – partial least squares discriminant analysis (PLS-DA) and random forest (RF). Binary classification models were constructed using the PRFFECT toolbox within R statistical software. Following classification, partial least squares regression (PLS-R) analysis was to obtain limits of detection and quantification. These methods are detailed in section 2.5.

For all classification models, the dataset was split using a 70:30 split where 70% of the dataset was used as a training set and 30% was used as a testing set. All samples were given a unique

sample ID which was used to ensure that all spectra obtained from the same sample were either in the training or test set. Prior to classification/regression analyses, a bootstrapping analysis was performed on the training dataset to determine the appropriate number of iterations to minimise error and maximise the accuracy and efficiency of the classification model. To evaluate the performance of these models in a real-world environment, k-fold cross-validation was carried out. Once the classification/regression models were built, they were evaluated with the independent test sets made up of the relevant drug compound.

For all PLS-DA models constructed in PRFFECT with all default values were used for all parameters except for ncomp which controlled the number of latent variables selected to build the analysis. It was selected to pick the best number of latent variables between 1 and 20 for the serum and urine datasets. This number was derived from the number of samples in each dataset using the following formula:

$$n\_samples \times trprop \times (k-1)/k \tag{3.1}$$

where n_samples is the number of samples in the dataset used for classification before being split into testing and training set, trprop is the proportion of data used as the training set which was 0.7, and k is the total number of folds in the cross-validation which was 5.

For all RF models, default values of 500 and 1 were used for *ntree* and *nodesize* respectively. The *mtry* values of 59 and 39 were used for serum and urine datasets respectively, which were based on the number of variables in those datasets. As described in **Chapter 2**, the performance of the classification model is reported in terms of sensitivity, specificity, kappa and balanced accuracy. All classification models were cross-validated using the k-fold cross-validation method where k was set to 5. For all regression models, ncomp was set to choose the optimum number of LVs between 1 and 20 and k was set to 10 for cross-validation. The limits of detection (LOD) and quantification (LOQ) were calculated using the following formulae:

$$LOD = 3 \times (Standard\ deviation\ of\ response\ variable/Slope) \tag{3.2}$$

$$LOQ = 10 \times\ Standard\ deviation\ of\ response\ variable/Slope \tag{3.3}$$

3.3 Results and Discussion

3.3.1 Peak Assignment

Spectra for all five drugs (MA and its metabolites) were inspected in their powder forms for peak assignment prior to analysis in serum and in urine matrices (Figure 3-3 and Table 3-2). The IR spectra for methamphetamine can broadly be categorized into four spectral domains. These include the vibrations due to the aromatic ring (Region A: 3100-3000 cm^{-1}, 1650-1400 cm^{-1}, 850-700 cm^{-1}), the vibrations indicating the type of substitution present on the ring (Region B: 2050-1700 cm-1, 1225-950 cm^{-1}), the aliphatic side chain vibrations (Region C: 2932-2715 cm^{-1}), and the vibrations reflecting the presence of amino group on the side chain (Region D: 3600-3300 cm^{-1}). The electron-donating or accepting properties of the substituents play an important role in determining the precise position of these absorption bands within the range of frequencies quoted here.[84] For instance, the C-H deformation bands represent the out-of-plane deformation vibrations of the hydrogen atoms on the aromatic rings, observed in region A between 1000-650 cm^{-1}. Both these bands are seen

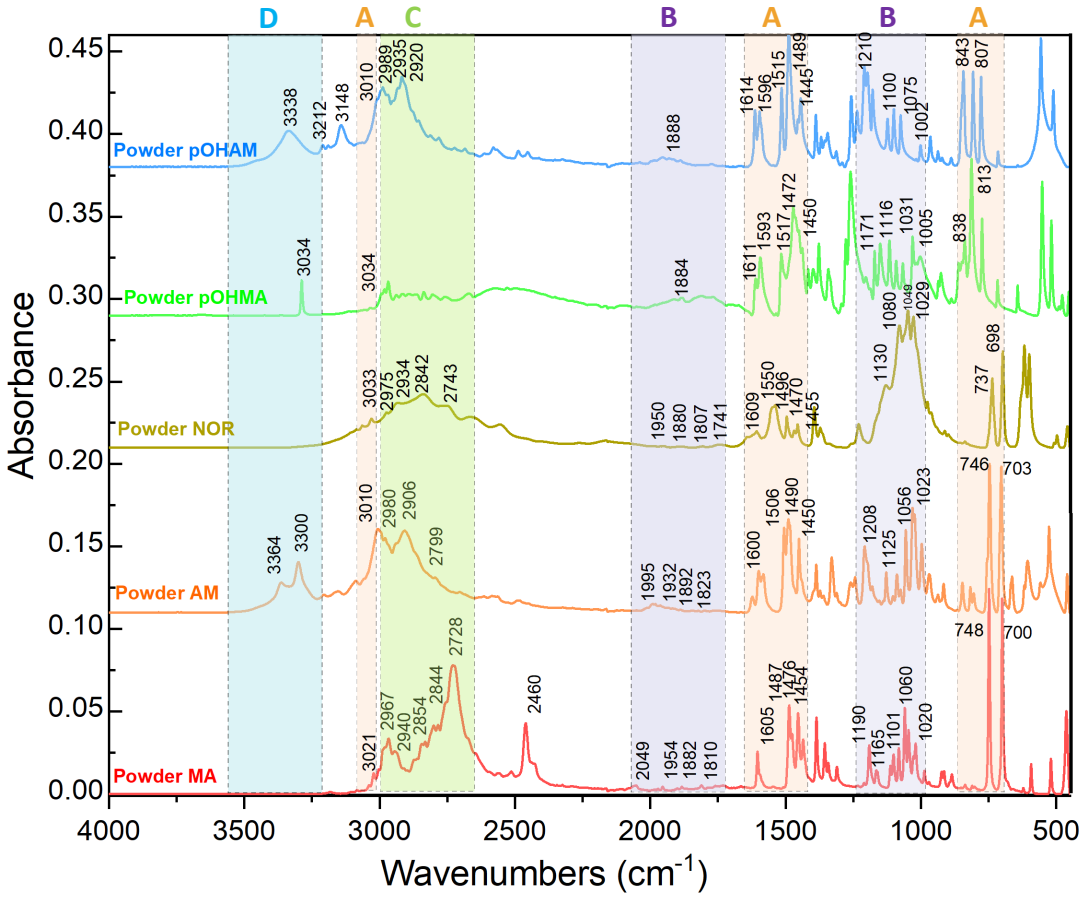

Figure 3-3: Stacked spectra for pure powder parent drug and its metabolite for each drug molecule. The descriptions for spectral regions A-D are given in Table 3-2.

between 750-695 cm^{-1} in MA, AM and NOR spectra due to their similar structures and the number of remaining hydrogens on the aromatic ring due to mono-substitution. However, these bands are found closer to 850-800 cm^{-1} in both pOHMA and pOHAM which is typical of para substitution of the aromatic ring with only two adjacent H's remaining between the substitutions.[84]

Table 3-4: Tentative spectral assignments of bond vibrations for all five drug molecules used in this study. Ref [84, 85]

Vibrational regions	Vibrational modes	MA	AM	NOR	pOHMA	pOHAM
Region A	Aromatic C-H stretch	3021	3010	3033	3033	3010
	Ring breathing modes – C-C double degenerate modes for aromatic ring	1605	1600	1609	1611	1614
	∂(C-H) aromatic, out-of-plane deformation	748, 700	746, 703	737, 698	838, 813	843, 807
Region B	Overtone and combination bands- for ring substitution	2049, 1954, 1882, 1810	1995, 1932, 1892, 1823	1950, 1880, 1807, 1741	1884	1950
	Ring substitution	1190, 1101, 1060, 1020	1208, 1125, 1056, 1023	1130, 1080, 1029	1171, 1116, 1005, 1031	1210, 1125, 1075, 1002
Region C	Aliphatic C-H stretches for side chains	2967, 2940, 2854, 2844	2980, 2906, 2865, 2799	2975, 2934, 2842	2960, 2838, 2807, 2959	2989, 2972, 2935, 2920
Region D	N-H		3364, 3300		3288	3338, 3212, 3148

While there are numerous spectral differences in the powder spectra, these are significantly masked by the spectral signatures of both matrices used. For instance, the ring substitution modes in Region B (1225 - 950 cm^{-1}) observed in the powder spectra are masked by the serum background, while the overtone and combination bands are masked by the strong thiocyanate peak at 2041 cm^{-1} in the urine samples (Figures 3-5, 3-6 and 3-7). However, as urine is a simpler biological fluid compared to serum, it allows for a greater number of drug peaks to be detected over the matrix background. As an example, MA in each matrix (at a concentration of 10 mg/mL) is shown in Figure 3-5. The superimposed spectra for all drugs in biofluids with the corresponding blank matrix are included in Appendix 1 (Figures A1-1 and A1-2).

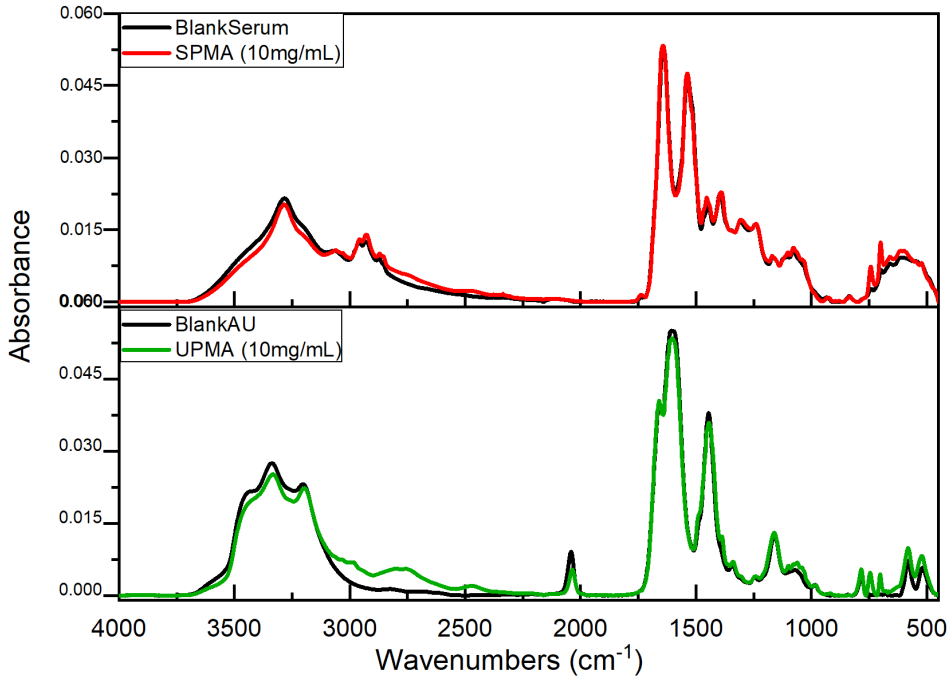

Figure 3-4: Blank biofluid spectra overlaid with MA in that biofluid. SPMA refers to MA in serum. UPMA refers to MA in urine.

In addition, difference spectra were calculated by subtracting blank serum/urine spectra from those containing drug samples in serum/urine (10 mg/mL) which were used to assess the spectral regions of importance. Difference spectra for all five compounds with serum and urine are shown in Figures 3-6 and 3-7, respectively.

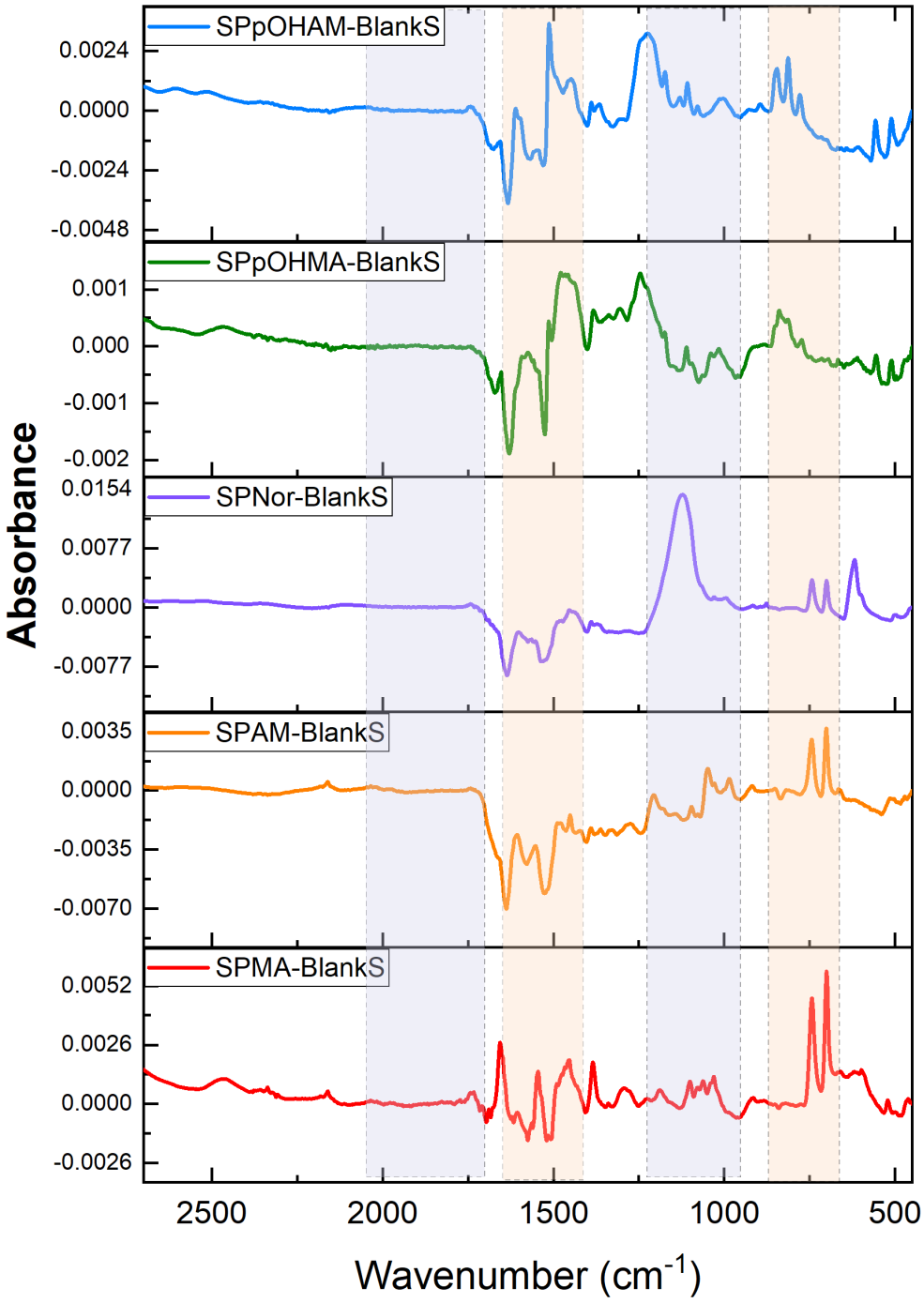

Figure 3-5: Stacked difference spectra for all five compounds where the blank serum spectra was subtracted from the spectra of drug samples in serum. All drug samples were at a concentration of 10 mg/mL except for pOHMA which is shown at 3 mg/mL. The regions denoted in the orange and purple boxes correlate with the spectral regions identified in Figure 3.4.

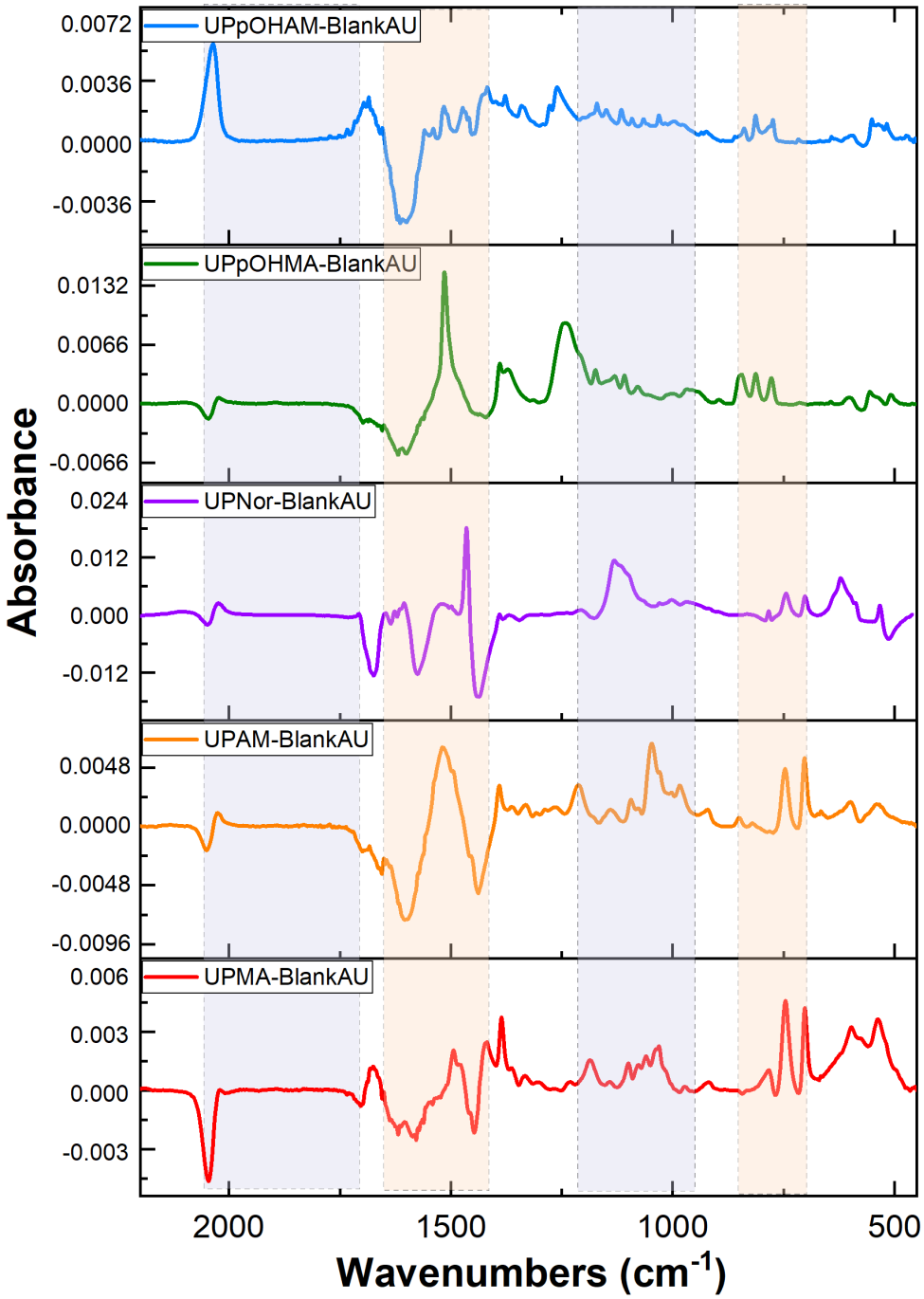

Figure 3-6: Stacked difference spectra for all five compounds where the blank urine spectra was subtracted from the spectra of drug samples in urine. All drug samples were at a concentration of 10 mg/mL except for pOHMA which is shown at 3 mg/mL. The regions denoted in the orange and purple boxes correlate with the spectral regions identified in Figure 3.4.

As the drug sample spectra were not normalized to any serum peaks prior to calculating difference spectra, the spectral differences observed are a combination of free drug and the protein-bound proportion of the total drug added to the sample. The spectral peaks relating

to the free drug proportion of MA would correspond to those highlighted in the powder spectra, while the protein-bound proportion would likely be reflected as changes to the protein peaks of the matrix. The peaks at 748 and 700 cm^{-1} corresponding to the aromatic stretching modes in the MA molecule remain visible above the matrix background reflective of the free drug portion. These are more clearly seen in the difference spectra (Figures 3-6 and 3-7). On the other hand, amide I and amide II bands at 1650 and 1550 cm^{-1} indicated in Figure 3-6 show conformational alterations from drug-protein interactions. This is further reflected in Figure 3-7 where decreasing concentration of the drug is correlated with the decreasing intensities of free drug-related peaks. Similarly, the changes in the amide I and II reflective of the drug-protein interactions are also seen to lessen (Figure 3-7). While it is possible to quantify drug-protein-related changes based on the protein binding percentage of the MA molecule, it was outwith the focus of this thesis. Furthermore, it is unlikely to possess such information about novel illicit drugs as there is minimal research conducted on elucidating their pharmacokinetic and pharmacodynamic properties.

As the focus of this thesis was distinguishing drug samples from drug-free samples, the drug spectral signatures were used as a whole in the multivariate models presented in this thesis.

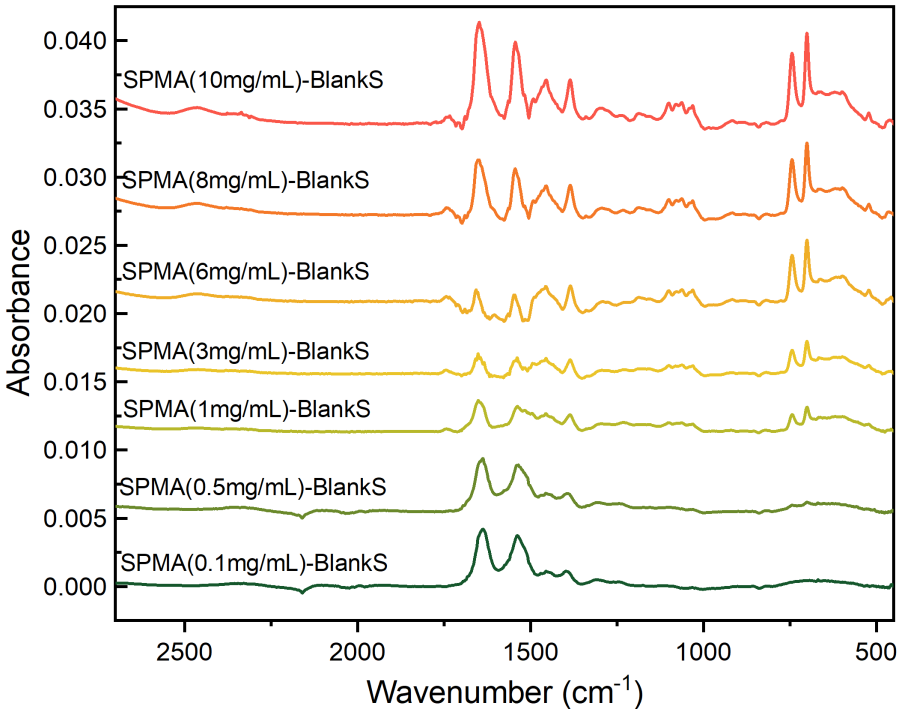

Figure 3-7: Stacked difference spectra covering a concentration range from 0.1 mg/mL to 10 mg/mL. Each spectrum is obtained by subtracting blank serum matrix spectrum from that of the drug sample spectrum of different concentrations.

3.3.2 Bootstrapping Analysis

Each PLS-DA model was performed numerous times so that the variance in the dataset was fully accounted for by the model. During the bootstrapping analysis, a total of 501 iterations were carried out on the MA samples versus blank control samples. This added significant time to the running of classification models making the process inefficient. The results of this analysis are presented in Figures 3-9 for serum and urine drug matrices respectively. At 51 iterations, the standard error for the test set was 0.12% for sensitivity and 0.8% for specificity, which was deemed to be an acceptable level with reasonable analysis time. This was also supported by previous work in the research group.[86] Therefore, all analyses from this point onwards were performed with 51 iterations.

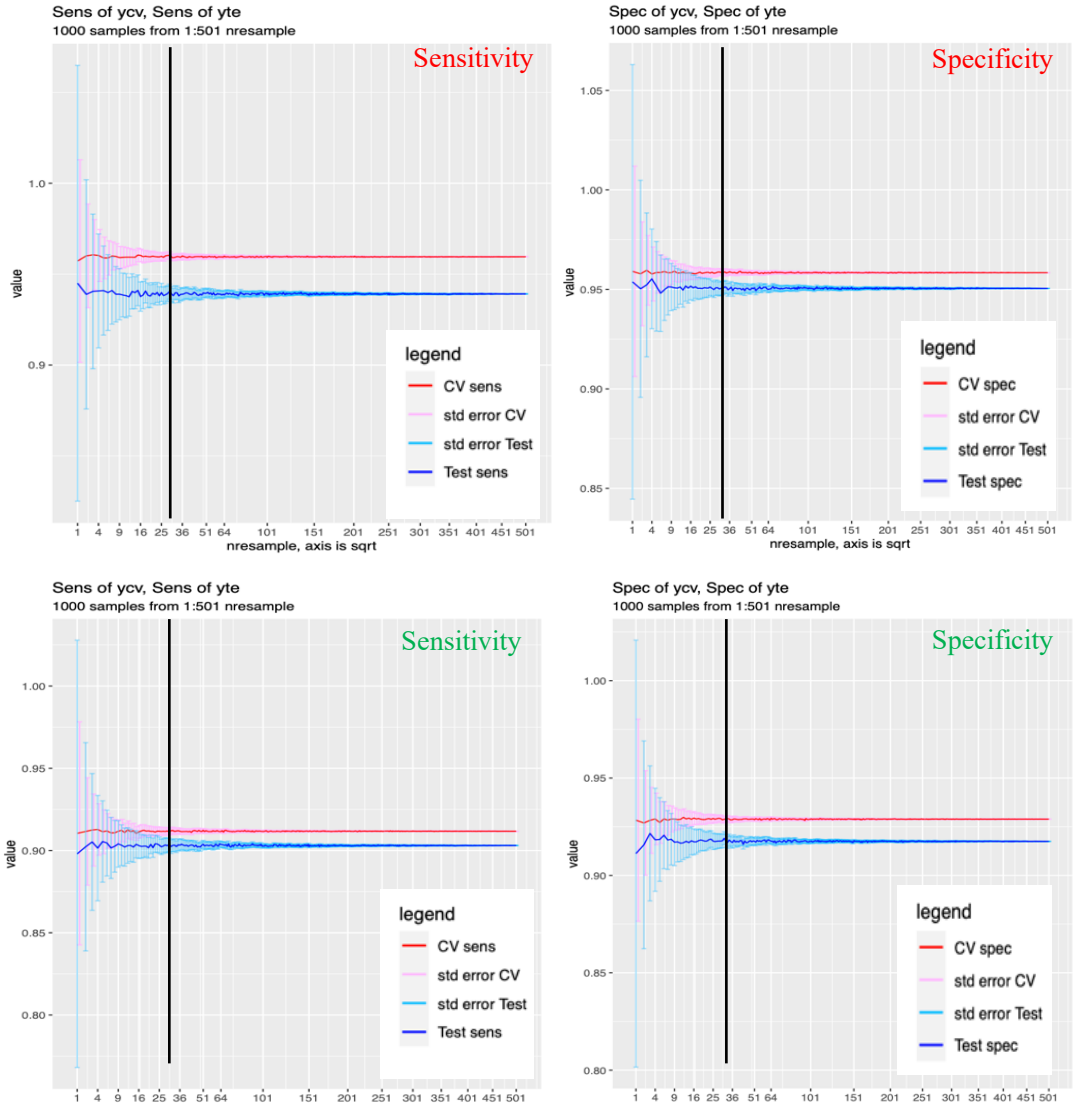

Figure 3-8: Bootstrapping analysis to determine the appropriate number of resample iterations required for the PLS-DA training dataset of blank serum vs MA in serum (top row) and blank urine vs MA in urine (bottom row). 51 iterations were chosen – indicated by black vertical like in all graphs.

3.3.3 Blank Samples *versus* MA Samples

3.3.3.1 PLS-DA

Before examining the classification results to distinguish MA spiked biofluid samples from blank samples, PLS-DA analysis was performed using up-sampling, down-sampling and SMOTE-sampling methods for the serum and urine datasets to determine the best resampling method. The results of this analysis are summarised in Tables 3-5 and 3-6. The PLS-DA model was performed 51 times as determined by the bootstrapping analysis in the previous section and the results were combined to give mean sensitivity and specificity values and the variation in the values obtained was described by the standard deviation.

Table 3-5: Comparison of sampling techniques for PLS classification of BlankS and SPMA samples. BlankS refers to blank serum samples and SPMA refers to MA in serum. Pre-processing steps included SG smoothing, vector normalisation, rubberband baseline correction and mean centring was performed during model construction. All values of mean and SD are provided for n = 51.

	Up-Sampling		**Down-sampling**		**SMOTE**	
	Mean	**SD**	**Mean**	**SD**	**Mean**	**SD**
Sensitivity (%)	90.4	11.6	91.5	9.5	82.9	14.8
Specificity (%)	92.3	9.5	91.9	9.7	95.8	7.1
Kappa	0.82	0.12	0.83	0.13	0.79	0.14
Balanced Accuracy (%)	91.4	6.3	91.7	6.6	89.3	7.6

Table 3-6: Comparison of sampling techniques for PLS classification of BlankAU and UPMA samples. BlankAU refers to blank urine samples and UPMA refers to MA in urine. Pre-processing steps included SG smoothing, vector normalisation, rubberband baseline correction and mean centring performed during model construction. All values of mean and SD are provided for n = 51.

	Up-Sampling		**Down-sampling**		**SMOTE**	
	Mean	**SD**	**Mean**	**SD**	**Mean**	**SD**
Sensitivity (%)	94.1	11.8	95.1	11.2	88.7	15.2
Specificity (%)	92.5	13.8	96.8	10.1	98.4	5.4
Kappa	0.93	0.15	0.92	0.14	0.87	0.14
Balanced Accuracy (%)	86.4	7.7	95.9	7.3	93.5	7.5

For the PLS-DA classifications, sensitivity and specificity values when using down-sampling were 91.5% and 91.9% respectively, which provided a balanced approach in comparison to up-sampling and SMOTE sampling (referring to samples in Table 3-5). Though up-sampling and SMOTE-sampling both provided higher specificities of 92.3% and 95.8%, respectively, (Table 3-5) than those of the down-sampling, the standard deviation associated with sensitivity values for both was much higher than that of down-sampling. This could have real-world implications when analysing real samples where biofluids with drugs present in them would be incorrectly identified. Similarly, for urine samples, the down-sampling method again presented the best balance between identifying true positives (95.1% ± 11.2) and true negatives (96.8% ± 10.1) while maintaining the lowest standard deviation values in comparison with the other two methods. In addition, the down-sampling protocol showed a relatively high Kappa value of 0.83 for serum and 0.92 for urine samples further adding to the reliability of this predictive model. Therefore, the down-sampling method was demonstrated to be more appropriate for both biofluids.

The sensitivities of 91.5% for serum samples and 95.1% for urine samples indicate that over 90% of the samples that contained MA were correctly assigned by the PLS-DA classification model. Similarly, the specificities of 91.9 and 96.8% in serum and urine respectively indicate that true negative samples i.e., samples that did not have any MA were correctly assigned 91.9 and 96.8% of the times. The high sensitivity demonstrated by this classification is promising as it has important implications in correctly identifying samples that need further confirmatory testing. The high specificity indicated by this model is particularly useful as a false positive screening test can have serious consequences such as unjust termination of a job and undue stress until confirmatory testing can be performed.

3.3.3.2 Random Forest

Following the same pre-processing protocol, RF classification models were built using the training datasets in both biofluids to evaluate the performance of the three resampling techniques. The bootstrapped RF model with 51 iterations was built for the dataset containing samples with MA and blank matrix with 5-fold cross-validation. The mean sensitivities and specificities along with their standard deviations are summarised in Tables 3-7 and 3-8.

When compared to the PLS-DA results of the same samples in the serum dataset, errors associated with RF sensitivity values were 6.6% and 8.5% higher for up- and down-sampling respectively and only 1.2% lower for SMOTE sampling (Tables 3-5 and 3-7). The opposite trend was seen in the specificities whereby up-sampling provided the highest specificity of 95.9% with the lowest error of 9.7% (Tables 3-5 and 3-7). PLS-DA was found to be a stronger classifier when comparing specificities which was also supported by the lower balanced accuracies of the RF models for all three sampling techniques in both biofluids (Tables 3-5 to 3-8).

Table 3-7: Summary of results showing sampling methods for MA in serum versus blank serum samples using RF classification. Pre-processing steps included SG smoothing, vector normalisation, rubberband baseline correction and mean centring was performed during model construction. All values of mean and SD are provided for n = 51.

	Up-Sampling		**Down-sampling**		**SMOTE**	
	Mean	**SD**	**Mean**	**SD**	**Mean**	**SD**
Sensitivity (%)	67.8	18.2	73.9	18.0	75.9	16.0
Specificity (%)	95.9	9.7	89.9	11.1	87.1	12.6
Kappa	0.64	0.19	0.64	0.19	0.63	0.18
Balanced Accuracy (%)	81.6	10.0	81.9	9.8	81.5	9.2

Table 3-8: Summary results showing sampling methods comparison for MA in urine versus blank urine samples using RF classification. Pre-processing steps included SG smoothing, vector normalisation, rubberband baseline correction and mean centring was performed during model construction. All values of mean and SD are provided for n = 51.

	Up-Sampling		**Down-sampling**		**SMOTE**	
	Mean	**SD**	**Mean**	**SD**	**Mean**	**SD**
Sensitivity (%)	91.1	15.6	88.7	15.2	91.6	13.8
Specificity (%)	87.8	12.1	83.5	14.8	83.1	18.9
Kappa	0.78	0.15	0.71	0.22	0.74	0.21
Balanced Accuracy (%)	89.5	7.9	86.1	11.3	87.4	10.2

While the PLS-DA sensitivity and specificity values were stronger in comparison to the RF classification results, the RF classification provided another output, the Gini importance

plots, which is significantly useful (Figure 3-10). While statistical metrics are valuable for model accuracy and reliability, the Gini importance plot provides wavenumbers that are significant in achieving classification between drug samples and blank (drug-free) biofluids.

Figure 3-9 shows the Gini importance plots for serum and urine RF classification models. The spectral regions of importance are shown by the orange, purple and green boxes in Figure 3-9. As previously described in section 3.3.1, the orange boxes highlight vibrational modes linked to the aromatic ring including the ring breathing modes and out-of-plane C-H stretches. The vibrational modes due to ring substitution in the drug molecule are shown in the purple boxes while the green box denotes vibrational modes of the aliphatic side chain in the molecules.

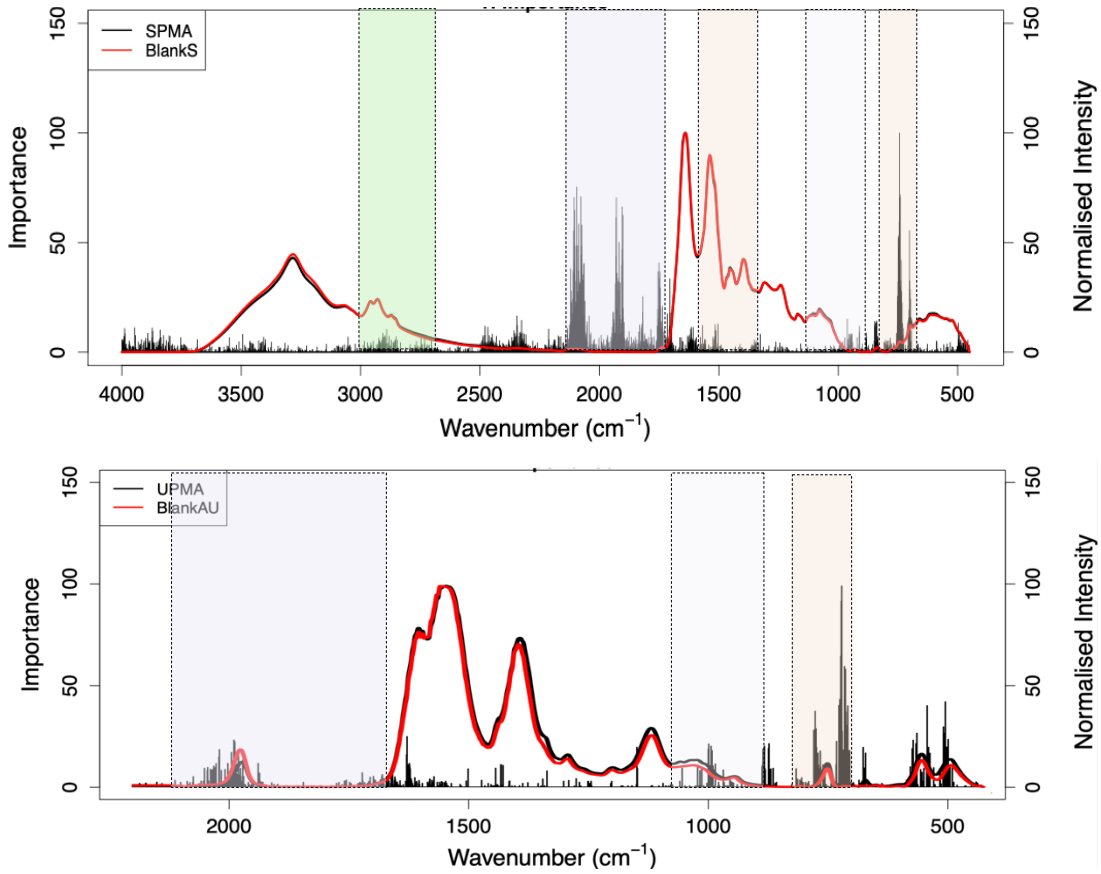

Figure 3-9: Random Forest Gini importance plot showing the most important features for classification between blank serum samples (labelled 'BlankS') and MA in serum (labelled 'SPMA') (top) and between blank urine (labelled 'BlankAU') and MA in urine, (labelled 'UPMA') (bottom). The orange box indicates substitution of the aromatic ring while the purple boxes are indicative of the overtone and combination bands.

The Gini importance plots determine that the most important region for discrimination in both matrices was the lower wavenumber end of the spectrum (850-700 cm^{-1}) due to the out-of-plane C-H stretching of the aromatic ring. This is also indicated in Figure 3-10 where the two strong sharp peaks at 748 and 700 cm^{-1} overlap with the same peaks in the MA spectra in serum and urine. The 1225-950 cm^{-1} region reflective of the ring substitution however was found to be of more importance in the urine dataset than that in the serum dataset.

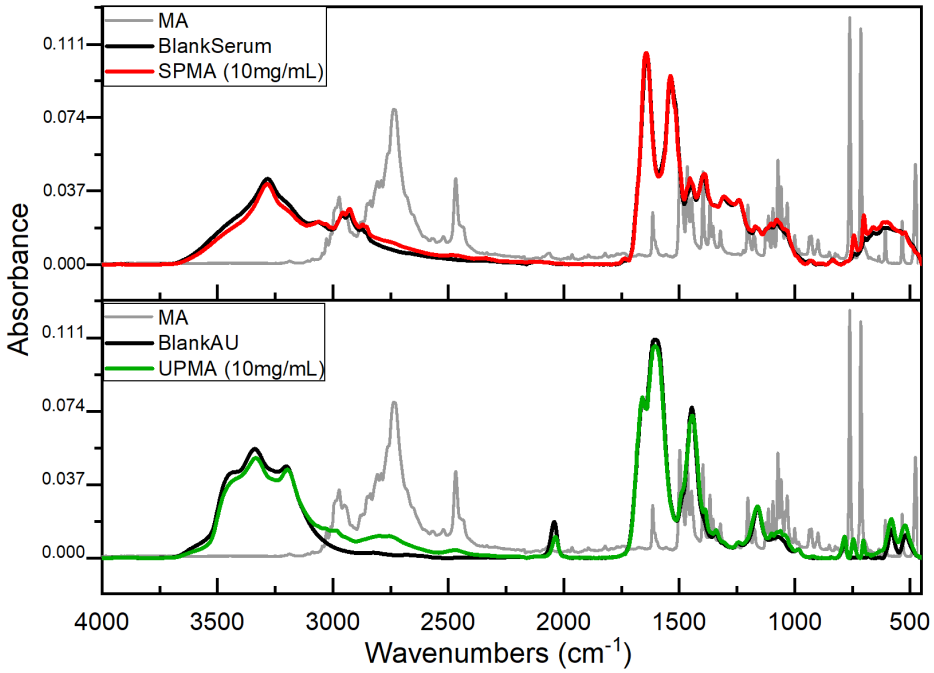

Figure 3-10: The powder spectra for MA are overlaid onto the blank matrix and MA samples spectra for serum (top) and urine (bottom).

The overtone bands in the 2050-1700 cm^{-1} region are much more significant for the classification of serum samples than for the urine dataset. In the urine dataset, this region has a strong thiocyanate peak at 2041 cm^{-1} which is part of the brand of urine matrix used in this thesis. This peak was seen change in absorbance when drug compounds were added to the sample which is reflective of a chemical reaction between the drug compound and the matrix. For the remaining compounds such as AM, NOR, and pOHMA, this reaction was seen to be stronger indicated by a greater decrease in the intensity of that peak (Figure 3.7). Moreover, it can be expected that the same spectral regions might be of significance in both

biofluids. However, it was found that this was not always the case, likely due to the interactions between the drug molecules and the matrix altering the spectral characteristics.

In summary, MA can be successfully distinguished from drug-free samples in both urine and serum using both classification methods presented here with high sensitivity and specificity. In terms of sampling methods, down sampling was seen to be more promising than that of others for this dataset. However, this was verified by performing all three for the remainder of this chapter, and the best values obtained for sensitivities and specificities are presented. For the rest of the chapter, both classification methods are presented as PLS-DA showed better sensitivities and specificities, while the RF method was important for highlighting wavenumber regions of significance.

The results are promising as they span a range of relevant concentrations including the upper limit of the clinical range as well as overdoses in a forensic toxicology situation. However, future experiments with lower concentrations are required for wider application. Both PLS and RF coupled with the advantages of IR illustrate that this method can be used to detect drugs in biofluids without sample extraction, it is sensitive to be applicable in both clinical and forensic settings and shows potential for use in the field when validated with portable instrumentation.

3.3.4 MA Samples *versus* Individual Metabolites Samples

As MA metabolises into many components, detection of only the consumed drug (MA) in a biofluid is not necessarily indicative of a true scenario as it is unlikely that the biological fluid being tested will contain only MA. Thus, it is imperative to consider MA along with its metabolites, AM, NOR, pOHMA and pOHAM, which produce their own unique spectral signatures, in order to distinguish MA from these similar compounds. However, it was not possible to access all the known metabolites of MA as individual compounds that can be purchased and analysed. Furthermore, there is a lack of information on the percentages of each of the metabolites in the samples making it difficult to create a more representative sample.

3.3.4.1 PLS-DA

Multiple binary classifications were performed by labelling the MA-only samples as the positive class and the metabolites were rotated in turn as the negative class, resulting in the production of four classification models. A summary of these results for the PLS-DA analyses

is provided in Tables 3-9 and 3-10 for serum and urine, respectively. In serum, mean sensitivities against AM, NOR and pOHAM are relatively similar however, pOHMA produced the lowest sensitivity. This is likely due to the lower concentration of pOHMA used due to its solubility (3 mg/mL) compared with the other metabolites (10 mg/mL) as well as the smaller number of samples belonging to that class.

Table 3-9: PLS-DA summary table of the parent drug, MA, against each individual metabolite in serum. Pre-processing steps included SG smoothing, vector normalisation, rubberband baseline correction and mean centring was performed during model construction. Sensitivities, specificities, and balanced accuracies are reported as means and standard deviations (SD) of 51 iterations.

Drug molecule against MA	Sampling	Sensitivity (%)		Specificity (%)		Balanced Accuracy (%)	
		Mean	SD	Mean	SD	Mean	SD
AM	Down	96.1	8.1	93.2	8.7	94.6	5.5
NOR	Down	96.9	5.9	92.9	9.6	94.9	5.0
pOHMA	Down	91.3	10.3	90.1	19.1	90.7	9.7
pOHAM	Down	96.9	7.1	95.5	9.2	96.2	6.1

Table 3-10: PLS-DA summary of the parent drug, MA against each of the metabolites in urine. Pre-processing steps included SG smoothing, vector normalisation, rubberband baseline correction and mean centring was performed during model construction. Sensitivities, specificities, and balanced accuracies are reported as means and standard deviations (SD) of 51 iterations.

Drug molecule against MA	Sampling	Sensitivity (%)		Specificity (%)		Balanced Accuracy (%)	
		Mean	SD	Mean	SD	Mean	SD
AM	Down	86.2	13.6	88.2	10.4	87.2	7.7
NOR	Down	96.8	7.3	89.8	12.2	93.3	6.5
pOHMA	Down	96.8	5.4	100	0	98.4	3.6
pOHAM	Down	94.5	7.3	98.4	5.4	96.4	4.8

However, in urine samples (Table 3-10) the lowest specificity and sensitivity values, 86.2% and 88.2% respectively, were observed from the classification of MA and AM. The structures

of MA and AM are almost identical except for a methyl group attached to the amine side chain which can be seen in the higher wavenumber region (Figure 3-2). While urine is a simpler matrix, the higher wavenumber region (3600 – 3000 cm^{-1}) of urine is dominated by broad and strong peaks of urea which are susceptible to drying conditions. Thus, these subtle differences between MA and AM are difficult to identify over the urine background in this region. The remaining three drugs, NOR, pOHMA and pOHAM, have stronger differences in the lower wavenumber region (850 - 650 cm^{-1}) allowing greater classification accuracies.

Upon use of the second derivative in addition to the previous pre-processing steps for the MA and AM samples, classification model accuracies indicated some improvement as it allowed for peaks characteristic of the methyl side chain (Region C, illustrated in Figure 3-4) to be more resolved. The results of this analysis are shown in Table 3-11. For serum samples, the sensitivity value was seen to decrease by 0.9% while the specificity value was seen to improve by 1.7%. For urine samples, the sensitivity and specificity of the PLS-DA classification model increased by 10.5 and 6.7% respectively when the second derivative was used.

Table 3-11: PLS-DA classification summary of MA against AM. Pre-processing steps included SG smoothing, vector normalisation, rubberband baseline correction and second derivative with mean centring being performed during model construction. Sensitivities, specificities, and balanced accuracies are reported as means and standard deviations (SD) of 51 iterations.

Biofluid	Drug molecule against MA	Sampling	Sensitivity (%)		Specificity (%)		Balanced Accuracy (%)	
			Mean	SD	Mean	SD	Mean	SD
Serum	AM	Down	95.2	6.8	94.9	8.4	95.1	5.6
Urine	AM	Down	96.7	10.0	94.4	16.8	95.5	9.6

3.3.4.2 Random Forest

Multiple RF classifications were performed by labelling MA-only samples as the positive class and rotating metabolites in turn as the negative class. This resulted in four classification models which are summarised in Tables 3-12 and 3-13.

Table 3-12: RF classification summary of parent drug MA against each of the metabolites in serum. Pre-processing steps included SG smoothing, vector normalisation, rubberband baseline correction and mean centring was performed during model construction.

Sensitivities, specificities, and balanced accuracies are reported as means and standard deviations (SD) of 51 iterations.

Drug molecule against MA	Sampling	Sensitivity (%)		Specificity (%)		Balanced Accuracy (%)	
		Mean	SD	Mean	SD	Mean	SD
AM	Down	91.1	11.7	90.4	11.3	90.7	8.1
NOR	Down	100	0	97.4	9.3	98.7	4.6
pOHMA	Down	92.4	11.9	92.1	17.1	92.3	10.5
pOHAM	Down	96.6	6.7	94.1	11.5	95.3	6.5

RF classification was also successful in classifying MA samples from their individual metabolites in both urine and serum. For NOR samples in serum, the RF sensitivity and specificity values were higher by 3.1 and 4.5% respectively when compared to that of the PLS-DA classification. In urine, however, PLS-DA classification performed better in distinguishing NOR samples from blank urine samples. For pOHAM samples, both classification models achieved similar results in both biofluids whereby the sensitivity and specificity values only differed by ± 1-3% and the standard errors associated with these values showed a similar trend. The pOHMA samples showed a similar trend for the serum dataset while the RF classification performed perfectly in the urine dataset with 100% sensitivity and specificity.

Table 3-13: RF classification summary of parent drug MA against each of the metabolites in urine. Pre-processing steps included SG smoothing, vector normalisation, rubberband baseline correction and mean centring was performed during model construction.

Sensitivities, specificities, and balanced accuracies are reported as means and standard deviations (SD) of 51 iterations.

Drug molecule against MA	Sampling	Sensitivity (%)		Specificity (%)		Balanced Accuracy (%)	
		Mean	SD	Mean	SD	Mean	SD
AM	Down	87.0	19.1	96.0	10.3	91.5	9.6
NOR	Down	93.3	11.0	87.0	13.1	90.1	8.3
pOHMA	Down	100	0	100	0	100	0
pOHAM	Down	91.7	17.0	98.4	6.7	95.1	8.8

The spectral regions highlighted in the difference spectra of serum samples in Figure 3-5 are also reflected in the Gini importance plots obtained from these four RF classification models. These are shown in Figure 3-11 for serum samples. The overlaid spectra of the blank matrix, drug samples in the matrix and the powder spectra of drugs for the 4 metabolites are presented alongside the parent drug MA in Appendix 1 (Figures A1-1 and A1-2). These figures illustrate the corresponding drug peaks These plots illustrate that the differences due to mono- and di-substitution of the ring highlighted by the purple boxes in the 1225 - 950 cm^{-1} region are significant in all four classification models MA and its metabolites, NOR, pOHMA and pOHAM.

The stretching vibrations at 2460 cm^{-1} attributed to the hydrochloride salt present in MA indicated by the grey box in plot 1 in Figure 3-11 is of particular significance for the classification of MA against its major metabolite and structurally very similar molecule, AM. The differences between the aliphatic side chains between MA and AM are also emphasised by the Gini importance plot (Green box in plot 1 in Figure 3-11). The same region C illustrated by the green box in plot 3 in Figure 3-14 is significant in the classification of MA against pOHAM. This is due to the stretching vibrations of the aliphatic side chain with the primary amine group in AM and pOHAM while both MA is a secondary amine.

For urine samples, a similar trend is observed whereby the spectral regions of importance highlighted in the Gini importance plot in Figure 3-12 are corroborated by those in the difference spectra shown in Figure 3-7. The region A (850 – 700 cm^{-1}) indicating the out-of-

plane deformation vibration modes presented in orange boxes in Figure 3-12 is significant in all four classification models.

The strong thiocyanate peak at 2041 cm^{-1} in the urine matrix showed a significant impact on the classification between MA and its metabolites owing to the reaction between the molecule and the matrix. The greatest example of this is seen in the classification between MA and pOHMA in plot 4 in Figure 3-12. While it was also of significance in the discrimination of MA from AM as well as MA from NOR, the 2041 cm^{-1} peak was relatively less significant in the classification of MA and pOHAM. This can likely be attributed to the varying strength of the reaction between the molecules and the matrix as is reflected by the varying intensities of the 2041 cm^{-1} peak in the difference spectra of the metabolites (Figure 3-7). Because the difference spectra for MA and pOHMA were at 10 mg/mL and 3 mg/mL, a more appropriate comparison of the same concentration is shown in Figure A1-3 in Appendix 1. The reaction between the matrix and pOHMA is stronger than that of MA indicated by the lower intensity of the 2041 cm^{-1} peak seen for pOHMA. As this reaction is an artefact of the brand of artificial urine employed in this study, its impact needs to be interpreted with caution on the classification models and its occurrence investigated should be in real urine samples.

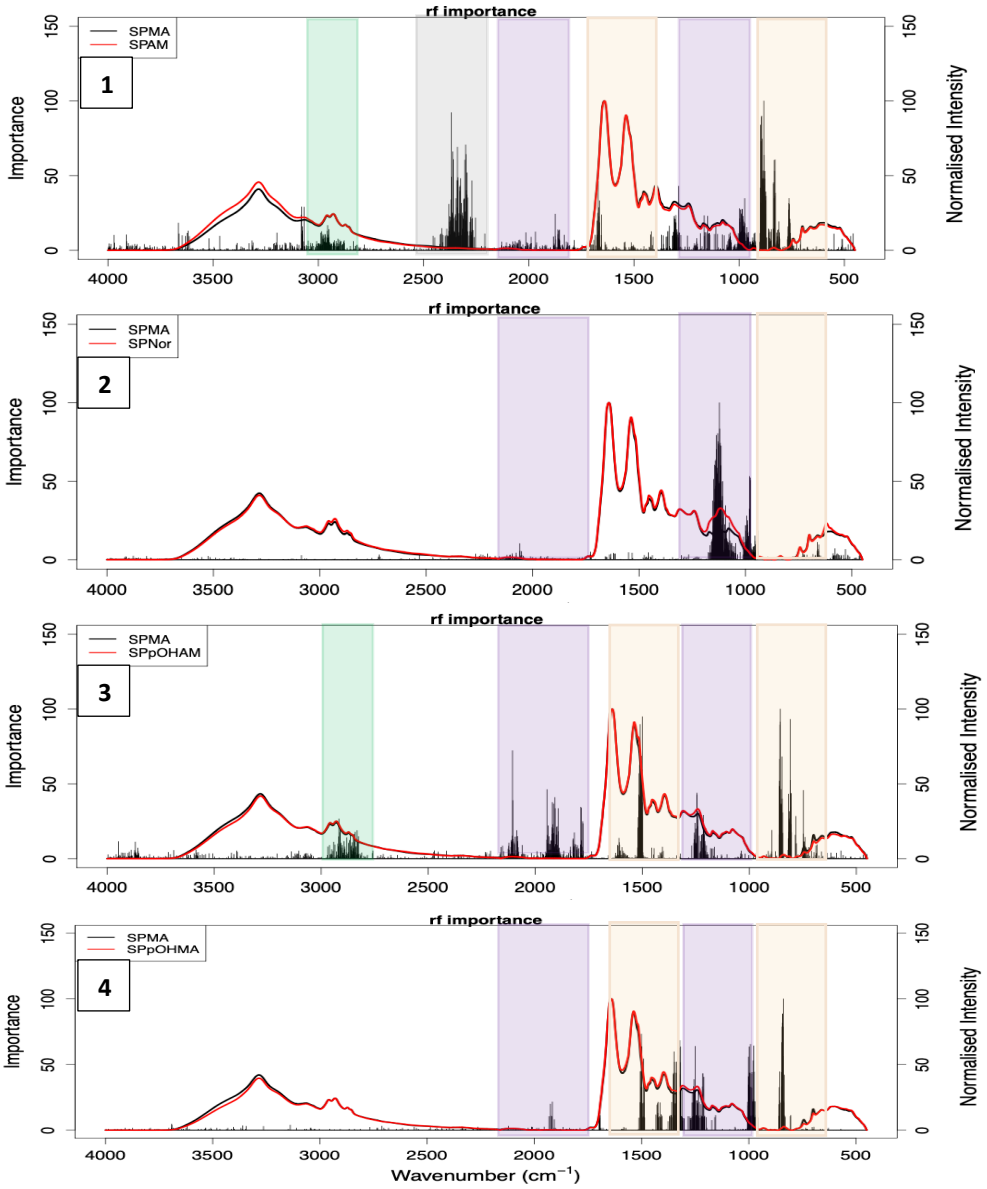

Figure 3-11: Gini importance plots for RF classification of MA against AM (1), NOR (2), pOHAM (3) and pOHMA (4) in serum. Spectral regions of importance are indicated by coloured boxes where orange boxes highlight region A (1650-1400 and 950-650 cm^{-1}; vibrations due to the aromatic ring), purple boxes highlight region B (2000-1650, 1225-950 cm^{-1}; vibrations indicating substitution on the ring) and green box highlights region C (2932-2715 cm^{-1}; aliphatic vibrations from the side chain). SPMA refers to MA samples in serum, SPAM refers to AM samples in serum, SPNOR refers to NOR samples in serum, SPpOHAM refers to pOHAM samples in serum and SPpOHMA refers to pOHMA samples in serum.

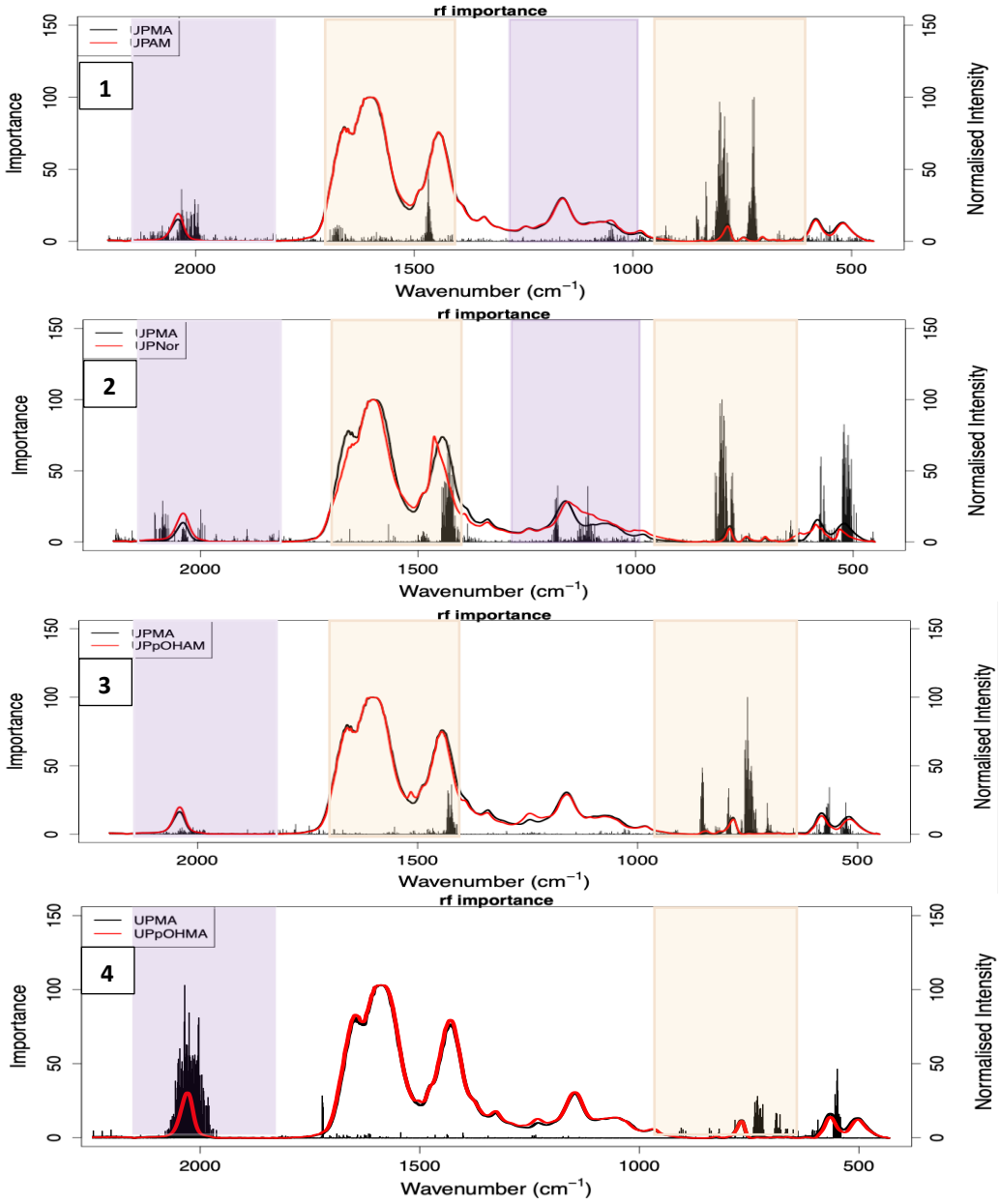

Figure 3-12: Gini importance plots for RF classification of MA against AM (1), NOR (2), pOHAM (3) and pOHMA (4) in urine. Spectral regions of importance are indicated by coloured boxes where orange boxes highlight region A (1650-1400 and 950-650 cm^{-1}; vibrations due to aromatic ring) and purple boxes highlight region B (2000-1650, 1225-950 cm^{-1}; vibrations indicating substitution on the ring). UPMA refers to MA samples in urine, UPAM refers to AM samples in urine, UPNOR refers to NOR samples in urine, UPpOHAM refers to pOHAM samples in urine and UPpOHMA refers to pOHMA samples in urine.

Upon the use of the second derivative, the RF sensitivity and specificity values improved for the serum dataset while the urine dataset showed a lower sensitivity by 13.1% and an improvement in the specificity by 6.4%. As much of the distinguishing features i.e., vibrations from the aliphatic side chains in the 3000-2700 cm^{-1} region useful in this classification are masked by the serum background, the use of the second derivative allows resolving these improving the overall sensitivity and specificity. For the urine dataset, however, the classification was mainly based on the features in regions A and B which meant that the key distinguishing structural region (region C; aliphatic side chain) was not included in the model due to higher variability in sample drying. Overall, RF models performed better for the serum dataset with lower standard deviations and higher balanced accuracies than that for PLS-DA classification.

Table 3-14: RF classification summary of MA against AM with the second derivative employed during pre-processing. Pre-processing steps included SG smoothing, vector normalisation, rubberband baseline correction and second derivative with mean centring being performed during model construction. Sensitivities, specificities, and balanced accuracies are reported as means and standard deviations (SD) of 51 iterations.

Biofluid	Drug molecule against MA	Sampling	Sensitivity (%)		Specificity (%)		Balanced Accuracy (%)	
			Mean	SD	Mean	SD	Mean	SD
Serum	AM	Down	99.7	2.0	98.6	4.2	99.1	2.3
Urine	AM	Down	83.6	27.7	100	0	91.8	13.8

3.3.5 Blank Samples versus Drug Samples

Finally, all drug compounds i.e. 1 parent drug and 4 metabolites were grouped together as a single class in order to distinguish between samples that contain drugs from those that do not. Tables 3-15 and 3-16 provide a summary of PLS and RF classification results respectively. The sensitivity and specificity values for this PLS classification of blank samples versus drug-spiked samples in serum were 95.2 ± 7.4% and 80.8 ± 6.8%. This indicates that the model was able to correctly identify drug-negative samples 95.2% of the time and drug-positive samples 80.8% of the time. PLS classification on the urine dataset achieved sensitivity and specificity of 91.6 and 91.1% which indicates that the model was able to correctly classify drug-free and drug-positive samples ~91% of the time. PLS classification was found to be stronger than RF

analysis of similar samples with higher values for sensitivities and specificities for serum and urine with higher overall balanced accuracies. However, the Gini importance plots for serum and urine datasets corroborate that the features contributing to the RF classification of drug-free samples from drug-positive samples fall in the spectral regions A to D identified in the powder and the difference spectra (Figures 3-4, 3-7, 3-8 and 3-13). The peak at 2460 cm^{-1} reflective of the hydrochloride salt form of MA, shows high significance in the Gini importance plot for the serum dataset, it is only present in the MA molecule. The position, intensity and shape of this peak are highly dependent on the molecular environment and therefore were not included in the regions identified in this analysis.[87]

Table 3-15: PLS-DA results of blank biofluid samples against all drug samples grouped together as 'Other', where Blank = positive class (sensitivity) and Other = negative class (specificity). Pre-processing steps included SG smoothing, vector normalisation, rubberband baseline correction and mean centring was performed during model construction. All values are reported as means and standard deviations (SD) of 51 iterations.

Blank against "Other" (Positive = Blank; Negative = Other)	Sampling	Sensitivity (%)		Specificity (%)		Balanced Accuracy (%)	
		Mean	SD	Mean	SD	Mean	SD
Serum	Up	95.2	7.4	80.8	6.8	88.0	4.5
Urine	Up	91.6	12.9	91.1	4.6	91.3	6.8

Table 3-16: RF results of blank biofluid samples against all drug samples grouped together as 'Other', where Blank = positive class (sensitivity) and Other = negative class (specificity). Pre-processing steps included SG smoothing, vector normalisation, rubberband baseline correction and mean centring was performed during model construction. All values are reported as means and standard deviations (SD) of 51 iterations.

Blank against "Other" (Positive = Blank; Negative = Other)	Sampling	Sensitivity (%)		Specificity (%)		Balanced Accuracy (%)	
		Mean	SD	Mean	SD	Mean	SD
Serum	Down	74.5	14.2	90.3	5.2	82.4	7.3
Urine	Down	85.2	18.2	86.5	6.2	85.9	9.4

To our knowledge, there are no publications that explore the application of ATR-FTIR spectroscopy combined with chemometrics to unextracted biological samples to identify the presence of drugs of abuse with such high sensitivities and specificities. Therefore, the results presented here of both classification models derived from clinically and forensically relevant concentrations are significant to the application of this method in and out of the lab.

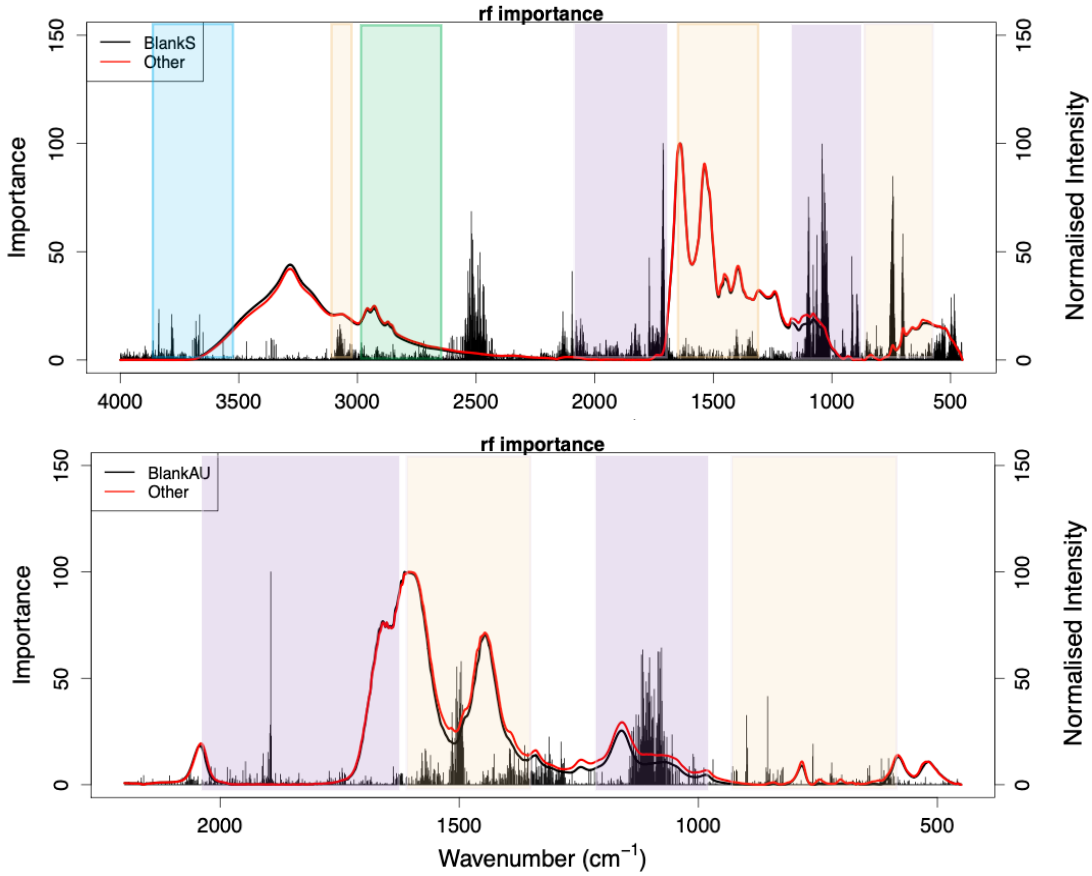

Figure 3-13: Gini importance plots of RF classification of blank biofluid against drug samples in that biofluid. In the top image, BlankS refers to drug-free serum samples and Other refers to drug-positive serum samples. In the bottom image, BlankAU refers to blank urine or drug-free urine samples and Other refers to urine samples with drugs in them. Orange box shows spectral region A (3100-3000 cm^{-1}, 1650-1400 cm^{-1} and 950-650 cm^{-1}), purple box indicates spectra region B (2050-1650 cm^{-1}, 1225-950 cm^{-1}), green box indicates spectral region C (2950-2700 cm^{-1}) and blue box indicates spectral region D (3600-3300 cm^{-1}).

Finally, PLS-DA was performed for the detection of MA-only samples from those that contain MA with its metabolites. For the classification, MA-only samples were kept as the positive class while the negative class was labelled as 'Other' which included samples containing its four metabolites. The classification results are summarised in Table 3-17 for both serum and

urine datasets. When classified against all metabolites, the sensitivity and specificity values of 83.4 and 88.8% for MA in serum respectively and 90.9 and 86.7% for MA in urine respectively were lower than that observed for individual analyses (Tables 3-7 and 3-8). This is likely due to many overlapping features in the negative class from all the metabolites.

For a similar analysis of the urine dataset, sensitivity improved by 7.5% which again can be attributed to the less complex nature of the urine matrix. However, it can be said that the PLS-DA model holds up well in the face of numerous spectral signatures in the negative class and is able to identify the presence of the parent drug in biofluids relatively well with strong sensitivities and specificities. This has clinical implications as the correct combination of MA with its major and minor metabolites could indicate time passed since the administration of MA.

Table 3-17: PLS-DA results of MA samples against all metabolites grouped together as 'Other', where MA = positive class(sensitivity) and Other = negative class (specificity). Pre-processing steps included SG smoothing, vector normalisation, rubberband baseline correction and mean centring performed during model construction. All values are reported as means and standard deviations (SD) of 51 iterations.

MA against "Other" (Positive = MA; Negative = Other)	Sampling	Sensitivity (%)		Specificity (%)		Balanced Accuracy (%)	
		Mean	SD	Mean	SD	Mean	SD
Serum	Up	83.4	13.5	88.8	6.8	86.1	6.3
Urine	Down	90.9	12.8	86.7	8.4	88.8	7.9

3.3.6 Blind Samples

Finally, three binary PLS-DA models were constructed using samples listed in Table 3-1 where the positive class was rotated between MA, AM and NOR, while the negative class, labelled as 'Other', consisted of the remaining two drug samples. Each binary classification model (for example - MA vs Other, AM vs Other or NOR vs Other) was trained to predict the positive class and was tested using an independent test set made up of two groups of samples – single drug samples (n=13) listed in Table 3-2 and a mixture of MA with a metabolite (n=4) listed in Table 3-3. Only AM, and NOR were included in the blind dataset as these two compounds are drugs sold on their own as well as being metabolites of MA. Hence it is more likely that they are found in illicit samples as well as in conjunction with illicit MA.

In Table 3-18, the cells highlighted in green indicate the correctly identified samples in relation to the positive class for that binary classification. The cells in red show those samples that were misclassified when they should have been identified as the positive class. Surprisingly, in the first binary classification with MA as the positive class, sample 9007 is misclassified as 'Other' even though it contains a high concentration of MA. This is likely an error either in the preparation of the sample or during the spectral collection and should be re-created and/or analysed.

Table 3-18: Blind single drug samples were classified using PLS-DA analysis where the three drugs, MA, AM and NOR, were rotated to be the positive class and the rest were included in as 'Other' that formed the negative class. Pre-processing steps included SG smoothing, vector normalisation, and rubberband baseline correction. Mean centring was performed during model construction. Those highlighted in green were correctly classified and those in red were misclassified by the PLS-DA model.

Sample ID	Actual Drug present	Concentration (mg/mL)	Predicted - Positive class		
			MA	AM	NOR
9001	NOR	0.4	Other	Other	NOR
9002	MA	0.3	MA	Other	Other
9003	AM	0.37	Other	Other	NOR
9004	MA	0.5	MA	Other	NOR
9005	MA	1	MA	Other	Other
9006	MA	4	MA	Other	Other
9007	MA	9	Other	Other	Other
9008	AM	2	Other	AM	Other
9009	AM	5	Other	AM	Other
9010	AM	7	Other	AM	Other
9011	NOR	1	Other	Other	NOR
9012	NOR	3	Other	Other	NOR
9013	NOR	9	Other	Other	NOR

For the second test set, that of mixed drug-metabolite samples (listed in Table 3-3), MA was labelled as the positive class, and the remaining drug samples as 'Other'. Here, the models were trained to predict MA-only samples as the positive class – implying that all samples that contain MA and its metabolites should have been classified as 'Other'. This was done to test the capabilities of the model built in this chapter to distinguish samples that contain MA and

other compounds – which can either be the metabolites of MA or any other adulterants present.

Table 3-19 shows the PLS-DA results whereby one out of the four mixed blind samples was correctly classified as 'Other' (shown in green). The potential reason for this misclassification of the three samples is that all mixed samples contain MA in dominating concentrations compared to the metabolite. Furthermore, sample 9014 contained AM as the metabolite which is much closer in structure to MA than NOR, potentially contributing to its correct classification. One limitation to note here is that street samples consumed in the real world are not only likely to contain MA and its metabolites including those not considered in this study but also cutting agents and potentially their metabolites. However, with a bigger training dataset containing a greater range of samples and concentrations, the application of these classification models to real-world samples is promising.

Table 3-19: PLS-DA classification predictions for mixed blind samples. Pre-processing steps included SG smoothing, vector normalisation, and rubberband baseline correction. Mean centring was performed during model construction. The classification was performed where MA was the positive class, and all others were included as 'Other' in the negative class.

Sample ID	Actual drug combination present	Predicted
9014	0.6 mg/mL MA + 0.1 mg/mL AM	Other
9015	0.8 mg/mL MA + 0.12 mg/mL NOR	SPMA
9016	1 mg/mL MA + 0.17 mg/mL AM	SPMA
9017	0.3 mg/mL MA + 0.1 mg/mL NOR	SPMA

3.3.7 PLS-R Results

As a final step in this proof-of-concept chapter, PLS regression analysis was performed to determine the limits of detection (LOD) and quantification (LOQ) for the parent drug and its metabolites in urine and serum. The dataset was split into an 80% training set and a 20% test set to build a PLS model with 10-fold cross-validation. All replicates for each sample were kept together when splitting the dataset into training and test set. The results of this are collated in Table 3-18 and an example graph is shown in Figure 3-20. The remaining graphs are included in Appendix 1 (Figures A1-4, A1-5, A1-6 and A1-7).

The PLS-R analysis showed good linearity across all drugs and performed well at predicting the limits of detection and quantification. For MA, the results are promising as the limit of

detection of 0.1 mg/mL and the limit of quantification of 0.3 mg/mL fall within the concentration range relevant to the clinical and forensic setting. Similar detection and quantification limits for the four metabolites of MA in both biofluids obtained without any sample extraction steps illustrate promising first steps of this protocol. With more samples per drug and a wider concentration range, it is possible to expand these detection and quantification limits on either end. When interpreting the concentrations from real-world samples using this PLS regression analysis, caution must be used in using exact numbers as these models are derived from single dose calculations not accounting for accumulation in the body. Furthermore, it is difficult to determine the effect of post-mortem redistribution on the antemortem and post-mortem concentrations in a forensic toxicology context as comparative samples from the same individuals are rarely available.[88]

Table 3-20: Summary table showing PLS-Regression analysis performed on the calibration standards ranging in concentration from 0.1-10 mg/mL for each drug molecule with the exception of pOHMA. The concentration range for pOHMA was 0.1 – 3 mg/mL. Blank serum samples were included to represent 0 mg/mL. Pre-processing steps included SG smoothing, vector normalisation, and rubberband baseline correction.

	Drug molecule	**Limit of detection (mg/mL)**	**Limit of Quantification (mg/mL)**	**R^2**	**RMSECV (mg/mL)**
Serum	MA	0.102	0.339	0.996	0.385
	AM	0.100	0.335	0.986	0.378
	NOR	0.125	0.418	0.995	0.242
	pOHAM	0.210	0.702	0.995	0.231
	pOHMA	0.076	0.255	0.994	0.068
Urine	MA	0.29	0.966	0.989	0.334
	AM	0.121	0.402	0.998	0.129
	NOR	0.157	0.523	0.992	0.297
	pOHAM	0.301	0.989	0.845	1.28
	pOHMA	0.29	0.92	0.820	0.40

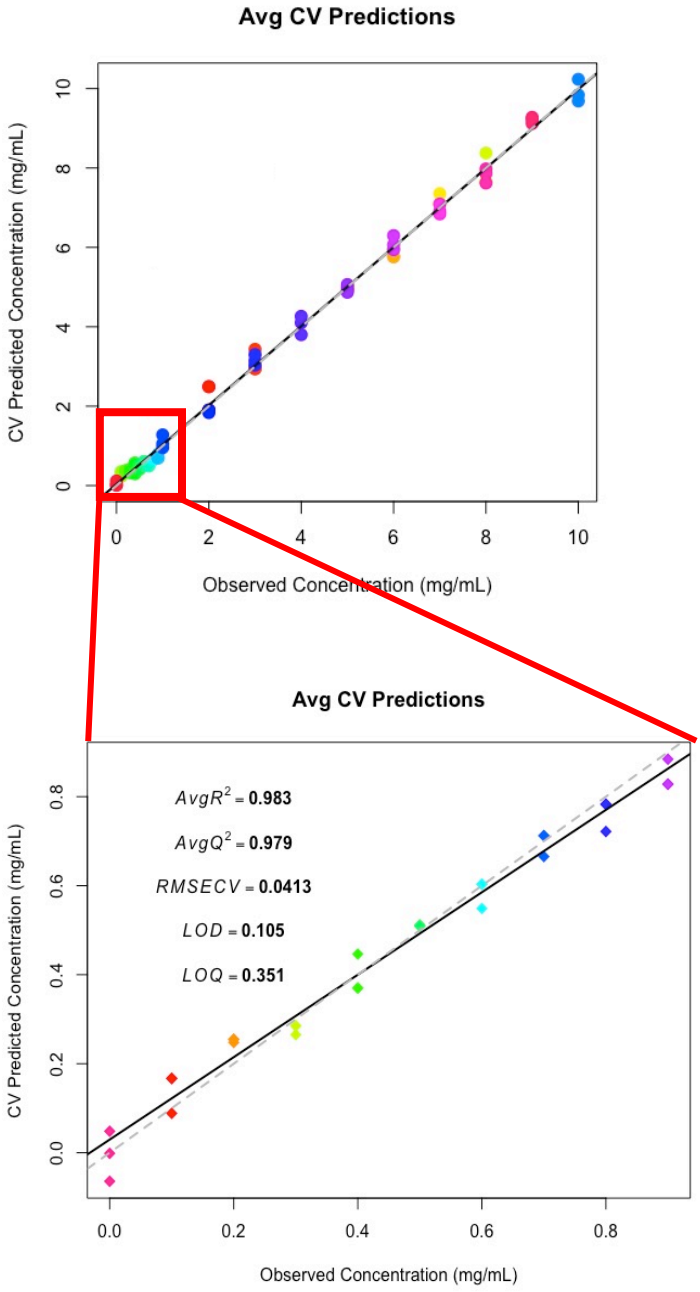

Figure 3-14: Graph showing PLS-R analysis for MA samples in serum across the concentration range of 0.1-10 mg/mL. The clinically and forensically relevant concentration range from 0.1 – 0.9 mg/mL is showed in an expanded graph at the bottom for clarity.

3.4 Conclusions

In this chapter, the ability of ATR-FTIR spectroscopy to analyse drug powders and liquid biological samples was combined to demonstrate the successful detection of MA in serum and urine without the use of prior sample extraction methods. Furthermore, the method was also applied to the detection of four metabolites of MA, namely AM, NOR, pOHMA and pOHAM, in serum and urine. Despite the complexity of serum and urine, detection of these comparatively small drug and metabolite molecules was possible through the use of multivariate analytical techniques.

Robust classification results were achieved through PLS-DA and were corroborated with visual spectral examination and random forest analysis. For the discrimination of MA-only samples from neat biofluids, sensitivities and specificities of ~91% in serum and ~95% in urine with balanced accuracies of 91.7 and 95.9% in serum and urine respectively are reported using PLS-DA classification. Furthermore, PLS-DA classification was able to discriminate MA from its metabolites, showing success even with the structurally similar AM, only differing from MA by a methyl group. This successful discrimination of MA from AM, with sensitivity and specificity values of 96.1% and 93.2% in serum and 86.2% and 88.2% in urine, illustrates the potential beneficial value of this method in a forensic setting. Overall, this protocol was able to discriminate between drug-free/blank samples from those that contained drugs in both biofluids with sensitivity and specificity values of 95.2 ± 7.4% and 80.8 ± 6.8% in serum and 91.6 ± 12.9% and 91.1 ± 4.6% in urine respectively. This is significant to clinical and forensic settings as the samples included here cover the upper limit of the clinical concentrations and overdose concentrations in forensic cases. It is also prudent to keep in mind that composition of real biological samples from patients are likely to show differences due to diet, ethnicity, gender, age, genetic differences in relevant metabolic enzymes and use of other medications. Therefore, it is important to view these results in light of these factors and make interpretations accordingly.

In addition, the predictive capabilities of this classification methodology were successfully tested in this study with blind samples. Out of 17 blind samples, 12 were successfully classified which included individual drug compound samples as well as MA+metabolite mixed samples. The blind samples containing drug-metabolite mixtures were more difficult to discriminate as the concentration of MA was higher in comparison to the metabolite

compounds and the models presented here do not account for mixtures and potential interactions between molecules.

In order to establish limits of detection and quantification of MA and its metabolites in both serum and urine, PLS-Regression was utilised and produced robust results for all 5 compounds examined. In particular, the regression model built for MA shows excellent linearity in serum and urine with R^2 values of 0.985 and 0.989 respectively. The limits of detection and quantification for MA from the PLS-R model were reported to be 0.102 and 0.339 mg/mL in serum and 0.29 and 0.966 mg/mL in urine respectively. While the concentrations studied here are more reflective of single-dose levels in serum and urine, chronic MA users show a tendency to accumulate MA from long-term abuse.[64] Moreover, real samples are likely to be more complex in composition and contain MA, its metabolites in varying concentrations and combinations as well as any cutting agents and impurities from illicit production. It is therefore important to exercise caution when interpreting concentrations of real-world samples using the regression models presented here. Improvements to the results presented here can be made by enriching the dataset with a variety of drugs, drug mixtures and concentrations. More specifically, lowering the concentration range to include concentrations from 0.006 -0.1 mg/mL would be beneficial for its application in the clinical setting. Air-drying of samples was employed in the development of this method. However, if a more standardised drying protocol is employed, it is likely to reduce spectral variation leading to improved results.

MA remains one of the most consumed drugs of abuse globally. With the rise of novel drugs and their consumption in polydrug settings, it is necessary to detect and identify these molecules not only in their powdered form but also upon consumption in biological fluids such as roadside drug testing. Furthermore, the consumption of drugs in an almost 'fashion/trendy' manner requires analytical methods to be quickly adaptable to be useful in detecting novel substances found in street drugs. The results reported here were successful in detecting and distinguishing MA in biological fluids from controls and other drug molecules without any sample extraction or use of other reagents. ATR-FTIR spectroscopy was demonstrated to be translatable across five drug molecules in this chapter without the need for altering the analytical protocol making it valuable in the analysis of novel substances. Additionally, once the multivariate models were trained, the results were obtained within a matter of minutes which is unmatched when compared to the current gold standard

techniques of hyphenated mass spectrometry. Therefore, the proof-of-concept work presented in this chapter utilising the quick, label- and reagent-free analysis afforded by ATR-FTIR spectroscopy combined with chemometrics provides a strong basis for future work in developing this method for a variety of drugs, drug-metabolite and drug-cutting agent mixtures in varying concentrations. This aspect of sample complexity arising from the adulteration of pure drug samples is explored in the upcoming chapter.

3.5 References

1. United Nations Office of Drugs and Crime, *World Drug Report Booklets 1-6*, United Nations Office of Drugs and Crime, Vienna, Austria, 2020.
2. United Nations Office on Drugs and Crime, *Understanding the Synthetic Drug Market Nps Factor*, United Nations Office on Drugs and Crime, Vienna, Austria, 2018.
3. United Nations Office on Drugs and Crime, *An Expanding Synthetic Drugs Market - Implications for Precursor Control*, 2020.
4. United Nations Office on Drugs and Crime, *Methamphetamine Continues to Dominate Synthetic Drug Markets*, United Nations Office on Drugs and Crime, Vienna, Austria, 2018.
5. United Nations Office of Drugs and Crime, *World Drug Report Booklet 4* United Nations Office of Drugs and Crime, Vienna, Austria, 2021.
6. T. Newton, R. De La Garza, A. Kalechstein and L. Nestor, *Pharmacology, Biochemistry, and Behavior*, 2005, **82**, 90-97.
7. T. F. Newton, R. De La Garza, T. Fong, N. Chiang, T. H. Holmes, D. A. Bloch, A. Anderson and A. Elkashef, *Pharmacology Biochemistry and Behavior*, 2005, **82**, 704-711.
8. M. Perez-Reyes, W. R. White, S. A. McDonald, J. M. Hill, A. R. Jeffcoat and C. E. Cook, *Life sciences*, 1991, **49**, 953-959.
9. C. E. Cook, A. R. Jeffcoat, J. M. Hill, D. E. Pugh, P. K. Patetta, B. M. Sadler, W. R. White and M. Perez-Reyes, *Drug metabolism and disposition: the biological fate of chemicals*, 1993, **21**, 717-723.
10. S. A. Shappell, G. L. Kearns, J. L. Valentine, D. F. Neri and C. A. DeJohn, *The Journal of Clinical Pharmacology*, 1996, **36**, 1051-1063.
11. R. J. F. Scheppers, J. M. Oyler, R. E. J. Joseph, E. J. Cone, E. T. Moolchan and M. A. Huestis, *Clinical Chemistry*, 2003, **49**, 121-132.
12. D. S. Harris, H. Boxenbaum, E. T. Everhart, G. Sequeira, J. E. Mendelson and R. T. Jones, *Clinical Pharmacology and Therapeutics*, 2003, **74**, 475-486.
13. United Nations Office of Drugs and Crime, *World Drug Report Booklet 2*, United Nations Office of Drugs and Crime, Vienna, Austria, 2021.
14. S. Graziano, L. Anzillotti, G. Mannocchi, S. Pichini and F. P. Busardo, *Journal of Pharmaceutical and Biomedical Analysis*, 2019, **163**, 170-179.
15. M. Philp and S. Fu, *Drug Testing and Analysis*, 2018, **10**, 95-108.
16. K. Kovar and M. Laudszun, *United Nations- Scientific and Technical Notes*, 1989, **89**, 1-19.
17. United Nations Office of Drugs and Crime, *Rapid Testing Methods of Drugs of Abuse*, United Nations Office of Drugs and Crime, Vienna, Austria, 1994.
18. C. L. O'Neal, D. J. Crouch and A. A. Fatah, *Forensic Science International*, 2000, **109**, 189-201.
19. C. Heesun and C. Sanggil, *Mass Spectrometry Letters*, 2019, **10**, 1-10.
20. G. Mercieca, S. Odoardi, M. Cassar and S. Strano Rossi, *Journal of Pharmaceutical and Biomedical Analysis*, 2018, **149**, 494-501.
21. F. Vaiano, F. P. Busardò, D. Palumbo, C. Kyriakou, A. Fioravanti, V. Catalani, F. Mari and E. Bertol, *Journal of Pharmaceutical and Biomedical Analysis*, 2016, **129**, 441-449.
22. M. K. Wozniak, M. Wiergowski, J. Aszyk, P. Kubica, J. Namiesnik and M. Biziuk, *Journal of Pharmaceutical and Biomedical Analysis*, 2018, **148**, 58-64.
23. C.-H. Chiang, H.-H. Lee, B.-H. Chen, Y.-C. Lin, Y.-Y. Chao and Y.-L. Huang, *Journal of Food and Drug Analysis*, 2019, **27**, 439-450.
24. A. El-Beqqali, L. I. Andersson, A. D. Jeppsson and M. Abdel-Rehim, *Journal of Chromatography B*, 2017, **1063**, 130-135.

25. A.-M. Dragan, M. Parrilla, B. Feier, R. Oprean, C. Cristea and K. De Wael, *Trends in Analytical Chemistry*, 2021, **145**, 116447.
26. J. Esteve-Romero, J. Albiol-Chiva and J. Peris-Vicente, *Analytica Chimica Acta*, 2016, **926**, 1-16.
27. L. Liu, S. E. Wheeler, R. Venkataramanan, J. A. Rymer, A. F. Pizon, M. J. Lynch and K. Tamama, *American Journal of Clinical Pathology*, 2018, **149**, 105-116.
28. E. Deconinck, C. Duchateau, M. Balcaen, L. Gremeaux and P. Courselle, *Reviews in Analytical Chemistry*, 2022, **41**, 228-255.
29. Scientific Working Group for the Analysis of Seized Drugs, *Construction of an Analytical Scheme*, United States Department of Justice, Drug Enforcement Administration, United States, 2020.
30. J. Hughes, G. Ayoko, S. Collett and G. Golding, *PLOS ONE*, 2013, **8**, e69609-e69609.
31. C. Y. Goh, W. Van Bronswijk and C. Priddis, *Applied Spectroscopy*, 2008, **62**, 640-648.
32. K. Tsujikawa, K. Kuwayama, H. Miyaguchi, T. Kanamori, Y. T. Iwata, T. Yoshida and H. Inoue, *Analytica Chimica Acta*, 2008, **608**, 95-103.
33. O. Barran, MASTER OF SCIENCE, Middle East Technical University, 2005.
34. D. Custers, T. Cauwenbergh, J. L. Bothy, P. Courselle, J. O. De Beer, S. Apers and E. Deconinck, *Journal of Pharmaceutical and Biomedical Analysis*, 2015, **112**, 181-189.
35. L. S. A. Pereira, F. L. C. Lisboa, J. Coelho Neto, F. N. Valladao and M. M. Sena, *Forensic Science International*, 2018, **288**, 227-235.
36. J. Coelho Neto, *Forensic Science International*, 2015, **252**, 87-92.
37. S. R. Al-Hussaini, *Science & Justice*, 1996, **36**, 139-142.
38. F. Been, Y. Roggo, K. Degardin, P. Esseiva and P. Margot, *Forensic Science International*, 2011, **211**, 83-100.
39. K. Banas, A. Banas, H. O. Moser, M. Bahou, W. Li, P. Yang, M. Cholewa and S. K. Lim, *Analytical Chemistry*, 2010, **82**, 3038-3044.
40. K. Castro, S. F. O. de Vallejuelo, I. Astondoa, F. M. Goñi and J. M. Madariaga, *Journal of Raman Spectroscopy*, 2011, **42**, 2000-2005.
41. C. Martín-Alberca, F. Zapata, H. Carrascosa, F. E. Ortega-Ojeda and C. García-Ruiz, *Talanta*, 2016, **149**, 257-265.
42. F. Bonnier, M. J. Baker and H. J. Byrne, *Analytical Methods*, 2014, **6**.
43. A. A. Bunaciu, Ş. Fleschin, V. D. Hoang and H. Y. Aboul-Enein, *Critical Reviews in Analytical Chemistry*, 2017, **47**, 67-75.
44. J. Ollesch, S. L. Drees, H. M. Heise, T. Behrens, T. Brüning and K. Gerwert, *Analyst*, 2013, **138**, 4092-4102.
45. C. M. Orphanou, L. Walton-Williams, H. Mountain and J. Cassella, *Forensic Science International*, 2015, **252**, e10-16.
46. J. Zhang, B. Li, Q. Wang, C. Li, Y. Zhang, H. Lin and Z. Wang, *Spectrochimica Acta Part A: Molecular and Biomolecular Spectroscopy*, 2017, **173**, 733-739.
47. P. Huang, Y. Ke, Q. Lu, B. Xin, S. Fan, G. Yang and Z. Wang, *Spectroscopy*, 2008, **22**, 21-31.
48. P. Huang, C. Su, S. Li, B. Xing, Y. Tuo, Q. Lu, Y. Ke and Z. Wang, *Fa yi xue za zhi*, 2010, **26**, 1-5.
49. Y. Tuo, P. Huang, Y. Ke, S. Fan, Q. Lu, B. Xin and Z. Wang, *Applied Spectroscopy*, 2010, **64**, 268-274.
50. K. M. Hans, S. Müller and M. W. Sigrist, *Drug Testing and Analysis*, 2012, **4**, 420-429.
51. K. M.-C. Hans, M. Müller, M. Gianella, P. Wägli and M. Sigrist, *Proceedings of Society of Photo-Optical Instrumentation Engineers*, 2013, **8591**.

52. K. M. C. Hans, M. Müller, T. Petrosyan and M. W. Sigrist, *Analytical Methods*, 2014, **6**, 666-673.
53. M. J. Baker, J. Trevisan, P. Bassan, R. Bhargava, H. J. Butler, K. M. Dorling, P. R. Fielden, S. W. Fogarty, N. J. Fullwood, K. A. Heys, C. Hughes, P. Lasch, P. L. Martin-Hirsch, B. Obinaju, G. D. Sockalingum, J. Sulé-Suso, R. J. Strong, M. J. Walsh, B. R. Wood, P. Gardner and F. L. Martin, *Nature Protocols*, 2014, **9**, 1771-1791.
54. M. Allendorf, A. Subramanian and L. Rodriguez-Saona, *Journal of the American Oil Chemists' Society*, 2012, **89**, 79-88.
55. G. Gorla, M. Mestres, R. Boqué, J. Riu, D. Spanu and B. Giussani, *Chemometrics and Intelligent Laboratory Systems*, 2020, **200**, 103995.
56. M. Ramsay, L. Gozdzialski, A. Larnder, B. Wallace and D. Hore, *Vibrational Spectroscopy*, 2021, **114**, 1-7.
57. F. Musshoff, *Drug Metabolism Reviews*, 2000, **32**, 15-44.
58. United Nations Office of Drugs and Crime, *World Drug Report 2019 Booklet 4 - Stimulants*, United Nations Office of Drugs and Crime, Vienna, Austria, 2019.
59. C. C. Cruickshank and K. R. Dyer, *Addiction*, 2009, **104**, 1085-1099.
60. T. E. Albertson, R. W. Derlet and B. E. Van Hoozen, *Journal*, 1999, **170**, 214.
61. J. M. Oyler, E. J. Cone, R. E. Joseph, Jr, E. T. Moolchan and M. A. Huestis, *Clinical Chemistry*, 2002, **48**, 1703-1714.
62. J. Mendelson, N. Uemura, D. Harris, R. P. Nath, E. Fernandez, P. Jacob, 3rd, E. T. Everhart and R. T. Jones, *Clinical Pharmacology and Therapeutics*, 2006, **80**, 403-420.
63. M. Perez-Reyes, W. R. White, S. A. McDonald, R. E. Hicks, A. R. Jeffcoat, J. M. Hill and C. E. Cook, *Clinical neuropharmacology*, 1991, **14**, 352-358.
64. N. D. Volkow, J. S. Fowler, G.-J. Wang, E. Shumay, F. Telang, P. K. Thanos and D. Alexoff, *PLOS ONE*, 2010, **5**, e15269-e15269.
65. L. P. Dwoskin, P. E. A. Glaser and M. T. Bardo, in *Addiction Medicine: Science and Practice*, ed. B. A. Johnson, Springer New York, New York, NY, 2011, pp. 1049-1061.
66. R. McKetin, E. Kelly and J. McLaren, *Drug and Alcohol Dependence*, 2006, **85**, 198-204.
67. K. S. Kalasinsky, T. Z. Bosy, G. A. Schmunk, G. Reiber, R. M. Anthony, Y. Furukawa, M. Guttman and S. J. Kish, *Forensic Science International*, 2001, **116**, 163-169.
68. C. E. Cook, A. R. Jeffcoat, B. M. Sadler, J. M. Hill, R. D. Voyksner, D. E. Pugh, W. R. White and M. Perez-Reyes, *Drug metabolism and disposition: the biological fate of chemicals*, 1992, **20**, 856-862.
69. R. De La Torre, S. Yubero-Lahoz, R. Pardo-Lozano and M. Farre, *Frontiers in Genetics*, 2012, **3**, 1-8.
70. L. Li, T. Everhart, P. Jacob Iii, R. Jones and J. Mendelson, *British Journal of Clinical Pharmacology*, 2010, **69**, 187-192.
71. L. Y. Lin, E. W. Di Steffano, D. A. Schmitz, L. Hsu, S. W. Ellis, M. S. Lennard, G. T. Tucker and A. K. Cho, *Drug Metabolism and Disposition*, 1997, **25**, 1059-1064.
72. I. Kim, j. Oyler, E. T. Moolchan, E. J. Cone and M. A. Huestis, *Therapeutic Drug Monitoring*, 2004, **26**, 664-672.
73. M. Carvalho, H. Carmo, V. M. Costa, J. P. Capela, H. Pontes, F. Remião, F. Carvalho and M. d. L. Bastos, *Archives of Toxicology*, 2012, **86**, 1167-1231.
74. R. de la Torre, M. Farre, M. Navarro, R. Pacifici, P. Zuccaro and S. Pichini, *Clinical Pharmacokinetics*, 2004, **43**, 157-185.
75. L. J. Schep, R. J. Slaughter and D. M. Beasley, *Clinical Toxicology*, 2010, **48**, 675-694.
76. N. Shima, H. T. Kamata, M. Katagi and H. Tsuchihashi, *Xenobiotica*, 2006, **36**, 259-267.

77. A. J. Barnes, M. L. Smith, S. L. Kacinko, E. W. Schwilke, E. J. Cone, E. T. Moolchan and M. A. Huestis, *Clinical Chemistry*, 2008, **54**, 172-180.
78. M. A. Huestis and E. J. Cone, *Annals of the New York Academy of Sciences*, 2007, **1098**, 104-121.
79. J. M. Cameron, H. J. Butler, D. S. Palmer and M. J. Baker, *Journal of Biophotonics*, 2018, **11**, e201700299.
80. J. R. Hands, K. M. Dorling, P. Abel, K. M. Ashton, A. Bordbelt, C. Davis, T. Dawson, M. D. Jenkinson, R. W. Lea, C. Walker and M. J. Baker, *Journal of Biophotonics*, 2014, **7**, 189-199.
81. A. Sala, K. E. Spalding, K. M. Ashton, R. Board, H. J. Butler, T. P. Dawson, D. A. Harris, C. S. Hughes, C. A. Jenkins, M. D. Jenkinson, D. S. Palmer, B. R. Smith, C. A. Thornton and M. J. Baker, *Journal of Biophotonics*, 2020, **13**, e202000118.
82. B. R. Smith, M. J. Baker and D. S. Palmer, *Chemometrics and Intelligent Laboratory Systems*, 2018, **172**, 33-42.
83. H. J. Butler, B. R. Smith, R. Fritzsch, P. Radhakrishnan, D. S. Palmer and M. J. Baker, *Analyst*, 2018, **143**, 6121-6134.
84. L. J. Bellamy, *The Infra-Red Spectra of Complex Molecules* Chapman and Hall, London, 3rd edn., 1075.
85. X. He, J. Wang, X. You, F. Niu, L. Fan and Y. Lv, *Spectrochimica Acta Part A: Molecular and Biomolecular Spectroscopy*, 2020, **241**, 118665.
86. J. Cameron, Doctor of Philosophy, University of Strathclyde, 2020.
87. V. Minaeva, B. Minaev, A. Panchenko and V. Pasychnik, *Journal of Molecular Modeling*, 2021, **27**, 1-15.
88. I. M. McIntyre, C. L. Nelson, B. Schaber and C. E. Hamm, *Journal of Analytical Toxicology*, 2013, **37**, 386-389.

CHAPTER FOUR

DETECTION OF ADULTERATED METHAMPHETAMINE IN BIOFLUIDS

Abstract

Access to drugs via other than legal channels means that neither developing nor developed countries are immune to the issue of adulterated drugs. In the case of clinically approved pharmaceuticals, for example, Desoxyn®, the adulteration generally stems from impurities left over during illicit manufacturing practices and any adulterants added post-production. For drugs not approved for therapeutic use and are illicitly manufactured such as MA, the likelihood of purchasing a pure product is slim to none. While some substances added to MA as cutting agents can be harmless, others can have serious consequences. However, such a detailed interrogation of samples is rarely conducted in routine toxicological analysis mainly due to resource constraints. Building on Chapter 3, this work provides an inexpensive solution to this problem by applying ATR-FTIR spectroscopy combined with chemometric analysis to distinguish pure MA samples from adulterated MA (10 to 90% purity) in serum and urine. Using three commonly found cutting agents in MA, this chapter demonstrates the successful discrimination of pure MA samples from those adulterated with either paracetamol, methylsulphonylmethane (MSM) or sugar using binary PLS-DA and RF models as well as multiclass PLS-DA models. For the multiclass model, sensitivities of 100%, 84% and 100% and specificities of 100%, 99% and 99% are reported for discriminating MA from MA mixed with MSM, paracetamol and sugar respectively. The type of analysis presented here demonstrates the potential of the protocol developed in this thesis, and the ATR-FTIR spectroscopy in general for the detection and discrimination of illicit substances of unknown composition in biological samples.

4.1 Introduction

Globally, the manufacture of amphetamine-type-stimulants (ATS) is dominated by methamphetamine (MA) as more than 95 per cent of all clandestine laboratories detected or dismantled worldwide were reported to have been manufacturing MA.[1] Historically, this manufacture was dependent on the precursors, ephedrine and pseudoephedrine which are naturally derived from the plant *Ephedra*, focusing its production in regions of the world conducive to its growth.[2] However, the discovery of synthetic routes for not only MA but also its precursors has expanded the geographical reach of clandestine production.[1] Illicitly produced MA is very rarely sold as a pure substance and its composition can change at any stage of production to consumption.[3] For MA, the purity levels have fluctuated from 1% to 44%, 3% to 83%, 7% to 44%, and 40% to 55% in Australia, Europe, the United Kingdom and the United States, respectively.[4-7] As the manufacturing processes of MA naturally create by-products and residues reflective of the method or precursors used, a product of less than 100% purity does not automatically imply adulteration.[8] The final product will however inevitably contain impurities characteristic of the route of synthesis in addition to any modifications made by the illicit drug vendors and/or the drug consumer. Critically, the final product will contain evidence to routes of production, thus potential identification of established users/dealers, both locally and regionally, providing forensic intelligence and aid towards elucidating trafficking patterns of illicit MA.[9-12]

While the drugs produced in pharmaceutical laboratories with good manufacturing practices have stringent quality control standards, illicit production has no such oversight. Further dilution of the pure drug substance is carried out during various stages of distribution for a variety of reasons by the wholesale supplier and local drug retailers. There are numerous ways in which such modifications can be made to the bulk drug content, which include the addition of cutting agents, contaminants, diluents or adulterants.[13, 14] By-products of the manufacturing process or unintentionally added substances, for example from cross-contamination, are often referred to as contaminants or impurities.[15] Cutting agents collectively include adulterants or diluents and comprise a range of substances,[3, 4] diluents refer to any pharmacologically inert and readily available substance added to bulk out the drug and decrease the amount of active ingredient,[3, 8, 14] and adulterants, on the other hand, are pharmacologically active ingredients that are added to achieve a specific physiological effect.[8, 14, 16] Therefore, it is very likely that consumers of illicit drugs may encounter drug mixtures that contain one or all of these types of modifications.

Many substances have been used to cut MA post-manufacture including sugars, bicarbonate of soda, caffeine, lidocaine, dimethyl sulfone, paracetamol, and phentermine.[4, 8, 13, 17-24] Sugars, mainly sucrose, are commonly used for bulking as they are legal and readily available.[8, 13] Dimethyl sulfone (methylsulphonylmethane (MSM)), classified as a non-controlled psychoactive substance, a sulphur-based dietary supplement and an industrial solvent, is a commonly occurring cutting agent in illicit MA seized in Korea, Japan, Australia, Canada and the United States.[15, 19, 21, 25-28] Its white colour and crystalline appearance, similar to MA crystals, gives the MSM adulterated MA the illusion of high purity.[8] Paracetamol, on the other hand, is a non-controlled analgesic medicine commonly used to relieve cold symptoms and has also been found in illicit MA samples as it is cheap and easy to acquire.[8] Aside from the toxicity associated with MA itself, cutting agents can also have individual as well as compounding toxic effects. Furthermore, all three of these compounds are usually orally consumed, while MA has numerous forms that can be smoked, snorted, ingested or injected. Therefore, MA adulterated with these compounds consumed via other than the oral route can alter their pharmacokinetic characteristics.[4] Consequently, it is important to investigate the composition of illicit MA to not only estimate the percentage purity of MA but also to characterise the presence of other substances in the samples.

Most forensic laboratories use hyphenated chromatographic methods such as GC-MS for the identification of illicit drugs and the presence of any cutting agents.[23, 28, 29] However, these methods are expensive, time-consuming, tedious and require much longer turnaround times. Routine drug detection in laboratories requires extraction protocols such as acid/base extraction, which may result in the concurrent removal of such substances prior to analysis.[4] With numerous additions to the pure drug compounds, it is often necessary to conduct multiple measurements to identify various substances present in the samples. Additionally, only those cutting agents that are known and controlled under the local/national legislation are reported in such analyses and information about other adulterants and/or diluents remains untested and/or unreported.[4]

ATR-FTIR spectroscopy is a fast, non-destructive, label-free technique that requires minimal to no sample preparation and provides highly structurally selective information about the samples in a range of physical states. The method is also particularly suitable for the detection and identification of adulterated samples as it is able to detect a variety of adulterations in a single analysis. In addition, the use of chemometrics for data analysis

makes this method extremely valuable in the analysis of illicit drugs. Numerous studies have demonstrated the use of ATR-FTIR spectroscopy combined with chemometrics for the analysis of adulteration in seized illicit MA.[19, 20, 30, 31] Pereira *et al.*[32] illustrated the power of ATR-FTIR spectroscopy in the screening of MDMA tablets while Tupper *et al.*[33] used FTIR for screening a range of illicit drug samples at drug-checking centres in Vancouver. An earlier study by Goh and colleagues[30] demonstrated the on-site applicability of ATR-FTIR spectroscopy to distinguish and quantify 3 adulterants including caffeine, glucose and paracetamol in MA, while Hughes *et al.*[20] built on this proof-of-concept study by building robust chemometric models to screen 92 seized samples and determine the MA percentages across a range of 0.1% to 78.6%. Though these studies are valuable in establishing the use of this technique in the forensic investigation of illicit drugs, they were all conducted on solid samples such as powders and tablets.

In this chapter, measurements of pure and adulterated MA in two biofluids, human serum and urine, are assessed in a bid to expand on the clinical and forensic relevance of drug detection. Using three common cutting agents of MA, dimethyl sulfone, sugar and paracetamol, as a proof-of-concept study, measurements of MA and its purity are explored using multivariate analysis methods. The application of ATR-FTIR spectroscopy allows the analysis of biofluid samples without any prior sample extraction or processing, demonstrating the potential of this methodology as a cheap, rapid alternative to current hyphenated methods for the complete characterisation of illicit samples.

4.2 Materials and Methods

4.2.1 Materials

(+)-Methamphetamine hydrochloride ($C_{10}H_{15}N \cdot HCl$, referred to as MA), paracetamol ($CH_3CONHC_6H_4OH$, here referred to as Para) and Surine™ Negative Urine Control (AU) were purchased from Merck Chemicals Ltd. Dimethyl sulfone ($(CH_3)_2SO_2$, here referred to as MSM) was purchased from Amazon UK and Icing Sugar ($C_{12}H_{22}O_{11}$, here referred to as Sug) was purchased from Sainsbury's, a local grocery store. Human pooled serum (here referred to as serum) was obtained from TSC Life Sciences Ltd., which was stored at -80 ℃ in a freezer when not in use.

4.2.2 Sample Preparation

Stock solutions for each cutting agent, Para, MSM and Sug, were created by dissolving 10 mg of each directly into 1 mL of both serum and AU, to create six stock solutions at a concentration of 10 mg/mL. Using these stock solutions, sample concentrations of 10, 5, 1, and 0.1 mg/mL were created for all three cutting agents in both serum and urine. Additionally, as paracetamol has known fatal, toxic and therapeutic levels, additional samples with paracetamol concentrations of 0.25 mg/mL, 12.5 µg/mL and 17.5 µg/mL, were obtained to reflect each of these scenarios, respectively.[34]

Adulterated samples were created whereby MA was mixed with one of the three cutting agents mentioned before, and prepared at the following purity levels: 10, 30, 50, 70 and 90%. For instance, 1 mg of MA and 9 mg of sugar were mixed to make up an adulterated MA sample of 10% purity. 10 mg of the mixed powder was then dissolved directly in serum or urine to create an adulterated MA sample of 10 mg/mL concentration. All the samples studied in this chapter are listed in Table 4-1.

Table 4-1: Summary of all the samples studied in this chapter.

Drug	Abbreviation	Set of samples	No. of samples
Blank	Serum: BlankS Urine: BlankAU	0 mg/mL	17 17
MA	Serum: SPMA Urine: UPMA	10, 9, 8, 7, 6, 5, 4, 3, 2, 1, 0.9, 0.8, 0.7, 0.6, 0.5, 0.4, 0.3, 0.2, 0.1 mg/mL	19 15
Paracetamol	Serum: SPPara Urine: UPPara	10, 5, 1, 0.1, 0.25, 0.125, 0.0175 mg/mL	21 21
MSM	Serum: SPMSM Urine: UPMSM	10, 5, 1, 0.1 mg/mL	12 12
Sugar	Serum: SPSug Urine: UPSug	10, 5, 1, 0.1 mg/mL	12 12
MA + Para	Serum: SPMAPara Urine: UPMAPara	10%, 30%, 50%, 70%, 90% purity	15 15
MA + MSM	Serum: SPMAMSM Urine: UPMAMSM	10%, 30%, 50%, 70%, 90% purity	15 15
MA + Sug	Serum: SPMASug Urine: UPMASug	10%, 30%, 50%, 70%, 90% purity	15 15

4.2.3 Spectral Collection

A PerkinElmer UATR Two FTIR spectrometer with the PerkinElmer ATR accessory was used to collect spectra for all samples. Spectra were the result of 16 co-added scans at a resolution of 4 cm^{-1} in the spectral region of 4000-450 cm^{-1}. More detail on the instrumentation and spectral collection procedure is provided in section 3.2.4.

4.2.4 Spectral Pre-processing and Analysis

The PRFFECT toolbox within R statistical computing environment software was utilised for spectral pre-processing. The pre-processing protocol followed here included a Savitzky-Golay (SG) filter for smoothing, vector normalisation and rubberband baseline correction in that order for serum and urine samples, as detailed in Chapter 2. Additionally, for urine samples, the spectra were cut to 2000-450 cm^{-1} as the higher region showed greater sensitivity to drying conditions. The urine spectra were cut to 2000-450 cm^{-1} region to exclude the thiocyanate peak which was seen to be variable in the presence of different drug compounds as previously explained in Chapter 3.

The spectral analysis consisted of a visual examination to identify the vibrational modes of importance in powder and biofluid samples for all molecules. Following this, multivariate classification analysis was performed on biofluid samples using two machine learning methods – Partial Least Squares Discriminant Analysis (PLS-DA) and Random Forest (RF). The binary classification models were performed in PRFFECT Toolbox within R statistical software, and the multiclass models were performed using PLS Toolbox by Eigenvector Research Ltd. in MATLAB in order to distinguish:

- Pure MA in biofluid from a pure cutting agent in biofluid.
- Pure MA in biofluid from adulterated MA (with three cutting agents) in biofluid.

Detailed descriptions of multivariate analysis methods are provided in **Chapter 2** Section 2.5. For the PLS-DA models constructed in PRFFECT with 51 iterations, all default parameters were used with one hyperparameter (ncomp) which controlled the number of latent variables selected to build the analysis. It was selected to pick the best number of latent variables between 1 and 20 for the serum and urine datasets. This number was derived from the number of samples in each dataset. In this chapter, mean centering was applied to all models built using PRFFECT.

For the multiclass analysis in PLS Toolbox, partial least squares discriminant analysis (PLS-DA) models were trained and cross-validated using the Venetian blinds cross-validation method. The training and test sets were created with 5 data splits and a maximum of 20 latent variables. An appropriate number of latent variables were selected based on the plot of root mean square errors of classification (RMSEC) and cross-validation (RMSECV) for each of the models. The performance of these models was evaluated using sensitivity, specificity and accuracy (total number of samples correctly identified). False positive rates were also reported. Permutation tests were performed in order to detect the overfitting and examine the extent to which 'chance correlation' might exist between x- and y-blocks in current modelling conditions.

4.3 Results and Discussion

4.3.1 Peak Assignment

IR spectra for all four compounds (MA plus three cutting agents) were obtained in their 'pure' powder forms (Figure 4-1). The vibrational bands seen here for 'pure' paracetamol, MSM and

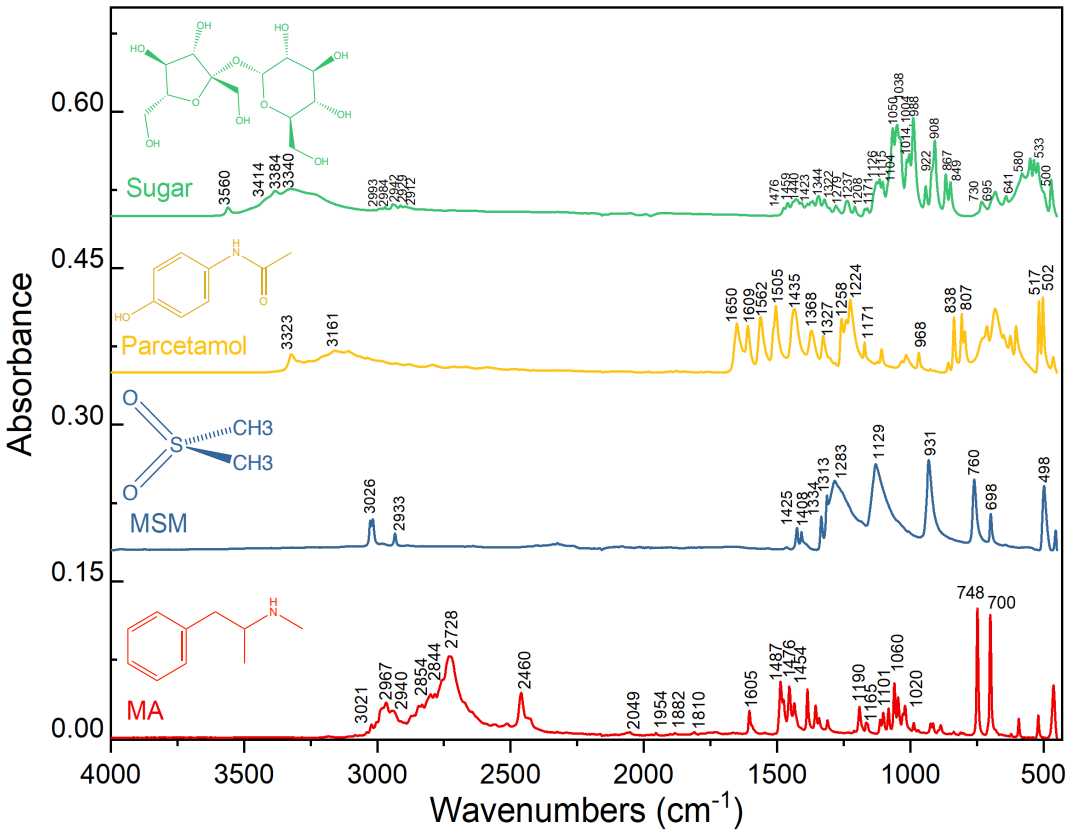

Figure 4-1: Stacked spectra for pure powder MA and three adulterants, MSM, paracetamol and sugar, with vibrational modes assigned for each molecule.

sugar (Table 4-2, refer to Table 3-2 in **Chapter 3** for band assignments for MA) are in agreement with those found in the literature.[35-38] Of these three molecules, paracetamol is structurally most similar to MA with one aromatic ring and an aliphatic sidechain, while MSM, a white crystalline substance, is physically most similar to MA. However, there are differences in their IR spectra that allow for their distinction. For instance, the para-substitution and out-of-plane ring deformation bands for the phenyl ring in paracetamol molecule are seen much lower in the spectrum at 838, 807 and at 517, 502 cm^{-1}, respectively, whereas they are found at 1190-1020 cm^{-1} and 748 and 700 cm^{-1} in the MA spectrum (Figure 4-1).[38] Additionally, the lack of an aromatic ring in the MSM and sugar molecules is distinctive when comparing it to the MA spectrum.

Following the comparison of powder spectra, the biofluid spectra of all three cutting agents were compared with that of MA. To determine which spectral regions/peaks were significant to each cutting agent in different biofluid mixtures during this comparison, difference spectra were obtained by subtracting the blank biofluid from that of samples of interest (biofluid + cutting agent at 10 mg/mL). These are shown in Figures 4-2 and 4-3. Though numerous spectral features of the molecules are masked by the biofluid background, the spectral region between 1800 – 450 cm^{-1} is most useful for differentiating between the three cutting agents in both biofluids. It is important to note here that not all wavenumbers would exactly match those in pure powder spectra due to the effects of solvents and the drug-matrix interactions. These drug-matrix interactions are further complicated by various cutting agents and combinations of these interactions with the matrix. As elucidating and identifying these for every molecule was outwith the focus of this study, all drug-related changes are included in this analysis.

Table 4-2: Tentative peak assignments of ATR-FTIR spectra of powder paracetamol, MSM and sugar (ν = stretching; ν_s and ν_{as} = symmetric and asymmetric stretching; δ = bending and δ_s = symmetric bending; τw = twisting; ρ = rocking).[35-39]

Paracetamol		MSM		Sugar	
Assignments	**Wavenumbers (cm^{-1})**	**Assignments**	**Wavenumbers (cm^{-1})**	**Assignments**	**Wavenumbers (cm^{-1})**
$\nu(\mathrm{OH})$	3323	$\nu_{as}(\mathrm{CH_2})$	3026	$\nu(\mathrm{OH})$	3560, 3384, 3340
$\nu(\mathrm{CH_3})$	3161	$\nu_s(\mathrm{CH_2})$	2934	$\nu_{as}(\mathrm{CH_2})$	2993, 2983
$\nu(\mathrm{C=O})$	1650	$\delta(\mathrm{CH_3})$	1426, 1335	$\nu_s(\mathrm{CH_2})$	2943, 2929, 2913
$\nu(\mathrm{C=C})$	1609	$\nu_{as}(\mathrm{SO})$	1290	$\delta(\mathrm{CH_2})$	1476, 1459, 1440
$\delta(\mathrm{NH})$	1562	$\nu_s(\mathrm{SO})$	1129	$\delta(\mathrm{OH})$	1237, 1208, 1161
$\delta_{as}(\mathrm{CH})$	1505	$\rho(\mathrm{S-CH_3})$	938	$\rho(\mathrm{CH_2})$	1348, 1344
$\nu(\mathrm{C-C})$	1435	$\nu(\mathrm{S-CH_3})$	760, 695	$\rho(\mathrm{CH})$	1323, 1280
$\delta_s(\mathrm{CH})$	1368			$\nu(\mathrm{CC})$	1171, 922, 695
$\nu(\mathrm{CN})$ (aryl)	1258			$\nu(\mathrm{CO})$	1126, 1115, 1104, 1050, 1038, 1014, 1004, 998
$\nu(\mathrm{CO})$	1171			$\tau w(\mathrm{CH_2})$	908, 847
$\nu(\mathrm{CN})$ (amide)	968				
Para substitution of aromatic ring	838, 800				
Ring deformation	517, 502				

For the MA molecule, the two sharp peaks at 747 and 702 cm^{-1} reflecting substitution on the aromatic ring are visible as was seen in **Chapter 3**. For the remaining three compounds, peaks at 1049 and 992 cm^{-1}, 1290 and 1129 cm^{-1} and 1506 and 832 cm^{-1} for sugar, MSM and paracetamol molecules stand out in both biofluids (Figures 4-2 and 4-3).

An interesting point to note here is that the thiocyanate peak at 2048 cm^{-1} in the urine samples shows varying absorbance. The peak is seen to decrease in absorbance as the concentration of the drug compounds is increased in the samples. However, it is prudent to

keep in mind that this peak is characteristic of this brand of artificial urine and the decrease in absorbance is reflective of the reaction between the matrix and the drug compound that is added. Additionally, this reaction between the matrix and the drug compound is not predictable across a range of drugs as seen here from the varying peak intensities for each of the compounds. Therefore, it may not be present in real-world samples consisting of a natural urine matrix and show predictable behaviour with all compounds that might be encountered. While it is possible to use this relationship between the change in absorbance and the concentration of the added compounds to predict the concentration of the cutting agent in the sample, it is not sufficiently discriminating to identify the compound present in an unknown sample. Figure 4-3 shows the urine spectra with the thiocyanate peak for illustrative purposes only. However, it is excluded from the classification analyses reported in this chapter.

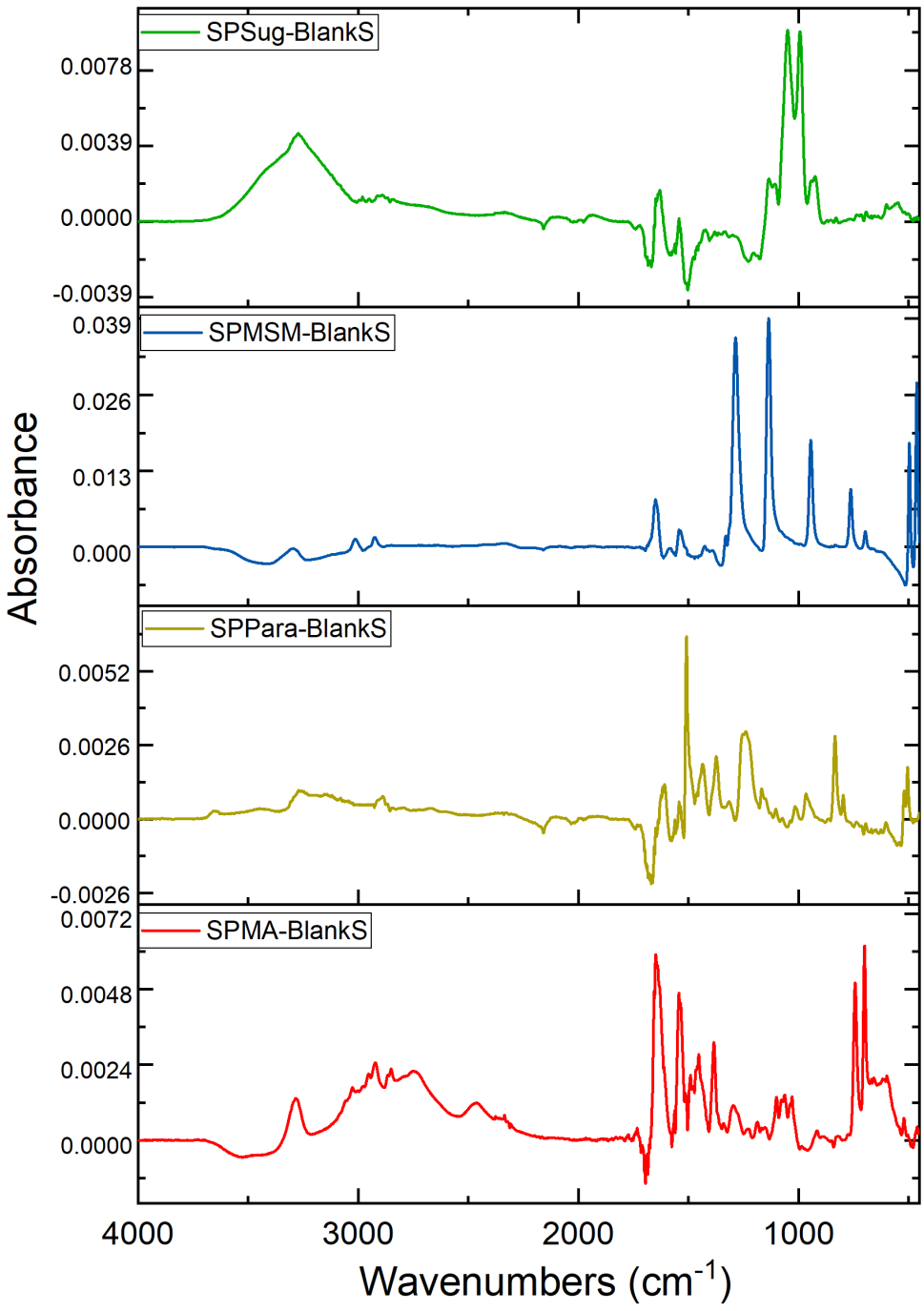

Figure 4-2: Stacked difference spectra for MA and three cutting agents in serum obtained by subtracting drug-serum samples from that of blank serum spectrum. (SPMA-BlankS = difference spectra for MA; SPPara-BlankS = difference spectra for paracetamol; SPMSM-BlankS = difference spectra for MSM and SPSug-BlankS = difference spectra for sugar). All drug samples were at concentration of 10mg/mL.

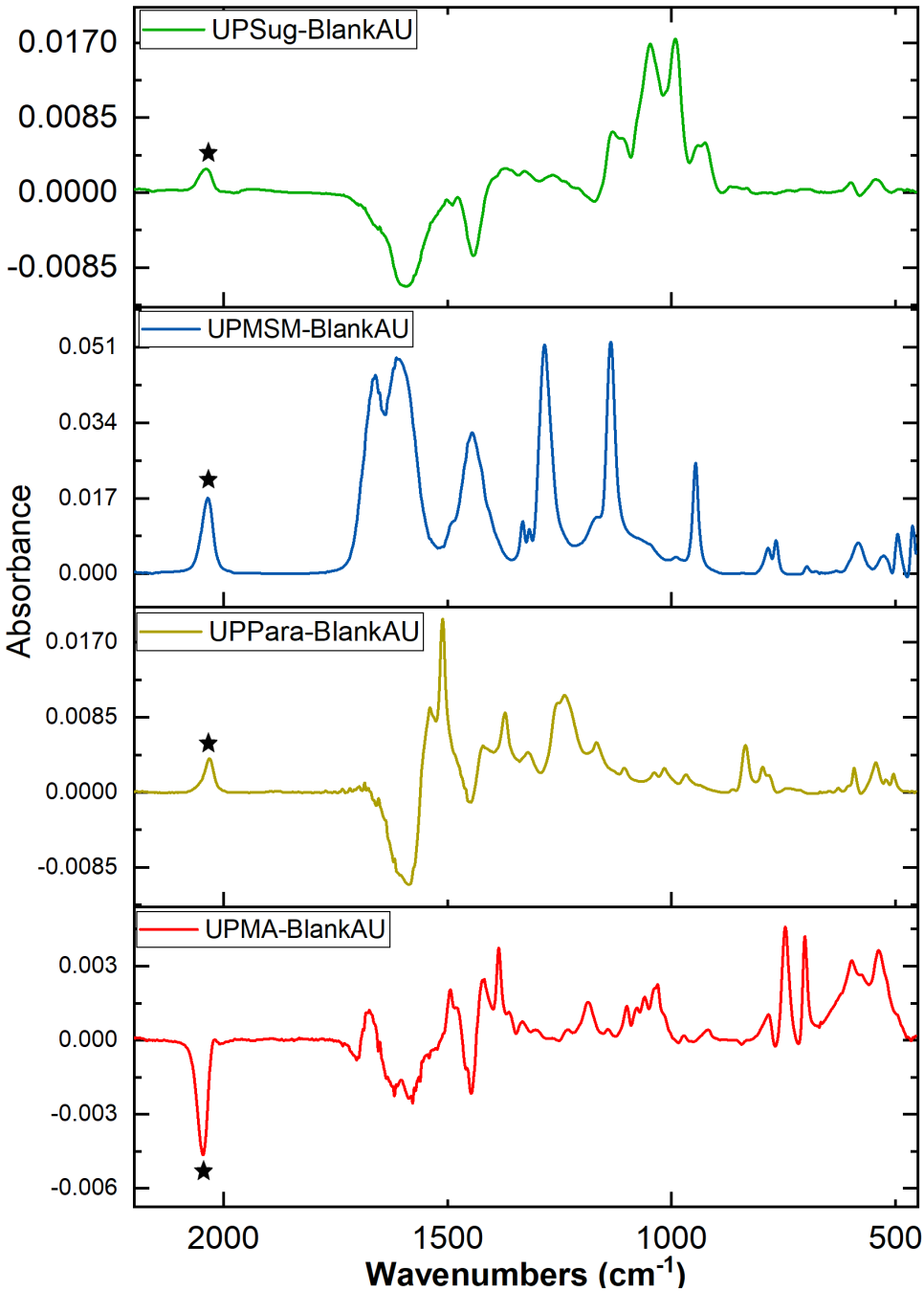

Figure 4-3: Stacked difference spectra for MA and three cutting agents in urine obtained by subtracting drug-urine samples from that of blank urine spectrum. (UPMA-BlankAU = difference spectra for MA; UPPara-BlankAU = difference spectra for paracetamol; UPMSM-BlankAU = difference spectra for MSM and UPSug-BlankAU = difference spectra for sugar). The black star indicates the thiocyanate peak. All drug samples were at concentration of 10mg/mL.

4.3.2 Pure MA *versus* Cutting Agents – Binary Models

First, individual cutting agents were distinguished from pure MA dissolved in both serum and urine using PLS-DA and RF analysis. These results are summarised in Tables 4-3 and 4-4. As in **Chapter 3**, all three sampling methods were applied for each of the classification models and the results were validated using 5-fold cross-validation. The results with the highest sensitivity and specificity are presented here.

All PLS-DA classification models showed high sensitivities and specificities across both serum and urine datasets (Table 4-3). When considering the serum dataset, samples containing the cutting agent sugar demonstrated the highest sensitivity, 99.1%, with the lowest standard deviation, 3.3%, associated with it. This is likely because MA and sugar are the most structurally distinct compounds of the four studied in this chapter and their characteristic vibrations visible above the biofluid do not overlap as indicated by the difference spectra in Figures 4-2 and 4-3. Conversely, the sensitivities and specificities for the classification MA against the cutting agents paracetamol and MSM in serum are comparable.

When discriminating pure MA samples in urine, the PLS classification models revealed a trend of increasing sensitivity values with the lowest sensitivity observed for the most structurally similar compound (paracetamol) to the highest sensitivity for the least structurally similar compound (sugar) (Table 4-3). While the specificity values for the PLS-DA classification did not follow this trend exactly, the observed values were excellent in identifying samples without any MA in them.

Table 4-3: Summary of results showing PLS-DA classification results for MA versus individual cutting agents in serum and urine. All values given are the mean of 51 iterations.

	Cutting agent against MA	Sampling method	Sensitivity (%)	SD	Specificity (%)	SD	Balanced Accuracy (%)	SD
Serum	**Para**	Down	95.5	6.7	99.0	4.9	97.2	4.7
	MSM	Down	94.9	7.4	97.1	11.8	96.0	6.9
	Sugar	Down	99.1	3.3	90.2	22.4	94.6	11.4
Urine	**Para**	Down	89.7	13.3	98.0	14.0	93.8	10.4
	MSM	Down	94.6	11.5	96.0	13.5	95.3	8.2
	Sugar	Down	98.5	5.9	99.0	7.0	98.7	4.5

Table 4-4: Summary of results showing RF classification results for MA versus individual cutting agents in serum and urine. All values given are the mean of 51 iterations.

	Cutting agent against MA	Sampling method	Sensitivity (%)	SD	Specificity (%)	SD	Balanced Accuracy (%)	SD
Serum	**Para**	Down	93.8	8.2	97.5	9.0	95.7	5.7
	MSM	Down	96.6	6.1	98.0	9.8	97.3	6.1
	Sugar	SMOTE	100	0	100	0	100	0
Urine	**Para**	Up	93.1	12.3	76.5	42.8	84.8	20.3
	MSM	Down	96.5	12.2	93.1	20.0	94.5	11.2
	Sugar	Up	97.5	7.5	81.3	31.5	89.4	15.4

A similar trend was seen in the sensitivities and specificities achieved by the RF classification models in the serum dataset, where the classification of MA samples against samples with sugar had the highest sensitivity and specificity values of 100% and the lowest sensitivity and specificity values were seen in the samples with paracetamol as it is the most structurally similar molecule to MA here. However, all models showed high balanced accuracy values indicating exceptional reliability of this model (Table 4-4).

On the whole, however, RF classification showed lower sensitivities and specificities than the PLS classification model for the urine dataset. As previously noted, the peak at 2048 cm^{-1} can be very useful in discriminating between the samples with drug molecules that react with thiocyanate, though, this classification was carried out by only using the 2000 - 450 cm^{-1} region as it is a more appropriate reflection of the real-world samples. Therefore, it is likely that the reduced number of variables is potentially responsible for the overall lower sensitivity and specificity values. Nevertheless, the trend of decreasing sensitivity and specificity values from samples with sugar towards samples with paracetamol is observed for urine samples in RF classification.

The Gini importance plots obtained from the RF classification highlight the spectral regions of significance which are shown in Figures 4-4 and 4-5. The spectral region from 1500 – 700 cm^{-1} is shown to be significant for classification against all cutting agents. Of note here, is the spectral region approximately between 2000 and 1700 cm^{-1} which is biologically silent allowing for the overtone and combination bands of the drug molecules to be visible.[40] These are seen for all three molecules in Figure 4-4 for the serum dataset. In the urine dataset, this

region appears to be of more importance in the classification between MA and Para molecules than that of the others (Figure 4-5). Overall, the Gini importance plots for serum and urine datasets are in agreement with the difference spectra shown in Figures 4-2 and 4-3 in emphasising the wavenumbers important for discriminating MA from the cutting agents.

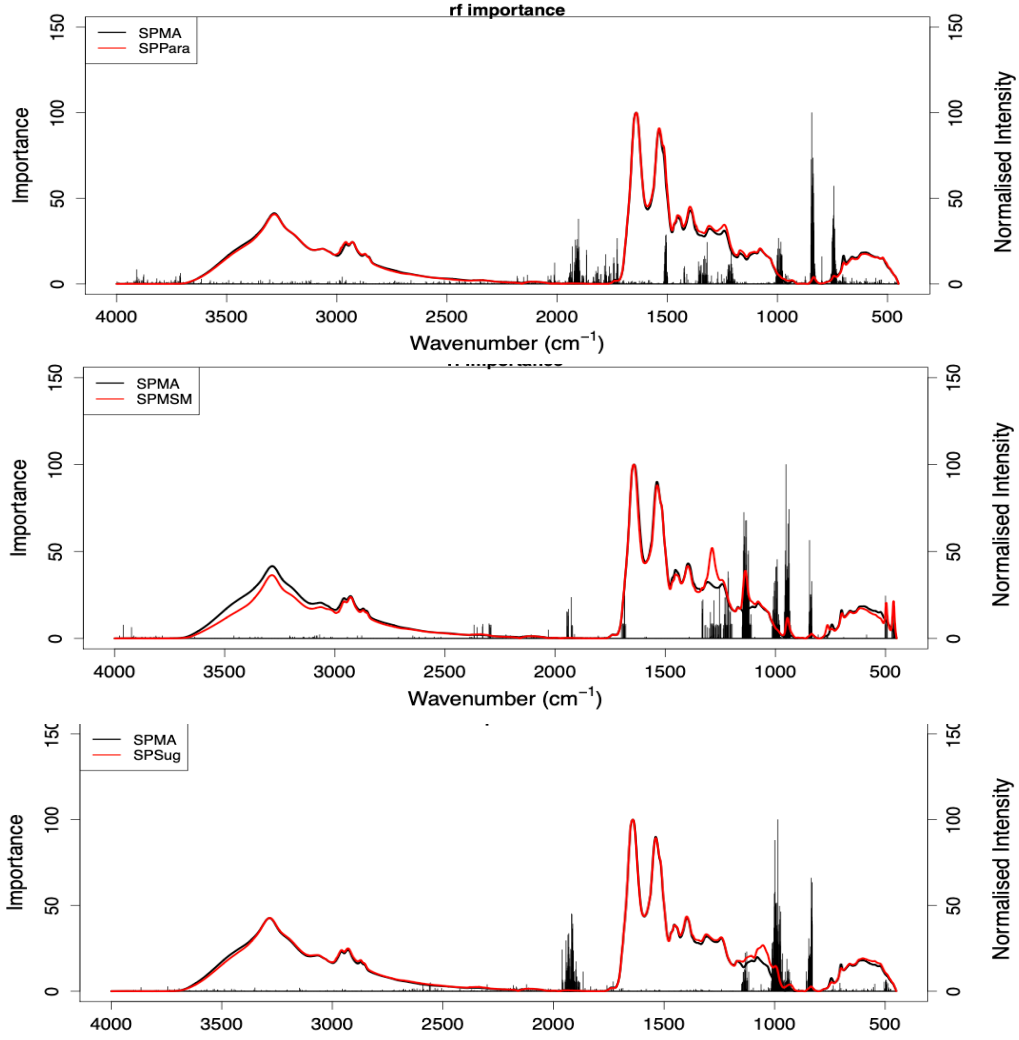

Figure 4-4: Gini importance plots from three RF classifications of SPMA against SPPara (top), SPMSM (middle) or SPSug (bottom) in serum. SPMA refers to MA samples in serum, SPMSM refers to MSM in serum, SPPara refers to paracetamol in serum and SPSug refers to sugar in serum.

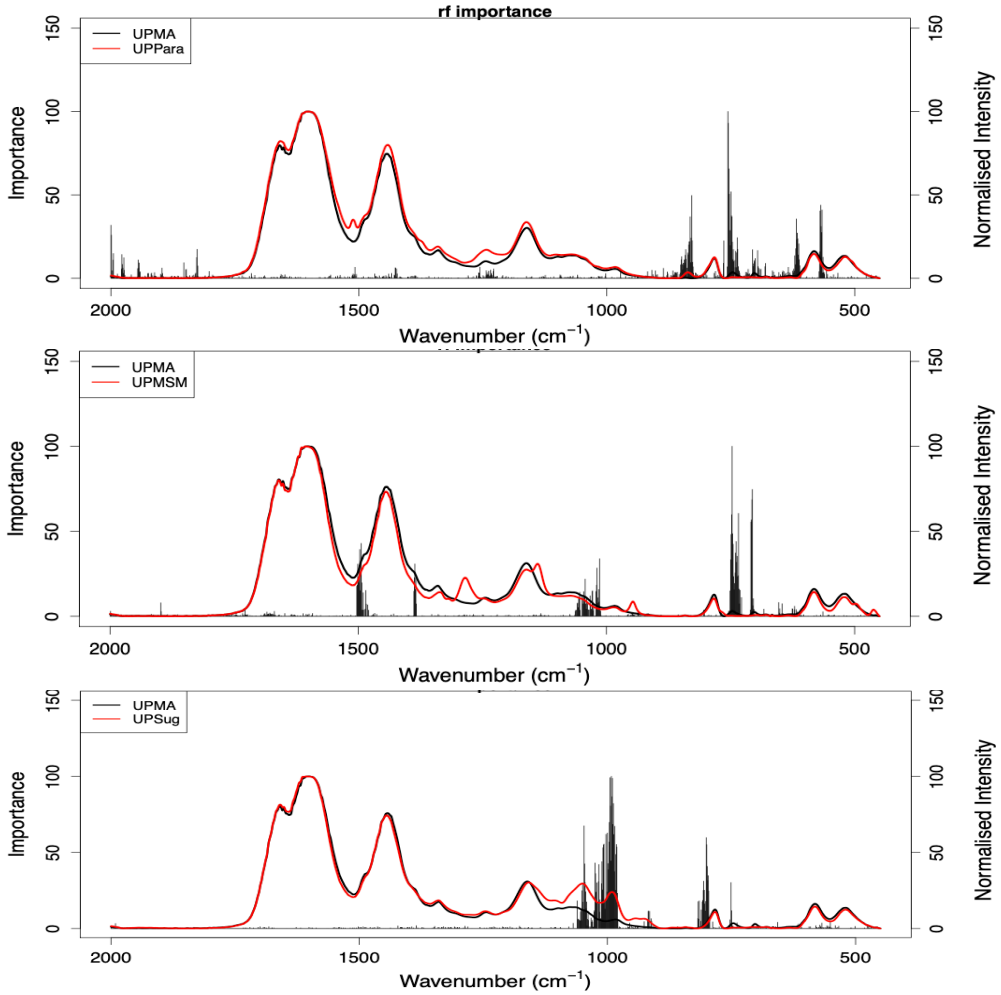

Figure 4-5: Gini importance plots from three RF classifications of UPMA against UPPara (top), UPMSM (middle) or UPSug (bottom) in urine. UPMA refers to MA samples in urine, UPMSM refers to MSM samples in urine, UPPara refers to paracetamol samples in urine and UPSug refers to sugar samples in urine.

4.3.3 Pure MA *versus* Adulterated MA – Binary Models

A second set of binary classification models were constructed to distinguish between pure and adulterated MA in both serum and urine. Both PLS-DA and RF models showed excellent discrimination between the pure MA and MA mixed with one of the three cutting agents (Tables 4-5 and 4-6). For the serum dataset, the PLS classification model for MA samples against adulterated MA samples with MSM showed the lowest sensitivity value of 99.7 ± 2% in comparison to the 100% sensitivities and specificities observed for the remaining models. This is likely due to the fact that peaks of significance for MSM and MA molecules are in the same spectral region of 1500 - 750 cm^{-1} and the differences outwith this region are not prominent over the serum matrix background.

In the urine dataset, discrimination of pure MA samples against those adulterated with paracetamol and MSM observed slightly lower sensitivities of 98.5 ± 5.9% and 98.0 ± 9.8%, respectively, for the PLS classification models. A specificity of 100% is obtained across all adulterated MA samples for both PLS-DA and RF models in serum and urine indicating that both models performed excellently in distinguishing adulterated MA with even the smallest amount of adulteration.

Table 4-5: Summary of results showing PLS-DA classification of MA versus MA adulterated with one cutting agent. Pre-processing steps included SG smoothing, vector normalisation, rubberband baseline correction and mean centring was performed during model construction.All values given are the mean of 51 iterations.

	Cutting agent against MA	Sampling method	Sensitivity (%)	SD	Specificity (%)	SD	Balanced Accuracy (%)	SD
Serum	**Para**	Down	100	0	100	0	100	0
	MSM	Down	99.7	2.0	100	0	99.8	1.0
	Sugar	Up	100	0	100	0	100	0
Urine	**Para**	Down	98.5	5.9	100	0	99.2	2.9
	MSM	SMOTE	98.0	9.8	100	0	99.0	4.9
	Sugar	Down	100	0	100	0	100	0

Table 4-6: Summary of RF classification results of MA versus MA adulterated with one cutting agent. Pre-processing steps included SG smoothing, vector normalisation, rubberband baseline correction and mean centring performed during model construction. All values are given as the mean of 51 iterations.

	Cutting agent against MA	Sampling method	Sensitivity (%)	SD	Specificity (%)	SD	Balanced Accuracy (%)	SD
Serum	**MSM**	Down	100	0	100	0	100	1.0
	Para	Down	100	0	100	0	100	0
	Sugar	Up	100	0	100	0	100	0
Urine	**MSM**	SMOTE	100	0	100	0	100	0
	Para	SMOTE	100	0	100	0	100	0
	Sugar	SMOTE	100	0	100	0	100	0

The RF classification models performed better with 100% sensitivities in comparison to the PLS models in distinguishing pure MA samples from the adulterated samples in both biofluids. Another valuable output provided by the RF classification, the Gini importance plots highlighted the spectral regions of significance for the discrimination of pure MA samples from those of adulterated MA in serum and urine. These are shown in Figures 4-6 and 4-7. The spectra regions highlighted here are in agreement with those found in the difference spectra and fall mostly in the 2000 – 450 cm-1 region. Interestingly, the C-N-C stretching mode seen at 2460 cm-1 in the MA molecule is seen to be significant for the discrimination of MA from MA adulterated with sugar (Bottom plot, Figure 4-6). There is a single line at the same position in the classification of MA against MA adulterated with MSM. While not seen in the same level of significance as in the classification of MA against MA adulterated with sugar, it remains another peak of discrimination when sugar or MSM are the cutting agents.

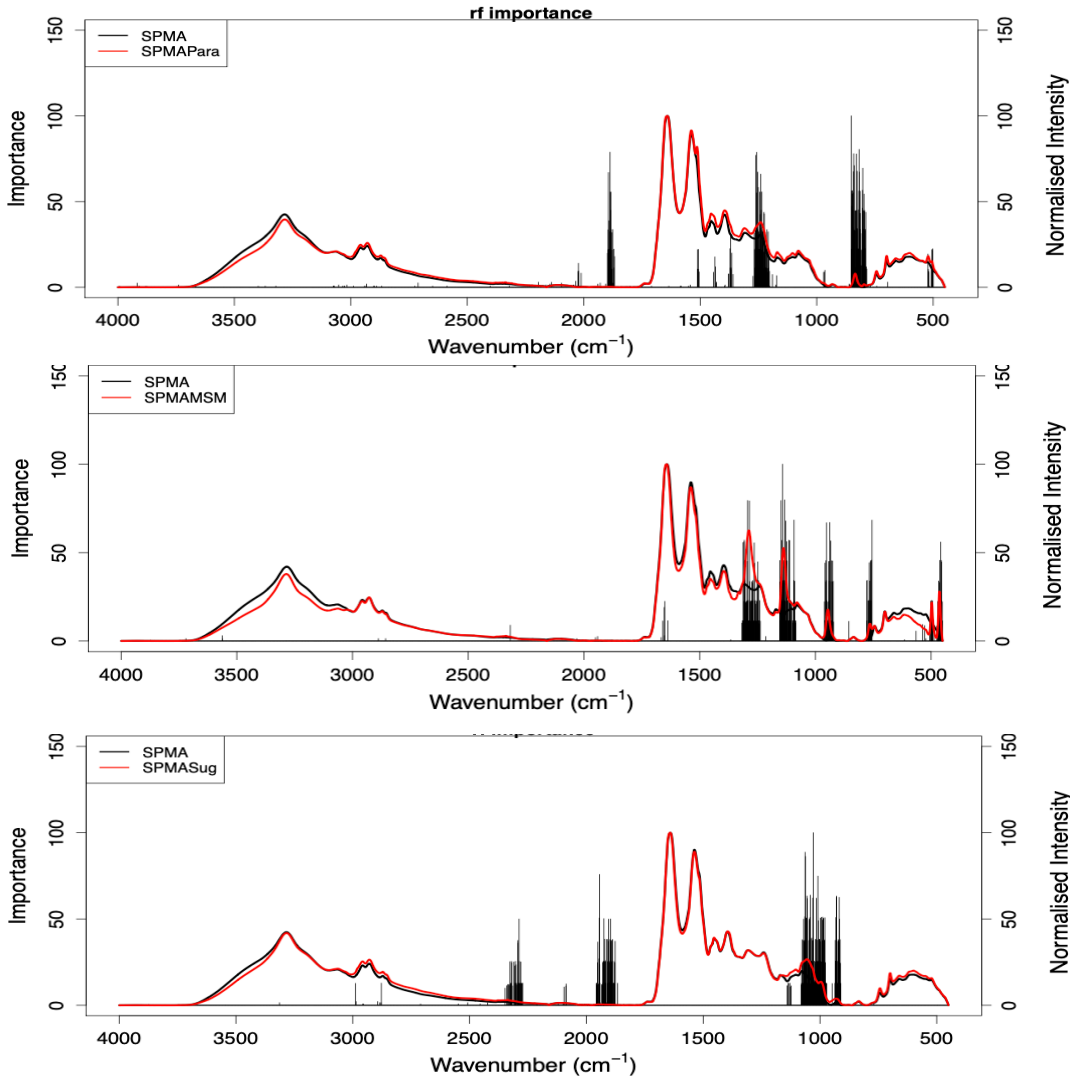

Figure 4-6: Gini importance plots from three RF classifications of SPMA against SPMAPara (top), SPMAMSM (middle) or SPMASug (bottom) in serum. SPMA refers to MA samples in serum, SPMAMSM refers to MA adulterated with MSM in serum, SPMAPara refers to MA adulterated with paracetamol in serum and SPMASug refers to MA adulterated with sugar in serum.

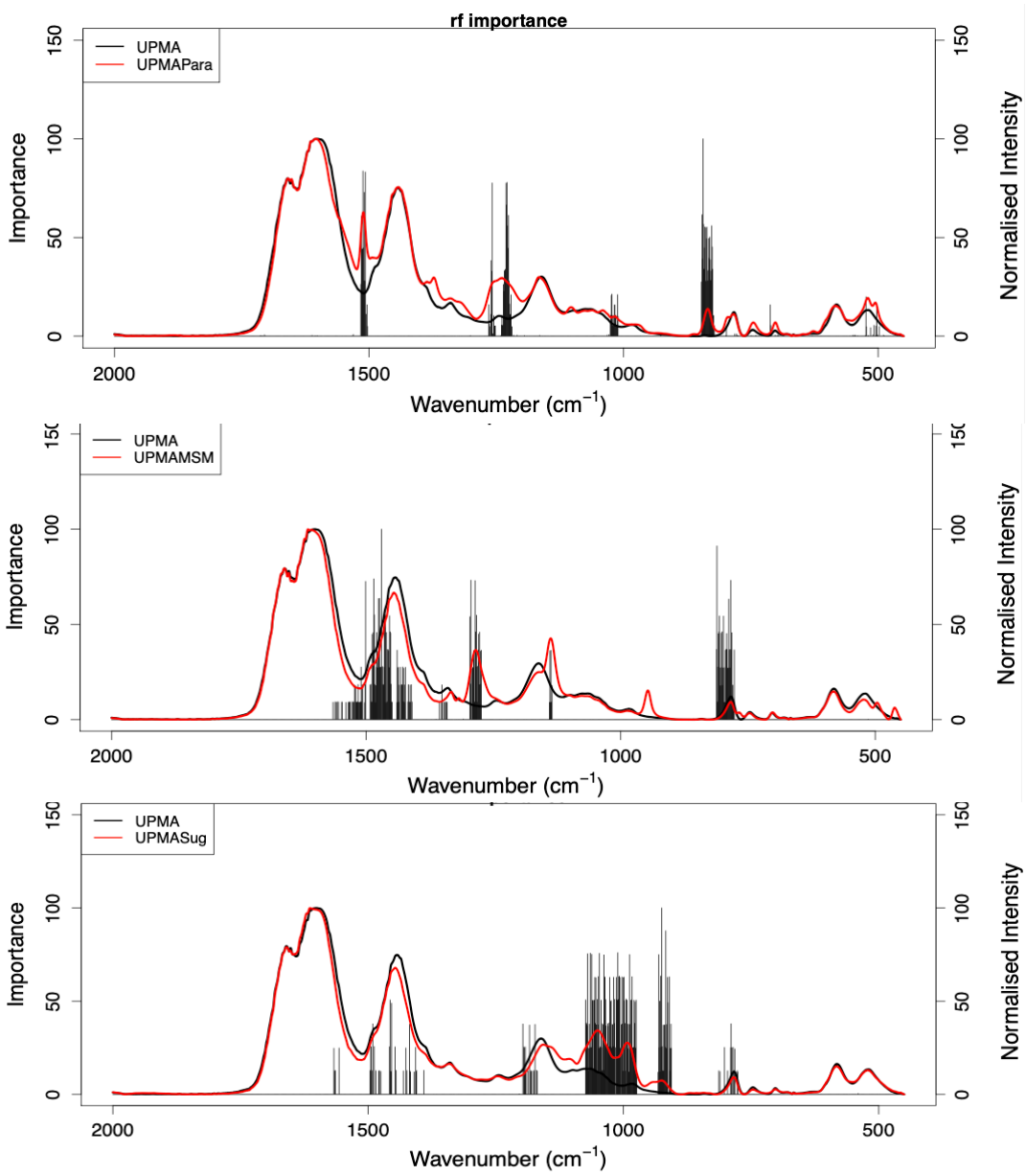

Figure 4-7: Gini importance plots from three RF classifications of UPMA against UPMAPara (top), UPMAMSM (middle) or UPMASug (bottom) in urine. UPMA refers to MA samples in urine, UPMAMSM refers to MA adulterated with MSM in urine, UPMAPara refers to MA adulterated with paracetamol in urine and UPMASug refers to MA adulterated with sugar in urine.

4.3.4 Pure MA *versus* Adulterated MA – Multiclass model

The multiclass PLS-DA model was performed for the discrimination of pure MA, MA+MSM, MA+Para and MA+Sug samples in both biofluids using the PLS Toolbox from Eigenvector Research Inc. This was performed to mimic a real-world scenario where samples from multiple sources with the presence of a range of cutting agents are likely to be encountered during analysis. The sensitivities and specificities for the 5-fold cross-validation are presented in Table 4-7. Overall, the sensitivity and specificity values from the multiclass model were within ± 1-2% of that achieved using binary classification models presented in the previous section. One exception here was the samples containing MA+Para in serum that showed the lowest sensitivity of 84.4% due to misclassification of six samples that contained MA mixed with paracetamol as pure MA samples. This is likely due to the higher relative percentage of MA in these samples in comparison to the percentage of paracetamol. Similarly, one pure MA sample was misclassified as MA adulterated with MSM, though the concentration of MA in this sample was much lower at 0.1 mg/mL.

Table 4-7: Summary of PLS2-DA classification results of MA versus MA adulterated with one cutting agent. The model consisted of 4 classes. The optimum number of LVs was determined to be 5 for both datasets (refer to Appendix 2, Figures A2-1 and A2-2).

Drug	Serum		Urine	
	Sensitivity (%)	Specificity (%)	Sensitivity (%)	Specificity (%)
MA	98.7	95.5	95.6	100
MA+MSM	100	100	100	99.4
MA+Para	84.4	99.4	100	100
MA+Sug	100	99.2	100	99.3

As the data were not mean-centred the loading plot for LV 1 resembled the blank serum spectra as it is the source of the most amount of variation in the dataset. The 3D scores plot for the above multiclass PLS-DA classification is shown in Figure 4-8, which shows LVs 2, 3 and 4 plotted against each other. It is expected that there will be some overlap between the samples as they all contain MA, and the overlap is mainly found where adulterated samples contain a lower percentage of cutting agents.

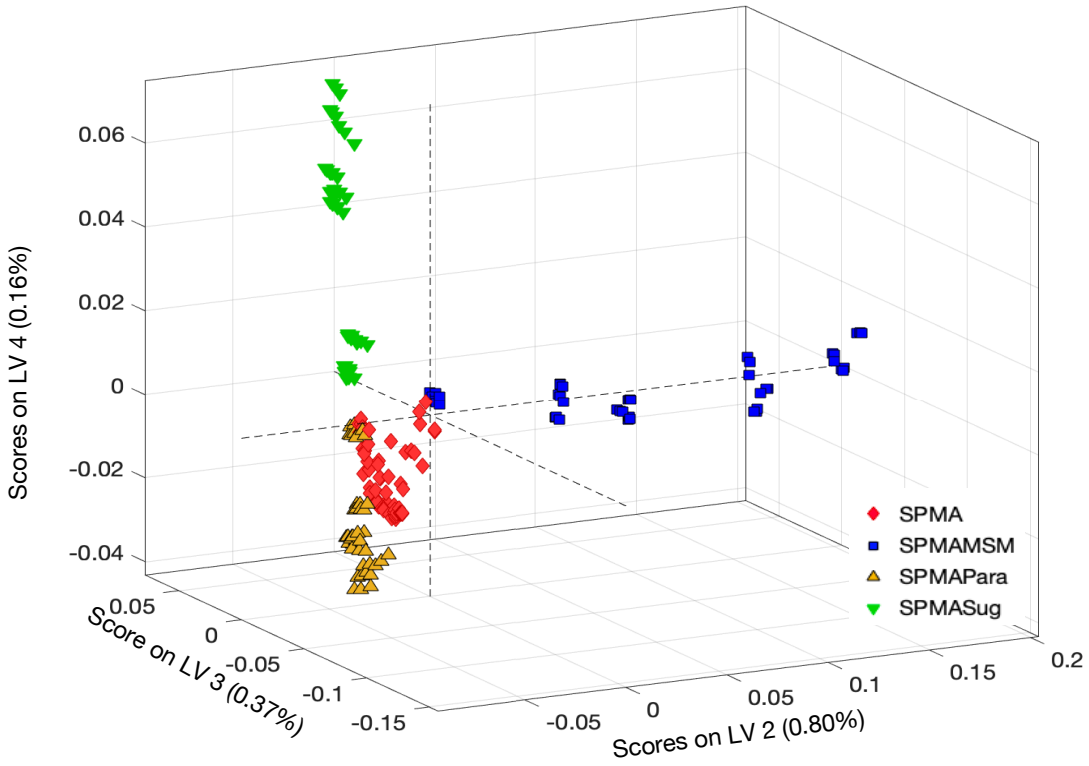

Figure 4-8: PLS-DA scores plot showing clear discrimination between Pure MA (red diamonds, here labelled as SPMA), MA+MSM (blue squares, here labelled as SPMAMSM), MA+Paracetamol (yellow triangles, here labelled as SPMAPara) and MA+Sugar (green triangles, here labelled as SPMASug) in serum using LV2 vs LV3 vs LV4 in a 3D plot created using PLS Toolbox.

When the remaining loading plots for latent variables 2, 3, 4 and 5 are inspected in relation to their difference spectra in serum and pure powder spectra, the characteristic vibrational bands for these compounds become apparent in them (Figure 4-9). When the scores plot is examined in relation to the loadings, each of the compounds is reflected independently by the separate latent variables. For instance, graph A in Figure 4-9 shows the LV2 loadings plot which is most influenced by the MSM molecule. Similarly, the loading plot of LV4 bears a resemblance to the IR spectrum of sugar molecules as seen in graph B in Figure 4-9. The LV 3 and 5 were more difficult to unpick due to the structural similarity between MA and paracetamol molecules. Though most of the spectral variation due to paracetamol is reflected in the loading plot of LV5, the two high-intensity peaks in the 750-700 cm^{-1} region

characteristic of the out-of-plane deformation of C-H bands in MA, are also seen in LV3. Similarly, peaks relating to the paracetamol molecule are seen in both LV5 and LV3.

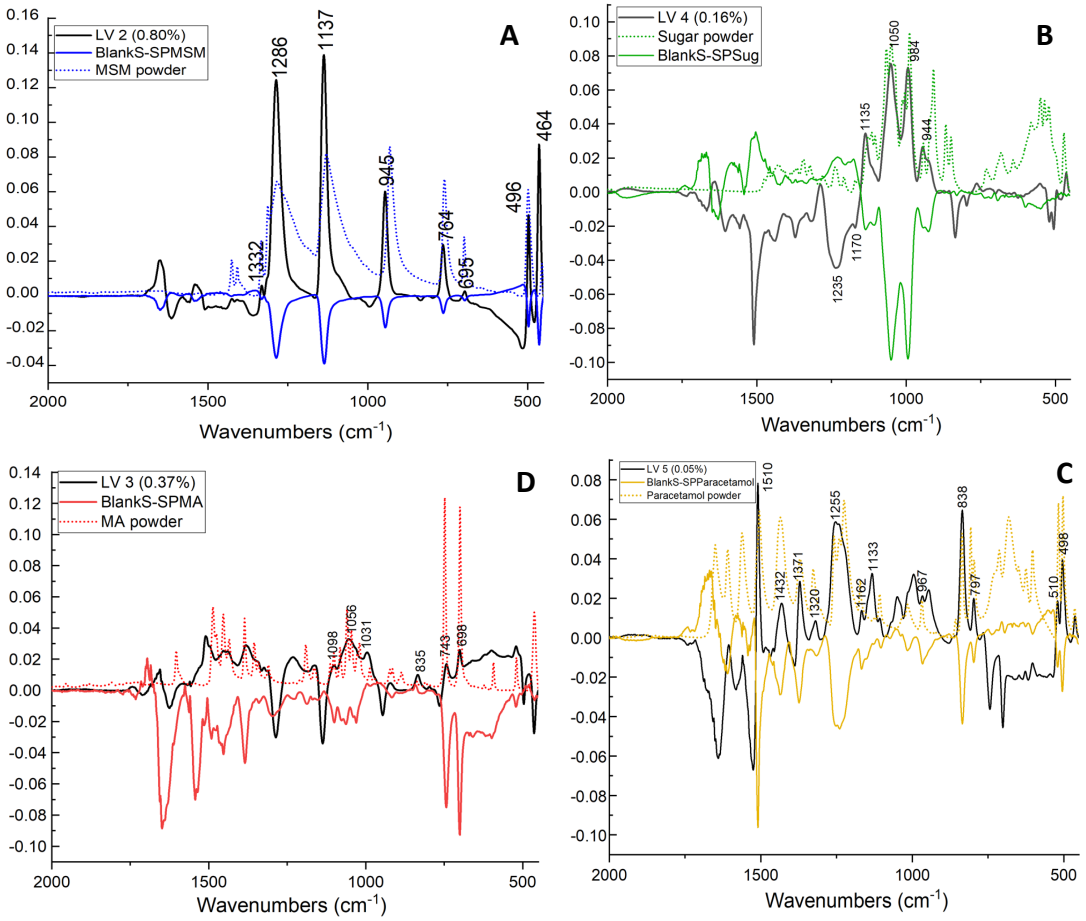

Figure 4-9: Graphs showing loadings for the respective LVs plotted with difference spectra (in bold coloured line) and powder spectra (in dotted coloured line) for the chemical compound in serum. **A** shows LV2 plotted with serum difference spectrum and powder spectrum of MSM; **B** shows LV4 plotted with serum difference spectrum and powder spectrum of sugar; **C** shows LV3 plotted with serum difference spectrum and powder spectrum of MA and **D** shows LV5 plotted with serum difference spectrum and powder spectrum of paracetamol. The vibrational bands belonging to each compound identified from the powder and difference spectra in serum are numbered in the loading plot for the corresponding latent variable.

A similar PLS-DA model was built for these compounds in urine samples. Figures 4-10 and 4-11 show the scores and loading plots for this model. As mean centring was not applied to this dataset, LV 1 describes the mean spectrum – which here resembles the urine matrix spectra. LV1 also showed influence from MA as it was present in all samples. In comparison to the serum model, this plot shows much clearer discrimination between all four classes. As with serum samples, some overlap between adulterated MA samples the pure MA samples is expected as they all contain varying amounts of MA.

When the loading plots are examined, LV4 bears a resemblance to the MSM IR spectrum as shown in graph A in Figure 4-11. Similarly, LV3 was seen to be influenced mostly by the variation from sugar molecules. However, unlike serum, there are a greater number of peaks visible in the urine samples due to the simplicity of the matrix. The loading plot of LV4 was more representative of the paracetamol molecule represented by the peaks identified in

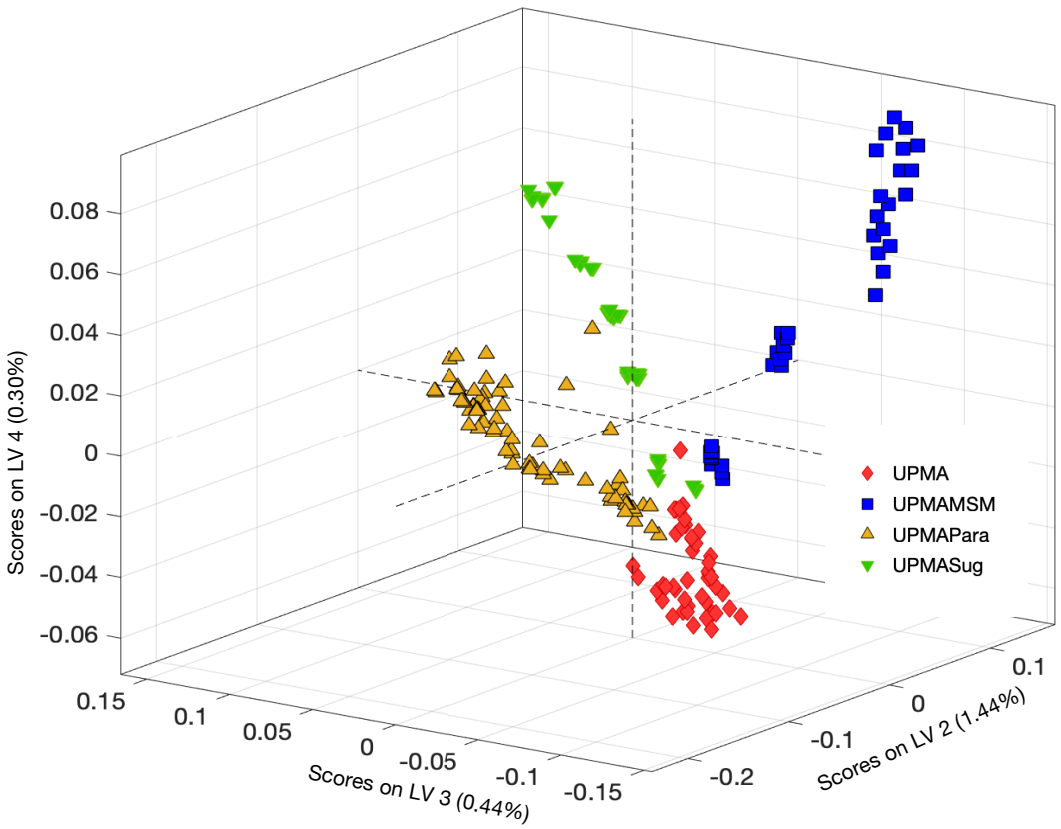

Figure 4-10: PLS-DA 3D scores plot for classification of Pure MA (red diamonds, here labelled as UPMA), MA+MSM (blue squares, here labelled as UPMAMSM), MA+Paracetamol (yellow triangles, here labelled as UPMAPara) and MA+Sugar (green triangles, here labelled as UPMASug) in urine using LV2 vs LV3 vs LV4 created using PLS Toolbox, Eigenvector Ltd.

graph D in Figure 4-7. However, smaller contributions from the 745 and 703 cm^{-1} bands of MA are visible in the loading plot for LV4.

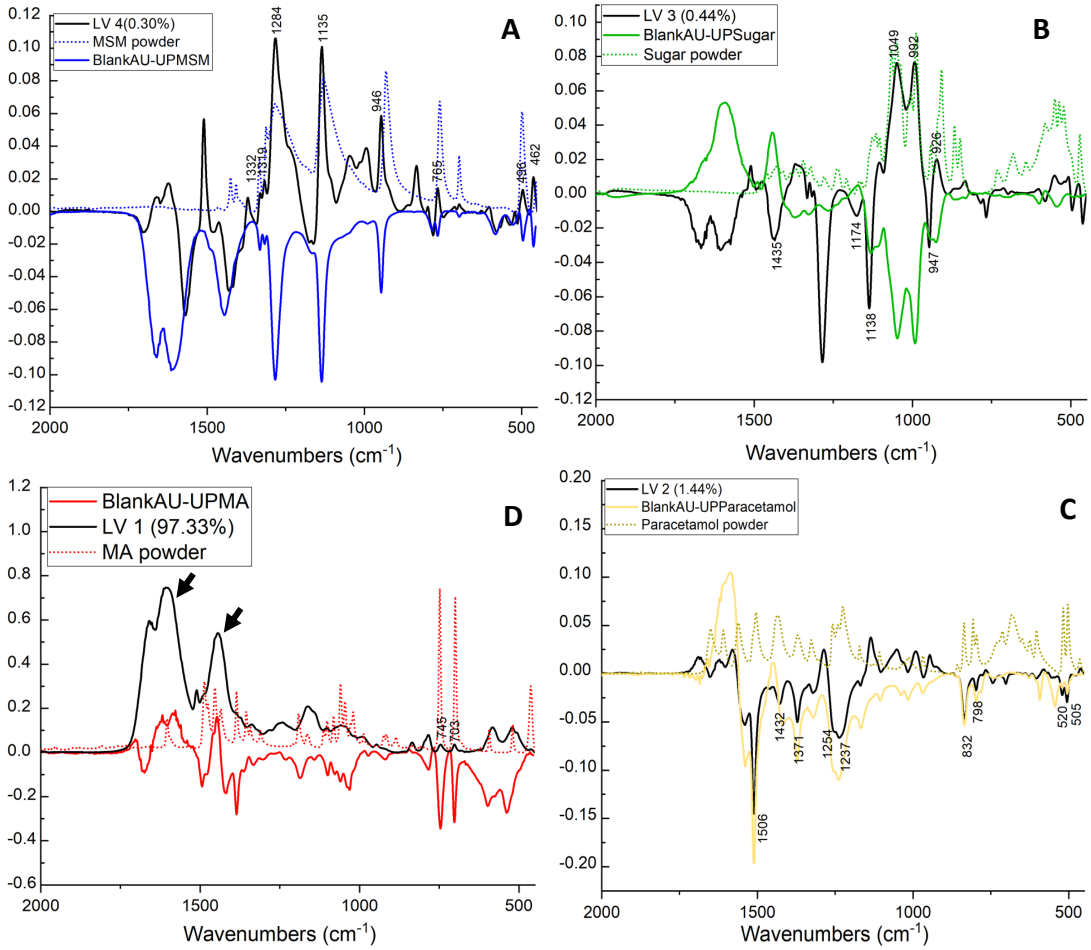

Figure 4-11: Graphs showing loadings for the respective LVs plotted with difference spectra (in bold coloured line) and powder spectra (in transparent coloured line) for the chemical compound in urine. **A** shows LV2 plotted with urine difference spectrum and powder spectrum of MSM; **B** shows LV4 plotted with urine difference spectrum and powder spectrum of sugar; **C** shows LV3 plotted with urine difference spectrum and powder spectrum of MA and **D** shows LV5 plotted with urine difference spectrum and powder spectrum of paracetamol. The vibrational bands belonging to each compound identified from the powder and difference spectra in serum are numbered in the loading plot for the corresponding latent variable. The black arrows in graph C indicate peaks characteristic of the urine matrix.

In summary, the classification models built using two different multivariate methods, PLS-DA and RF analysis on two different software platforms agreed with each other to show excellent discrimination between pure MA and MA adulterated with these three cutting agents. The

models presented here were not evaluated using an independent test set. Moreover, the combined interactions of the drug+cutting agent with the matrix were used in the classification models. Predictions of how these interactions would play out with different compounds and concentrations etc in classification models cannot be made based on the information presented here. Therefore, caution must be exercised when interpreting or drawing comparisons with samples that have different combinations and permutations of drugs with cutting agent concentrations. However, there are no other studies as per the author's knowledge that are similar to that presented in this chapter to allow for a direct comparison.

4.3.5 PLS-R Analysis

As a final step, PLS regression was explored to mimic a real-world scenario whereby unknown adulterations are encountered which need to be investigated against reference collection of pure samples. Using the pure MA dataset, PLS-R models were built in serum and urine. 5 LVs were chosen for both datasets based on the plot of calibration error (RMSEC) and cross-validation error (RMSECV) as a function of the number of latent variables (Appendix 2, Figure A2-1 and A2-2). The calibration set consisted of all pure MA samples in serum and urine, while an independent validation set was made up of samples that contained MA adulterated with MSM in the respective biofluid (Table 4-8). MSM was chosen as the cutting agent for this model as it is the most used substance when adulterating MA.

Table 4-8: Summary of samples included in building PLS regression models in the calibration and validation sets.

Model	Calibration set	Total samples	Validation set	Total samples
A	SPMA	19	SPMAMSM	5
B	UPMA	19	UPMAMSM	5

PLS-R model A was built using a serum dataset of MA samples with known purities and was validated using 5-fold cross-validation (Appendix 2, Figure A4-1). The MA samples are shown in red diamonds, while the MA+MSM samples shown in the green squares in Figure 4-12 range from 10% to 90% MA purity. The root mean square error of prediction (RMSEP) was found to be 0.86 mg/mL with an R^2 value of 0.965 indicating excellent applicability of the model to future samples.

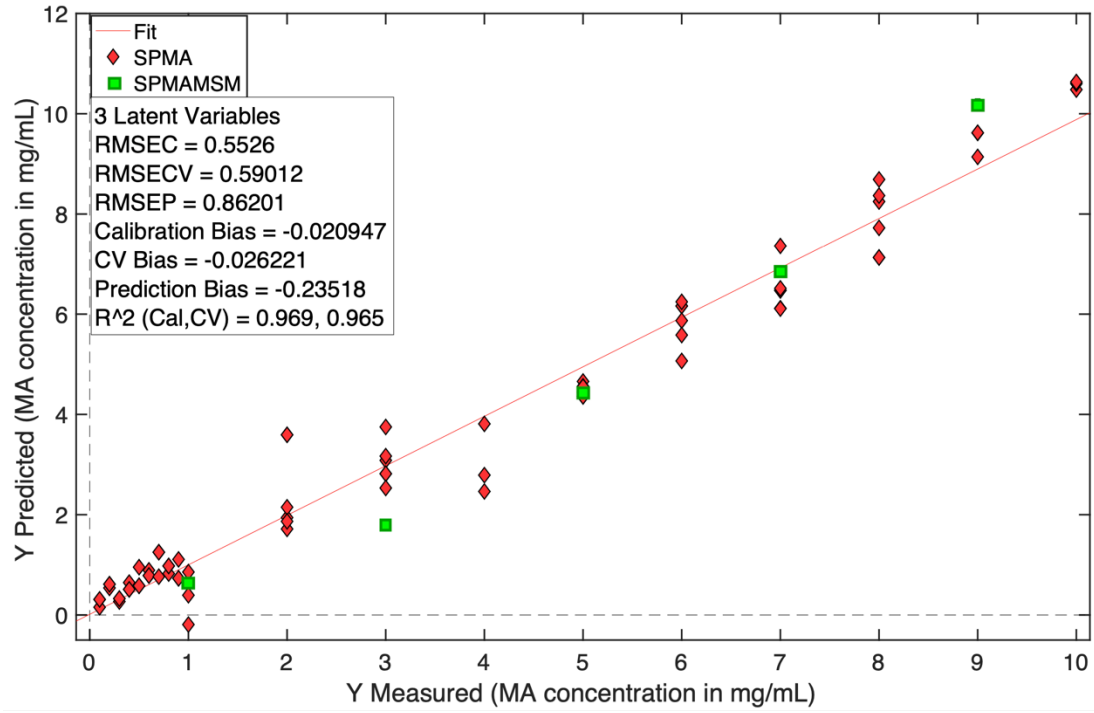

Figure 4-12: PLS regression model built with pure MA dataset in serum (here labelled as SPMA) which was then tested using samples containing MA adulterated with MSM (here labelled as SPMAMSM) for its predictive abilities for MA samples with unknown adulterations. Results using 3 latent variables: RMSEC = 0.5526 mg/mL, RMSECV = 0.5901 mg/mL, RMSEP = 0.8620 mg/mL, R^2 (Cal,CV) = 0.969 and R^2 (Pred) = 0.965.

PLS-R model B was built using a urine dataset of MA samples with known MA purities and was validated using three latent variables and a 5-fold cross-validation (Figure A4-2). The scores plot for the regression model is shown in Figure 4-13 where the calibration set of pure MA samples in urine is shown in red diamonds and the independent validation set of MA+MSM samples is shown in green squares. The root mean square error of prediction (RMSEP) was found to be 0.70 mg/mL, lower than that of the serum dataset. Similarly, the observed R^2 value of 0.985 was also higher than that for the serum dataset. This is likely because serum is a more complex matrix than urine and tends to mask the spectral signatures of the drug compounds in the sample.

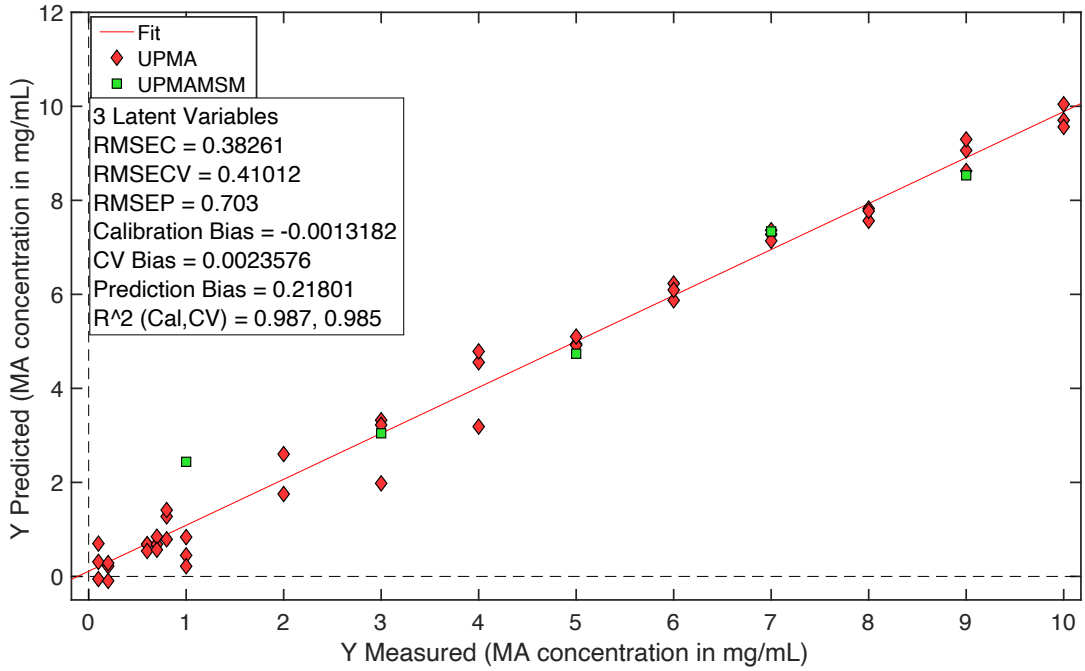

Figure 4-13: PLS regression model built with pure MA dataset in urine (here labelled as UPMA) which was then tested using urine samples containing MA adulterated with MSM (here labelled as UPMAMSM) for its predictive abilities for MA samples with unknown adulterations. Results using 3 latent variables: RMSEC = 0.3826 mg/mL, RMSECV = 0.4101 mg/mL, RMSEP = 0.703 mg/mL, R^2 (Cal,CV) = 0.987 and R^2 (Pred) = 0.985.

4.4 Conclusion

Alternative methods for direct, quick, and accurate detection of adulteration in drugs are urgently needed in a clinical setting as well as in forensic investigations. This novel study examining the ability of the ATR-FTIR spectroscopy to distinguish pure drug samples from samples with no MA in them as well as adulterated MA samples in serum and urine directly illustrated the excellent potential of this technique by delivering promising statistical outputs.

The cutting agents included in this chapter, MSM, paracetamol and sugar were investigated owing to their prevalence as cutting agents in today's global drug market and additionally represent a group of substances that are often unreported in routine forensic analysis of illicit MA samples. The purity percentage of MA included in this study varied from 10% to 90% which is typical of the purity values found in the majority of adulterated MA samples seized worldwide. Initially, three cutting agents in their powder form were characterised using FTIR

spectroscopy to identify spectral regions of importance in discriminating them from pure MA powder.

Following powder analysis, drug samples in serum and urine biofluids were analysed. Firstly, pure MA samples were discriminated against samples with only cutting agents using PLS-DA and RF classification models. Overall, both classification methods showed similar statistical outputs when discriminating MA from cutting agents that in physical appearance can resemble MA. In the serum dataset, the highest sensitivity values of 96.6 ± 6.1% and 100% and specificity values of 98.0 ± 9.8% and 100% were seen for discrimination against MSM and sugar respectively using the RF classification model. For discrimination of MA against paracetamol, however, the PLS-DA model performed better providing sensitivity and specificity values of 95.5 ± 6.7% and 99.0 ± 4.9% respectively.

For the discrimination of pure MA from adulterated MA samples in both biofluids RF classification performed better than PLS-DA to provide outstanding sensitivities and specificities of 100% for all cutting agents. In order to simulate a real-world situation where samples from varying sources with a range of cutting agents could be encountered during analysis, a multiclass PLS classification model was performed in both biofluids. Comparable results were observed with 98.7% sensitivity and 95.5% specificity for the correct classification of pure MA samples.

Finally, PLS regression models constructed using a training dataset of pure MA samples demonstrated adequate predictive power in determining the percentage of MA in adulterated samples from an independent validation set of MA adulterated with MSM. With RMSEP of 0.86 and 0.70 mg/mL for the serum and urine datasets, the regression models were able to show strong linearities with R^2 values of ~ 0.95. Though this is lower than that found in the literature and the threshold recommended for an analytical method, it is an excellent result for a proof-of-principle study with a limited sample size. Additionally, the results achieved here were achieved in biofluids without any sample preparation or pre-treatment which is unparalleled in the literature.

In conclusion, the use of ATR-FTIR spectroscopy combined with chemometrics has demonstrated successful discrimination of pure MA samples from adulterated samples without the need for prior time-consuming sample extractions or preparations. This study has significant implications when treating patients in the emergency department where

quick results are needed for appropriate patient care when an unknown drug, similar in appearance to MA, or street MA with an unknown degree of adulteration is ingested or when the patient is unable to communicate. In addition, the identification of cutting agents and their relative percentages in a timely manner could provide useful intelligence regarding adulteration practices and linkages with regional/local dealers which could be crucial in a forensic investigation.

Improvements in the discrimination of pure MA from adulterated MA could be achieved using a larger dataset where a greater range of MA purity percentages is covered. Moreover, though the applicability of this methodology to MA samples with impurities that occurred from illicit production would be challenging due to their much lower concentrations, it would benefit from the inclusion of a greater variety of cutting agents for its wider application. While this study looked at the total (free and bound) drug compound portions, it is important to note that differences in drug-protein binding abilities of a variety of compounds is likely to have an impact on the results presented here. However, this was outside the scope of this study and requires more directed research. Therefore, though GC-MS remains the gold standard for confirmatory analyses, the methodology presented in this Chapter presents a more efficient alternative to the current methods that can be performed outwith a dedicated laboratory leading to significant savings in both time and expenditure as well as providing vital forensic intelligence in a timely manner.

4.5 References

1. United Nations Office of Drugs and Crime, *World Drug Report Booklet 4* United Nations Office of Drugs and Crime, Vienna, Austria, 2021.
2. W. D. Barker and U. Antia, *Forensic Science International*, 2007, **166**, 102-109.
3. J. Broséus, N. Gentile, F. Bonadio Pont, J. M. Garcia Gongora, L. Gasté and P. Esseiva, *Forensic Science International*, 2015, **257**, 307-313.
4. T. R. Fiorentin, A. J. Krotulski, D. M. Martin, T. Browne, J. Triplett, T. Conti and B. K. Logan, *Journal of Forensic Sciences*, 2019, **64**, 888-896.
5. A. Fries, R. W. Anthony, A. Cseko, C. C. Gaither and E. Schulman, *The Price and Purity of Illicit Drugs: 1981-2007*, Institute for Defence Analyses, Virginia, USA, 2008.
6. T. Hand, R. Mulchandani and L. K. Panesar, *Seizures of Drugs in England and Wales 2009/10*, Home Office, London, 2009.
7. European Monitoring Centre for Drugs and Drug Addiction, *The State of Drugs Problem in Europe*, European Monitoring Centre for Drugs and Drug Addiction, Luxemburg, Germany, 2009.
8. C. Cole, L. Jones, J. McVeigh, A. Kicman, Q. Syed and M. Bellis, *Cut: A Guide to Adulterants, Bulking Agents and Other Contaminants Found in Illicit Drugs*, Liverpool John Moores University, LIverpool, 2010.
9. I. Onoka, A. T. Banyika, P. N. Banerjee, J. J. Makangara and L. Dujourdy, *Forensic Science International: Synergy*, 2020, **2**, 194-205.
10. B. A. Perillo, R. F. X. Klein and E. S. Franzosa, *Forensic Science International*, 1994, **69**, 1-6.
11. UN Office for Drug Control and Crime Prevention, *Drug Characterization/Impurity Profiling: Background and Concepts*, Report 9211481392, United Nations Office for Drug Control and Crime Prevention, Vienna, Austria, 2001.
12. L. Dujourdy, V. Dufey, F. Besacier, N. Miano, R. Marquis, E. Lock, L. Aalberg, S. Dieckmann, F. Zrcek and J. S. Bozenko, *Forensic Science International*, 2008, **177**, 153-161.
13. C. Cole, L. Jones, J. McVeigh, A. Kicman, Q. Syed and M. Bellis, *Drug Testing and Analysis*, 2011, **3**, 89-96.
14. R. J. Hamilton, J. Perrone, R. Hoffman, F. M. Henretig, E. H. Karkevandian, S. Marcus, R. D. Shih, B. Blok and K. Nordenholz, *Journal of Toxicology: Clinical Toxicology*, 2000, **38**, 597-608.
15. D. Payer, M. Young, B. Maloney-Hall, C. Mill, P. LeClerc and J. Buxton, *Adulterants, Contaminants and Co-Occurring Substances in Drugs on the Illegal Market in Canada: An Analysis of Data from Drug Seizures, Drug Checking and Urine Toxicology*, Canadian Centre on Substance Use and Addiction, Ottawa, Canada, 2020.
16. V. M. Singh, T. Browne and J. Montgomery, *Public Health Reports*, 2019, **135**, 6-10.
17. A. Żubrycka, A. Kwaśnica, M. Haczkiewicz, K. Sipa, K. Rudnicki, S. Skrzypek and L. Poltorak, *Talanta*, 2022, **237**, 1-8.
18. C. S. Johnson, C. R. Stansfield and V. R. Hassan, *Forensic Science International*, 2020, **313**, 110367.
19. H. Segawa, K. Kumisaka, R. Sugita, Y. T. Iwata, T. Yamamuro, K. Kuwayama, K. Tsujikawa, T. Kanamori and H. Inoue, *Forensic Science International*, 2018, **282**, 86-91.
20. J. Hughes, G. Ayoko, S. Collett and G. Golding, *PloS one*, 2013, **8**, e69609-e69609.
21. Drug Enforcement Administration Office of Forensic Sciences, *Microgram Bulletin*, 2007, **40**, 111.
22. J. S. Lee, H. S. Chung, K. Kuwayama, H. Inoue, M. Y. Lee and J. H. Park, *Analytica Chimica Acta*, 2008, **619**, 20-25.

23. V. Puthaviriyakorn, N. Siriviriyasomboon, J. Phorachata, W. Pan-ox, T. Sasaki and K. Tanaka, *Forensic Science International*, 2002, **126**, 105-113.
24. R. Coomber, *Addiction Research*, 1997, **5**, 297-306.
25. Y. Qi, I. D. Evans and A. McCluskey, *Forensic Science International*, 2006, **164**, 201-210.
26. H. Inoue, K. Kuwayama, Y. T. Iwata, T. Kanamori, K. Tsujikawa and H. Miyaguchi, *Forensic Toxicology*, 2008, **26**, 19-22.
27. D. T. Vu, *Journal of Forensic Sciences*, 2001, **46**, 1014-1024.
28. S. Choe, S. Heo, H. Choi, E. Kim, H. Chung and J. Lee, *Forensic Science International*, 2013, **227**, 48-51.
29. A. R. Khajeamiri, M. Faizi, F. Sohani, T. Baheri and F. Kobarfard, *Forensic Science International*, 2012, **217**, 204-206.
30. C. Y. Goh, W. Van Bronswijk and C. Priddis, *Applied Spectroscopy*, 2008, **62**, 640-648.
31. K. Tsujikawa, K. Kuwayama, H. Miyaguchi, T. Kanamori, Y. T. Iwata, T. Yoshida and H. Inoue, *Analytica Chimica Acta*, 2008, **608**, 95-103.
32. L. S. A. Pereira, F. L. C. Lisboa, J. Coelho Neto, F. N. Valladão and M. M. Sena, *Forensic Science International*, 2018, **288**, 227-235.
33. K. W. Tupper, K. McCrae, I. Garber, M. Lysyshyn and E. Wood, *Drug and Alcohol Dependence*, 2018, **190**, 242-245.
34. M. Schulz, A. Schmoldt, H. Andresen-Streichert and S. Iwersen-Bergmann, *Critical Care*, 2020, **24**, 195.
35. R. D. McLachlan and V. B. Carter, *Spectrochimica Acta Part A: Molecular Spectroscopy*, 1970, **26**, 1121-1127.
36. A. B. Brizuela, L. C. Bichara, E. Romano, A. Yurquina, S. Locatelli and S. A. Brandán, *Carbohydrate Research*, 2012, **361**, 212-218.
37. J.-J. Max and C. Chapados, *The Journal of Physical Chemistry A*, 2001, **105**, 10681-10688.
38. M. Trivedi, S. Patil, H. Shettigar, K. Bairwa and S. Jana, *Chemical Sciences Journal*, 2015, **6**.
39. A. M. Amado, C. Azevedo and P. J. A. Ribeiro-Claro, *Spectrochimica Acta Part A: Molecular and Biomolecular Spectroscopy*, 2017, **183**, 431-438.
40. M. Huber, K. V. Kepesidis, L. Voronina, F. Fleischmann, E. Fill, J. Hermann, I. Koch, K. Milger-Kneidinger, T. Kolben, G. B. Schulz, F. Jokisch, J. Behr, N. Harbeck, M. Reiser, C. Stief, F. Krausz and M. Zigman, *eLife*, 2021, **10**, e68758.

CHAPTER FIVE

APPLICATION OF ATR-FTIR SPECTROSCOPY AS AN ALTERNATIVE TO IMMUNOASSAYS FOR DRUG SCREENING IN BIOFLUIDS

Abstract

Immunoassays are currently the standard screening methods used in routine toxicological screening of biofluids. These are employed in numerous settings including workplace drug testing, and therapeutic drug monitoring for verifying drug consumption and abstinence making them an indispensable screening tool. However, they are plagued by several issues relating to the cross-reactivity of antibodies employed in their operation. While some studies take advantage of cross-reactivities to detect drugs that otherwise go undetected, in a clinical setting false positives due to cross-reactivities can have serious implications. Such a problem is frequently encountered in immunoassay testing of MA whereby many commonly prescribed drugs are mistakenly identified as MA. ATR-FTIR spectroscopy in combination with chemometric analysis is employed as an alternative screening technique to immunoassays for the discrimination of MA from such prescription drugs. Six prescription drugs were chosen in this chapter because they are known for testing positive on commercially available amphetamine immunoassays. Two-step binary and single-step multiclass PLS-DA models provided sensitivities and specificities of 100% for the discrimination of MA samples from drug-free and samples containing prescription drugs. Though there are limitations to this analysis such as a small sample size and a lack of independent testing sets, this chapter provides a promising proof-of-concept work for more detailed future investigations.

5.1 Introduction

Methamphetamine is one of the most abused drugs with almost 34 million users worldwide.[1] In the UK, there are an estimated 1.5 million people addicted to prescription and over-the-counter drugs and approximately 300,000 people have accessed drug and alcohol services in 2021.[2] Approximately 6% of the emergency department presentations for seizures are drug-related in the US, while the drug-related mortality rates have increased by 171%, 149% and 61% in Scotland, Northern Ireland, and England and Wales between 2010 and 2019, respectively.[3, 4] On average, a third of the UK's prison population – approximately 82,000 people on a given day, are incarcerated for a drug-related offence.[5, 6] As a response to increasing drug-related crimes, mandatory drug testing upon arrest was introduced in the UK to monitor compliance with rehabilitation programmes to provide the necessary help to detainees and avoid future relapse.[7, 8] In addition, between 67 and 80% of corporations have established workplace testing programmes in the US currently, while there has been a 470% increase in such testing in the UK workplaces.[9, 10] Though this list of scenarios requiring drug testing is not comprehensive, it highlights that drug screening tests are prolific and have become ubiquitous in numerous situations.

Immunoassays (IAs) are the most common first step in drug screening making them indispensable for evidence-based reporting and resolutions.[11, 12] IAs are performed to verify drug abstinence, identify non-medical drug use and monitor adherence to prescribed controlled substances at hospitals, point-of-care locations and in dedicated laboratories for clinical, legal and forensic purposes.[13-15] IAs typically used for urine drug screening are broadly categorised into two – those targeting a drug class with multiple clinically and forensically relevant compounds and targeting a single drug and/or its unique metabolites.[16, 17] The choice of assay used is situation-dependent with varying consequences. In a forensic/legal setting, identifying the presence of controlled substances is often a priority while in a clinical setting identification of all possible drugs present is essential for correct patient care.

Though presumptive positive samples via IAs are required to be sent for confirmatory testing in an accredited laboratory in forensic/legal situations, confirmatory testing may not always be available in a timely manner for effective patient management in a clinical setting.[12] With increasing global substance abuse leading to high volumes of routine drug screening, it is not always feasible to send all samples for expensive confirmatory analysis and screening

methods such as IAs are employed in ruling out drug-free samples. IAs, therefore, remain the most prevalent first line of testing for drugs of abuse steadily replacing other screening methods such as thin layer chromatography and colourimetric tests due to their simple and fast operation, lower cost and high-throughput analysis of samples with the availability of numerous automated commercial kits.[12, 18-20] The Point-of-care devices are also advantageous in the simultaneous testing of multiple drugs or drug classes and offer even faster turnaround times.[21]

Despite the benefits mentioned above, IAs suffer from many important limitations. The primary design of an IA relies on binding specifically designed antibodies with the target molecules of interest and its detection using various technologies.[19, 22] This makes IAs inherently susceptible to interferences due to the cross-reactivity profiles of the assay antibodies and/or cut-off concentrations of the assay leading to false positives and/or false negatives.[13, 23] With the proliferation of commercial IAs consisting of different antibodies from a variety of manufacturers that target the same drug, the cross-reactivity profiles and range of compounds tested for interference are not standardised.[13, 16] Furthermore, IAs are often developed with the parent drug in mind while the drug metabolites are not always targeted either in the assay or the list of compounds tested for interferences.[16] Therefore, overall interpretation is complicated by the availability of a range of assays for the same drug compound that may not provide concordant results and lack of information on their susceptibility to all possible interfering compounds.[16, 21, 24]

In addition, the cut-off concentrations are arbitrarily determined by government organisations such as the Substance Abuse and Mental Health Services Administration (SAMHSA) in the US which have little to no correlation with the therapeutic or toxic concentrations of the drug in question.[16] For instance, the threshold for positive opiate drug screens was increased from 300 μg/L to 2000 μg/L in order to avoid false positives due to poppy seed ingestion in the late 1990s.[25] While this solution might increase the specificity of assays, it can also lead to an increase in false negatives thus reducing the overall sensitivity. Conversely, the cut-off for marijuana metabolite was lowered in 1994 to increase the frequency of positive specimens reflecting advances in IA technology.[25] Therefore, the application of such cut-off concentrations outwith the dictated settings needs to be situationally specific to achieve the correct balance between specificity and sensitivity.

Many studies have shown that amphetamine IAs are particularly susceptible to interferences from numerous prescribed and over-the-counter drugs.[11, 12, 26-29] Methamphetamine and amphetamine are both structurally simple sympathomimetic compounds making it difficult to develop specific antibodies for their detection.[27] Most commercially available IAs target the amine functional group in amphetamines which makes them vulnerable to interferences from many other compounds commonly ingested.[26, 27] The most commonly mentioned drugs responsible for false positives due to cross-reactivities with methamphetamine IAs in the literature - bupropion, labetalol, metformin, ofloxacin, promethazine and trazodone are the focus of this chapter. These drugs are routinely prescribed to patients to treat depression (bupropion), high blood pressure in pregnant women (labetalol), type II diabetes (metformin), infections (ofloxacin), allergies (promethazine) and a combination of depression and anxiety (trazodone). While some of these drugs such as bupropion have similar 2D structures to methamphetamine, others have significantly differing structures (Figure 5-1).

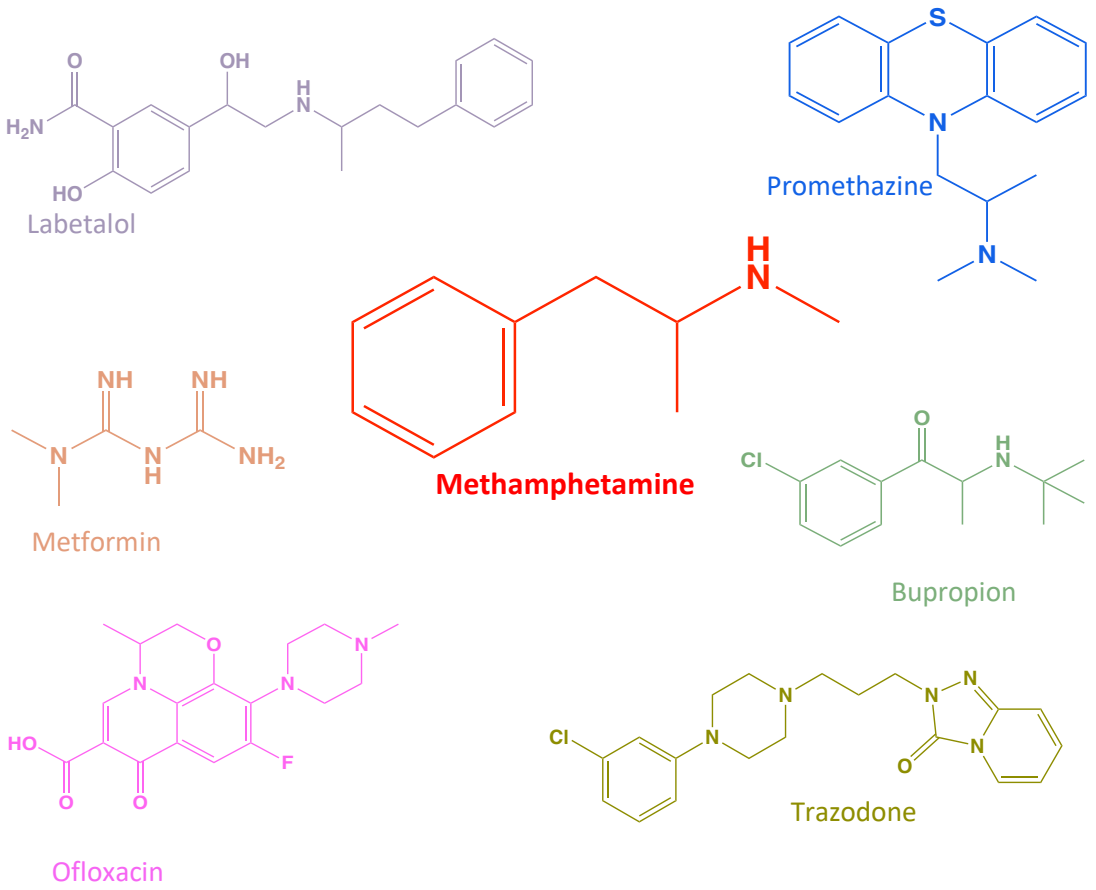

Figure 5-1: Structures of the six drugs investigated in this chapter along with methamphetamine.

Some studies have attempted to predict cross-reactivities of compounds based on molecular similarities using chemoinformatic methods. For instance, Pope *et al.* calculated the molecular similarity scores based on 2D structures of methamphetamine and a range of interfering compounds as a simple means of estimating cross-reactivity whereby higher scores reflect a higher probability of immunoreactivity.[12] However, the varying similarity scores of 0.69, 0.40, 0.18 and 0.19 for bupropion, labetalol, metformin and trazodone respectively suggest that predicting cross-reactivity is more complicated as antibody-analyte interactions are three-dimensional and take place in complex biological samples.[12, 20, 30] Therefore, it might be difficult to know which compounds cross-react without specific testing.

In varying patient populations with prescriptions for the therapeutic use of one or more of these drugs, studies have reported false positive rates ranging from 3.9% - 9.9%,[12] 13.8%,[13] 26%,[31] 35%[32, 33] to as high as 49.5%.[17] Casey *et al*.[32] reported that 41% of the total number of false positives in their study were due to the therapeutic administration of bupropion in patients while the rest were attributed to labetalol and other antipsychotics. Melanson *et al.*[31] reported a similar false positive rate (40%) in their patient population representing a typical emergency department, however, promethazine and its metabolite chlorpromazine were identified to be responsible. These authors also examined the same samples with 5 other immunoassays available on the market which produced varying results.[31] These studies overall highlight three main points: first, even therapeutic concentrations of these commonly prescribed drugs can produce false positive drug screens for amphetamines; second, it is important to investigate not only such drug compounds but also their metabolites for cross-reactivities; and third, different immunoassays will not necessarily provide concordant results and require careful interpretation on the clinician's part. Finally, though some of these discrepancies in the false positive rates can be explained by the varying patient populations, the numbers highlight the need for a more effective and reliable screening method.

Table 5-1 highlights the prevalence of these six drugs in the US and the UK by the large numbers of prescriptions annually dispensed to patients. Furthermore, many of the presenting symptoms such as altered mental state (hallucinations and seizures), cardiovascular toxicity (tachycardia) and gastrointestinal issues caused by the misuse of these six drugs in patients at emergency departments can also be present in cases of methamphetamine abuse.[4, 32, 34] Therefore, it may not be possible to rule out such drugs

simply based on symptoms without a drug test. Moreover, a false positive result on a drug screen may require further testing and delay patient management. The number of retesting or confirmatory tests needed in light of the high false positive rates and high volumes of drugs consumed leads to additional expenditure.

Aside from the economic and practical concerns, there can be damaging social and legal implications to testing positive on a Drugs of Abuse test for the patient in the short term. For instance, Fucci *et al.*[35] reported a patient, who, even after showing a 10-year-long prescription for metformin lost his taxi permit and driving licence upon testing positive on the amphetamine screening test leading to loss of livelihood. Similarly, Yee *et al.*[34] reported three cases where inaccurate interpretation of urine drug screen in the presence of labetalol could have led to mismanagement of pregnant patients and caused mental trauma with a wrongful diagnosis of illicit drug use. Finally, in court-ordered or work-related drug screening, a false positive test can lead to legal interventions, employment denials, and questions of honesty which can have detrimental effects on the person's personal and professional life.

In this chapter, the application of ATR-FTIR spectroscopy as an alternative to current immunoassay methods is explored. As demonstrated by the method developed in Chapters 3 and 4, ATR-FTIR spectroscopy applied without prior sample extraction methods can reveal the presence of all possible drug compounds within a sample. With urine as the primary biological fluid of choice, this chapter aims to explore if ATR-FTIR spectroscopy along with chemometric analysis can produce lower rates of false positives in distinguishing methamphetamine from these six drugs in a given sample population. Furthermore, the application of this method in serum samples is also explored as these drugs are likely to be found in blood, i.e., serum upon consumption allowing comparison across matrices. Considering the pharmacokinetics of each of the drugs involved, the concentration ranges explored here include therapeutic, toxic and fatal-comatose levels making this study clinically and forensically relevant (Table 5-1).

Table 5-1: Pharmacologic and usage data for the six drugs included in this chapter, data are collated from Ref[36-44].

Drug		Bupropion	Labetalol	Metformin	Ofloxacin	Promethazine	Trazodone
Daily Dose Range (mg)		200-400	800-2400	500-2550	400-800	25-50	150-600
Average Oral Bioavailability (%)		5-20	11-86	50-60	95	25	63-91
Half-life (hrs)		24	1.7-6.1	6	9	12-15	4
Plasma-protein binding (%)		84	50	Negligible	10-30	93	85-95
Unchanged parent drug eliminated in urine (%)		4	5	90	90	0.64	0.13
Concentration in urine at 12 hrs (mg/mL)		0.013-0.026	0.067-0.2	0.75-3.825	0.6-1.2	0.0003-0.0005	0.0003-0.001
Concentration in Blood (mg/L)	Therapeutic	0.01-1.5	0.03-0.2	0.1-2	2-5.5	0.01-0.2	0.7-2
	Toxic	1.2-2	1-2.9	5-10	39	0.1-2	1.2-4
	Comatose-Fatal	4-7.3	1.7	91-166	-	1.8-5.4	9-15
USA (in 2020)	Number of prescriptions	28,889,368	2,301,044	92,591,486	1,844,982	2,309,125	26,210,731
England (GP prescriptions in 2022)	Quantity of drug	3,023,368	8,149,236	1,947,931,06	1,057,396	83,518,321	48,734,235

5.2 Materials and Methods

5.2.1 Materials

Surine™ Negative Urine Control (here referred to as AU), Ofloxacin ($C_{18}H_{20}FN_3O_4$, here referred to as OF) and the hydrochloride salts of bupropion ($C_{13}H_{18}ClNO$ • HCl, here referred to as BU), metformin ($C_4H_{11}N_5$ • HCl, here referred as MET), labetalol ($C_{19}H_{24}N_2O_4$ • HCl, here referred as LB), promethazine ($C_{17}H_{20}N_2S$ • HCl, here referred as PR), and trazodone ($C_{19}H_{22}ClN_5O$ • HCl, here referred as TR) were purchased from Merck Chemicals Ltd. Human pooled serum was purchased from TSC Life Sciences Ltd., which was stored at -80℃ in a freezer when not in use. All chemicals were in powder form. All solutions were prepared directly in the human serum and AU, without any other solvents or reagents.

5.2.2 Sample Preparation

Stock solutions of the six drug molecules were created by directly dissolving powders into biofluids. Using these stock solutions, samples of varying concentrations reflecting therapeutic, toxic and comatose-fatal levels were made up in urine and serum (Table 5-2). The stock solutions were made up at 10 mg/mL or at the maximum solubility of the drug molecule in aqueous media as indicated in Table 5-2. Details for the MA samples mentioned in this chapter are provided in Chapter 3 (Section 3.2.2).

Table 5-2: Stock and sample solutions concentrations for the six drugs in urine and serum. The therapeutic, toxic and comatose-fatal concentrations are indicated in brackets as described in ref. [42, 45]

Drug	Abbreviation	Stock Solution (mg/mL)	Sample Solutions (mg/mL)	No. of samples
Bupropion	Urine: UPBU Serum: SPBU	10	10, 1, 0.1, 0.0073 (comatose-fatal), 0.0012 (toxic), 0.0001 (therapeutic)	32
Labetalol	Urine: UPLB Serum: SPLB	8	8, 4, 1, 0.1, 0.01, 0.001 (comatose-fatal/toxic)	24
Metformin	Urine: UPMET Serum: SPMET	10	10, 5, 0.2 (comatose-fatal), 0.1 (toxic), 0.004 (therapeutic)	19
Ofloxacin	Urine: UPOF Serum: SPOF	6	5, 1, 0.1, 0.04 (toxic), 0.0055 (therapeutic)	18
Promethazine	Urine: UPPR Serum: SPPR	10	1, 0.1, 0.0054 (comatose-fatal), 0.0004 (therapeutic)	25
Trazodone	Urine: UPTR Serum: SPTR	2	1, 0.1, 0.015 (comatose-fatal), 0.004 (toxic)	15

5.2.3 Spectral Collection

The instrumentation and spectral collection procedure used were previously described in section 3.2.3.

5.2.4 Spectral Pre-processing and Analysis

The PRFFECT toolbox within R statistical computing environment software was utilised for spectral pre-processing. The pre-processing protocol followed here included Savitzky-Golay (SG) filter for smoothing, vector normalisation and rubberband baseline correction in that order for all samples, while an additional step of picking the 2200-450 cm^{-1} region for urine samples was performed.

The spectral analysis was performed in MATLAB (version 2018b) using the PLS Toolbox (version 9.6.2) add-on created by Eigenvector Research Inc. Mean centring was applied to the complete dataset after it was imported into PLS_Toolbox. Binary and multi-class partial least squares discriminant analysis (PLS-DA) models were trained and cross-validated using the Venetian blinds cross-validation method. The training and test sets were created with 5 data splits and a maximum of 20 latent variables. An appropriate number of latent variables were selected based on the plot of root mean square errors of classification and cross-validation for each of the models. The performance of these models was evaluated using sensitivity, specificity and accuracy (total number of samples correctly identified). False positive rates were used for comparison with those noted in section 5.1. Permutation tests were performed in order to detect the overfitting and examine the extent to which 'chance correlation' might exist between x- and y-blocks in current modelling conditions.

5.3 Results and Discussion

IR spectra for all drug powders were collected for peak assignment. These are provided in Appendix 3 Figures A3-1, A3-2 and A3-3. The difference spectra for all seven compounds were calculated by subtracting the blanks urine spectra from drug sample spectra (at a concentration of 10 mg/mL) shown in Figure 5-2. These were important in highlighting the peaks of importance for each of the drugs that stand out above the urine matrix background. These peaks were later used as characteristic indicators for that drug in loading plots of the classification models. The term 'prescription drugs' is used to refer to the group of six drugs (BU, LB, OF, MET, PR, and TR) mentioned while the term 'all drugs' refers to seven compounds which include the six prescription drugs and MA.

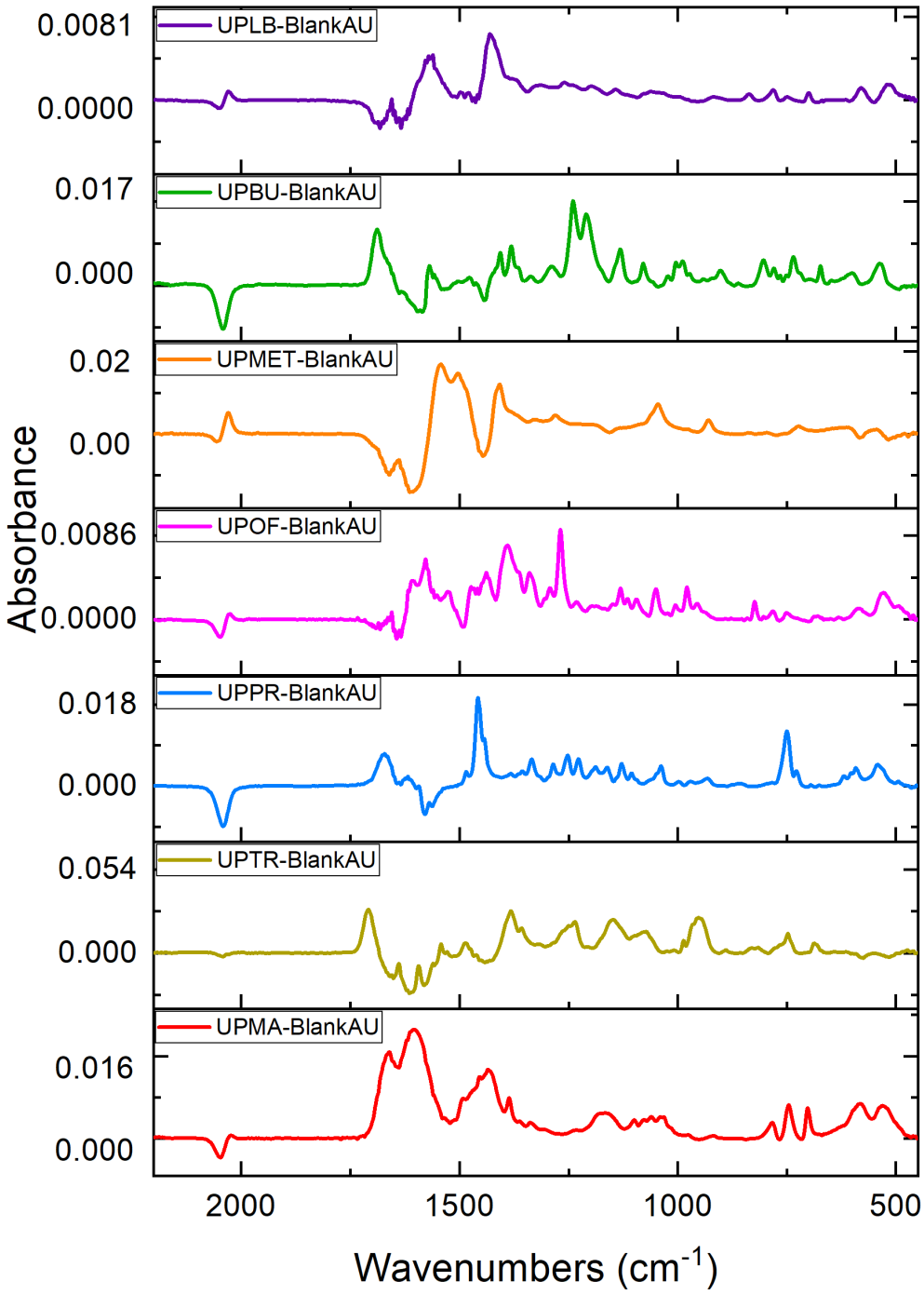

Figure 5-2: Stacked difference spectra for all seven drug compounds where blank urine spectra were subtracted from the spectra of the drug samples in urine. UPMA-BlankAU = difference spectra for MA; UPTR-BlankAU = difference spectra for trazodone; UPOF-BlankAU = difference spectra for ofloxacin; UPMET-BlankAU = difference spectra for metformin; UPBU-BlankAU = difference spectra for bupropion and UPLB-BlankAU = difference spectra for labetalol.

5.3.1 Urine Dataset

5.3.1.1 Binary Models – PLS-DA

The discrimination of MA samples from the prescription drugs was carried out in a two-step analysis. The binary PLS model was constructed first to distinguish all drug samples from the drug-free samples in the urine dataset. The drug-free cohort consisted of blank urine samples (n = 17), while the drug cohort consisted of samples spiked with bupropion, labetalol, metformin, ofloxacin promethazine, trazodone and methamphetamine (n = 148). The PLS-DA model (number of LVs = 6) for discriminating between these two cohorts performed exceptionally well with a sensitivity and specificity of 95% and 96%, respectively. The accuracy of this model calculated at 95.7%. Excellent performance in the cross-validated

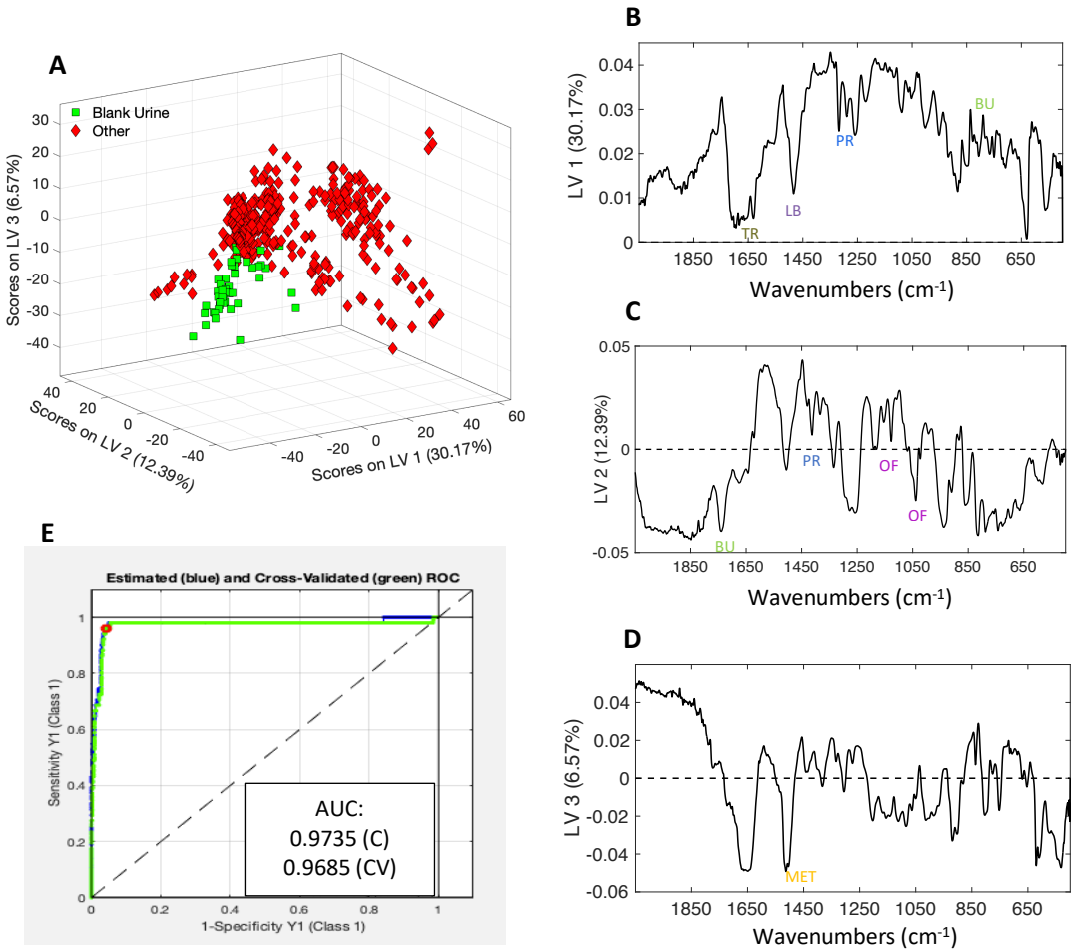

Figure 5-3: Results from PLS-DA model built using urine dataset. **A**: 3D scores plot for drug samples (denoted here as 'Other' in red) and drug-free samples (denoted here as 'Blank Urine' in green). **B**, **C** and **D** present latent variables 1, 2 and 3 respectively which were used to construct the scores plot in **A**. **E**: Indicates receiver operator curve (ROC) with area under the curve (AUC) of 0.9685 for the cross-validated PLS model.

model was also indicated by the AUC 0.9635 (Figure 5-3). Overall, the false positive rate for drug-free samples was 4.5% while the false positive rate for drug samples was 3.9%. These cross-validated results suggest that this model performed remarkably well in this sample population in this sample population with compounds of varying structures.

Following this, a second binary PLS model (number of LVs = 5) was constructed to specifically distinguish those samples with MA from the prescription drugs. This PLS-DA model performed exceptionally well with 100% sensitivity and specificity. This is illustrated in Figure 5-4 where a clear distinction between the two classes is evident. Furthermore, the loading plots for latent variables 1, 3 and 3 (Figure 5-4, plots B, C and D) show characteristic peaks

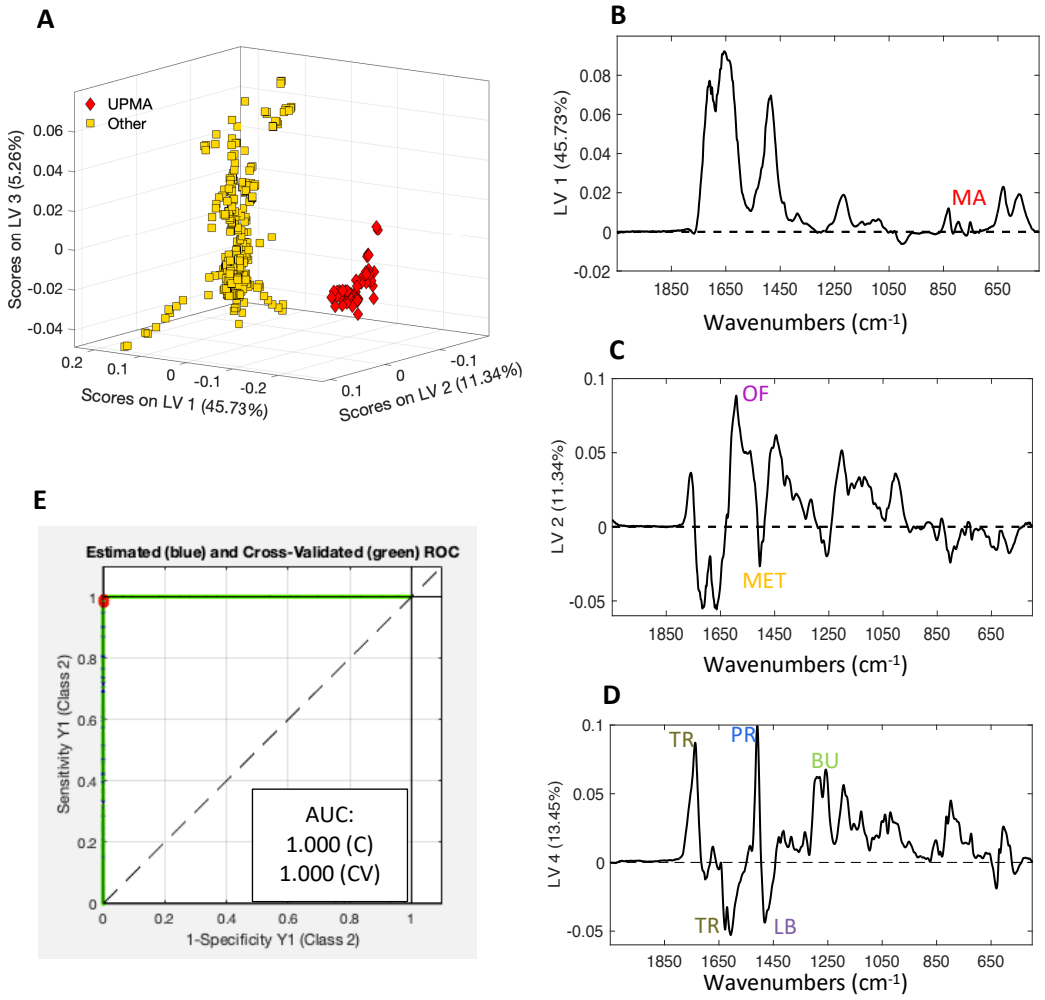

Figure 5-4: Results from PLS-DA model built using urine dataset. **A**: 3D scores plot for two classes – 'UPMA' shown in red diamonds consists of MA samples in urine and 'Other' shown in yellow squares consists of all samples with one of the six drugs mentioned in this chapter. **B**, **C** and **D** present latent variables 1, 2 and 3 respectively which were used to construct the scores plot in **A**. **E**: Indicates receiver operating curve (ROC) with area under the curve (AUC) of 1.000 for the cross-validated PLS model.

for each of the drugs that were identified from the difference spectra (Figure 5-2). The permutation tests conducted on both models demonstrated their statistical significance at 95% confidence interval.

This two-step analysis consisting of two PLS-DA binary models displayed promising results in distinguishing firstly, drug samples from drug-free samples and then more specifically methamphetamine samples from the prescription drugs commonly known to give false positives in current IAs. Furthermore, the false positive rates reported here were found to be better than those reported in the literature.[12, 13, 17, 32] It is likely that these cross-validated results presented here are overly optimistic as they were not evaluated with an independent dataset obtained from real-world samples. However, permutation tests conducted for both models highlighted indicating statistical significance of these models at a 95% confidence level. Therefore, with the range of concentrations presented here covering clinical and forensic ranges highlight the strong potential of this method as an alternative to the immunoassay methods currently in use.

5.3.1.2 Multi-class Models – PLS-DA

Following the success of the two-step analysis, a multiclass PLS-DA model was constructed to combine both analyses into one step. This PLS-DA model (with optimum number of LVs = 7) consisted of three classes – 'Blank Urine' referring to drug-free samples, 'UPMA' referring to urine samples containing MA and 'Other' refers to samples that contained one of the prescription drugs.

This cross-validated multi-class PLS model performed very well in terms of total accuracy whereby 94.9% of the samples were correctly classified (Table 5-3). This is comparable with the binary models presented in the previous section and was particularly effective in distinguishing MA samples from the rest with 100% sensitivity and specificity. This is also depicted by the scores plot in Figure 5-5 where there is no overlap between MA samples and the remaining two classes.

Table 5-3: Results for cross-validated multi-class PLS-DA model where blank urine class consisted of drug-free samples, Other class consisted of samples with one of the prescription drugs and UPMA class consisted of all samples containing MA.

Class	Sensitivity (%)	Specificity (%)	False Positive Rate (%)
Blank Urine	74.5	97.4	2.5
Other	97.1	86.3	13.6
UPMA	100	100	0

The sensitivities of 74.5% and 97.1% for drug-free samples and 'other' drug class respectively indicated that this model was less precise than the binary classification. Upon closer examination of the data, the overlap between blank urine samples and the 'Other' drug samples is due to the low concentrations included in this analysis. It was, however, essential to include these samples as they are most likely to be encountered in a clinical setting where

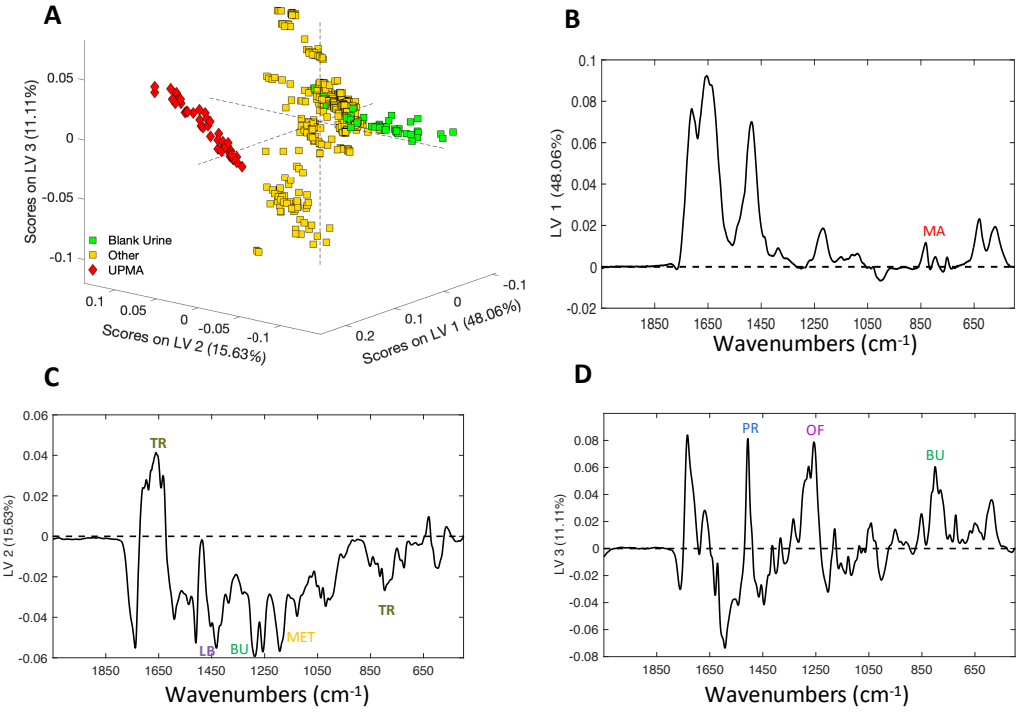

Figure 5-5: Results from PLS-DA multiclass model built using urine dataset. **A**: 3D scores plot for three classes – 'UPMA' shown in red diamonds consists of MA samples in urine, 'Other' shown in yellow squares consists of all samples with one of the six drugs mentioned in this chapter and 'Blank Urine' shown in green squares consists of all drug-free urine samples. **B**, **C** and **D** present latent variables 1, 2 and 3 respectively which were used to construct the scores plot in **A**.

patients have been prescribed these drugs in therapeutic doses. This also adds to the class imbalance seen in this model which can also impact the model performance. In spite of this, 97.1% of the drug samples were correctly identified in the 'Other' drug class and the false positive rate of 13.6% was comparable to those reported in the literature. Finally, the area under the curve (AUC) values of 0.913, 0.945 and 0.100 for the 'Blank Urine', 'Other' and 'UPMA' classes respectively suggest excellent detection capability.

To take this multi-class analysis one step further for an effective application in the field, an eight-class PLS model was built to attempt to classify all samples in their respective classes in one analysis. The results of this model (optimum number of LVs = 4) are presented in Table 5-4 in the form of sensitivities, specificities and false positive rates for each of the classes. The accuracy, i.e., the total number of samples correctly assigned using this model was 51.6%. This is significantly less than those obtained from either the two-step analysis or the three-class PLS model. However, this model still achieved 100% sensitivity and specificity classifying all the MA samples correctly. Furthermore, the second highest correct identification was found to be for the blank/drug-free samples with a sensitivity of 72.5%. While this is lower than those achieved by the two previous analyses, with a specificity of 95.4%, it is still a significant finding as it would reduce unnecessary further testing.

Table 5-4: Table showing results for cross-validated eight-class PLS model.

Class	Sensitivity (%)	Specificity (%)	False Positive Rate (%)
UPMA	100	100	0
UPTR	60	82.1	17.8
UPPR	62.6	96.1	3.8
UPOF	50	94.1	5.9
UPMET	35	100	0
UPBU	37.5	99.2	0.75
UPLB	23.6	77.7	22.2
Blank Urine	72.5	95.4	4.5

The drug classes with two of the highest false positive rates of 22.2% and 17.8% were labetalol and trazodone respectively (Table 5-4). This high false positive rate is due to

trazodone samples being classified as labetalol and *vice versa*. For trazodone, the highest concentration possible was 2 mg/mL due to the low solubility of the drug in aqueous media. This severely limited the proportion of characteristic peaks visible over the urine matrix background in the spectra leading to low sensitivity. For labetalol, while the solubility was higher than trazodone, the characteristic peaks highlighted in the difference spectra (Figure 5-2) are in the same region of 1600 – 1400 cm^{-1} as those found in trazodone. This is also the region where major contributions from urea as part of the urine matrix are visible. The lack of any other distinctive spectral features in the rest of the spectrum along with this likely explains the difficulty in their identification.

While the above model showed limited success in classifying all samples in one step, it highlighted that MA samples can be distinguished even in the presence of a structurally diverse sample population using this method. Therefore, for a situation where one potential interferant is expected i.e. when the patient is known to have a prescription for one of these drugs, a three-class PLS model specifically targeted towards that drug would be beneficial. To this effect, six three-class PLS models were constructed and their results are presented below (Figure 5-6). The scores and loadings plots are given in Appendix 3 (Figures A3-4 and A3-5). When these sensitivities and specificities are examined, all six models illustrate the correct classification of all MA samples. In addition, when false positive rates were examined, they were all below the lowest reported false positive rates i.e. 3.9% in the literature.[12] In particular, the results for the model with bupropion samples are excellent whereby only 1.1% of the samples were incorrectly identified in this analysis (Table A, Figure 5-6). With the use of only one of the six drugs as one of the three classes, the classes become more balanced, thus allowing for more confidence in the results. However, the performance of these models was not evaluated using independent test sets in this study. Therefore, the comparisons with the literature values of false positives should be done cautiously and with a caveat that these models may be overly optimistic in their predictive performance.

A **Blank v UPMA v UPBU**

	Sens (%)	*Spec (%)*	*FPR (%)*
Blank	98.0	98.5	1.4
UPMA	100	100	0
UPBU	97.9	98.9	1.1

B **Blank v UPMA v UPTR**

	Sens (%)	*Spec (%)*	*FPR (%)*
Blank	96.1	96.5	3.4
UPMA	100	100	0
UPTR	93.1	97.8	2.1

C **Blank v UPMA v UPPR**

	Sens (%)	*Spec (%)*	*FPR (%)*
Blank	93.3	100	6.7
UPMA	100	97.5	2.5
UPPR	100	100	0

D **Blank v UPMA v UPOF**

	Sens (%)	*Spec (%)*	*FPR (%)*
Blank	82.3	100	0
UPMA	100	92.3	7.6
UPOF	100	98.9	1.1

E **Blank v UPMA v UPMET**

	Sens (%)	*Spec (%)*	*FPR (%)*
Blank	98	100	0
UPMA	100	100	0
UPMET	100	98.9	1.1

F **Blank v UPMA v UPLB**

	Sens (%)	*Spec (%)*	*FPR (%)*
Blank	98	100	0
UPMA	100	100	0
UPLB	100	98.9	1.1

Figure 5-6: Results for six multi-class PLS models constructed for the urine dataset including sensitivity (here referred to as Sens), specificity (here referred to as Spec) and false positive rates (here referred to as FPR). Blank = drug-free urine samples; UPBU = urine samples containing bupropion, UPLB = samples containing labetalol, UPTR = samples containing trazodone; UPPR = samples containing promethazine; UPOF = samples containing ofloxacin; and UPMET = samples containing metformin.

In summary, the results of the various PLS models using the urine dataset presented here provide robust results in the correct identification of MA samples with low rates of false positives. However, some models with unbalanced classes should be interpreted with restraint and must be repeated with a larger dataset consisting of independent test sets from real patient samples.

5.3.2 Serum Dataset

While there are no studies on these drugs causing false positives in a serum immunoassay, blood samples are commonly taken in drug screening situations in a clinical setting. Therefore, a similar two-step analysis was performed on the serum dataset. A binary PLS classification model was built to distinguish drug-free samples from those containing any one

of the seven drugs. Following this, another binary PLS model was constructed to discriminate between samples containing MA from those containing one of the prescription drugs. These results are shown below (**A** and **B** in Figure 5-7).

A **Blank Serum v Other**

	Sens (%)	Spec (%)	FPR (%)
Blank	84.4	89.2	10.7
Other	89.2	84.4	15.5

B **SPMA v Other**

	Sens (%)	Spec (%)	FPR (%)
SPMA	83.5	96.2	16.4
Other	96.2	83.5	3.7

C **Blank serum v SPMA v Other**

	Sens (%)	Spec (%)	FPR (%)
Blank	83.3	88.4	11.5
SPMA	60	94.5	5.4
Other	90.5	94.5	5.4

Figure 5-7: Results of the PLS models build on the serum dataset. A and B show the results of two binary PLS models carried out in the two-step analysis. C shows results of multiclass PLS model. Blank serum class includes all drug free samples. SPMA class includes all samples with MA in them. Other class includes all samples containing one of the six drugs. Sens = sensitivity; Spec = specificity; FPR = false positive rate.

For discriminating drug-free samples, the cross-validated model produced sensitivity and specificity of 84.4% and 89.2%, respectively. Moreover, the false positive rate for drug-free samples incorrectly identified here was 10.7% while the false positive rate for drug samples was 15.5%. In the second step of the analysis, the cross-validated PLS model constructed for the discrimination of MA samples from those of the six drugs produced sensitivity and specificity of 83.5% and 96.2%, respectively. The optimum number of LVs were determined to be 6, 3 and 5 for plot A, B and C in Figure 5-7 respectively. The false positive rate for the MA sample class in this classification was higher at 16.4% than that observed from the urine dataset (Table 5-3). In comparison to the urine dataset, the sensitivity and specificity values of both of these models were lower on the serum dataset leading to higher rates of misclassifications. This is unsurprising as the serum is a more complex biological matrix with large protein molecules with strong IR absorptions which tend to mask a lot of spectral signatures of the drug compounds.

Following this, a multiclass PLS model was constructed for the serum dataset similar to that of the urine dataset to classify drug-free, MA and prescription drug samples. in this model, the sensitivity for the MA class was significantly lower at 60% in comparison to the other two classes (**C** in Figure 5-7). The high false positive rate of 11.5% for the drug-free samples in comparison to the 5.4% false positive rate for the other two classes suggests that many of the samples containing drugs are being classified as drug-free by this model. Upon further examination, the samples with the lowest drug concentrations have been misclassified by this model indicating that this method might not be sensitive enough to detect drugs in low concentrations in serum samples. Therefore, it might be necessary to further investigate the application of this method to serum samples either with more balanced larger datasets or with some preliminary sample preparation steps such as protein precipitation performed prior to analysis. Moreover, it would be beneficial to investigate the detection limits for each of the drugs in this dataset with a full set of standards with wide concentration ranges than that employed in this chapter.

5.4 Conclusion

With the convenient availability of drugs worldwide, the need for drug testing has increased in a variety of situations. The most common first test conducted for drug screening is immunoassays. However, there are several prescription medications taken in therapeutic doses that cause false positives on these Drugs of Abuse immunoassays. While in forensic/legal cases, confirmatory testing is mandatory, clinical laboratories are often not equipped with the expensive instrumentation necessary for confirmatory testing. This can lead to significant mental trauma and damage to the patient's personal and professional life. Therefore the application of ATR-FTIR spectroscopy as an alternative method for drug testing using immunoassays is presented in this chapter. The drugs investigated in this study were six compounds commonly shown to test false positives on methamphetamine IAs including bupropion, labetalol, ofloxacin, promethazine, metformin and trazodone. The chapter focused mainly on the analysis of urine samples while preliminary work on serum samples was also presented.

Using binary PLS-DA classification models with Venetian blinds cross-validation, excellent sensitivity and specificity values of 96% and 95.4% respectively, were obtained for the discriminating drug-free samples from drug samples containing at least one of the drugs mentioned in this study. Following this, a second binary PLS-DA model was constructed to

discriminate MA samples from the prescription drugs with 100% sensitivity and specificity. The AUC-ROC values of 0.96 and 0.100 for these two binary models demonstrated good predictive capabilities.

A third multiclass PLS-DA model was constructed to combine these two steps and to categorise drug-free, MA and prescription drug samples in one step. The results of this cross-validated multiclass model also displayed promising results with sensitivity values of 74.5%, 97.1% and 100% for drug-free, prescription drug and MA samples respectively. Furthermore, the sensitivity of 100% for MA samples obtained here illustrated that none of the prescription drug samples were misclassified as MA. Therefore, based on these results the method described here is a strong contender as an alternate screening test for the detection of MA in urine samples.

The multiclass PLS classification model for the serum dataset was decidedly less accurate with sensitivity values of 83.3%, 90% and 60% for prescription drugs, drug-free and MA samples, respectively. However, the examination of class assignments for samples indicated that this was due to the low sensitivity of the instrument in detecting low-concentration samples. A false positive rate of 5.4% was obtained for MA samples, which was fairly respectable considering the complexity of the serum matrix.

The results reported here are very promising, and emphasise the applicability of ATR-FTIR spectroscopy as an alternative method of drug screening for MA in urine. There are, however, some important considerations to note. The classes included in this analysis were very unbalanced in some instances and thus would require further samples with a wider concentration range for a more robust analysis. Furthermore, this chapter only included the parent drugs in the analysis. This was due to time and resource constraints. However, it would be greatly beneficial to include major metabolites of these drug compounds in the analysis as it is the metabolites that tend to cause false positives for some drugs. It would also be prudent to consider poly-drug use where an analysis that includes combinations of these drugs would be useful as some patients might be prescribed more than one from this list. Following this theme of false positives, the next chapter investigates the capability of this method in the detection and discrimination of a class of drugs that are specifically designed to mimic the effects of MA.

5.5 References

1. United Nations Office of Drugs and Crime, *World Drug Report Booklets 1-6*, United Nations Office of Drugs and Crime, Vienna, Austria, 2020.

2. Office for Health and Improvement & Disparities, *Adult Substance Misuse Treatment Statistics 2021 to 2022: Report*, Office for Health and Improvement & Disparities, London, 2023.

3. A. Holland, A. Stevens, M. Harris, D. Lewer, H. Sumnall, D. Stewart, E. Gilvarry, A. Wiseman, J. Howkins, J. McManus, G. W. Shorter, J. Nicholls, J. Scott, K. Thomas, L. Reid, E. Day, J. Horsley, F. Measham, M. Rae, K. Fenton and M. Hickman, *Journal of Public Health*, 2022, fdac114.

4. J. C. Drees, J. A. Stone, K. R. Olson, K. H. Meier, A. M. Gelb and A. H. B. Wu, *Clinical Chemistry*, 2009, **55**, 126-133.

5. C. Black, *Review of Drugs: Summary*, Home Office, London, 2020.

6. HM Scottish Government, *Recorded Crime in Scotland, 2021-2022*, United Kingdom Statistics Authority, Edinburgh, 2021.

7. H. G.-U. Kingdom, *From Harm to Hope - a 10-Year Drugs Plan to Cut Crime and Save Lives*, London, 2021.

8. M. Connor, G. Green, N. Thomas, A. Sondhi and D. Pevalin, *Health & Justice*, 2020, **8**, 3.

9. S. Warren and E. Wray-Bliss, *New Technology, Work and Employment*, 2009, **24**, 163-176.

10. J. Wicks, The State of Workplace Drug Testing in 2019, https://blog.cansfordlabs.co.uk/uk-workplace-drug-testing-in-2019, (accessed 21 March, 2023).

11. J. M. Boyd and S. M. H. Sadrzadeh, in *Accurate Results in the Clinical Laboratory*, eds. A. Dasgupta and J. L. Sepulveda, Elsevier, Cambridge, United States, 2nd edn., 2019, ch. 14, pp. 233-242.

12. J. D. Pope, O. H. Drummer and H. G. Schneider, *Journal of Analytical Toxicology*, 2022, **47**, 263-270.

13. K. L. Johnson-Davis, A. J. Sadler and J. R. Genzen, *Journal of Analytical Toxicology*, 2016, **40**, 97-107.

14. K. E. Moeller, K. C. Lee and J. C. Kissack, *Mayo Clinic Proceedings*, 2008, **83**, 66+.

15. M. D. Krasowski and T. C. Kwong, in *Critical Issues in Alcohol and Drugs of Abuse Testing*, ed. A. Dasgupta, Academic Press, London, 2nd edn., 2019, ch. 30, pp. 441-448.

16. J. M. Reschly-Krasowski and M. D. Krasowski, *Academic Pathology*, 2018, **5**, 2374289518811797.

17. B. M. Kapur, *Clinical Biochemistry*, 2012, **45**, 603-604.

18. J. Dupouy, V. Mémier, H. Catala, M. Lavit, S. Oustric and M. Lapeyre-Mestre, *Drug and Alcohol Dependence*, 2014, **136**, 11-20.

19. P. Datta, in *Critical Issues in Alcohol and Drugs of Abuse Testing*, ed. A. Dasgupta, Academic Press, London, 2nd edn., 2019, ch. 9, pp. 121-128.

20. M. D. Krasowski, A. F. Pizon, M. G. Siam, S. Giannoutsos, M. Iyer and S. Ekins, *BMC Emergency Medicine*, 2009, **9**, 5.

21. M. D. Krasowski, G. A. McMillin, S. E. F. Melanson, A. Dizon, B. Magnani and C. L. H. Snozek, *Archive of Pathology and Laboratory Medicine*, 2020, **144**, 177-184.

22. S. E. F. Melanson, *Clinics in Laboratory Medicine*, 2012, **32**, 429-447.

23. A. S. Maharjan and K. L. Johnson-Davis, in *Critical Issues in Alcohol and Drugs of Abuse Testing*, ed. A. Dasgupta, Academic Press, London, 2nd edn., 2019, ch. 10, pp. 129-139.

24. S. E. F. Melanson, L. Baskin, B. Magnani, T. C. Kwong, A. Dizon and A. H. B. Wu, *Archives of Pathology & Laboratory Medicine*, 2010, **134**, 735-739.

25. V. I. Luzzi, A. N. Saunders, J. W. Koenig, J. Turk, S. F. Lo, U. C. Garg and D. J. Dietzen, *Clinical Chemistry*, 2004, **50**, 717-722.

26. L. Broussard, in *Critical Issues in Alcohol and Drugs of Abuse Testing*, ed. A. Dasgupta, Academic Press, London, 2nd edn., 2019, ch. 16, pp. 207-214.

27. A. Saitman, H. D. Park and R. L. Fitzgerald, *Journal of Analytical Toxicology*, 2014, **38**, 387-396.

28. A. G. Verstraete and F. V. Heyden, *Journal of Analytical Toxicology*, 2005, **29**, 359-364.

29. N. C. Brahm, L. L. Yeager, M. D. Fox, K. C. Farmer and T. A. Palmer, *American Journal of Health-System Pharmacy*, 2010, **67**, 1344-1350.

30. M. D. Krasowski, M. G. Siam, M. Iyer, A. F. Pizon, S. Giannoutsos and S. Ekins, *Clinical Chemistry*, 2009, **55**, 1203-1213.

31. S. E. F. Melanson, E. Lee-Lewandrowski, D. A. Griggs, W. H. Long and J. G. Flood, *Archives of Pathology & Laboratory Medicine*, 2006, **130**, 1834-1838.

32. E. R. Casey, M. G. Scott, S. Tang and M. E. Mullins, *Journal of Medical Toxicology*, 2011, **7**, 105-108.

33. J. M. Baron, D. A. Griggs, A. L. Nixon, W. H. Long and J. G. Flood, *Journal of Analytical Toxicology*, 2011, **35**, 364-368.

34. L. M. Yee and D. Wu, *Obstetrics & Gynecology*, 2011, **117**.

35. N. Fucci, *Forensic Science International*, 2012, **223**, e60.

36. M. A. Al-Omar, in *Profiles of Drug Substances, Excipients and Related Methodology*, ed. H. G. Brittain, Academic Press, London, 2009, vol. 34, ch. 6, pp. 265-298.

37. D. J. Buysse and S. Tyagi, in *Principles and Practice of Sleep Medicine*, eds. M. Kryger, T. Roth and W. C. Dement, Elsevier, London, 6th edn., 2017, ch. 42, pp. 432-445.e437.

38. J. N. Connarn, R. Luo, J. Windak, X. Zhang, A. Babiskin, M. Kelly, G. Harrington, V. L. Ellingrod, M. Kamali, M. McInnis and D. Sun, *Biopharmaceutics and Drug Disposition*, 2016, **37**, 550-560.

39. J. N. Connarn, S. Flowers, M. Kelly, R. Luo, K. M. Ward, G. Harrington, I. Moncion, M. Kamali, M. McInnis, M. R. Feng, V. Ellingrod, A. Babiskin, X. Zhang and D. Sun, *Journal of the American Association of Pharmaceutical Scientists*, 2017, **19**, 1513-1522.

40. E. P. MacCarthy and S. S. Bloomfield, *Pharmacotherapy: The Journal of Human Pharmacology and Drug Therapy*, 1983, **3**, 193-217.

41. G. G. Graham, J. Punt, M. Arora, R. O. Day, M. P. Doogue, J. Duong, T. J. Furlong, J. R. Greenfield, L. C. Greenup, C. M. Kirkpatrick, J. E. Ray, P. Timmins and K. M. Williams, *Clinical Pharmacokinetics*, 2011, **50**, 81-98.

42. M. Schulz, A. Schmoldt, H. Andresen-Streichert and S. Iwersen-Bergmann, *Critical Care*, 2020, **24**, 195-199.

43. OpenPrescribing.net).

44. ClinCalc DrugStats Database, *Medical Expenditure Panel Survey (Meps) 2013-2020*, Agency for Healthcare Research and Quality (AHRQ), Rockville, MD, 2022.

45. M. Schulz, S. Iwersen-Bergmann, H. Andresen and A. Schmoldt, *Critical Care*, 2012, **16**, 1-4.

CHAPTER SIX

SAME SAME BUT DIFFERENT - USING ATR-FTIR SPECTROSCOPY TO DISTINGUISH BETWEEN TRADITIONAL AND NOVEL STIMULANTS IN BIOFLUIDS

Abstract

The screening of NPS in biofluids is challenging for many reasons including structural diversity, constantly evolving new variants, low concentrations, lack of reference materials, instability of compounds during extraction and analysis, as well as limited knowledge of metabolism and excretion parameters. Furthermore, they are very rarely included as part of the routine toxicological strategy. This creates a challenge for not only detecting newly emerging compounds but also unsuspected ones. In this chapter, ATR-FTIR spectroscopy is utilised to provide a solution to this problem by analysing biological samples containing drugs as a whole without prior sample extraction. This chapter reports a forensic application of the method using real drug samples from the synthetic stimulant drug class obtained from police seizures for the discrimination of traditional stimulant, MA, from its NPS analogues, synthetic cathinones, in biofluids. Using chemometric analysis, the results reported here illustrate respectable sensitivity and specificity values for four structurally different groups of synthetic stimulants. Some important considerations highlighted through this analysis are the need for a wider range of concentrations and drug compounds, balanced datasets, independent test sets with real patient samples and research into drug-protein binding abilities of these novel stimulants for more robust model performance and reliable application.

6.1 Introduction

With increasing globalisation and new technologies, Novel psychoactive substances (NPS) have seen exponential growth in the last decade. Over 1150 substances are reported to the Early warning systems by the UNODC worldwide.[1] The term NPS includes any substance, either in pure form or preparation that is not currently controlled under the United Nations Single Convention on Narcotic Drugs, 1961 or the 1971 United Nations Convention of Psychotropic Substances, but may pose a public health threat comparable to the substances listed under these.[2] While some compounds were initially sold as 'legal highs' and 'research chemicals', NPSs are essentially legal alternatives to psychotropic substances currently controlled under national legislation.[3-5] Small changes continuously made to NPS structures, ensure their psychoactivity and, more importantly, their legality. While some countries regulate whole classes of NPSs, others choose to invoke the principle of 'chemical similarity' to an existing controlled drug to curb the potential for harm caused by these substances.[6] Therefore, the number of compounds in each class of drugs is constantly evolving with newer analogues appearing on the market when older ones are being controlled by law.[7] Furthermore, the advanced chemical capabilities and adaptabilities of the drug suppliers are intensified with the use of the Internet making any compounds available to anyone anywhere in the world.[8] The combination of all these issues creates the legal challenge where evidence-based reporting of harm is necessary for these new compounds to be included in the national legislation.

The capability and capacity to detect, identify and report NPS events are integral for the legal framework of early warning, risk assessment and control measures to be implemented effectively.[9, 10] However, the consumers of NPS often are unaware of the substances they are consuming which makes understanding the emergence, patterns of use and prevalence of these NPSs difficult to gauge.[11-14] Consequently, carrying out NPS risk assessments is difficult as research relating to their biological effects, bioavailability, metabolism, toxicity and long-term health effects are limited or anecdotal at best.[15-19] With the continuous growth of NPS structural variations, maintaining a working knowledge of their pharmacological parameters is almost impossible leading to under-detection and under-reporting of their use and prevalence.[9, 10, 20, 21] Additionally, the time required to maintain this working knowledge of all such compounds oftentimes exceeds their lifespan on the drug markets. This evolving NPS market creates a challenging legal and analytical problem.

Synthetic cathinones, the second largest group of NPS, mimic the effects of stimulants such as MA and other amphetamines.[2, 22, 23] Synthetic cathinones are a class of molecules derived from cathinone – a beta ketone amphetamine analogue which is a naturally occurring psychoactive compound present in the *Khat* plant.[5] While *Khat* has been used for centuries in parts of East Africa and the Arabian peninsula, currently, bupropion is the only cathinone derivative that has known therapeutic uses.[23] Others including 4-methylethcathinone (4-MEC), 3-methylmethcathinone (3-MMC), N-ethylpentylone and dipentylone have been used for recreational purposes (Figure 6-1).[15, 24, 25]

Over 130 novel cathinones have been reported to the EMCDDA in 2018 with little to no pharmacological information on most of them.[26] While the prevalence of synthetic cathinones is difficult to gauge as with many other drugs of abuse, their popularity began partly due to the decrease in the availability and purity of the more typical drugs of abuse.[15, 27] Cathinones are consumed in numerous forms and via various routes of administration.[15] The information regarding the typical dosage of such compounds is mostly obtained from user surveys and case studies and can be as low as 5 mg or as high as 1g per session.[15, 28] This is also reflected in the wide range of blood concentrations (1 to 50,000 ng/mL) of cathinones found in various case studies reported in the literature.[19, 28-36] These case studies also highlight an important aspect of NPS use which is poly-drug use. Whether this is achieved intentionally or accidentally due to unknown contents, it makes identifying the drug responsible for causing harm difficult.[27, 37-39] Moreover, like its traditional analogue MA, synthetic cathinones have adverse effects consistent with their sympathomimetic toxicity including flushing sweating, chills, anorexia, restlessness, hypertension and tachycardia.[40, 41] Therefore, in cases of acute intoxication, it is difficult for a clinician to ascertain the specific drug compound responsible. This means that forensic toxicological analyses of biological samples are much more important to not only gauge emergence and consumption trends but also to identify adverse effects.

The two-step analytical strategy of preliminary screening followed by a confirmatory test commonly applied to traditional illicit drugs to maximise diagnostic sensitivity in the first step and to optimise diagnostic specificity amongst all the presumptive positives is also applicable to synthetic cathinones.[42] However, the standard screening methods including immunoassays such as those ordered in emergency departments, will not typically detect the presence of cathinones.[7, 40] While some case studies have reported false positives generated

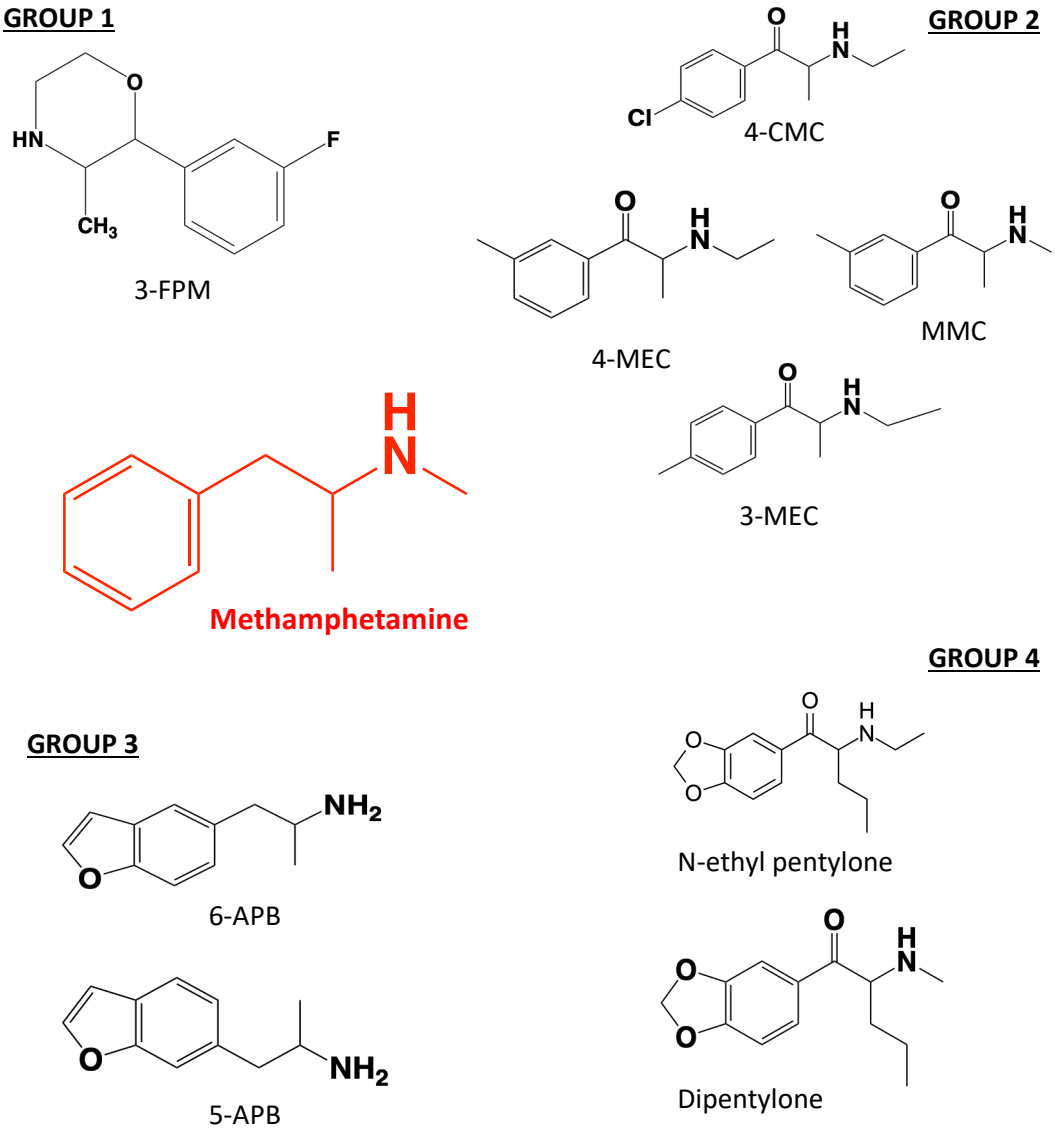

Figure 6-1: Figure shows structures for all NPS stimulants included in this chapter for comparison with MA (shown in red). Group 1 (Top left) includes 3-flurophenmetrazine (3-FPM). Group 2 (Top right) includes 4-chloromethcathinone (4-CMC), 4-methylethcathinone (4-MEC), 3-methylethcathinone (3-MEC) and methylmethcathinone (MMC). Group 3 (Bottom right) includes 6-(2-aminopropyl)benzofuran (6-APB) and 5-(2-aminopropyl)benzofuran (5-APB). Group 4 (Bottom left) includes N-ethyl pentylone and dipentylone.

for amphetamines and PCP, it is possible to employ this immunoassay cross-reactivity for toxicological screening.[43-46] Such studies, however, have reported highly variable results depending on the structural diversity of compounds included, concentrations and commercial test manufacturers.[47, 48] Therefore, specific testing for NPS that would allow

timely information for guided patient management in a clinical setting is still not available even with the most advanced instrumentations.[10, 40, 49]

Furthermore, when suspected samples are sent for more specific laboratory testing using hyphenated mass spectrometry techniques, NPSs are not commonly included on the drug panels in routine toxicology unless there is a strong suspicion of NPS use.[50, 51] Moreover, when NPS detection is requested, even the gold standard techniques such as LC-MS/MS are not all-inclusive leaving emerging compounds undetected.[50] Such methods require reference samples, lengthy method development, extensive drug database, and expert evaluation of results making them of limited use in the clinical setting for timely patient management.[40] Such detailed investigations can't be carried out on NPSs as they are essentially transient on the drug markets.

From the above discussion, it is evident that the screening of unknown substances is the weak point in the analytical strategy employed in the toxicological analysis of drug samples. This chapter aims to provide a potential solution to this problem by using the method developed in this thesis. The ability of ATR-FTIR spectroscopy to distinguish between MA, a traditional drug of abuse from its novel analogues, a selection of synthetic cathinones, in biological fluids is investigated as a rapid, adaptable and single-analysis method alternative to current screening methods.

6.2 Materials and methods

6.2.1 Materials

The reference standards for NPSs studied here were obtained from Cambridge Biosciences Ltd, in Cambridgeshire, UK. The street NPS samples analysed in this study were provided by the Defence Science and Technology Laboratory (DSTL) in Hertfordshire, UK in line with all legalities associated with controlled substances under UK legislation. Detailed information for these samples is given in Table 6-1. Reference standards were received in sealed vials with reference documentation, while street NPS samples were received in a variety of packaging such as small ziplock bags and plastic screw-top bottles which were sealed in an evidence bag. Examples of these are shown in Figure 6-2. The samples were divided into four groups based on their structural similarities (Figure 6-1) and these were used as classes in the classification models presented in this chapter.

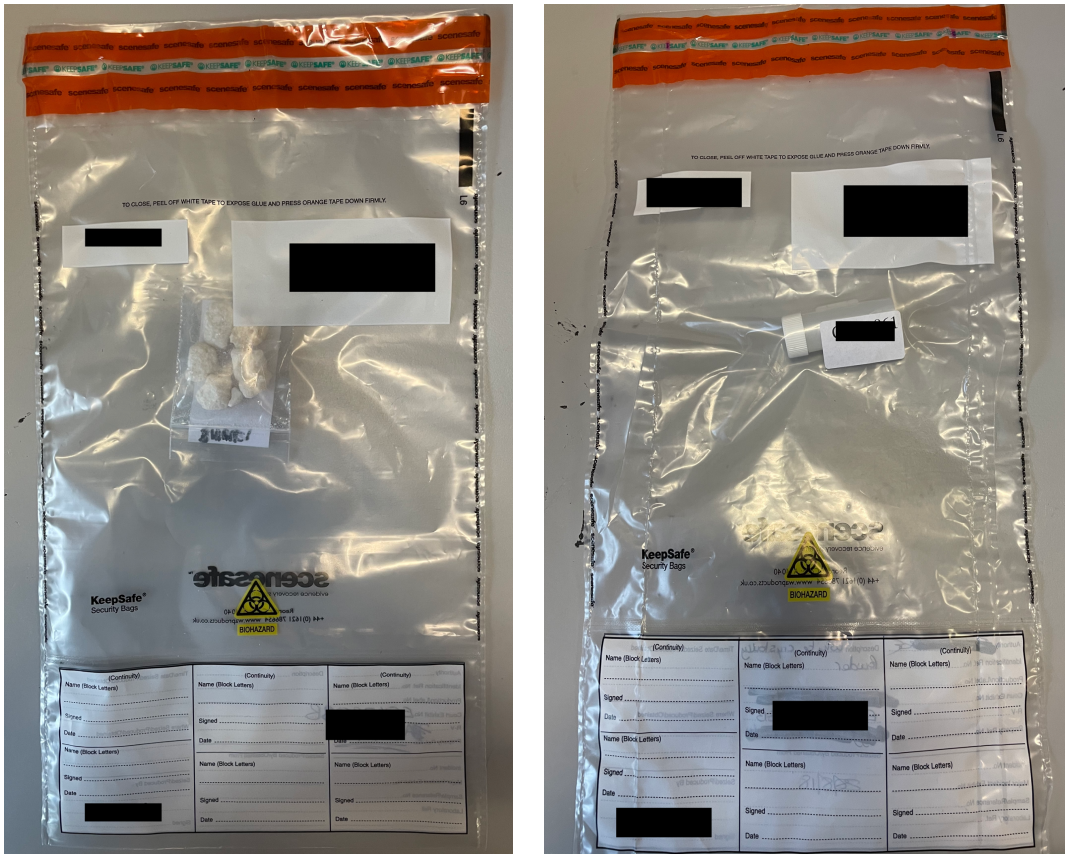

Figure 6-2: Photographs showing example of the condition in which street NPS samples arrived in from DSTL. The left photo shows a zip lock bag while the right photo shows a screw top bottle inside the sealed evidence bag. The photographs were taken by the author on their personal camera. Black boxes are used to remove sensitive information on the evidence bags.

Table 6-1: Details of all samples used in this study are shown in this table. Ref refers to reference standards; Street NPS refers to samples donated by DSTL. Total number of samples indicates the number of samples in each biofluid, urine and serum. Groups 1-4 refer to classes created using the structural similarity of the drug molecules in the street samples.

Sample Type	Sample ID	Drug/ Abbreviation	Total No of samples	Allocated Group
Ref	CAY17208	Flurophenmetrazine (FPM)	15	-
Ref	CAY11222	Methylethylcathinone (3-MEC)	15	-
Ref	CAY9001069	Methylethylcathinone (4-MEC)	15	-
Ref	CAY11224	Methylmethcathinone (MMC)	15	-
Ref	CAY16436	4-chloromethcathinone (4-CMC)	15	-
Ref	CAY11079	Aminopropylbenzofuran (6-APB)	15	-
Ref	CAY11134	Aminopropylbenzofuran (5-APB)	15	-
Ref	CAY9001933	Dipentylone	15	-
Street NPS	E5139347	3F-phenmetrazine (Street3FPM)	15	1
Street NPS	EH662856491GB	3-methylethylcathinone (Street3MEC)	15	2
Street NPS	E5147950 (A)	Clephedrone or 4-chloromethcathinone (Street4CMC)	15	2
Street NPS	E5147050 (B)	Methylmethcathinone (StreetMMC)	15	2
Street NPS	E5140038 (1)	4-methylethylcathinone (StreetMEC)	15	2
Street NPS	E5110349-K03	Methylmethcathinone (StreetMMC2)	15	2
Street NPS	E5140038 (2)	6-(2-aminopropyl)benzofuran (Street6APB)	15	3
Street NPS	E5110349-K01	*N*-ethylpentylone (StreetnEP)	15	4
Street NPS	E5110349-K02	*N*-ethylpentylone (StreetnEP2)	15	4
Street NPS	E4407010129	Dipentylone (StreetDipentylone)	15	4

6.2.2 Sample Preparation

Stock solutions of the six drug molecules were created by directly dissolving 10 mg of powders into 1 ml of biofluids. Using these stock solutions, samples of 10, 5, 1, 0.1 and 0.01 mg/mL concentrations were prepared for all reference standards and street NPS samples. Details for the MA samples mentioned in this chapter are provided in Chapter 3 (Section 3.2.2).

Powder samples were analysed in the form they were received in and did not require any further sample preparation such as milling or grinding.

6.2.3 Spectral Collection

The instrumentation and spectral collection procedure used were previously described in section 3.2.3.

6.2.4 Spectral Pre-processing and Analysis

The PRFFECT toolbox within R statistical computing environment software was utilised for spectral pre-processing. The pre-processing protocol followed here included a Savitzky-Golay (SG) filter for smoothing, vector normalisation and rubberband baseline correction in that order for all samples, while an additional step of picking the 2200-450 cm^{-1} region for urine samples was performed.

The spectral analysis was performed in MATLAB (version 2018b) using PLS Toolbox (version 9.6.2) created by Eigenvector Research Ltd. The mean centre and autoscale parameters provided in the PLS Toolbox were employed when they enhanced the model performance. This was evaluated for each dataset during analysis. Binary and multi-class PLS-DA models were trained and cross-validated using the Venetian blinds cross-validation method. The training and test sets were created with 5 data splits and a maximum of 20 latent variables. An appropriate number of latent variables were selected based on the plot of root mean square errors of classification and cross-validation for each model. The performance of these models was evaluated using sensitivity, specificity and accuracy (total number of samples correctly identified) and false positive rates. Permutation tests were performed in order to detect the overfitting and examine the extent to which 'chance correlation' might exist between x- and y-blocks in current modelling conditions.

6.3 Results and Discussion

6.3.1 Powder Spectra

Firstly, all powder samples – reference standards and street NPSs were analysed to understand the composition of the street samples. The individual spectra for reference standards with labelled peaks are provided in Appendix 4 Figures A4-1, A4-2, A4-3 and A4-4. The examination of the powder spectra of groups 1 - 4 samples revealed spectral regions of importance that were similar to those identified in **Chapter 3**. These regions include vibrations of the aromatic ring deformation and bending modes in the 1650 – 1400 cm^{-1} and 850 – 700 cm^{-1} regions, the type of substitution indicated by the sets of peaks in the 1225 – 950 cm^{-1} region, the symmetric and asymmetric stretches of the aliphatic side chains are found in the 2950 – 2700 cm^{-1} region and the N-H stretching modes in the higher 3600 – 3300 cm^{-1} region. However, some differences were also observed. For instance, the presence of strong C=O stretching mode at ~1685 cm^{-1}, a characteristic of cathinones not present in MA, was found in all sample spectra belonging to group 2. Similarly, the strong C-O stretching mode at ~1250 cm^{-1} indicating the presence of methylenedioxy group in the samples from group 4 was also evident.

The difference spectrum for each street sample powder was calculated by subtracting the reference standard spectrum from the corresponding street sample. These are provided in Figure 6-3. If these samples were pure, the difference spectra should be a flat line rather than showing any peaks. When these difference spectra were examined, none were found to be a flat line indicating the presence of impurities and/or contaminations. Of particular interest here, are the two different MMC samples from the street drugs cohort indicating two different illicitly made products whose disparities are visible in their unidentical difference spectra (labelled as MMC 1 and MMC 2 in Figure 6-3). This suggests that these two samples, though labelled and sold as MMC, are either likely to be from a different batch with unique adulterants or have retained different impurities from the individual illicit manufacturing processes. While it is highly likely that these street samples contain some cutting agents, it is also possible that these spectral differences are due to different salt forms of the compounds as well as impurities retained through the illicit manufacturing process. Though these differences were not investigated further in this chapter, the difference spectra were included here to illustrate the inconsistencies in the compositions of street drugs.

Difference spectra for these NPS samples calculated in serum and urine are given in Appendix 4 Figures A4-5, A4-6, A4-7 and A4-8.

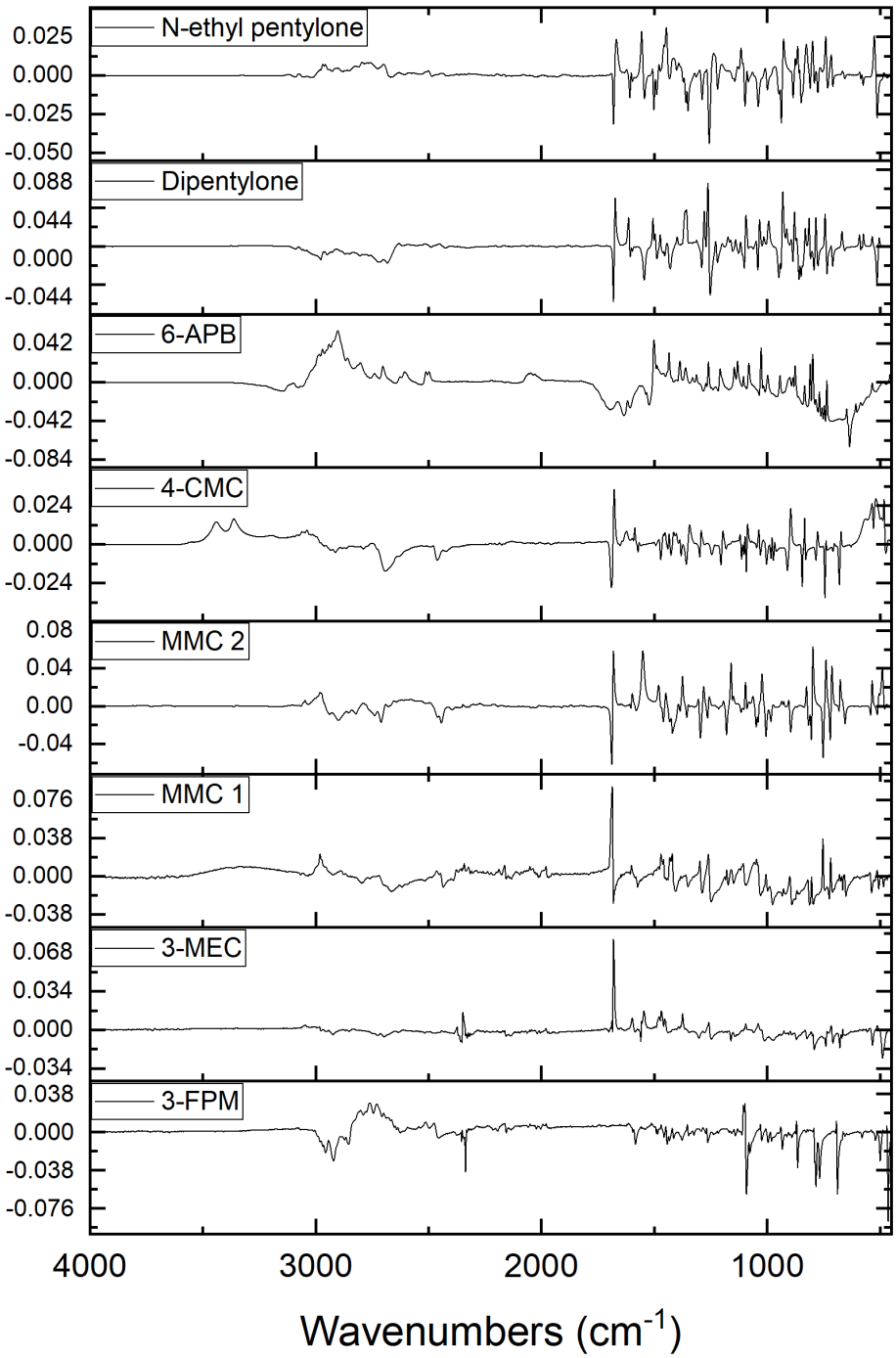

Figure 6-3: Difference spectra for the powder samples is shown. Each were calculated by the substracting the powder spectra of the respective reference standards from that of the street versions.

For the remainder of this chapter, the street NPSs are categorised into four groups based on their structural similarities for ease of analysis. These are also shown in column 5 of Table 6-1. Group 1 consisted of spectra from only 3-FPM samples as it was the only street sample with that structure. Group 2 consisted of spectra from MMC (2 samples), 4-CMC, 3-MEC and 4-MEC. Group 3 consisted of 6-APB, a benzofuran stimulant. Finally, group 4 consisted of N-ethyl pentylone and dipentylone samples.

6.3.2 PLS-DA – Binary Models

The analysis was conducted in two steps as previously shown in **Chapter 5**. The first PLS model was built using the drug-free cohort (n = 30 in serum; n = 17 in urine) and drug samples (here referred to as 'Drug; n = 76 in serum; n = 50 in urine) which included all street NPSs and MA samples (Figure 6-4). With 5-fold cross-validation, the optimum number of LVs was found to be 6 for both serum (with mean centre) and urine (without mean centre) datasets. The accuracy of the models was found to be 84.% for the serum dataset and 78.6% for the urine dataset suggesting a reasonable predictive performance, especially considering the structural diversity represented in the drug cohort. The sensitivity and specificity values for the serum dataset were 92.2% and 80% with an AUC-ROC value of 0.92. Similarly, for the urine dataset, the sensitivity and specificity values of 92.1% and 74% were obtained with an AUC-ROC of 0.91. The false positive rates were found to be high for drug-free samples at 19.2% in the serum dataset and 26% in the urine dataset suggesting that many of the drug samples were misclassified as drug-free samples. This issue was seen in other analyses presented in this thesis, where low-concentration drug samples in serum and urine were often misclassified. This is likely due to the strong absorptions from biological matrices in comparison to the low concentration of the drugs present in the samples.

Following this, the second PLS-DA model was constructed to discriminate MA samples (here referred to from that of the street NPSs. With 5-fold cross-validation, the optimum number of LVs were found to be 6 and 4 for serum (without mean centre) and urine (with mean centre) datasets respectively. This model showed excellent sensitivity and specificity values of 98.6% and 98.1% for the serum dataset and 97.7% and 92.6% for the urine dataset (Figure 6-4). The scores plots included in Figure 6-4 visually present the discrimination between the two classes with some overlap which is reflected in the sensitivity and specificity values. The AUC-ROC values of 0.99 and 0.98 for the serum and urine models respectively highlight good discriminatory capabilities.

A1

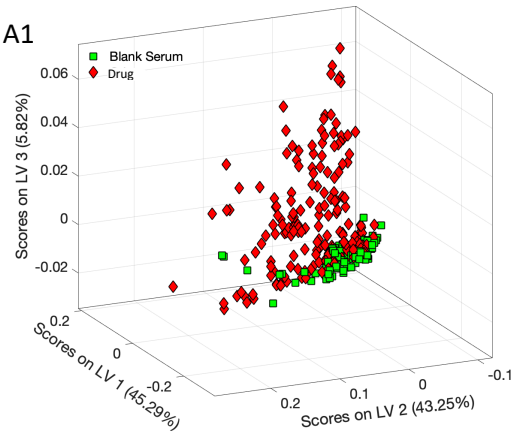

C1

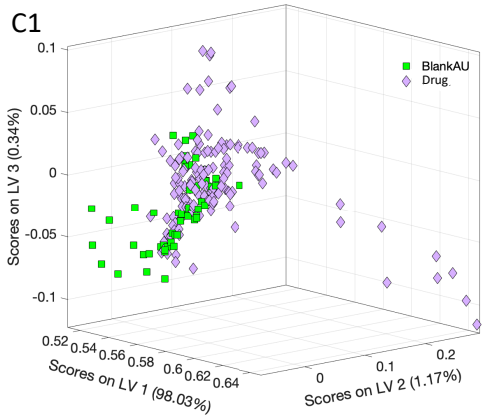

B1

BlankS v Other
AUC = 0.92

	Sens (%)	*Spec (%)*	*FPR (%)*
BlankS	92.2	80.8	19.2
Drug	80.8	92.2	7.7

D1

BlankAU v Other
AUC = 0.92

	Sens (%)	*Spec (%)*	*FPR (%)*
BlankAU	92.1	74	26
Drug	74	92.1	7.8

A2

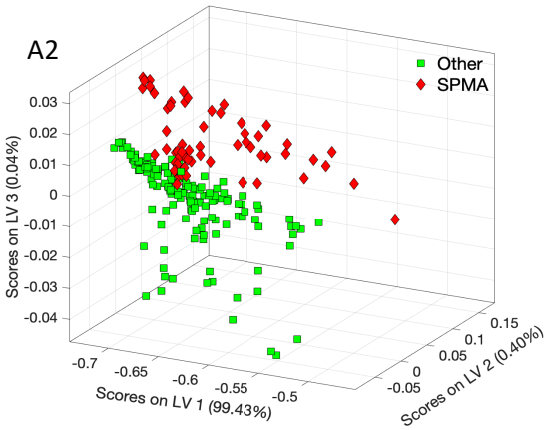

C2

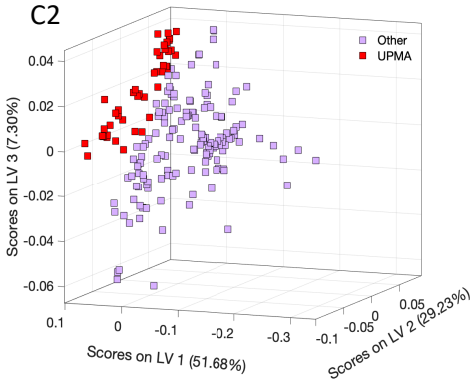

B2

SPMA v Other
AUC = 0.99

	Sens (%)	*Spec (%)*	*FPR (%)*
SPMA	98.6	98.1	1.9
Other	98.1	98.6	1.3

D2

UPMA v Other
AUC = 0.98

	Sens (%)	*Spec (%)*	*FPR (%)*
UPMA	97.7	92.6	7.3
Other	92.6	97.7	2.2

Figure 6-4: Results of the two-step binary PLS-DA model for discriminating between drug (here referred to as 'Other' and drug-free samples (here referred to as 'BlankS' for serum and 'BlankAU' for urine) are shown for serum (A1, A2, B1 and B2) and urine (C1, C2, D1 and D2) datasets. The scores plots for this classification in the serum dataset are shown in A and for the urine dataset in C. The sensitivity (here referred to as Sens) and specificity (here referred to as Spec) values as well as the AUC-ROC values for the serum dataset are shown in B and for the urine dataset in D.

The loading plots for the aforementioned two-step analysis are provided in Figure 6-5. In the models where mean centring was not applied (E2 and F1 in Figure 6-5), LV1 resembled the respective matrix. The remaining latent variables show influences from multiple functional groups belonging to different drugs included in the drug class. For instance, the two strong peaks at 748 and 700 cm $^{-1}$ reflecting the presence of MA are seen to be present in multiple latent variables. As identified in **Chapter 3**, the spectra regions of 850-700 cm^{-1} and 1225 – 950 cm^{-1} are also of significance here as they represent the aromatic ring and the types of substitutions present on the ring. RF analysis which was most useful in identifying the contributions from these two regions, was not performed here but remains a promising approach to explore in future studies.

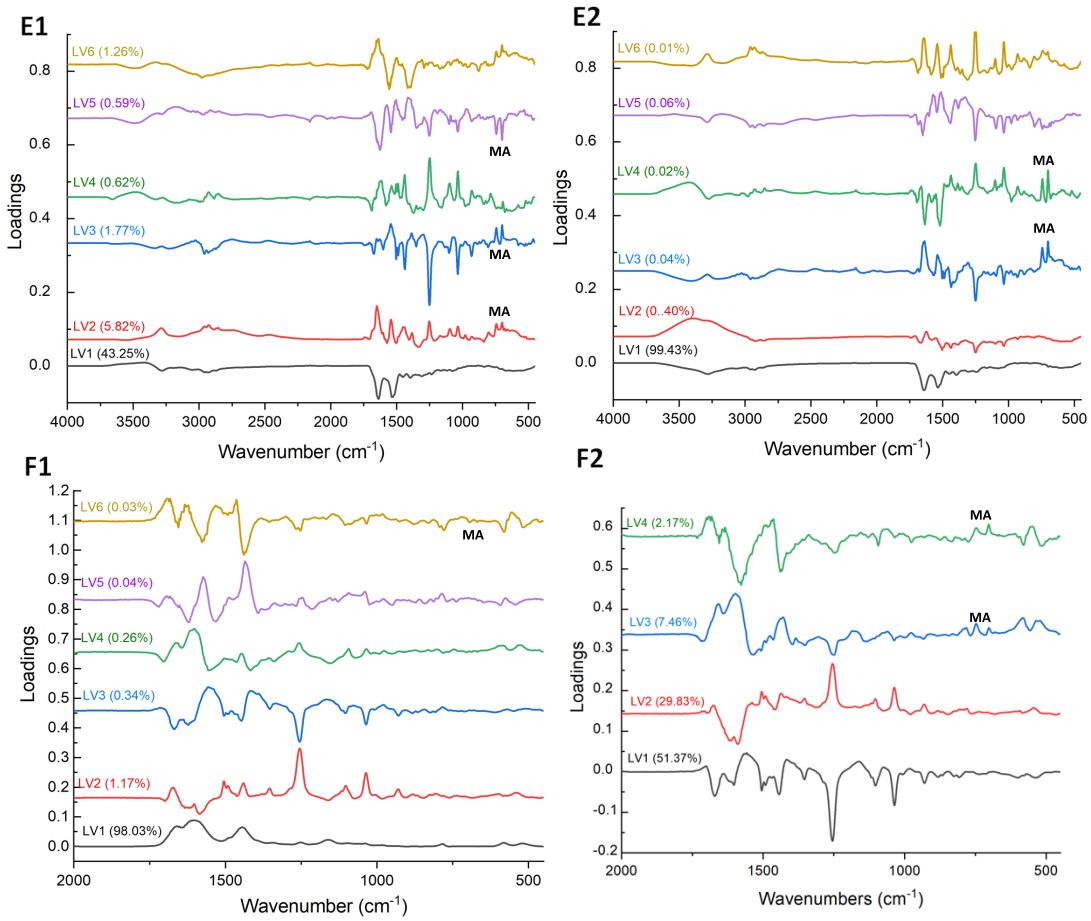

Figure 6-5: Loading plots for the two step PLS-DA classification of drug samples from drug free samples (E1 and F1) and MA from combined set of groups 1-4 (E2 and F2). Top row shows loadings from serum dataset while urine dataset is represented in the bottom row.

The sensitivities and specificities reported from this two-step analysis demonstrate the ability of this analysis to discriminate these sample classes. Interestingly, both serum and urine

datasets provided similar values of sensitivities and specificities, unlike previous chapters where the results of classification models for urine datasets were decidedly better. Whether this is likely to occur for all NPSs or a characteristic of this set of street samples, would require further research. It is also important to note here that spectral signatures of the total drug in the sample (free drug portion and bound drug portion) were used in this analysis. As information such as the protein binding abilities of NPSs is rarely available in the literature, it is not possible to account for such interactions. However, the existence of such interactions is demonstrated by the changes observed in the amide I and amide II bands of the serum in the difference spectra as well as the loading plots from this section.

While the false positive rates for MA were high in the first step, these were significantly reduced in both serum and urine datasets following the removal of drug-free samples (B2 and D2, Figure 6-4). This indicates that these are likely related to the difficulty in the classification of lower-concentration samples.

It is also prudent to note that these models were built using imbalanced classes and their performances were not validated using an independent set of biological samples containing these drugs. While powder drugs were obtained from DSTL without much hassle, obtaining real patient samples containing such drugs is more difficult due to legal and ethical considerations. This means that the CV results presented here could likely be overly optimistic in their sensitivity and specificity values. However, permutation tests conducted for both models highlighted indicated the statistical significance of these models at a 95% confidence level. Therefore, further analysis using a more representative dataset with greater sample numbers and concentration range would provide a more robust model.

6.3.3 PLS-DA – Binary Models for Individual NPS Groups

Following the preliminary classification of MA samples from all NPSs, a set of 4 more specific classifications between MA and each group of NPSs. The results of these cross-validated PLS-DA models are presented in Figure 6.6 for serum (A1 to A4) and urine (B1 to B4). The optimum number of LVs was determined to be 4, 5, 4 and 5 classification of MA against groups 1, 2, 3 and 4 respectively, for both datasets. All binary classification models presented in Figure 6-6 show excellent sensitivities and specificities for both datasets. A sensitivity of 100% was seen when discriminating MA against groups 1 and 2 in serum and groups 2 and 3 in urine, while the remaining sensitivity values were above 96%. This is especially significant

A1 SPMA v Group 1

	Sens (%)	Spec (%)	FPR (%)
SPMA	100	100	0
Group 1	100	100	0

B1 UPMA v Group 1

	Sens (%)	Spec (%)	FPR (%)
UPMA	97.7	100	0
Group 1	100	97.7	2.2

A2 SPMA v Group 2

	Sens (%)	Spec (%)	FPR (%)
SPMA	100	98.7	1.2
Group 2	98.7	100	0

B2 UPMA v Group 2

	Sens (%)	Spec (%)	FPR (%)
UPMA	100	97.2	2.7
Group 2	97.2	100	0

A3 SPMA v Group 3

	Sens (%)	Spec (%)	FPR (%)
SPMA	96	96.7	3.3
Group 3	96.7	96	4

B3 UPMA v Group 3

	Sens (%)	Spec (%)	FPR (%)
UPMA	100	96.7	3.3
Group 3	96.7	100	0

A4 SPMA v Group 4

	Sens (%)	Spec (%)	FPR (%)
SPMA	96	100	0
Group 4	100	96	4

B4 UPMA v Group 4

	Sens (%)	Spec (%)	FPR (%)
UPMA	95.5	95.4	4.5
Group 4	95.4	95.5	4.5

Figure 6-6: Results of four sets of PLS-DA models for discrimination of MA from each group of the NPSs in serum (A1 – A4) and urine (B1 – B4) datasets. The sensitivity (here referred to as Sens) and specificity (here referred to as Spec) values. FPR refers to false positive rates.

for the discrimination of MA from group 2 samples as these molecules are structurally most similar to MA and AM differing only by the presence of a carbonyl group at the β-position of the side chain. The false positive rates were found to be under 5% in all models suggesting reasonable discrimination of MA samples in these datasets.

The scores and loading plots for this classification are provided in Appendix 4 Figures A4-9 to A4-12. LV1 was influenced by the mean spectrum of the respective matrix as the data was

not mean-centred. The remaining loading plots in each of the classifications show influences from the drugs included in the group. For instance, loading plots of LV3 and LV4 in the classification of MA from group 4 samples in serum display significant influence from the ~1246 cm^{-1} peak characteristic of the methylenedioxy group (Appendix 4, Figure A4-12). Additionally, differences in the aromatic rings from MA and 3-FPM are also reflected in these loading plots.

The better performance of these models with MA samples and a single NPS group in comparison with all NPSs grouped suggests that it is beneficial to utilise the structural similarities to achieve better discrimination and class assignments in a real sample dataset when a certain type of NPS is suspected. Though these models, as previously noted, were not evaluated using independent samples and could be presenting overly optimistic results, the permutation tests conducted here highlight their statistical significance.

6.3.4 Multiclass Models

With the excellent performance of the binary models presented in the previous section, multi-class PLS-DA models were constructed so that MA can be distinguished from drug-free samples as well as samples containing NPSs in a single step. The results of the cross-validated PLS-DA model are included in Figure 6-7 along with the scores plot for LVs 1, 2 and 3. The optimum number of latent variables was determined to be 5 for both serum and urine datasets. The loadings for these are provided in Appendix 4, Figure A4-13.

The sensitivity values of 63. 5%, 63. 5% and 71.7% for drug-free, MA and Street NPS samples respectively in the serum dataset were much lower than those observed in the binary models Figure 6-7). This was also observed for the urine dataset with the lowest sensitivity value of 46% for the drug-free class. The drug-free class was also found to have a higher false positive rate in comparison to MA and street NPS classes in both serum and urine datasets. When the misclassified samples were closely examined, it was observed that they stemmed from the lower-concentration samples being misclassified as drug-free samples. Additionally, the higher AUC-ROC values of 0.95 and 0.94 in the serum dataset and 0.98 and 0.80 in the urine dataset for MA and street NPS suggest an excellent ability of the model to classify these two classes.

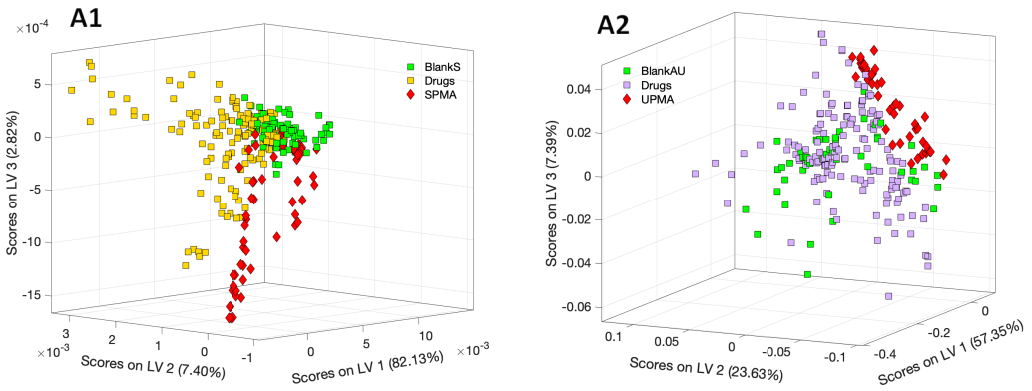

B1 **Blank v SPMA v Street NPS**

	Sens (%)	*Spec (%)*	*FPR (%)*	*AUC*
Blank	63.5	93.8	28.5	0.826
SPMA	63.5	93.8	6.1	0.954
Street NPS	71.4	92.0	7.9	0.944

B2 **Blank v UPMA v Street NPS**

	Sens (%)	*Spec (%)*	*FPR (%)*	*AUC*
Blank	46	86.5	13.4	0.749
UPMA	93.1	71.5	8.5	0.982
Street NPS	75.3	86.6	25	0.804

Figure 6-7: Results of multiclass PLS-DA models for discriminating between MA (here referred to as 'SPMA' for serum and 'UPMA' for urine), combined class of all NPS groups (here referred to as 'Street NPS') and drug-free samples (here referred to as 'BlankS' for serum and 'BlankAU' for urine) are shown for serum (A1 and B1) and urine (A2 and B2) datasets. The scores plots for this classification are shown in A and results are given in B. The sensitivity (here referred to as Sens) and specificity (here referred to as Spec) values as well as the AUC-ROC values for both datasets are shown.

In order to make this analysis more applicable to field deployment, the 5-class PLS-DA model was constructed for the classification of MA and all groups of NPSs in one single step. The PLS model with 5-fold cross-validation and 5 latent variables, provided promising results for a model involving such diverse classes. The scores plots and the results of these models are presented in Figure 6-8. For the MA samples, the sensitivities and specificities of 84% and 98.7% for the serum dataset and 97.7% and 94.6% for the urine dataset were observed. Conversely, the lowest sensitivity values of 60% were observed for group 3. However, the specificity values for group 3 were found to be very good (98.1% and 100% for serum and urine datasets respectively). This highlights a previous point regarding the difficulties encountered in this thesis when classifying samples with lower concentrations. However, the significant differences in the structures of MA and group 3 compounds are reflective of the high specificity values obtained here.

The loading plots for all the latent variables selected in these models are given in Appendix 4, Figure A4-14. The optimum number of LVs was determined to be 6 for both datasets and LV1 was a mean spectrum resembling the respective biofluids. The contributions from groups 1 and 2 to the loading plots were evident due to the distinctive peaks present in the sample spectra. Conversely, the low sensitivities identified for group 3 are also likely explained by the lack of strong, distinctive peaks that stand out above the matrix background.

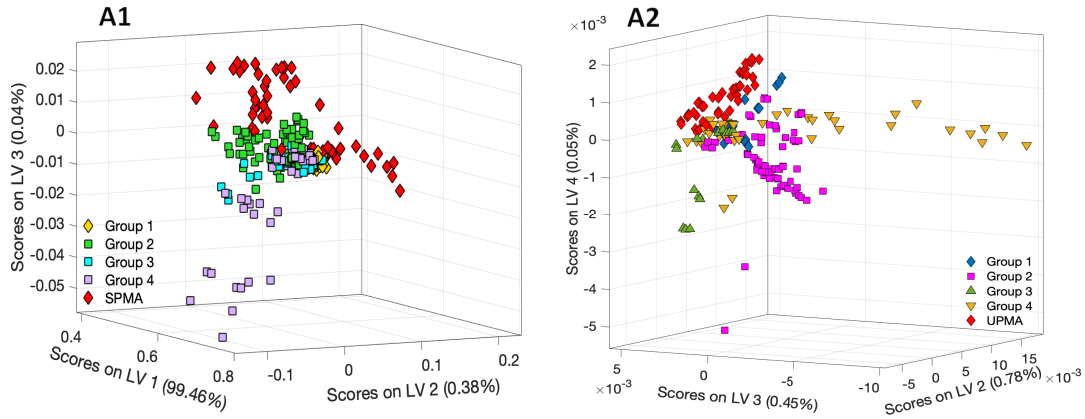

B1	*Sens (%)*	*Spec (%)*	*FPR (%)*
Group 1	100	95.7	4.2
Group 2	83.5	88.6	11.3
Group 3	60	98.1	1.8
Group 4	66.7	92.3	7.6
SPMA	84	98.7	1.2

B2	*Sens (%)*	*Spec (%)*	*FPR (%)*
Group 1	80	91.1	8.9
Group 2	82.7	95.7	4.2
Group 3	60	100	0
Group 4	71.1	95.3	4.6
UPMA	97.7	94.6	5.3

Figure 6-8: Results of 5 class PLS-DA models for classification of MA (here referred to as 'SPMA' for serum and 'UPMA' for urine), group 1, group 2, group 3 and group 4 of street NPS samples are shown for serum (A1 and B1) and urine (A2 and B2) datasets. The scores plots for this classification are shown in A and results are given in B. The sensitivity (here referred to as Sens) and specificity (here referred to as Spec) values as well as the false positive rates are shown.

These multiclass models were able to demonstrate that the discrimination of MA can be done in a single-step analysis of both biofluids using ATR-FTIR spectroscopy. However, it is prudent to note that these models were not evaluated using independent test sets or real patient samples containing NPSs. Furthermore, groups 1 and 3 consisted only of one street

compound making the sample size much smaller and less representative than the other groups of samples included here. Another important point to note here is that the drug-matrix interactions were not investigated here and the spectral contributions from the total drug portions were included in the classification process. While it is inevitable in terms of NPSs as such data is rarely available for them, further studies exploring this could lead to better classification.

6.4 Conclusion

With the increasing use of NPSs globally, the need for good screening methods has increased for legal as well as public health reasons. The standard toxicological screening performed using immunoassays is inadequate for testing NPSs in biological fluids due to unpredictable cross-reactivities and variable results due to disparities in substances, concentrations and manufacturers. This chapter presented an alternative method for screening NPSs, more specifically synthetic cathinones, in biological fluids, with the use of ATR-FTIR spectroscopy.

The drugs obtained from the DSTL laboratory consisted of a range of drug compounds from the synthetic stimulant NPS class. As synthetic stimulants are the most common legal alternatives to MA to achieve the same physiological effects, the range included in this study was a good representative of real-world situations.

Using a two-step analysis consisting of binary PLS-DA classification models with Venetian blinds cross-validation, first, drug-free samples were distinguished from all drug samples with sensitivity and specificity values of ~92% and ~80% in two biofluids. Following this, discrimination of MA from all street NPSs was achieved with sensitivity and specificity values of ~98 and ~97%. This model performance was supported by high AUC-ROC values of >0.92 in both serum and urine datasets. This two-step analysis protocol was successful in discriminating MA samples and achieving one of the primary aims of this chapter.

The multiclass models were constructed here to demonstrate the applicability of this method as a one-step screening method to be able to distinguish MA from a range of samples including drug-free samples. The results of the cross-validated three-class PLS-DA model were promising in terms of specificity values but provided much lower sensitivities than the binary models. This was also reflected in the high false positives obtained for the drug-free class indicating that lower concentration samples were often misclassified by the models

presented here. This was also supported by the relatively low AUC-ROC values obtained for the drug-free class in both datasets.

Finally, expanding the multivariate analysis even more, two 5-class PLD-DA models were built to distinguish individual groups of drugs present in this study for serum and urine datasets. With sensitivities and specificities of 84% and 98% in the serum dataset and 97% and 94% in the urine dataset for MA samples, this application of ATR-FTIR spectroscopy was shown to be successful in achieving the original aims. However, there are important considerations to note which are mentioned throughout this study. The sample set employed here was unbalanced and limited in number and the variety of drug compounds represented in each of the groups. The use of an independent test set with real patient samples would be invaluable in testing the efficacy and applicability of this analysis to a real-world scenario. Moreover, the impacts of the interactions between drugs and the matrix on the spectral signatures were observed but not investigated here. It would be beneficial to explore these in order to delineate the specific spectral features of specific drug compounds. Constructing such a database would allow this method to be more accurate in its discrimination and more versatile in its application.

6.5 References

1. Early Warning Advisory and United Nations Office of Drugs and Crime, *Current Nps Threats Volume V*, United Nations Office of Drugs and Crime, Vienna, Austria, 2022.

2. United Nations Office of Drugs and Crime, *The Challenge of Nps Global Smart Programme: A Report from Global Smart Programme*, United Nations Office of Drugs and Crime, Vienna, Austria, 2013.

3. S. Beharry and S. Gibbons, *Forensic Science International*, 2016, **267**, 25-34.

4. J. B. Zawilska and J. Wojcieszak, *Forensic Science International*, 2013, **231**, 42-53.

5. M. Protti, in *Critical Issues in Alcohol and Drugs of Abuse Testing*, ed. A. Dasgupta, Academic Press, London, 2nd edn., 2019, ch. 21, pp. 259-271.

6. P. Reuter and B. Pardo, *Addiction*, 2016, **112**, 25-31.

7. A. Namera, M. Kawamura, A. Nakamoto, T. Saito and M. Nagao, *Forensic Toxicology*, 2015, **33**, 175-194.

8. B. K. Logan, A. L. A. Mohr, M. Friscia, A. J. Krotulski, D. M. Papsun, S. L. Kacinko, J. D. Ropero-Miller and M. A. Huestis, *Journal of Analytical Toxicology*, 2017, **41**, 573-610.

9. M. Evans-Brown and R. Sedefov, in *New Psychoactive Substances : Pharmacology, Clinical, Forensic and Analytical Toxicology*, eds. H. H. Maurer and S. D. Brandt, Springer International Publishing, Cham, 2018, pp. 3-49.

10. J. R. H. Archer, in *Novel Psychoactive Substances (Second Edition)*, eds. P. Dargan and D. Wood, Academic Press, Boston, 2022, pp. 131-156.

11. M. Baron, M. Elie and L. Elie, *Drug Testing and Analysis*, 2011, **3**, 576-581.

12. M. M. Schmidt, A. Sharma, F. Schifano and C. Feinmann, *Forensic Science International*, 2011, **206**, 92-97.

13. S. D. Brandt, H. R. Sumnall, F. Measham and J. Cole, *Drug Testing and Analysis*, 2010, **2**, 377-382.

14. A. M. Araújo, M. J. Valente, M. Carvalho, D. Dias da Silva, H. Gaspar, F. Carvalho, M. de Lourdes Bastos and P. Guedes de Pinho, *Archives of Toxicology*, 2015, **89**, 757-771.

15. J. M. Prosser and L. S. Nelson, *Journal of Medical Toxicology*, 2012, **8**, 33-42.

16. K. N. Ellefsen, S. Anizan, M. S. Castaneto, N. A. Desrosiers, T. M. Martin, K. L. Klette and M. A. Huestis, *Drug Testing and Analysis*, 2014, **6**, 728-738.

17. R. A. S. Couto, L. M. Gonçalves, F. Carvalho, J. A. Rodrigues, C. M. P. Rodrigues and M. B. Quinaz, *Critical Reviews in Analytical Chemistry*, 2018, **48**, 372-390.

18. M. Kraemer, A. Boehmer, B. Madea and A. Maas, *Forensic Science International*, 2019, **298**, 186-267.

19. P. Adamowicz, *Clinical Toxicology*, 2021, **59**, 648-654.

20. D. Baumeister, L. M. Tojo and D. K. Tracy, *Therapeutic Advances in Psychopharmacology*, 2015, **5**, 97-132.

21. L. Wagmann and H. H. Maurer, in *New Psychoactive Substances : Pharmacology, Clinical, Forensic and Analytical Toxicology*, eds. H. H. Maurer and S. D. Brandt, Springer International Publishing, Cham, 2018, pp. 413-439.

22. J. B. Zawilska and J. Wojcieszak, in *Synthetic Cathinones: Novel Addictive and Stimulatory Psychoactive Substances*, ed. J. B. Zawilska, Springer International Publishing, Cham, 2018, pp. 11-24.

23. C. L. German, A. E. Fleckenstein and G. R. Hanson, *Life Sciences*, 2014, **97**, 2-8.

24. Early Warning Advisory and United Nations Office of Drugs and Crime, *Large Seizures of Synthetic Cathinones in Europe Reflect Their Growing Importance on the Illicit Stimulants Market*, United Nations Office of Drugs and Crime, Vienna, Austria, 2022.

25. S. Odoardi, F. S. Romolo and S. Strano-Rossi, *Forensic Science International*, 2016, **265**, 116-120.

26. K. Layne, P. I. Dargan and D. M. Wood, in *Novel Psychoactive Substances*, eds. P. Dargan and D. Wood, Academic Press, Boston, 2nd edn., 2022, ch. 13, pp. 333-380.

27. F. Measham, K. Moore, R. Newcombe and Z. Zoë, *Drugs and Alcohol Today*, 2010, **10**, 14-21.

28. J. L. Gonçalves, V. L. Alves, J. Aguiar, H. M. Teixeira and J. S. Câmara, *Critical Reviews in Toxicology*, 2019, **49**, 549-566.

29. P. Adamowicz, J. Gieroń, D. Gil, W. Lechowicz, A. Skulska and B. Tokarczyk, *Drug Testing and Analysis*, 2016, **8**, 63-70.

30. S. Elliott and J. Evans, *Forensic Science International*, 2014, **243**, 55-60.

31. A. Maas, C. Wippich, B. Madea and C. Hess, *International Journal of Legal Medicine*, 2015, **129**, 997-1003.

32. S. L. Thornton, J. Lo, R. F. Clark, A. H. B. Wu and R. R. Gerona, *Clinical Toxicology*, 2012, **50**, 1165-1168.

33. E. Tomczak, M. K. Woźniak, M. Kata, M. Wiergowski, B. Szpiech and M. Biziuk, *Forensic Toxicology*, 2018, **36**, 476-485.

34. M. Wiergowski, J. Aszyk, M. Kaliszan, K. Wilczewska, J. S. Anand, A. Kot-Wasik and Z. Jankowski, *Journal of Chromatography B*, 2017, **1041-1042**, 1-10.

35. M. K. Woźniak, L. Banaszkiewicz, M. Wiergowski, E. Tomczak, M. Kata, B. Szpiech, J. Namieśnik and M. Biziuk, *Forensic Toxicology*, 2020, **38**, 42-58.

36. M. Zawadzki, K. Nowak and P. Szpot, *Forensic Toxicology*, 2020, **38**, 255-263.

37. C. f. D. C. a. Prevention, *Mobility Mortality Weekly Report*, 2011, **60**, 624-627.

38. S. Davies, D. M. Wood, G. Smith, J. Button, J. Ramsey, R. Archer, D. W. Holt and P. I. Dargan, *QJM: An International Journal of Medicine*, 2010, **103**, 489-493.

39. A. J. Dickson, S. P. Vorce, B. Levine and M. R. Past, *Journal of Analytical Toxicology*, 2010, **34**, 162-168.

40. R. Abbott and D. E. Smith, *Journal of Psychoactive Drugs*, 2015, **47**, 368-371.

41. F. Schifano, J. Corkery and A. H. Ghodse, *Journal of Clinical Psychopharmacology*, 2012, **32**, 710-714.

42. D. Favretto, J. P. Pascali and F. Tagliaro, *Journal of Chromatography A*, 2013, **1287**, 84-95.

43. M. Coppola and R. Mondola, *Toxicology Letters*, 2012, **211**, 144-149.

44. K. Kesha, C. L. Boggs, M. G. Ripple, C. H. Allan, B. Levine, R. Jufer-Phipps, S. Doyon, P. Chi and D. R. Fowler, *Journal of Forensic Sciences*, 2013, **58**, 1654-1659.

45. A. M. Macher and T. M. Penders, *Drug Testing and Analysis*, 2013, **5**, 130-132.

46. M. Coppola and R. Mondola, *Toxicology Letters*, 2012, **208**, 12-15.

47. K. N. Ellefsen, S. Anizan, M. S. Castaneto, N. A. Desrosiers, T. M. Martin, K. L. Klette and M. A. Huestis, *Drug Test Anal*, 2014, **6**, 728-738.

48. M. J. Swortwood, W. L. Hearn and A. P. DeCaprio, *Drug Testing and Analysis*, 2014, **6**, 716-727.

49. C. Yates and P. M. Kabata, in *Novel Psychoactive Substances*, eds. P. Dargan and D. Wood, Academic Press, Boston, 2nd edn., 2022, ch. 7, pp. 181-202.

50. K. E. Grafinger, M. E. Liechti and E. Liakoni, *British Journal of Clinical Pharmacology*, 2020, **86**, 429-436.

51. E. Liakoni, C. Yates, A. M. Dines, P. I. Dargan, F. Heyerdahl, K. E. Hovda, D. M. Wood, F. Eyer, M. E. Liechti and D. E. N. P. R. G. Euro, *Medicine*, 2018, **97**, e9784-e9793.

CHAPTER SEVEN

CONCLUSIONS

Global drug markets and patterns of use are becoming increasingly complex with the emergence of new drugs and the prevalence of poly-drug habits that include both licit and illicit drugs. However, the constantly changing landscape of drug markets creates numerous challenges in monitoring and regulating drug compounds to reduce public harm. Hence, drug detection is of great importance as it lies at the heart of all drug-related social, economic and legal issues.

Attenuated total reflectance – Fourier transform infrared spectroscopy has shown great promise in detecting seized drug samples and in biofluid spectroscopy mainly owing to quick, versatile and nondestructive analysis, minimal sample volumes required and simple instrumentation. Its wider application and acceptance in the forensic analytical field have been heightened by the commercial availability of portable instrumentations. However, a combined application for the detection of drugs in biological fluids using this technique needs further research. With this in mind, this thesis conducted a proof-of-concept study for the direct detection and quantification of drugs in biological samples. An important and distinctive aspect of the method presented throughout this thesis was the lack of tedious sample extraction and preparation methods. This was directly influenced by the constant struggle to keep up with the testing of newly emerging unknown drugs efficiently and cost-effectively. Therefore, the preliminary study was expanded to include cutting agents and NPSs common in the illicit drug markets, as well as prescription drugs erroneously screened as controlled substances. Through this, this thesis demonstrated the adaptability of the method presented here and presented a potential solution for the analytical challenges encountered in the detection of drugs in biofluids in clinical and forensic drug analysis.

In **Chapter 3**, MA is used as a target molecule to present a proof-of-concept study in detecting MA and its metabolites in serum and urine without prior sample extraction. Despite the strong absorption of biofluids, the successful detection of MA and its metabolites in clinically and forensically relevant concentrations was demonstrated with the help of chemometric multivariate analysis. Multivariate analyses presented in this chapter were able to distinguish MA samples in serum and urine at sensitivity and specificity values of ~91% in serum and ~95% in urine matrices. Additionally, the high discriminatory power of this analysis was demonstrated by distinguishing MA from its major metabolite AM, a psychoactive drug on its own, with sensitivity and specificity values of 96.1% and 93.2% in serum and 86.2% and 88.2% in urine respectively. A preliminary regression analysis was presented for the

quantification of MA and its metabolites with a detection limit of ~0.1 and ~0.3 mg/mL in serum and urine respectively.

With the increasing consumption of illicit drugs which are rarely pure, the applicability of the method was successfully demonstrated for discriminating adulterated MA samples in **Chapter 4**. MSM, paracetamol and sugar were the cutting agents included in this analysis as they are similar to MA in physical appearance as well as are commonly found in illicitly manufactured MA. Using two methods of classification, PLS-DA and RF analysis, the multivariate analysis was successful in discriminating pure MA samples from adulterated MA samples in biological fluids. The sensitivity and specificity values of ~95-100% were obtained for this classification using PLS-DA analyses, though RF analysis performed better with 100% sensitivities and specificities. Quantification attempted to determine the amount of MA in adulterated samples using PLS regression models demonstrated strong linearities (R^2 = 0.95). These results highlight the promising future for this method in clinical situations for instance when quick analysis of body fluids is necessary following ingestion of unknown substances for effective patient management.

Chapter 5 demonstrated the capability of ATR-FTIR spectroscopy as an alternative to urine immunoassays which are routinely performed for the screening of MA in clinical and forensic situations. Six drugs including bupropion, labetalol, ofloxacin, promethazine, metformin and trazodone commonly known to give false positive results on an MA immunoassay were investigated in this chapter. The binary and multiclass PLS models performed exceptionally well in discriminating MA samples from these prescription drugs. For the urine dataset, the sensitivities and specificities obtained from these analyses were in the range of 95-100% and the false positive rates obtained for misclassifying other samples as MA remained under 5% which are at least comparable to those reported in the literature making this method a strong alternative to the current IA-based methods.

Following the theme of detecting imitators, this method was used to distinguish between traditional stimulants such as MA and NPS stimulants such as synthetic cathinones in **Chapter 6**. Successful analysis was conducted on real street samples provided by DSTL, UK and showed promising results suggesting the abundant potential of this method. The sensitivity and specificity values of ~94% - 98% were reported in serum and urine datasets for

distinguishing MA from its NPS analogues. This has huge implications in both forensic and clinical applications where current screening methods are unable to detect these differences.

Chapter 3 was also important in the development of the experimental protocol followed throughout this thesis. While there was previous work available in the research group to guide the basic protocol of biofluid spectroscopy, this was mainly developed for the detection of cancer biomarkers. The adaptation of this protocol for the detection of drugs presented a few different challenges. For instance, preliminary work was conducted to determine that dissolving the drug powders directly into the biofluids provided the best results. This also reduced the amount of biofluids and drug powders needed throughout this thesis. The drying protocol was kept simple by design to allow future operations by non-experts. Based on the previous work in the research group, sample amounts and drying times for serum were known. Such analysis on urine samples had not been conducted previously. For analysis of urine samples, the sample volume had to be reduced so that the sample remained on the crystal surface upon drying. Much more variability was observed in the drying of urine samples than in the serum samples. This was mainly observed in the higher wavenumber end of the spectrum and led to that section being excluded from the analyses presented here.

Therefore, during the method development phase of this work, some limitations of this method became apparent. While almost all drugs chosen in this study were adequately soluble in water, the application of this method to investigate drug compounds insoluble in water would not be possible by the protocol devised here. The air-drying employed here was found to be dependent on temperature and humidity in the lab and can get very time-consuming. The analyses presented here consisted of small and in some cases, imbalanced datasets. Therefore it is necessary to evaluate these performance statistics with a larger dataset and real-world samples. Furthermore, the complex spectral signatures of the biological matrices tend to increase the limits of detection and are the limiting factor for the widespread application of this method. However, the research presented here was overall successful in addressing the aims and objectives set out and provides a promising future for using the existing FTIR instrumentations in most laboratories for developing a simple, rapid and highly adaptable drug screening test for biofluids.

CHAPTER EIGHT

FUTURE WORK

Drug detection is a complex and dynamic field not only in terms of the analytes that are targeted but also the technologies that are utilised and developed. The use of ATR-FTIR instruments for characterising unknown substances is well known in many fields including forensic chemistry for analysing powders as previously stated in **Chapter 1**. The intrinsic benefits of this technique including simple operation and instrumentation, minimal sample volumes and direct analysis make it applicable in a variety of situations. Availing of all these benefits, this thesis has demonstrated the significant potential of ATR-FTIR spectroscopy for the detection of drugs in biological fluids without the need for extensive sample extraction and preparation steps.

It is important to note that the method presented here is a proof-of-concept study and comprehensive analytical method validation is necessary prior to practical field deployment. The experimental protocol described here would need a thorough validation to investigate the effects of specific parameters and to optimise them. This is significant to preserve the integrity of the samples by optimising sample collection and storage protocols for the analysis of simulated and real-world samples. Another crucial factor to consider here is the effects of sample drying. The drying protocol followed in this study was kept simple by design to minimise the need for complex procedures and make it easy to follow by a non-expert. However, variables such as temperature and humidity etc. were observed to impact drying times during experiments. This along with the heterogeneous deposition of samples during the drying process and its impacts in this context need to be evaluated for reliable application. There are extensive studies that investigate such pre-clinical factors for biofluid spectroscopy in clinical diagnostics.[1-5] With the help of this knowledge base, it would be highly beneficial to conduct such pre-clinical investigations to ensure experimental reproducibility across instruments and laboratories for its practical application. As more data is collected, it is important to optimise and validate the data processing protocols presented here for widespread application. The multivariate models built here will require continuous maintenance throughout data collection for their reliable application. Therefore, organising a dynamic and comprehensive reference library and developing automation for library matching would be beneficial for the efficient detection and identification of newly emerging drugs in the field.

One time-consuming factor identified here was the drying of samples on the one ATR crystal which needed to be analysed and cleaned before the next sample. Sample multiplexing

where multiple samples are analysed sequentially on the same ATR crystal would be highly beneficial in reducing the analysis time and mitigating the potential for sample contamination. This has been demonstrated in the literature for other applications such as detecting COVID-positive sera using ATR-FTIR spectroscopy coupled with chemometrics. Investigating the application of such protocol to prepare drug samples would be a valuable next step to investigate for a high throughput analysis.[6] Other than the aforementioned methodological opportunities, the work presented in this thesis can be expanded in numerous avenues in chemistry, pharmacology, and clinical and forensic scenarios. Some recommendations for future directions are presented below.

Chapter 3 evaluated the presence of MA along with 4 of its metabolites in two biological matrices – urine and serum. Though this proof-of-concept study targeted MA, the method and the instrument are infinitely adaptable to any drug compounds, their metabolites and any adulterants. It is important to note here that all drug compounds included in this thesis displayed adequate solubility in aqueous media such as serum and urine. While this is not an issue when analysing real-world samples, it would be prudent to investigate and devise a protocol for drugs that are insoluble in aqueous media for conducting preliminary reference studies. Due to the adaptability of this method, it can also be applied to other NPSs than those covered in **Chapter 6.** Furthermore, it is widely recognised that testing only the parent compounds is not enough to understand the complete picture in clinical and forensic toxicology.[7-10] Similarly, as explored in **Chapter 5**, metabolites of prescription drugs can be responsible for false positives on drug screens. For instance, synthetic cannabinoids are one such drug group that are commonly insoluble in aqueous media and are extensively metabolised in the body. Therefore, expanding the application of this method to other relevant drugs as well as their metabolites could provide valuable information allowing for this method to be an efficient drug screening procedure for early warning as well as routine toxicological testing.

MA and other illicit drugs are rarely ever consumed in their pure form. **Chapter 4** of this thesis explored three of the common adulterants found in illicit MA samples. In some instances, the compounds besides the drug itself are responsible for the adverse reactions. However, the common drug panels utilised in either clinical or forensic settings rarely include these adulterants. In addition, even when such impurity is known or detected, only the percentage of relevant drug compounds is often reported. This method allows for the

detection of the drug and the adulterants in one test reducing the number of extra tests required. Therefore, the application of this method to detect other adulterants would be valuable for reducing harm and producing forensic intelligence.

Both clinical and forensic situations involve the analysis of various biofluids to investigate the presence of drugs. The work presented here in **Chapters 3** to **6** was focused on human pooled serum and urine. However, there is scope for expanding this work to other relevant biofluids for example oral fluid and sweat. Oral fluid is easy to collect and thus would be valuable in a roadside testing situation. Other methods tend to be weary of sweat samples for drug detection as this biofluid is difficult to collect in enough quantities or they are often collected on paper patches requiring extraction procedures. However, the ATR sampling method employed here only required volumes in the range of 0.5 – 3 μL and can also analyse papers and films. Therefore, it would be valuable to investigate the application of this method to sweat samples for the detection of drugs in either collection medium.

In pharmacology, the protein binding ability of a drug compound is one of its essential characteristics as it determines the amount of compound that is available for therapeutic activity. Therefore, when detecting these compounds in biofluids, in particular blood products, it is necessary to know if the whole drug amount is being detected or if only the free drug compound is of interest. With the use of protein precipitation as a quick additional sample clean-up step, the method developed here would allow for isolating the free drug amount (in the supernatant) from the protein-bound (in the pellet) portion in the sample. The supernatant carrying the free-drug component could also allow for assessing the psychoactivity of new compounds as it would be the actual amount of the compound available for the psychoactive effect. Furthermore, by investigating the protein-bound component in the pellet, it might be possible to estimate the concentration of the drugs that are therapeutically relevant even when the free drug portion might have already been metabolised. This would be particularly of use when analysing fast-metabolising drugs such as synthetic cannabinoids or characterising novel compounds with unknown pharmacokinetics. Application of protein precipitation prior to FTIR analysis would allow for lowering the detection limits presented in this work as the strong IR absorbances from large proteins are removed from the spectrum making this method applicable to potent drugs that are often found in low concentrations in biofluids.

Another avenue for expanding this work is in the analysis of post-mortem biofluids. All work presented in this thesis uses antemortem biological samples. However, the human body undergoes numerous changes upon death which can alter the composition of biological fluids. Therefore, more research is needed in post-mortem toxicology to understand not only the composition of biofluids following death but also the interaction between the biofluid and the exogenous compounds. To conserve the limited resources usually available to forensic toxicology laboratories, it would be beneficial to expand the application of this method in post-mortem toxicology to test for unusual compounds as well as investigate the biofluids themselves.

Finally, all experiments presented in this thesis have been spiking studies where drug compounds are spiked into the biofluids. However, it would be interesting to apply this method to samples generated by drug metabolism simulation studies using liver hepatocytes. These samples represent the closest analogues to real toxicology samples. Therefore, the application of this method to such a dataset would allow for evaluating the applicability and efficacy of this method in a real situation.

In conclusion, future projects could include the expansion of this drug detection study in pharmacology, toxicology, clinical and forensic settings in the hope of making it a widespread drug screening tool.

8.1 References

1. J. M. Cameron, H. J. Butler, D. J. Anderson, L. Christie, L. Confield, K. E. Spalding, D. Finlayson, S. Murray, Z. Panni, C. Rinaldi, A. Sala, A. G. Theakstone and M. J. Baker, *Vibrational Spectroscopy*, 2020, **109**, 103092.

2. L. Lovergne, P. Bouzy, V. Untereiner, R. Garnotel, M. J. Baker, G. Thiéfin and G. D. Sockalingum, *Faraday Discussions*, 2016, **187**, 521-537.

3. L. Lovergne, G. Clemens, V. Untereiner, R. A. Lukaszweski, G. D. Sockalingum and M. J. Baker, *Analytical Methods*, 2015, **7**, 7140-7149.

4. L. Lovergne, J. Lovergne, P. Bouzy, V. Untereiner, M. Offroy, R. Garnotel, G. Thiéfin, M. J. Baker and G. D. Sockalingum, *Journal of Biophotonics*, 2019, **12**, e201900177.

5. H. J. Butler, P. M. Brennan, J. M. Cameron, D. Finlayson, M. G. Hegarty, M. D. Jenkinson, D. S. Palmer, B. R. Smith and M. J. Baker, *Nature Communications*, 2019, **10**, 4501.

6. C. C. S. Bandeira, K. C. R. Madureira, M. B. Rossi, J. F. Gallo, A. da Silva, V. L. Torres, V. A. de Lima, N. K. Júnior, J. D. Almeida, R. M. Zerbinati, P. H. Braz-Silva, J. A. L. Lindoso and H. da Silva Martinho, *Sci Rep*, 2022, **12**, 4269.

7. F. T. Peters, *Bioanalysis*, 2014, **6**, 2083-2107.

8. L. H. J. Richter, H. H. Maurer and M. R. Meyer, *Toxicology Letters*, 2017, **280**, 142-150.

9. A. E. Steuer, E. Williner, S. N. Staeheli and T. Kraemer, *Drug Testing and Analysis*, 2017, **9**, 1085-1092.

10. F. Schifano, L. Orsolini, G. D. Papanti and J. Corkery, *World Psychiatry*, 2015.

Appendix 1

Supplementary information for Chapter 3

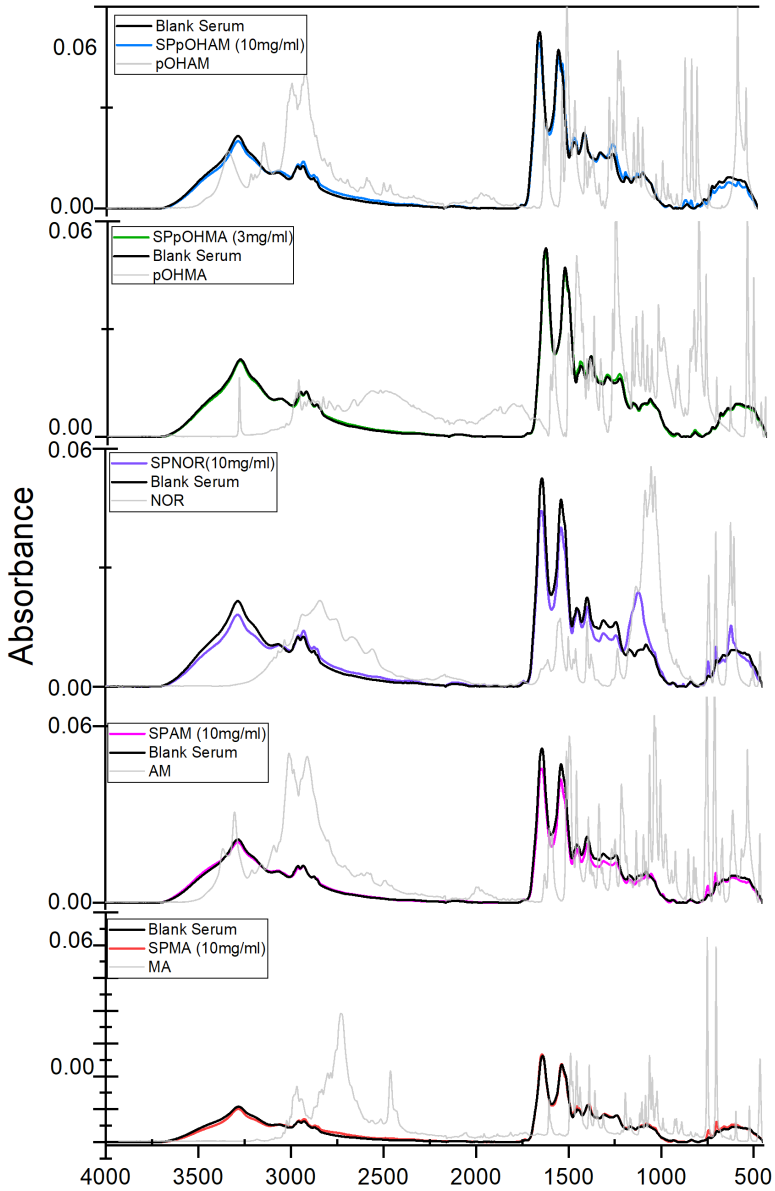

Figure A1-1: Stacked IR spectra of blank serum overlapped with serum samples spiked with drug compounds. The concentration of all drugs in urine was 10mg/mL except for UPpOHMA which was at 3 mg/mL. The spectra in grey show the IR spectra for respective powder drug compounds.SPMA refers to serum samples with MA, SPAM refers to serum samples with AM, SPNOR refers to serum samples with NOR, SPpOHAM refers to serum samples with pOHAM and SPpOMA refers serum samples with pOHMA.

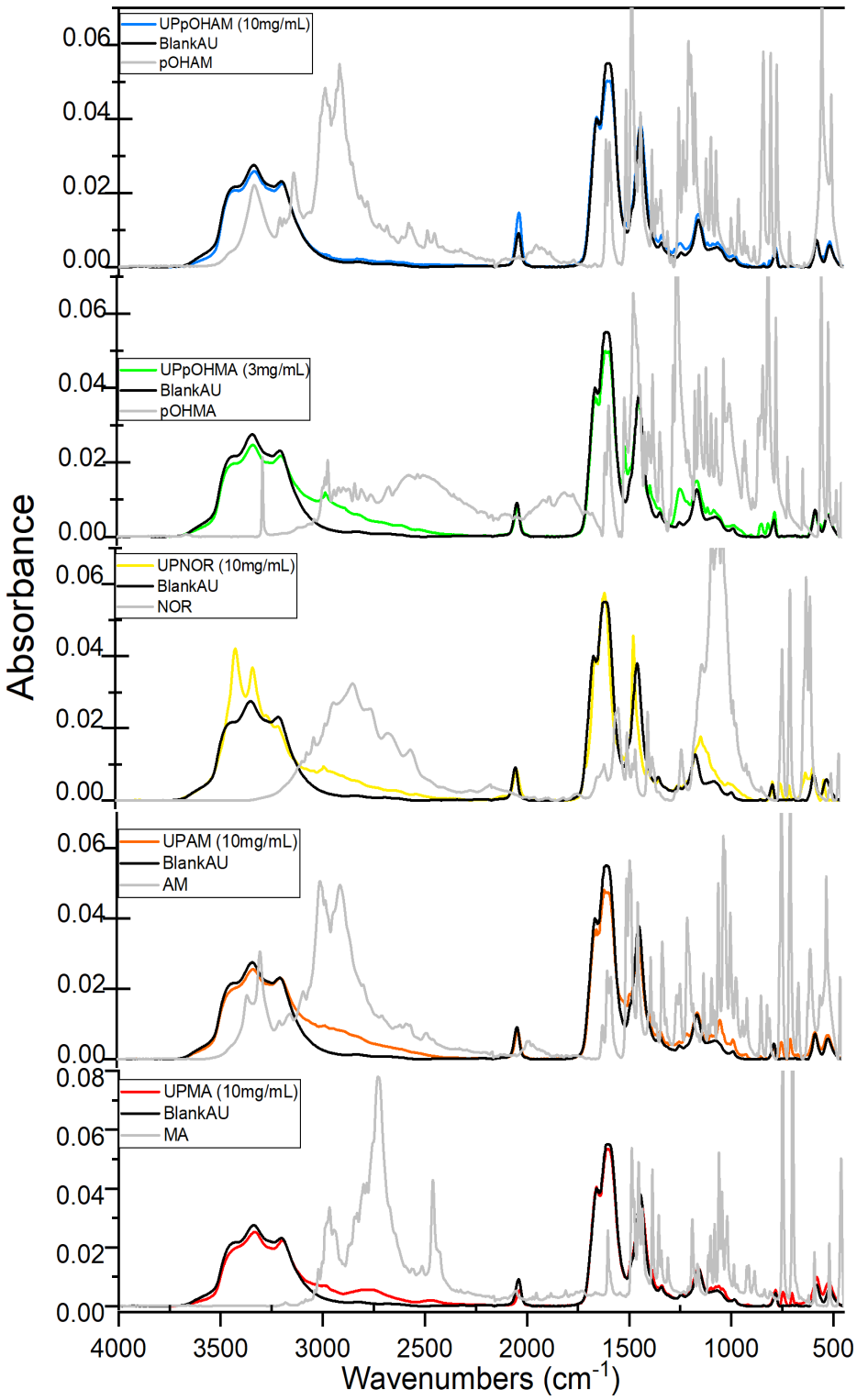

Figure A1-2 Stacked IR spectra of blank urine overlapped with urine samples spiked with drug compounds. The concentration of all drugs in urine was 10mg/mL except for UPpOHMA which was at 3 mg/mL. The spectra in grey show the IR spectra for respective powder drug compounds. UPMA refers to urine samples with MA, UPAM refers to urine samples with AM, UPNOR refers to urine samples with NOR, UPpOHAM refers to urine samples with pOHAM and UPpOMA refers urine samples with pOHMA.

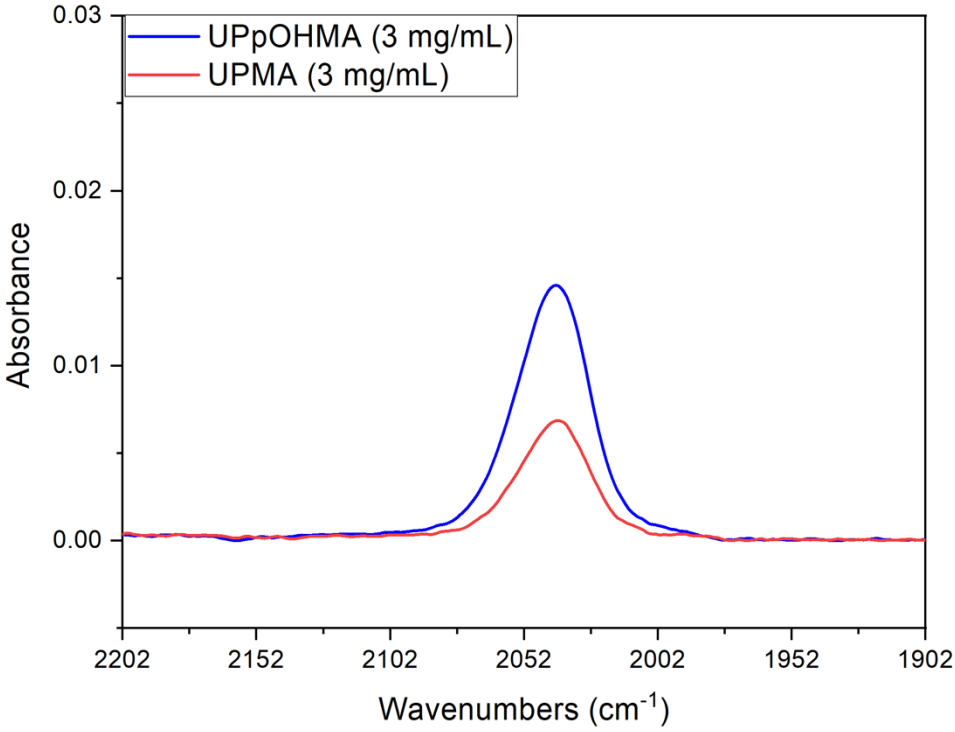

Figure A1-3: Comparison of MA and pOHMA peaks at 2040 cm-1 in urine at 3 mg/mL

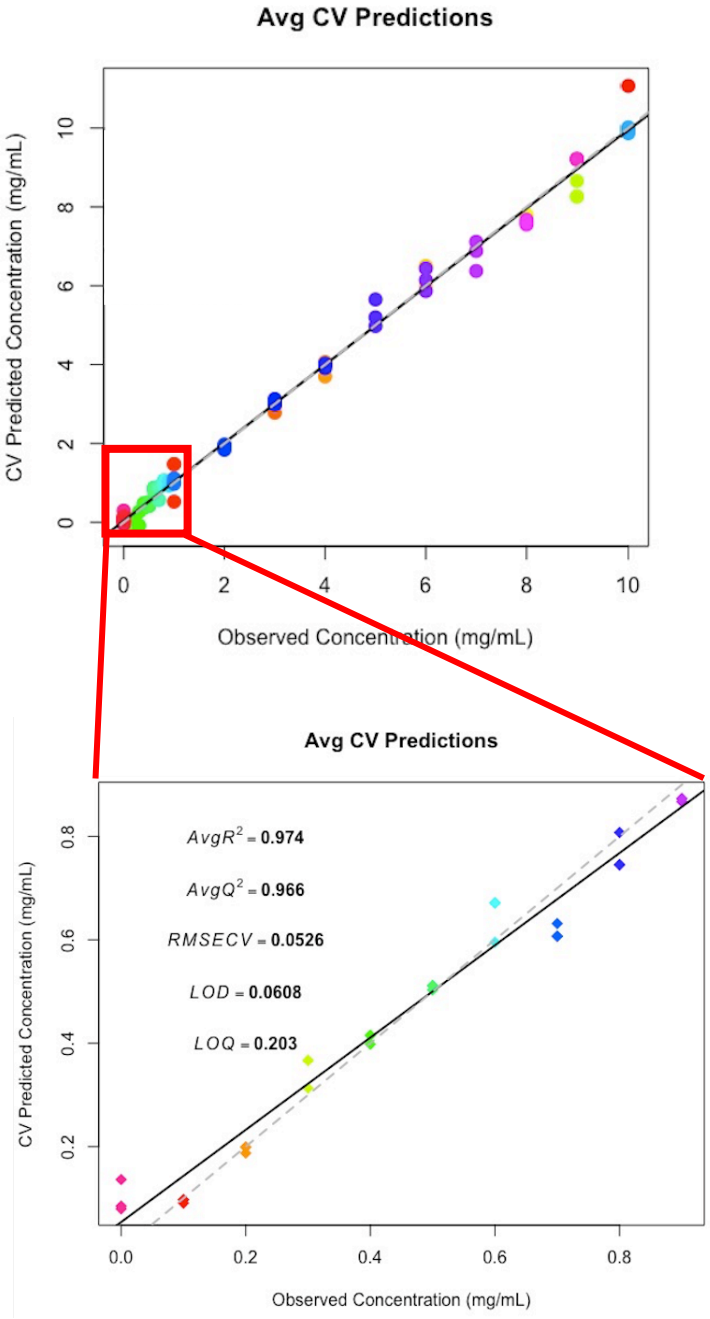

Figure A1-4: Graph showing PLS-R analysis for AM samples in serum across the concentration range of 0.1-10 mg/mL. The clinically and forensically relevant concentration range from 0.1 – 0.9 mg/mL is showed in an expanded graph at the bottom for clarity.

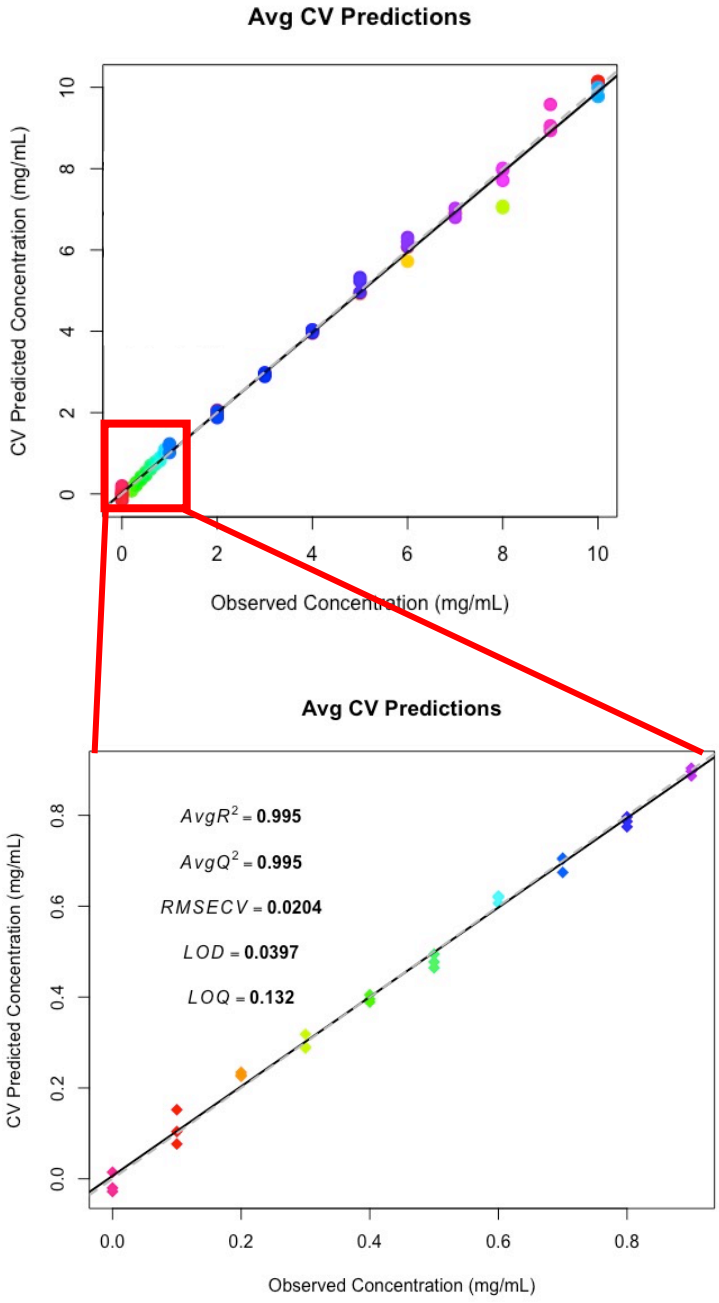

Figure A1-5: Graph showing PLS-R analysis for NOR samples in serum across the concentration range of 0.1-10 mg/mL. The clinically and forensically relevant concentration range from 0.1 – 0.9 mg/mL is showed in an expanded graph at the bottom for clarity.

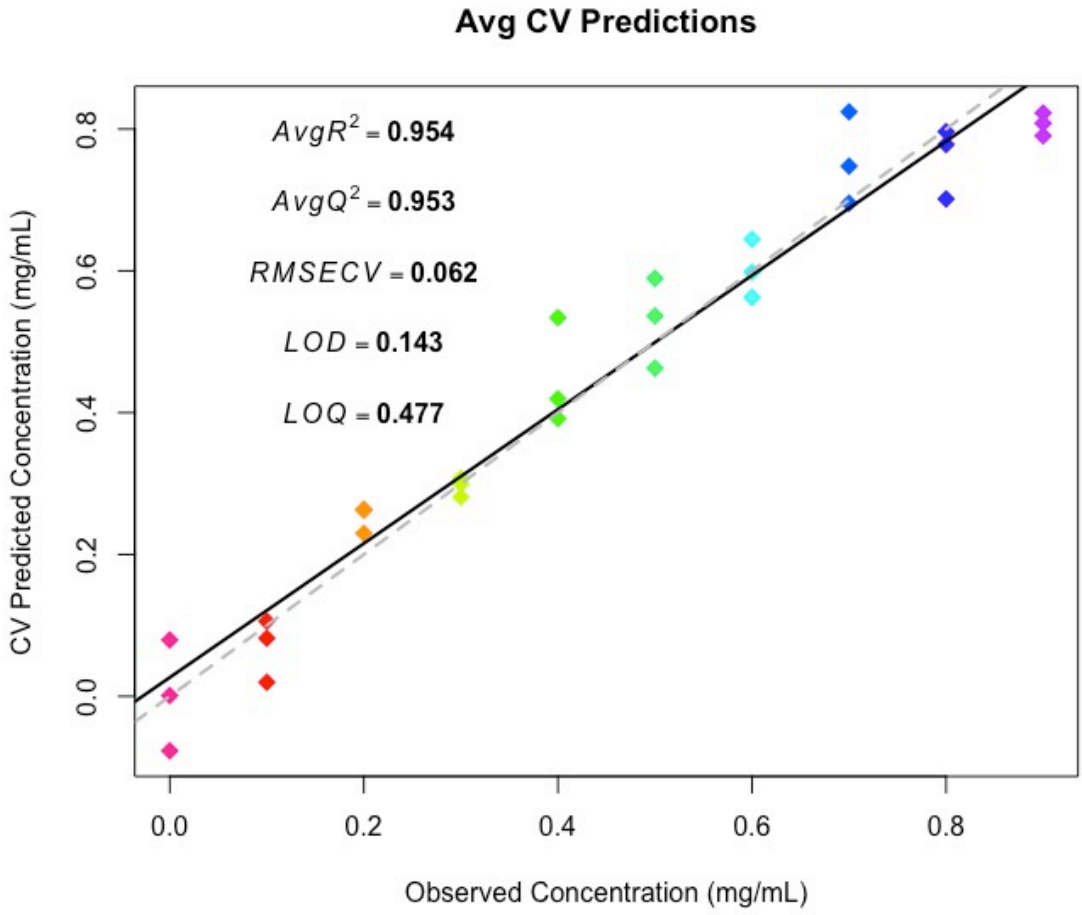

Figure A1-6: Graph showing PLS-R analysis for pOHMA samples in serum across the concentration range of 0.1-0.9 mg/mL which is the clinically and forensically relevant concentration range. Samples with higher concentration than 3 mg/mL were not possible due to the low solubility of pOHMA.

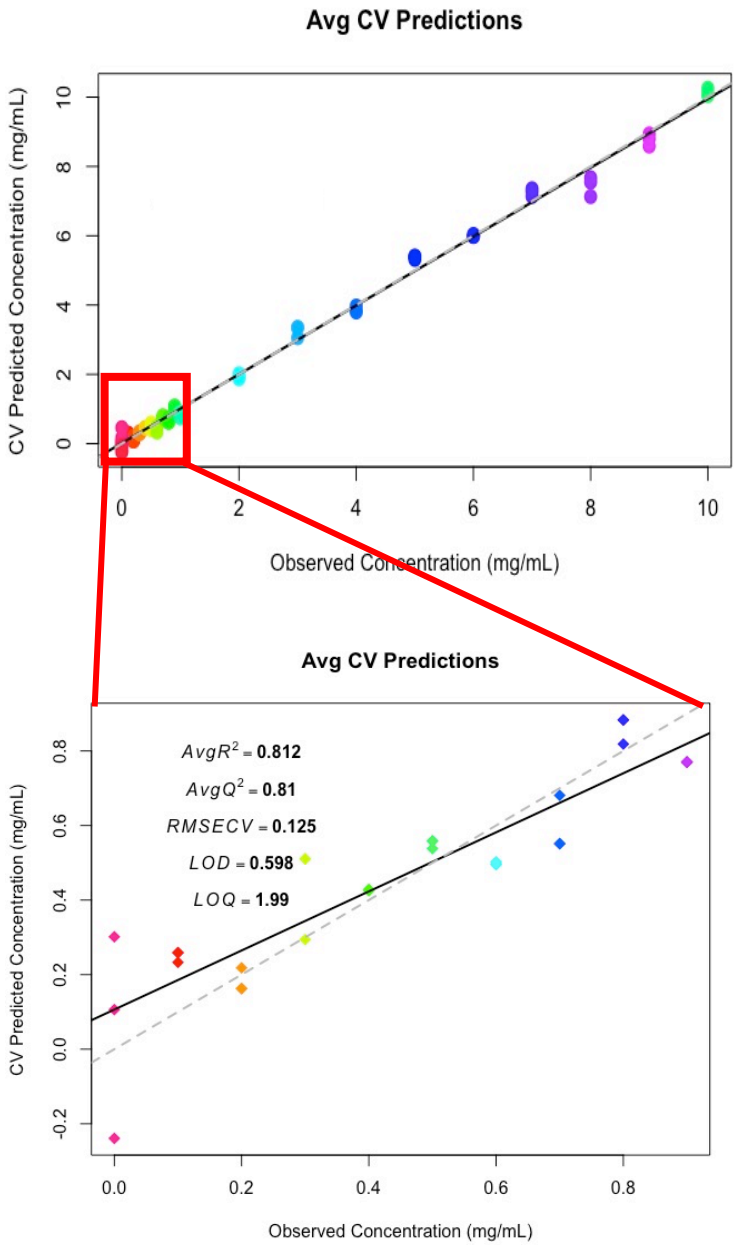

Figure A1-7: Graph showing PLS-R analysis for pOHAM samples in serum across the concentration range of 0.1-10 mg/mL. The clinically and forensically relevant concentration range from 0.1 – 0.9 mg/mL is showed in an expanded graph at the bottom for clarity.

Appendix 2

Supplementary information for Chapter 4

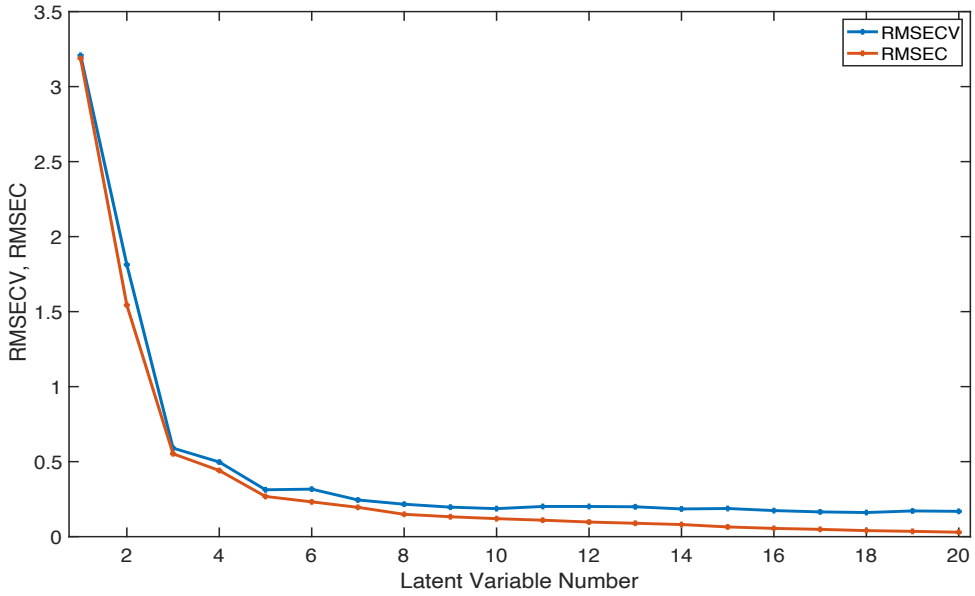

Figure A2-1: The plot of calibration error (RMSEC) and cross-validation error (RMSECV) as a function of the number of latent variables of the PLS regression model for MA samples in serum.

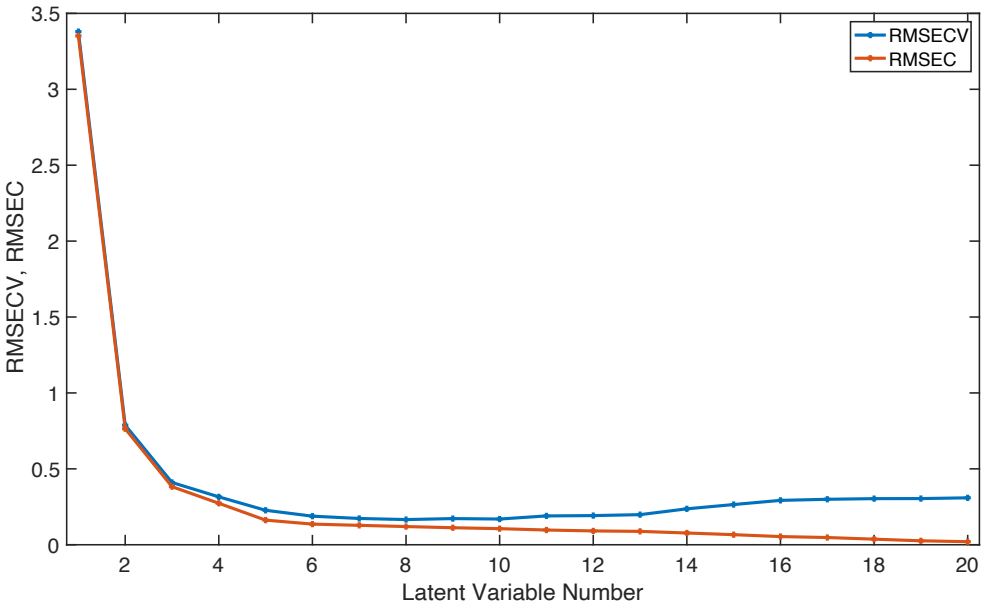

Figure A2-2: The plot of calibration error (RMSEC) and cross-validation error (RMSECV) as a function of the number of latent variables of the PLS regression model for MA samples in urine.

Appendix 3

Supplementary information for Chapter 5

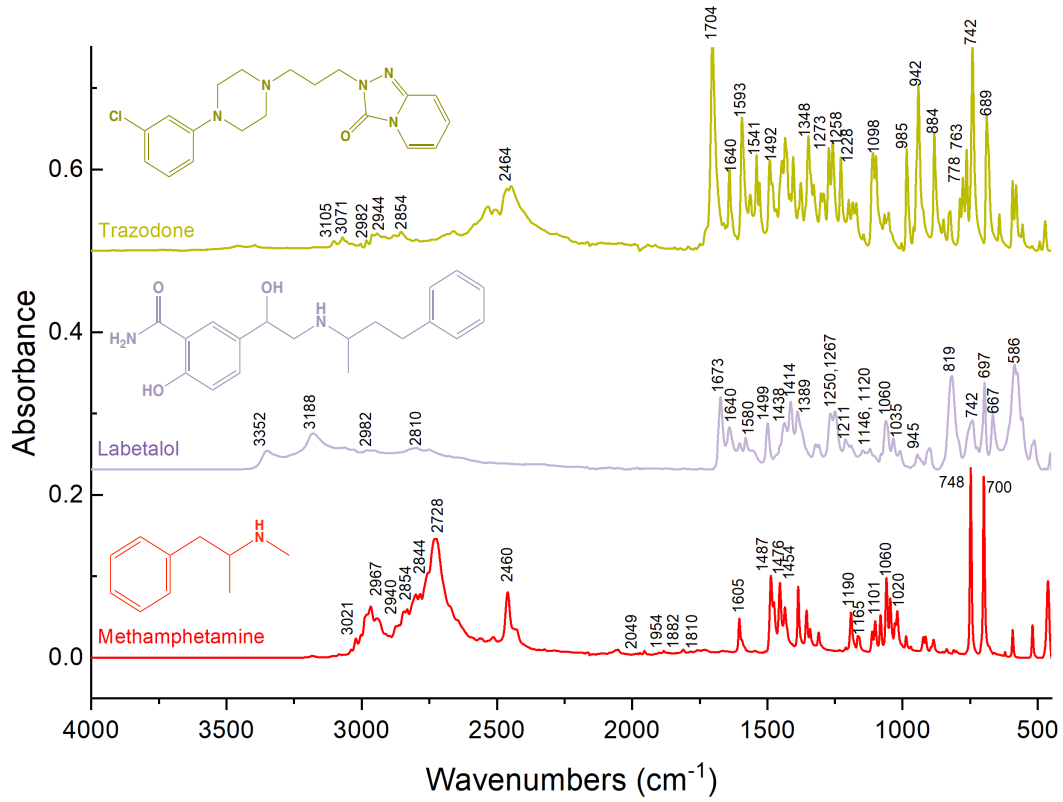

Figure A3-1: Stacked spectra of powder MA, Labetalol and Trazodone with labelled peaks.

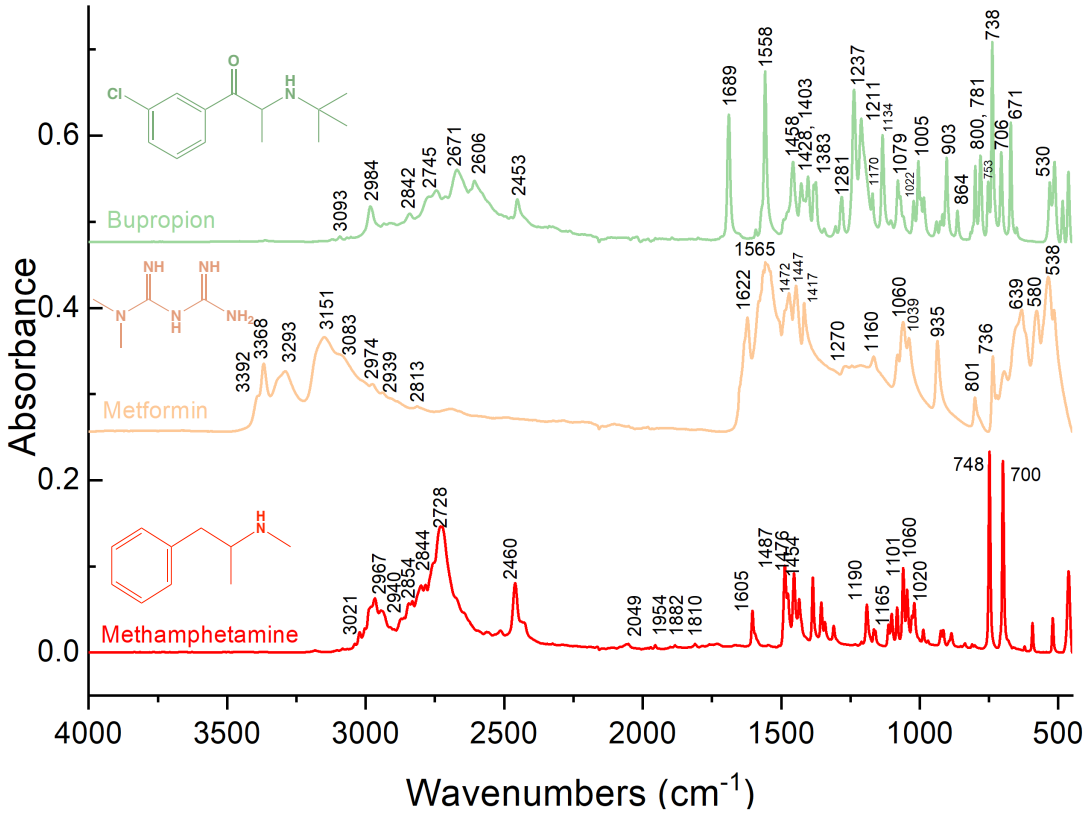

Figure A3-2: Stacked spectra for powder bupropion and metformin with labelled peaks.

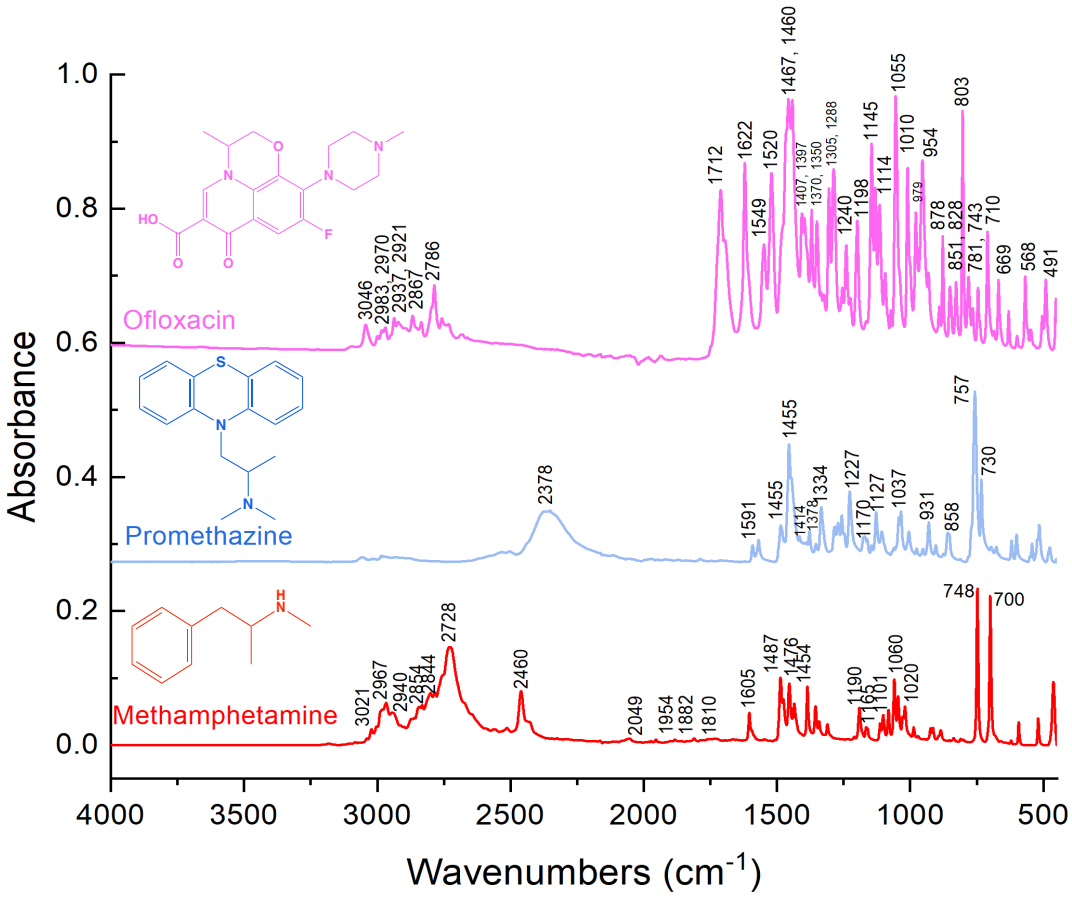

Figure A3-3: Stacked spectra for powder promethazine and ofloxacin with labelled peaks.

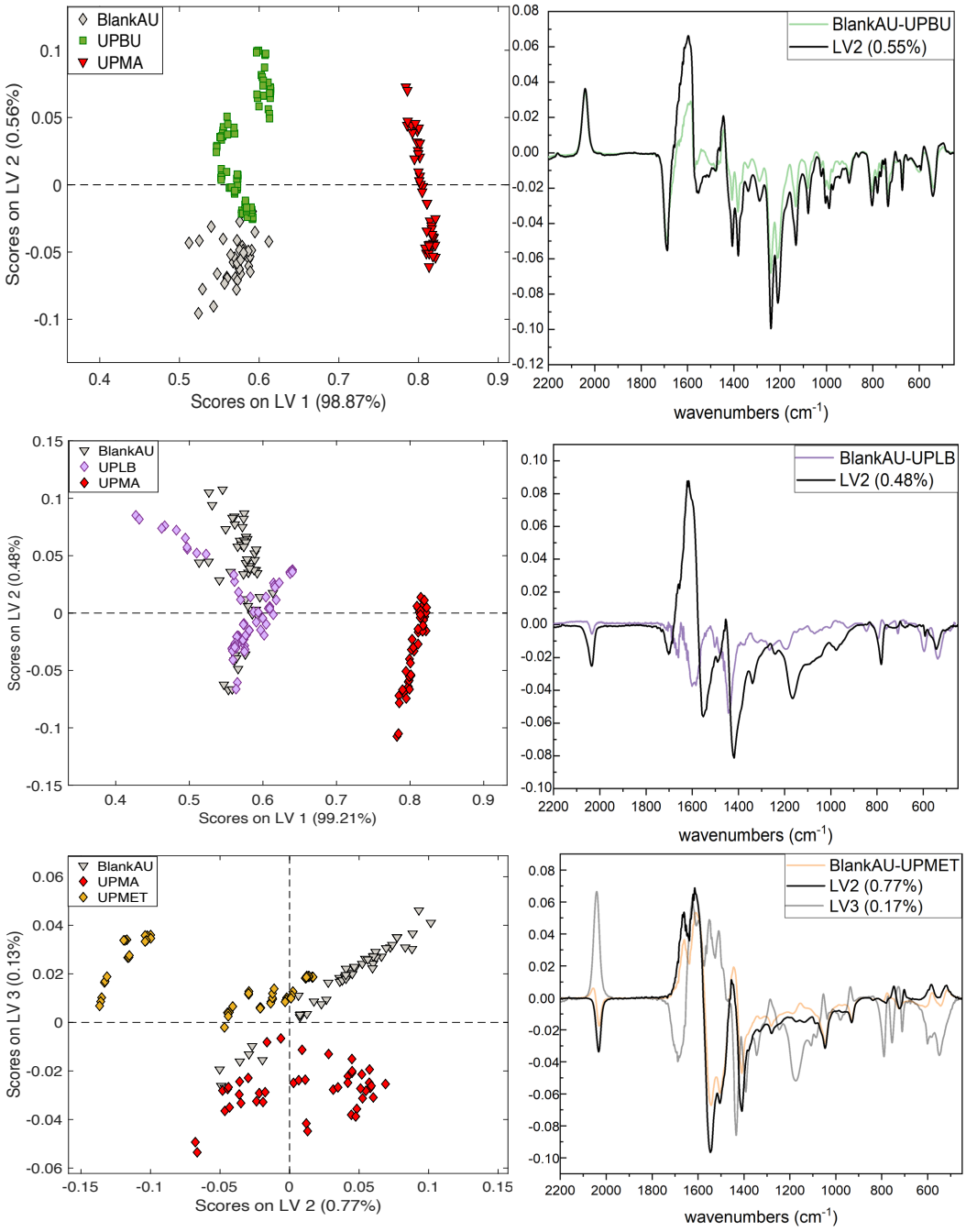

Figure A3-4: Scores (left) and loadings (right) plots for three multiclass PLS models are shown here. Top level shows plots for PLS classification between blank urine (BlankAU), MA samples in urine (UPMA) and bupropion samples in urine (UPBU). Middle level shows plots for classification between blank urine (BlankAU), MA samples in urine (UPMA) and labetalol in urine (UPLB). Bottom level shows plots from classification of blank urine (BlankAU), MA in urine (UPMA) and metformin in urine (UPMET). The loadings plots on the right are shown in colour with difference spectra for the respective drugs for comparison.

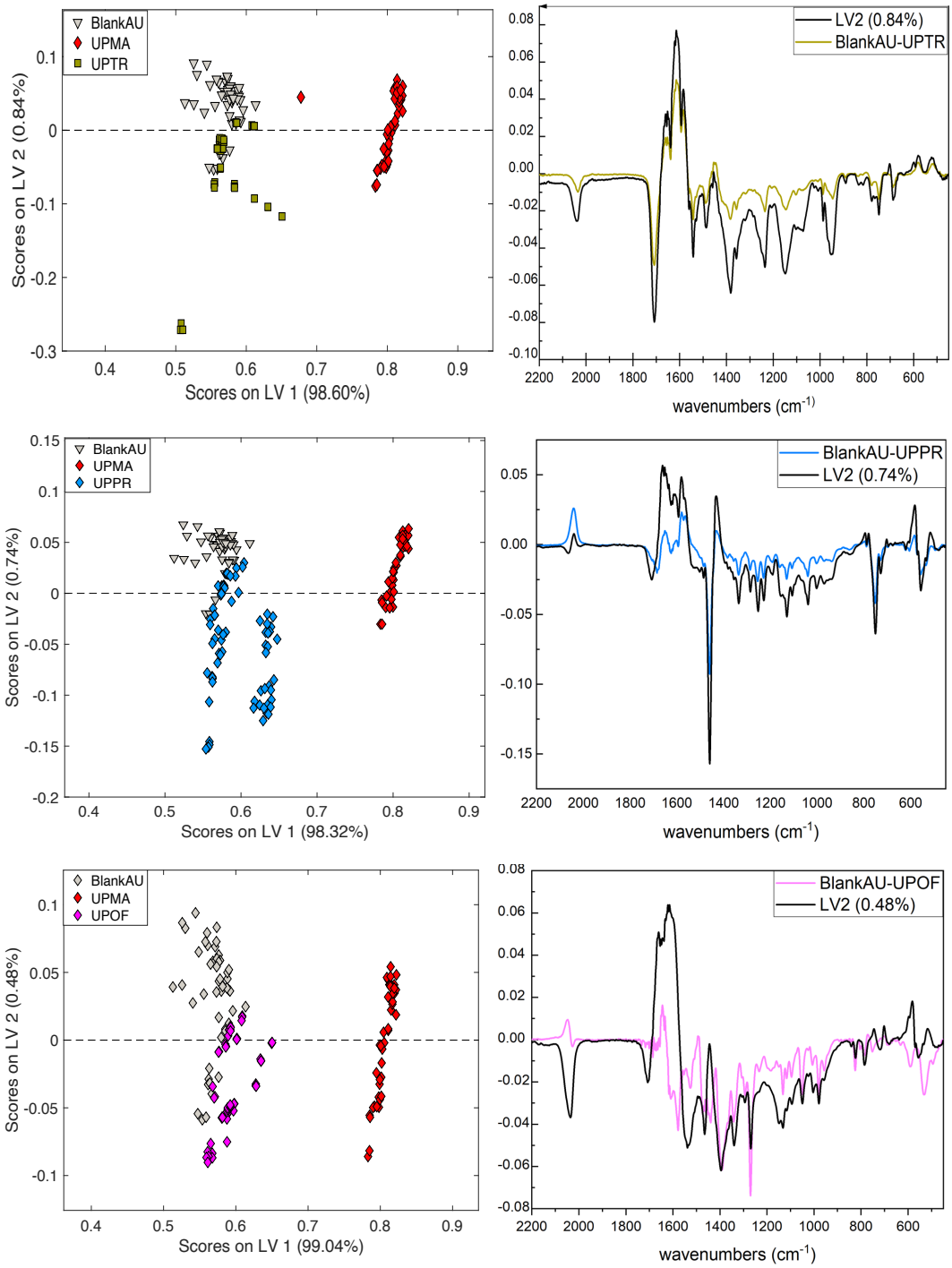

Figure A3-5: Scores (left) and loadings (right) plots for three multiclass PLS models are shown here. Top level shows plots for PLS classification between blank urine (BlankAU), MA samples in urine (UPMA) and trazodone samples in urine (UPTR). Middle level shows plots for classification between blank urine (BlankAU), MA samples in urine (UPMA) and promethazine in urine (UPPR). Bottom level shows plots from classification of blank urine (BlankAU), MA in urine (UPMA) and ofloxacin in urine (UPOF). The loadings plots on the right are shown in colour with difference spectra for the respective drugs for comparison.

Appendix 4

Supplementary information for Chapter 6

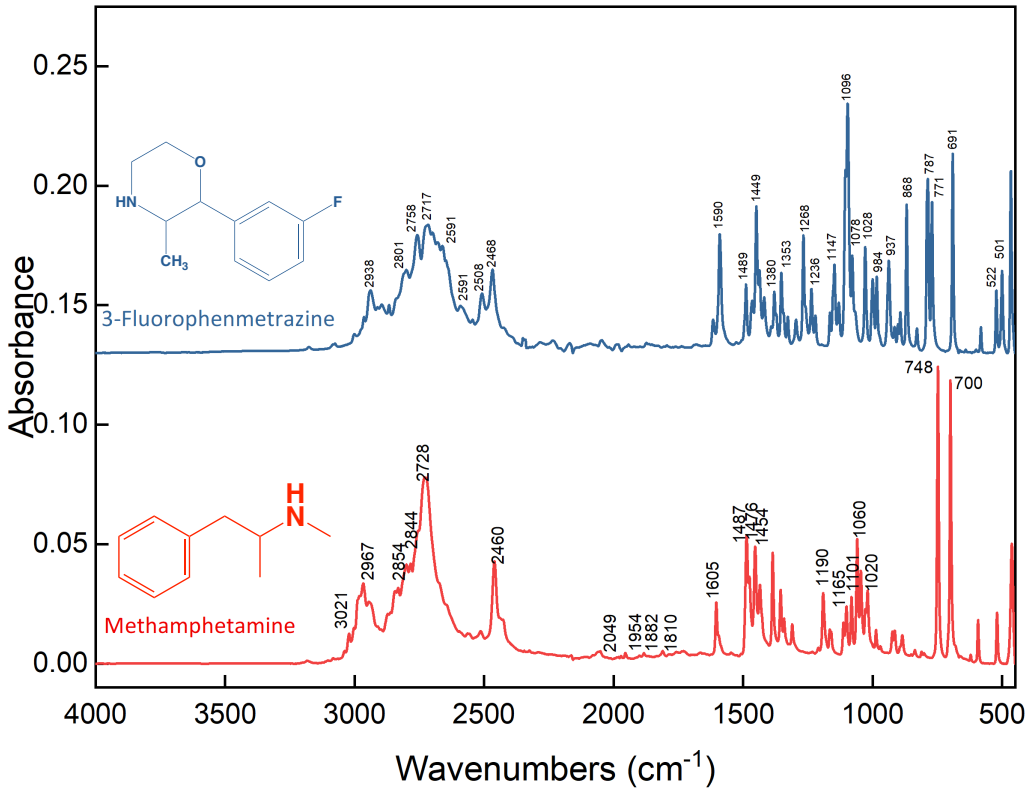

Figure A4-1: Stacked powder spectra for reference standards in Group 1 is shown here with methamphetamine. Group 1 only contains 3-flurophenmetrazine.

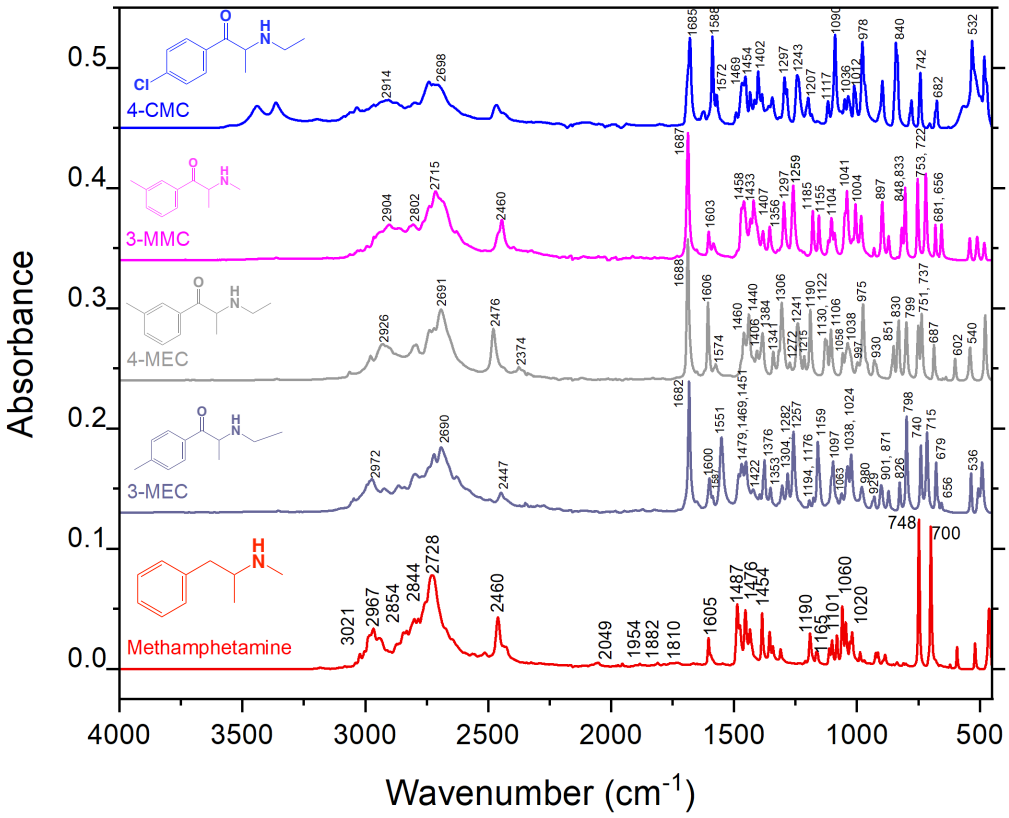

Figure A4-2: Stacked powder spectra for reference standards in Group 2 are shown here with MA in red. Group 2 contains 4-chloromethacathinone (4-CMC), 3-methylmethcathinone (3-MMC), 4-methylethcathinone (4-MEC) and 3-methylethcathinone (3-MEC).

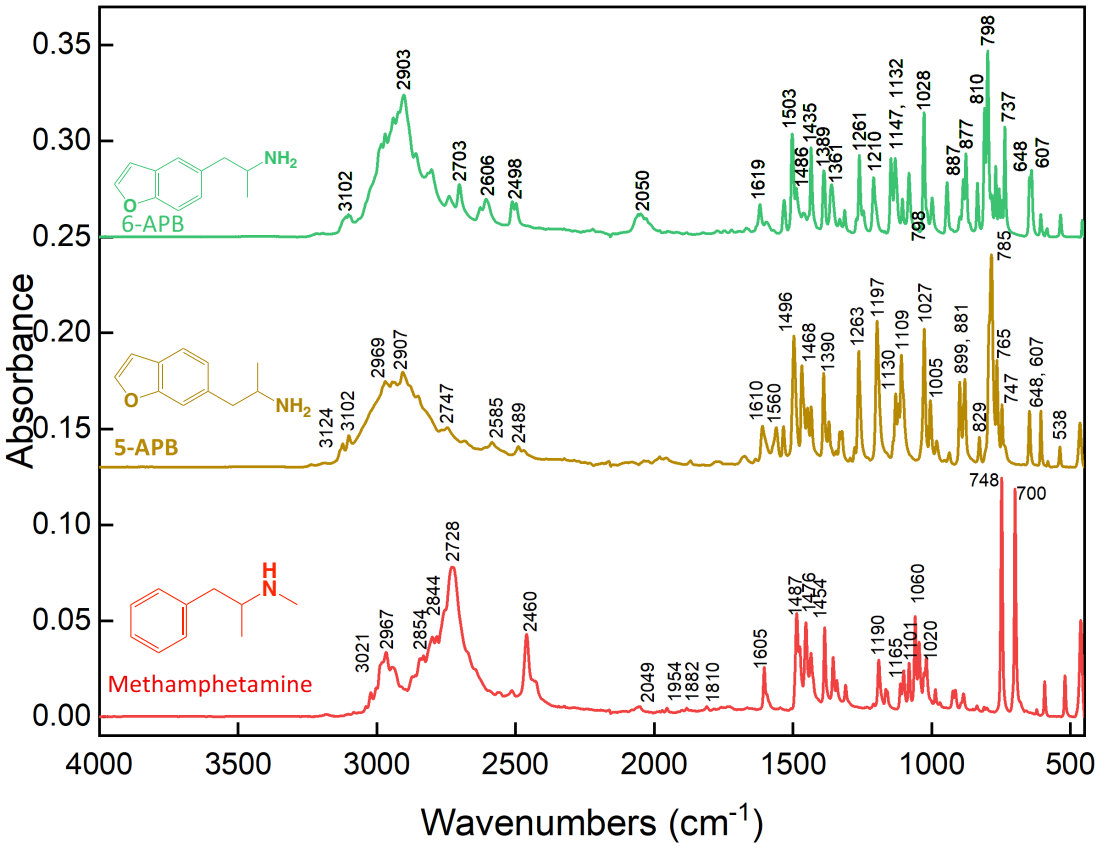

Figure A4-3: Stacked powder spectra for reference standards in Group 3 are shown here with MA in red. Group 3 consists of 6-(2-aminopropyl)benzofuran (6-APB) and 5-(2-aminopropyl)benzofuran (5-APB).

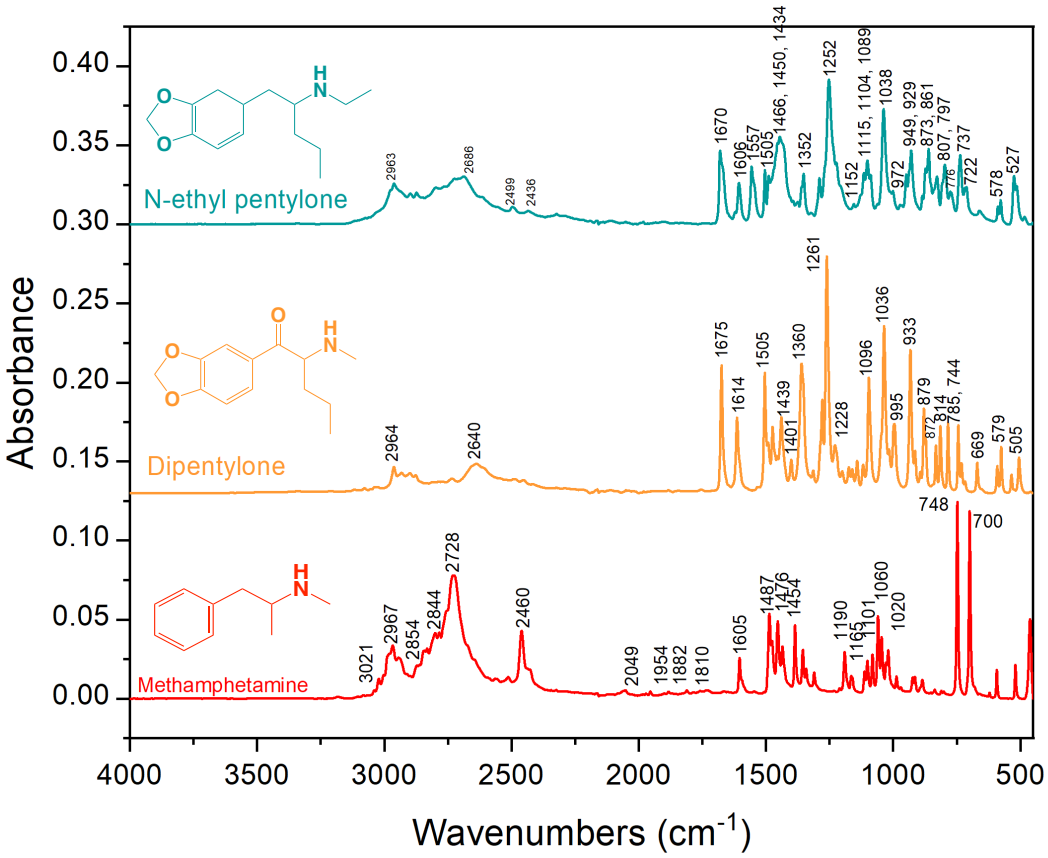

Figure A4-4:Figure shows stacked spectra for powder N-ethyl pentylone and dipentylone with MA in red. These are reference standards for Group 4.

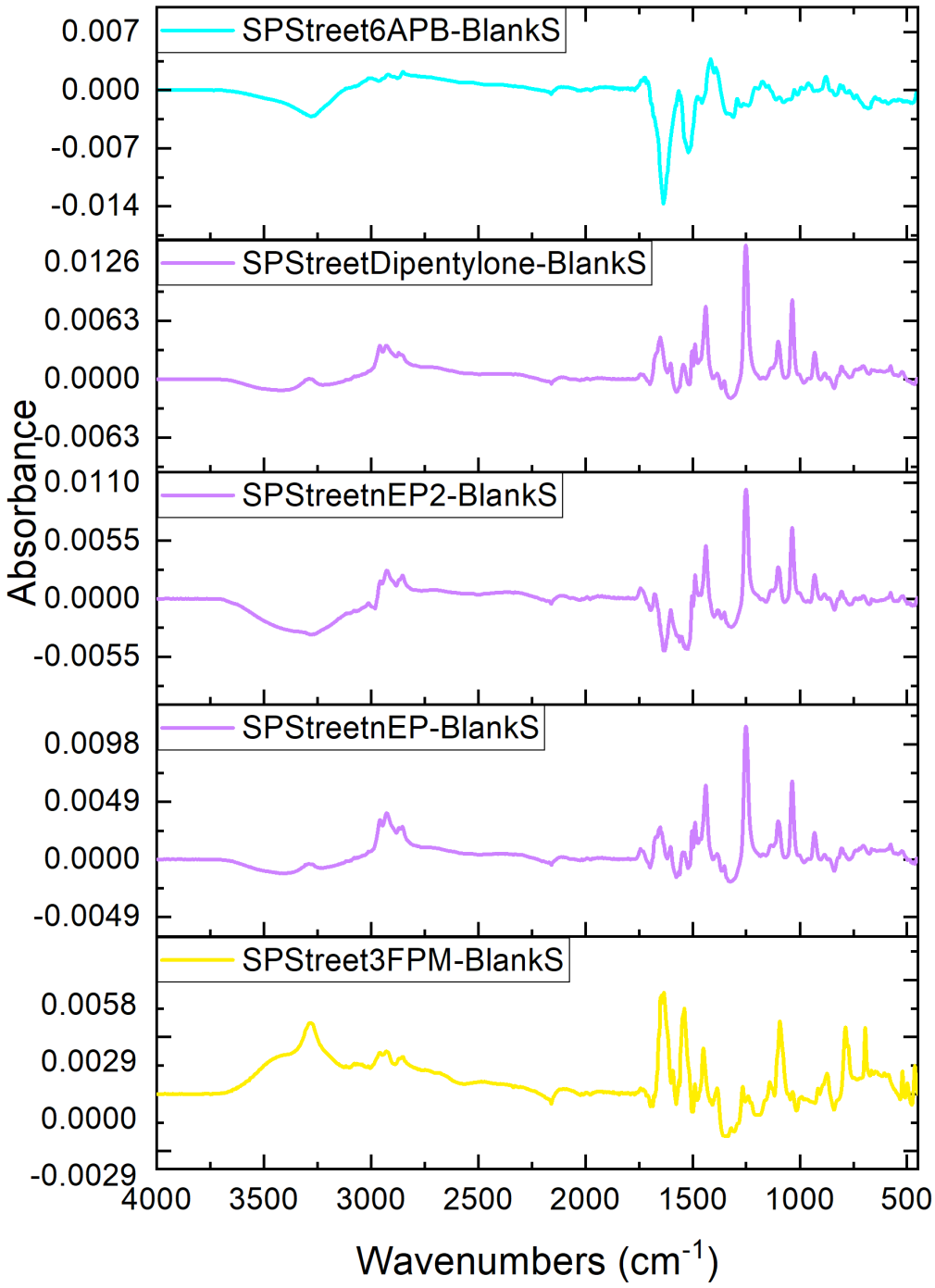

Figure A4-5: Stacked difference spectra for group 1 (yellow), group 4 (Purple) and group 3 (blue) are shown. All drug samples were at a concentration of 10 mg/mL in serum. These were obtained by subtracting blank serum spectra from that of the drug sample spectra.

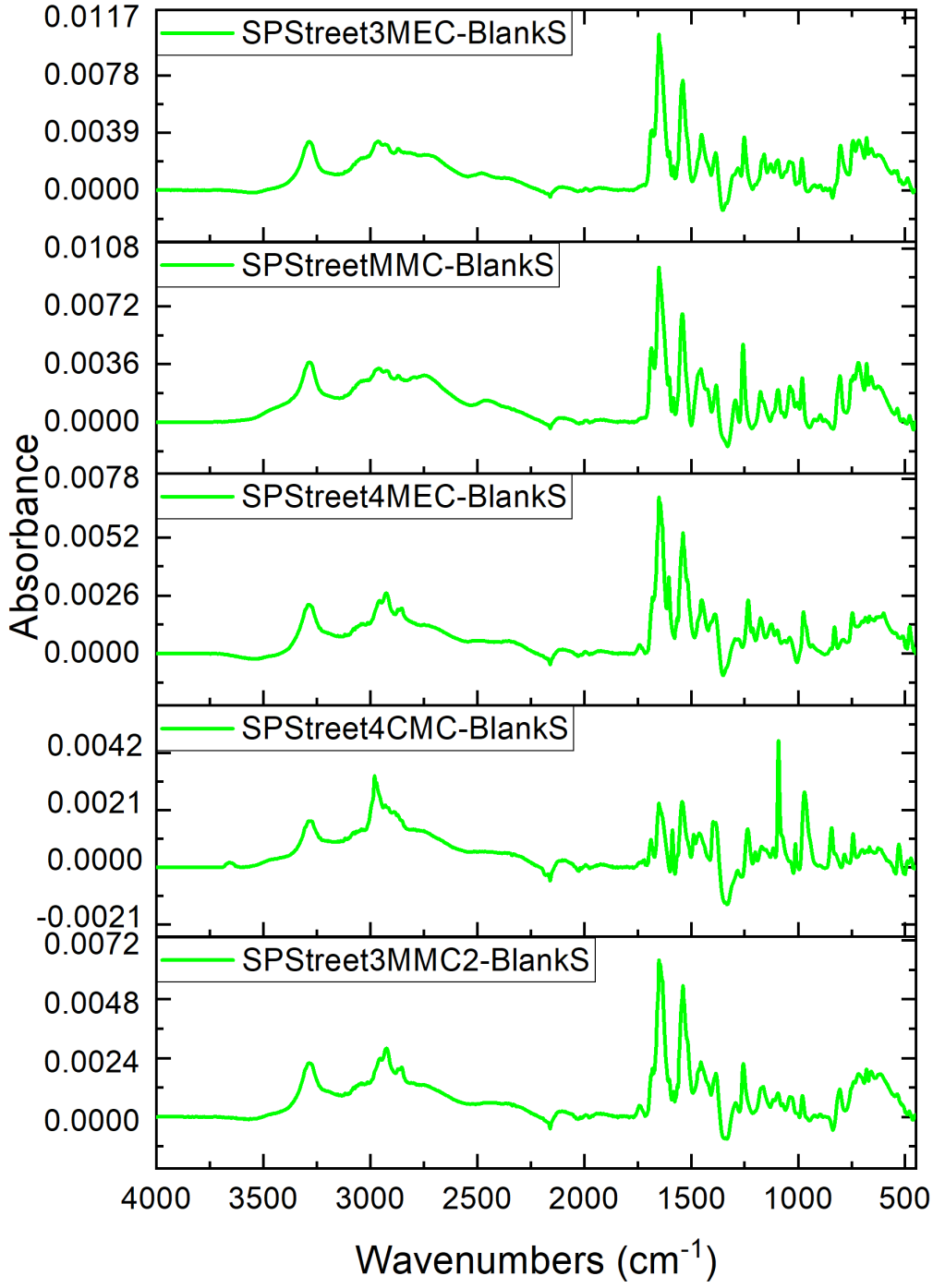

Figure A4-6: Stacked difference spectra for group 2 (green) are shown. All drug samples were at 10 mg/mL in serum. These were obtained by subtracting blank serum matrix spectra from that of the drug sample spectra.

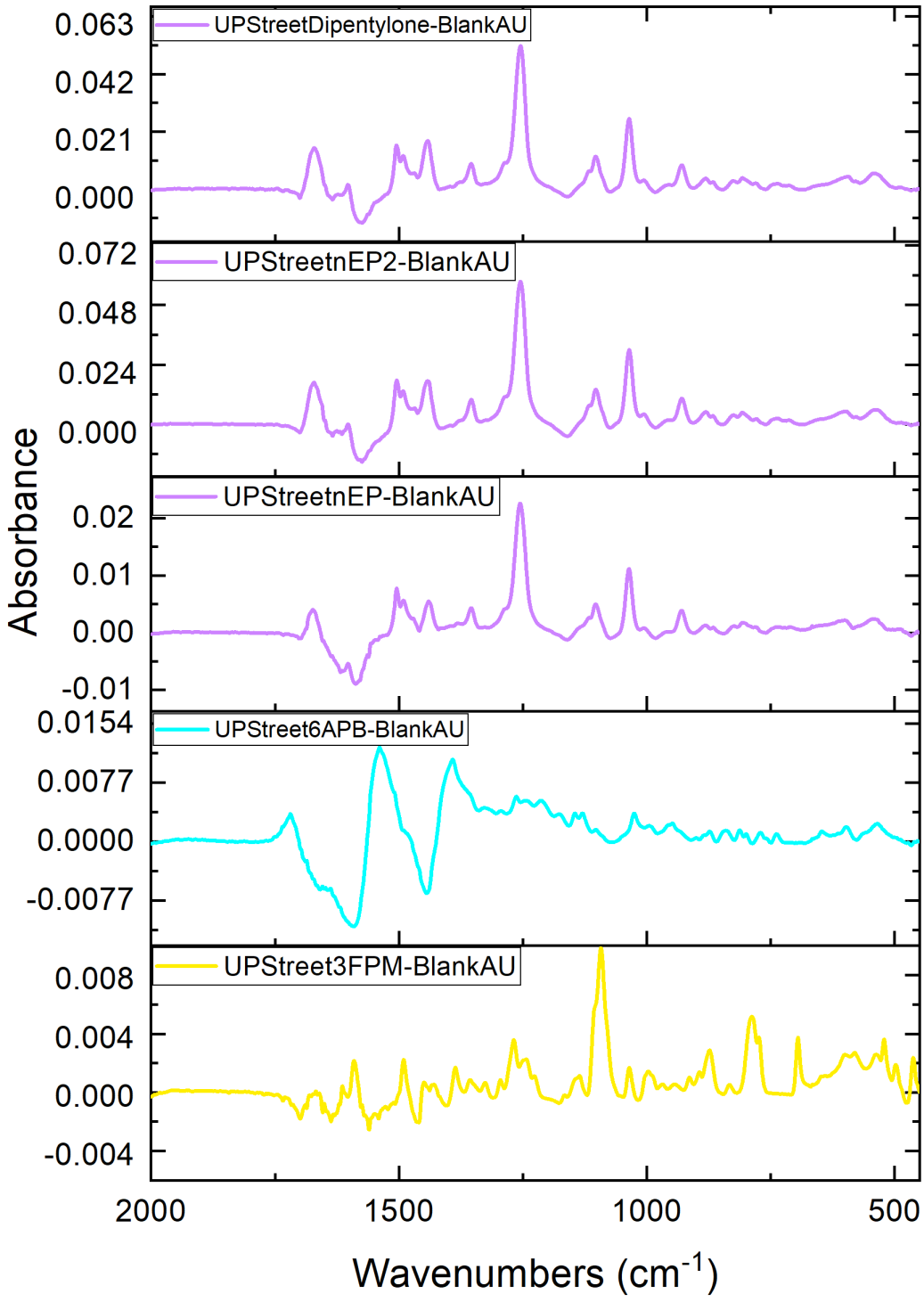

Figure A4-7: Stacked difference spectra for group 1 (yellow), group 4 (Purple) and group 3 (blue) are shown. All drug samples were at a concentration of 10 mg/mL in urine. These were obtained by subtracting blank urine spectra from that of the drug sample spectra.

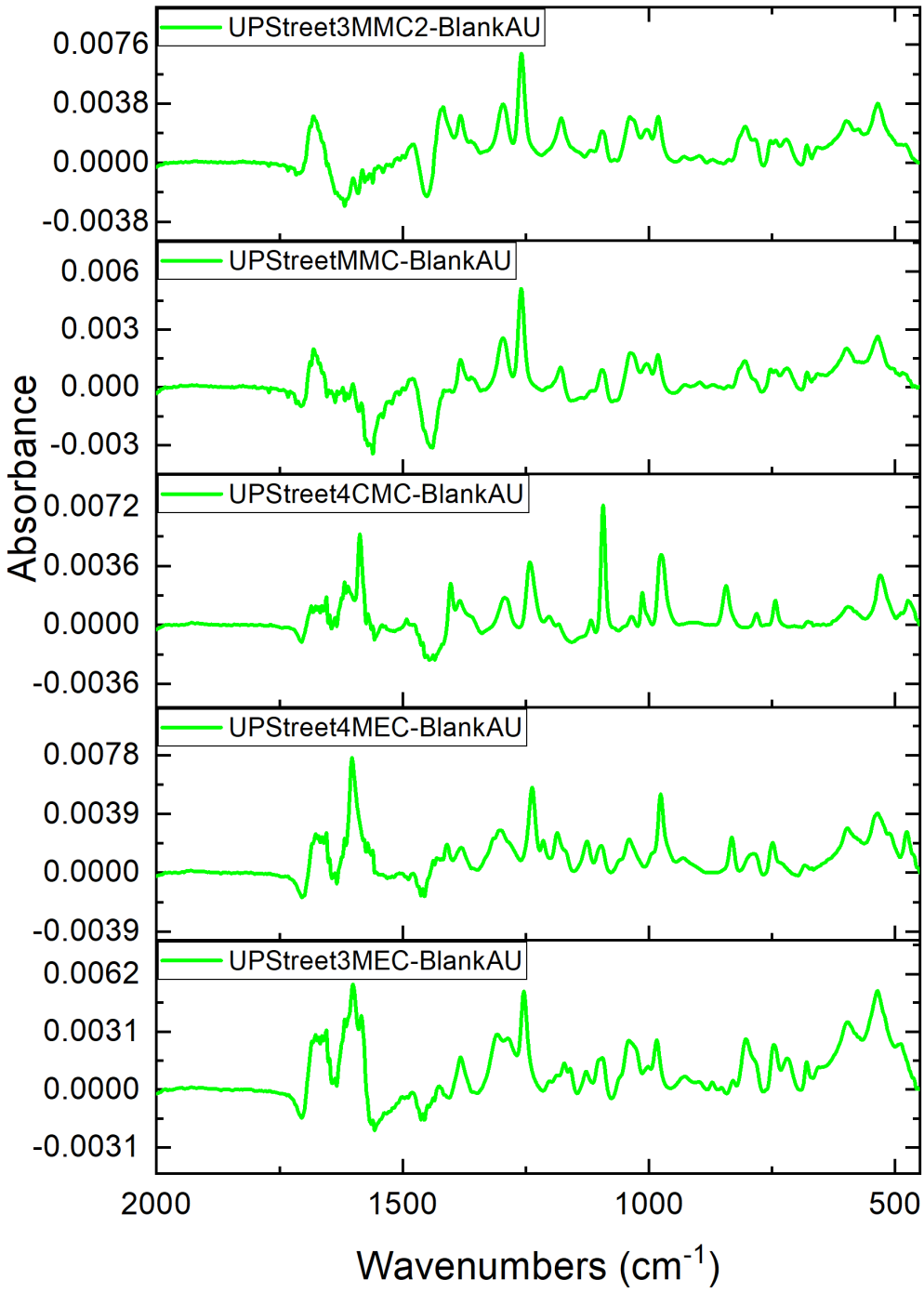

Figure A4-8: Stacked difference spectra for group 2 (green) are shown. All drug samples were at a concentration of 10 mg/mL in serum. These were obtained by subtracting blank serum spectra from that of the drug sample spectra.

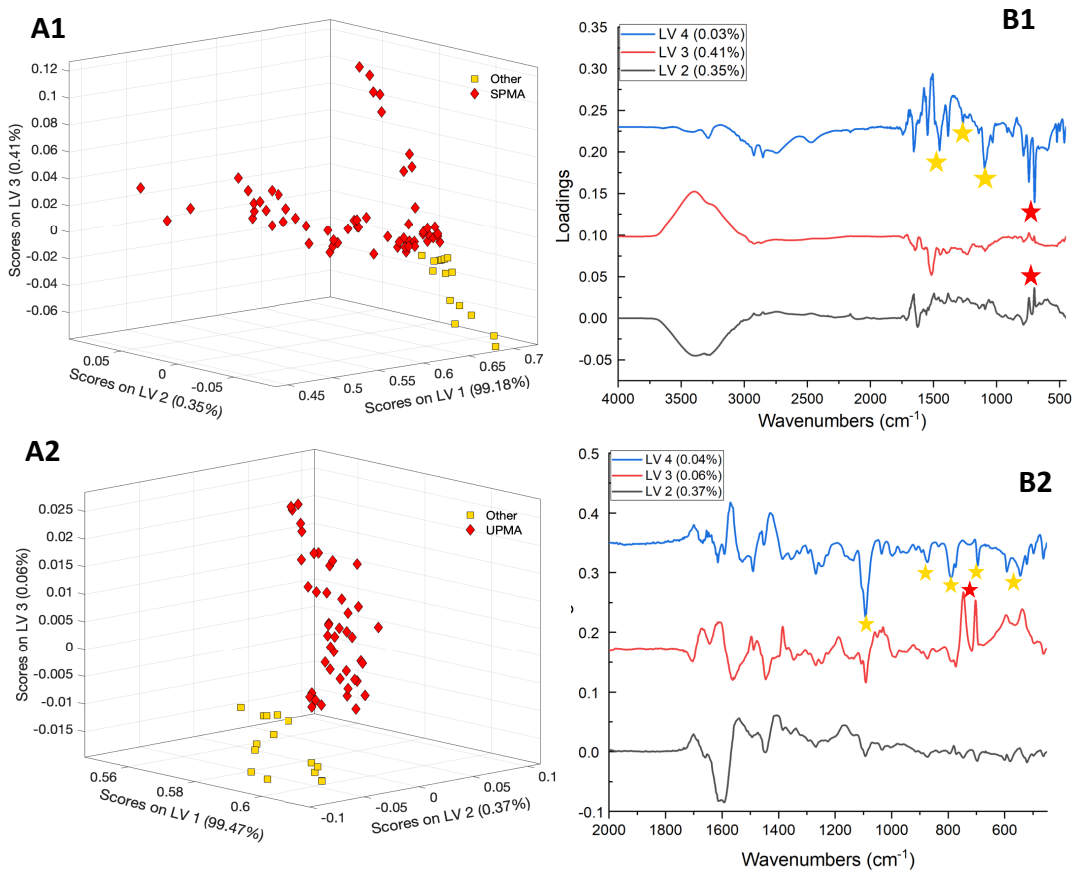

Figure A4-9: Scores and loading plots for PLS-DA classification of MA samples (red diamonds in scores plots, here denoted as 'SPMA' or 'UPMA) from those in group 1 (yellow squares in scores plots, here denoted as 'Other') are shown for serum (A1 and B1) and urine (A2 and B2) datasets. The optimum number of LVs for both models were found to be 4 and their loadings are given in B1 and B2. LV1 is not shown here as it was the mean spectrum in both datasets resembling the respective matrices. The yellow stars highlight the peaks from group 1 samples while the red stars highlight the influence of MA samples in the loading plots.

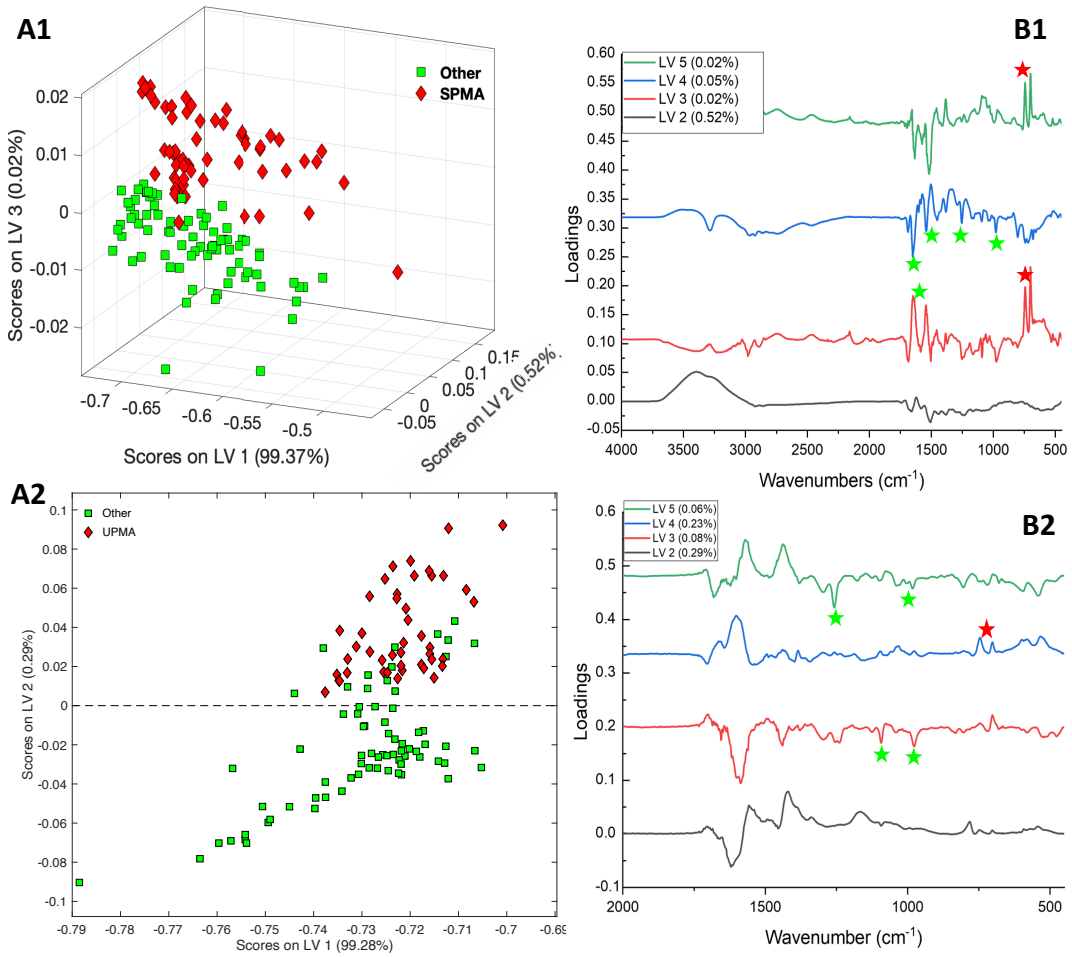

Figure A4-10: Scores and loading plots for PLS-DA classification of MA samples (red diamonds in scores plots, here denoted as 'SPMA' or 'UPMA) from those in group 2 (green square in scores plots, here denoted as 'Other') are shown for serum (A1 and B1) and urine (A2 and B2) datasets. The optimum number of LVs for both models were found to be 5 and their loadings are given in B1 and B2. LV1 is not shown here as it was the mean spectrum in both datasets resembling the respective matrices. The green stars highlight the peaks from group 2 samples while the red stars highlight the influence of MA samples in the loading plots.

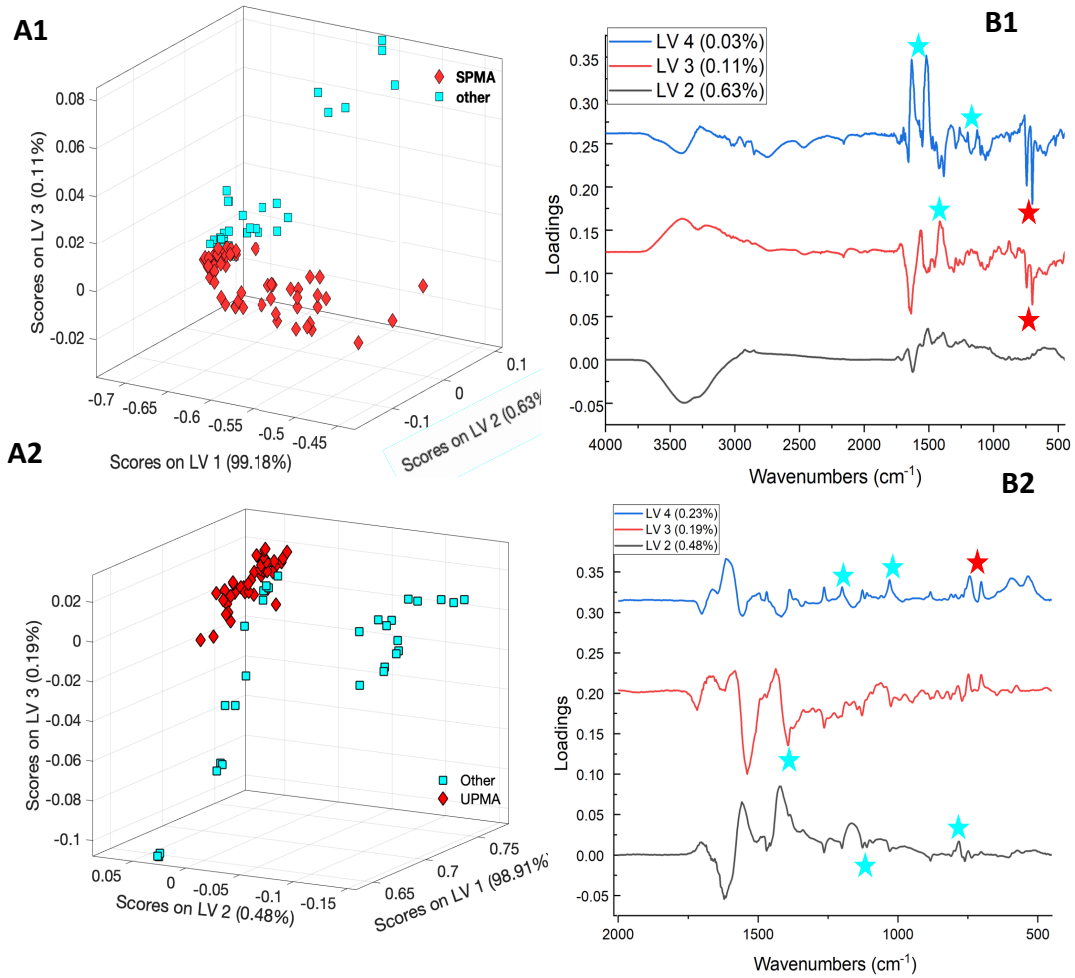

Figure A4-11: Scores and loading plots for PLS-DA classification of MA samples (red diamonds in scores plots, here denoted as 'SPMA' or 'UPMA) from those in group 3 (blue square in scores plots, here denoted as 'Other') are shown for serum (A1 and B1) and urine (A2 and B2) datasets. The optimum number of LVs for both models were found to be 4 and their loadings are given in B1 and B2. LV1 is not shown here as it was the mean spectrum in both datasets resembling the respective matrices. The blue stars highlight the peaks from group 3 samples while the red stars highlight the influence of MA samples in the loading plots.

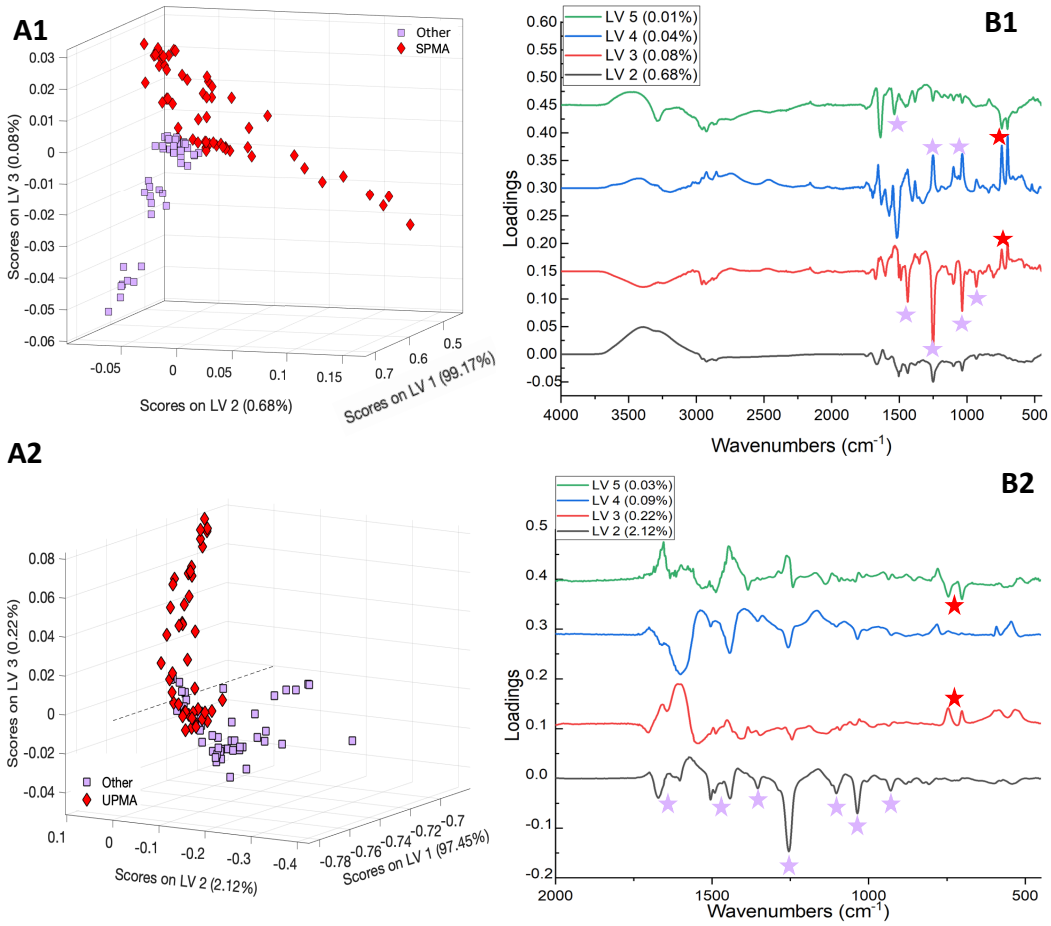

Figure A4-12: Scores and loading plots for PLS-DA classification of MA samples (red diamonds in scores plots, here denoted as 'SPMA' or 'UPMA) from those in group 4 (purple square in scores plots, here denoted as 'Other') are shown for serum (A1 and B1) and urine (A2 and B2) datasets. The optimum number of LVs for both models were found to be 5 and their loadings are given in B1 and B2. LV1 is not shown here as it was the mean spectrum in both datasets resembling the respective matrices. The purple stars highlight the peaks from group 4 samples while the red stars highlight the influence of MA samples in the loading plots.

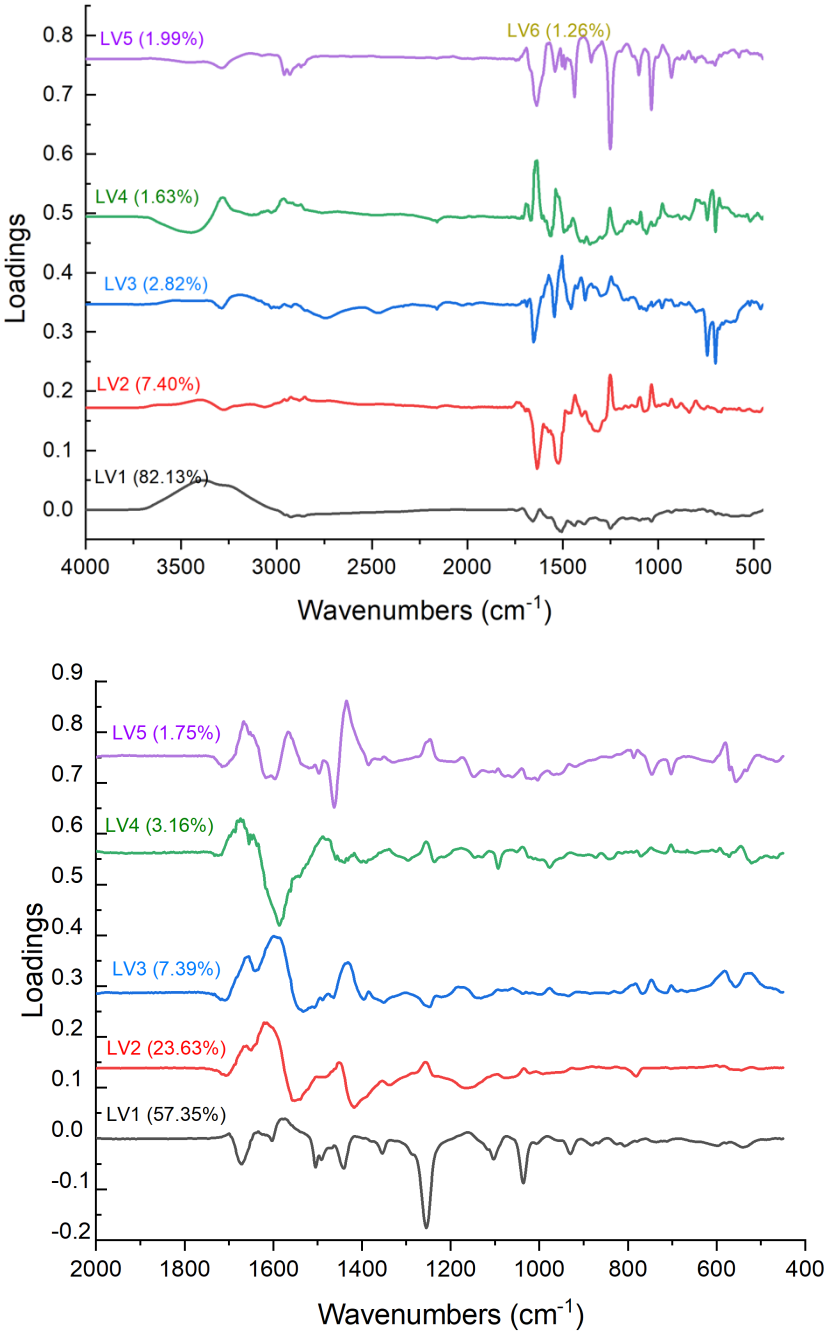

Figure A4-13: Loading plots latent variables from for multiclass PLS-DA model for classification of MA, Street NPS and drug-free samples are shown here for serum (top) and urine (bottom) datasets.

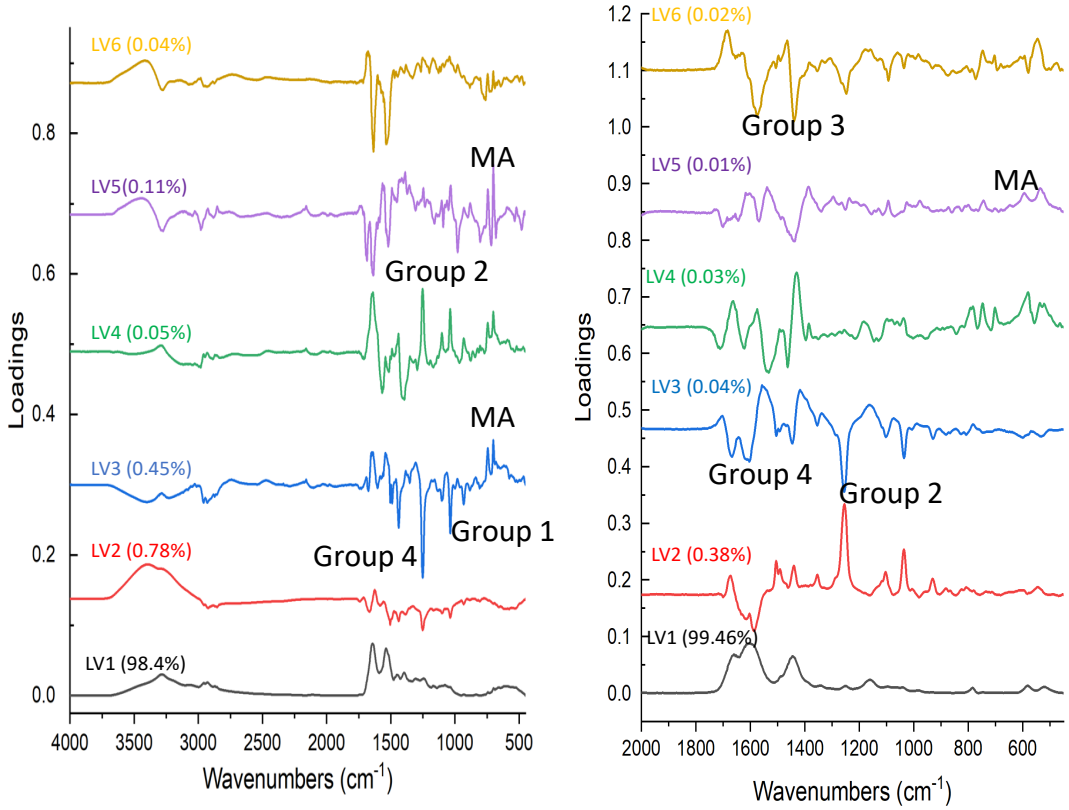

Figure A4-14: Loading plots 6 LVs from multiclass PLS-DA classification for serum (left) and urine (right) datasets are given here. The classes included MA, groups 1 to 4. The first LV (shown in black) resembles the mean spectrum of respective matrix. The contributions to the loading plots from MA samples are indicated by 'MA'. Similarly, the contributions from NPS groups are also indicated by their group labels.